The Thermodynamics, Mechanism and Kinetics of the Catalytic Conversion of Propylene and Water to Diisopropyl Ether over Amberlyst 15

Frank Patrick Heese
B.Sc. Eng. (Chem.) (University of the Witwatersrand)

Submitted to the University of Cape Town
in fulfilment of the requirements for the degree of

DOCTOR OF PHILOSOPHY

November 1998

Department of Chemical Engineering
University of Cape Town
Rondebosch
Cape Town
South Africa

Acknowledgements

My thanks go to my supervisors Prof. Mark Dry and Dr. Klaus Möller for their help and guidance without which this thesis would not have been. Many thanks also to Assoc. Prof. Eric van Steen for his valuable contributions, both to this thesis and to my wine appreciation skills.

Thanks to all the fellow postgraduates who made life enjoyable. In particular to Rein and Andrew who indulged my rampant caveman musings; to Peter, Linda, Heiko and Uwe for the crayfish and the sparkling wine; to Warwick for teaching me the finer points of body art; to Richard for waiting patiently while I retrieved my errant golf balls; to Sandra for being just a phone call away and to Melissa for that bottle of Cabernet.

A special mention must, of course, go to dear departed Freddie, Blinky and of course Squidgy who contrived to make the last few months a more pleasurable experience than it otherwise would have been.

My appreciation goes to all the members of staff who made my stay in the department that little bit easier. Especially to Pam for ensuring orders arrived when I least expected them and to Peter and Joachim for keeping my experimental rig alive and kicking.

Abstract

Diisopropyl ether (DIPE) was synthesised in a single step from a feed of propylene and water over Amberlyst 15 ion exchange resin catalyst. It was produced in a trickle bed reactor at pressures between 1 bar and 60 bar, at temperatures between 70 °C and 160 °C and at overall propylene to water ratios between 1 : 5 and 10 : 1. Reaction proceeded in the liquid phase within the catalyst particles. The only reactions that occurred in the system were the hydration of propylene to form isopropanol (IPA), the alkylation of IPA with propylene to form DIPE and the bimolecular dehydration of IPA to form DIPE and water. No side reactions such as propylene oligomerisation were observed. Starting from a feed of propylene and water the primary reaction product was IPA. IPA was subsequently consumed in two secondary reactions which produced DIPE. DIPE was produced either by the alkylation of IPA with propylene or by the bimolecular dehydration of IPA. It was generally not possible to study the two DIPE formation reactions separately as they are linked via the propylene hydration reaction. All experimental data was thus reported in terms of a hydration rate and an etherification rate, the latter being the sum of the IPA alkylation and the bimolecular IPA dehydration rates.

The reactions to produce IPA and DIPE over Amberlyst 15 proceeded via two different mechanisms, the so-called Type I and Type II mechanisms. The ratio of apolar (propylene and DIPE) to polar (water and IPA) species and the overall species concentration in the reaction medium determined the dominant mechanism. Type I mechanisms predominated at low ratios of apolar to polar species in the reaction medium. When the ratio of apolar to polar species about 1:2 the Type II mechanisms became predominant.

In Type I mechanisms a number of polar molecules cluster around each active site. Reactions proceed between a polar molecule adsorbed in such a cluster and a molecule from the solution phase. Propylene hydration occurs via reaction between an adsorbed water and solution phase propylene; IPA alkylation occurs between adsorbed IPA and solution phase propylene; and bimolecular IPA dehydration occurs between adsorbed IPA and solution phase IPA. In Type II mechanisms, the clusters of polar molecules around individual active sites are disrupted by the increased concentration of apolar species. Single polar molecules now hydrogen bond with multiple active sites. Reactions proceed between multiply hydrogen bonded polar species and solution phase species. As the reaction intermediates in Type II mechanisms are stabilised by additional active sites, these mechanisms are more catalytically active than the corresponding Type I mechanisms. The dependence of reaction rate on acid site density of the catalyst gives an indication of the number of active sites involved in each type of mechanism. It was found that propylene hydration via a Type I mechanism takes place on one active site and etherification (whether IPA alkylation or bimolecular IPA dehydration) takes place on 2 or 3 active sites at a pressure of 50 bar and a temperature of 120 °C.

In both types of mechanisms, the polar species adsorb onto the active sites far more strongly than the apolar species. Single component adsorption studies gave a Henry constant for water of 12000 compared to the Henry constant for propylene of 1400 at 60 °C. As long as there are sufficient polar species to saturate the active sites, practically all apolar species will be displaced from the active sites. Any side reactions involving only apolar species, e.g. propylene oligomerisation, are thus strongly inhibited by competitive adsorption.

The DIPE system contains highly polar water and IPA together with apolar DIPE and apolar propylene under supercritical conditions. The Peng-Robinson-Stryjek-Vera equation of state in conjunction with either the Wyczesany or the Wong-Sandler (WS) mixing rules was used to model the thermodynamic behaviour of this highly nonideal mixture. The binary interaction parameters of the Wyczesany mixing rule were obtained from literature; those of the Wong-Sandler mixing rule were regressed from binary vapour-

liquid equilibrium data from literature. It was found that the Wong-Sandler mixing rule correlated the phase behaviour of binary mixture of the components in the DIPE system considerably more accurately than the Wyczesany mixing rule. The Peng-Robinson-Stryjek-Vera equation of state together with the Wong-Sandler mixing rule (the WS-PRSV model) was thus chosen to predict the thermodynamic behaviour of the DIPE system. The accuracy of prediction of the WS-PRSV was verified by comparing multi-component predictions of the chemical equilibrium composition to experimentally obtained chemical equilibrium compositions.

It was decided to first study the effect of various system parameters on the individual reactions within the DIPE system before studying all three reactions combined. Consequently, the effect of system parameters on IPA synthesis from a feed of propylene and water in a 2 : 1 mole ratio and the synthesis of DIPE from a feed of propylene and IPA in a 1 : 1 ratio was studied. It was verified experimentally and through the use of various criteria that all experimental kinetic data was collected free of significant internal and external mass transfer effects, i.e. temperature and concentration gradients within the catalyst particles and within the catalyst bed were negligible. It could thus be assumed that reaction rates were controlled by kinetics only. In addition, all experimental runs with carbon balances with deviations greater than 5% were rejected.

The rates of propylene hydration and etherification showed a typical Arrhenius dependence on reaction temperature between 70 °C and 130 °C. Above 130 °C the propylene hydration reaction rate deviated from Arrhenius behaviour due to mass transfer limitations. Activation energies of 90.0 kJ mol^{-1} and 74.3 kJ mol^{-1} were determined for the hydration and the etherification reactions respectively. The rate of propylene hydration and etherification was markedly slower (approximately three orders of magnitude) than the reported rates of isobutylene or isoamylene hydration and etherification over the same catalyst at identical reaction conditions. This difference in rate is due to the difference in stability of the intermediate carbocations - the secondary carbocations in propylene chemistry being less stable than the tertiary carbocations which occur in isobutylene chemistry.

Increasing pressure increased both the rate of IPA formation and the rate of DIPE formation. In the case of IPA formation, reaction rate increased linearly with pressure due to a linear increase in the propylene activity between 15 bar and 70 bar. In DIPE formation, the reaction rate increased linearly from 15 bar to 30 bar. Above 30 bar the reaction rate increased with pressure to the third order. Between 15 bar and 30 bar the concentration of propylene in the liquid phase is low and the Type I mechanism predominates. The increase in etherification rate in this region is due to the increasing propylene activity with increasing pressure. Above 30 bar the concentration of propylene in the liquid phase is great enough to disrupt the Type I mechanism and the transition to a more catalytically active Type II mechanism begins to take place. In this region, the greater order with reaction pressure is thus due to a combination of increasing propylene activity and a change in the reaction mechanism.

The overall propylene to water ratio had little effect on the reaction rate. In the case of propylene hydration to form IPA, the reaction rate remained constant between propylene to water mole ratios of 1 : 5 and 10 : 1. Propylene oligomerisation only occurred at mole ratios greater than 10 : 1 due to poor interphase mixing. The rate of etherification increased with propylene to IPA mole ratios up to a ratio of 1 : 1, after which the reaction rate remained constant. At low mole ratios Type I reaction mechanisms dominated due to low liquid phase propylene concentrations. At mole ratios greater than 1 : 1, the liquid phase was saturated with propylene, Type II mechanisms dominated and no further change with propylene to IPA mole ratio was observed. At ratios of propylene to IPA greater than 6:1, oligomerisation of propylene once again took place due to poor interphase mixing.

Chemical reaction equilibrium composition of the DIPE system was measured experimentally at 100 °C, 120 °C and 140 °C at a pressure of 50 bar and an overall propylene to water ratio of 2 : 1; at 1 atm, 30 bar, 50 bar and 70 bar at 120 °C and an overall propylene to water ratio of 2 : 1 and at 1 atm and 50 bar at a temperature of 120 °C and an overall propylene to water mole ratio of 1 : 1. The chemical equilibrium product distribution obtained from experiment agreed well with the predicted product distribution using the

WS-PRSV model. At high pressure, in the liquid phase, the equilibrium distribution was a strong function of temperature and the overall propylene to water mole ratio only. The greatest equilibrium DIPE yield was obtained at the lowest reaction temperature.

The catalyst used for the majority of the experimental work in this study was Amberlyst 15. It showed no loss of activity over a period of three months on-line at a temperature of 120 °C. The same lifetime behaviour can be expected for Amberlyst 35 and Amberlyst 36 as they are almost identical in structure, differing only in acid site density and in the extent of cross-linking; the deactivation behaviour of zeolite H-Y and Deloxan ASP is not known. It is thus difficult to compare catalysts on the basis of lifetime or selectivity. Amberlyst 15, though, displayed the greatest activity per unit volume of catalyst bed under "process" conditions and any process design utilising this resin would thus result in the most economical reactor design. Amberlyst 35 and Amberlyst 36 are reported to be more thermally stable than Amberlyst 15. The lifetime of these catalysts may thus extend beyond that of Amberlyst 15 and, consequently, even though the initial reactor costs may be greater due to their lower activity, the catalyst replacement costs may be lower. No side reactions were observed on any of the tested catalysts.

Four kinetic models (a pseudo-homogeneous, two Eley-Rideal and the so-called "changing-mechanism" model) were examined for their ability to describe the DIPE system. Kinetic equations were formulated in terms of species activities rather than concentrations or partial pressures as the system was highly non-ideal. The species activities were calculated using the WS-PRSV model. The three parameter "changing-mechanism" model gave the best description of the DIPE system It is an empirical model based on the pseudo-homogeneous kinetic model, which incorporates an empirical term that changes the magnitude of the kinetic rate constant of each reaction to account for changes in the reaction mechanism from a Type I to a Type II, as the ratio of apolar to polar species changes. Even though it consistently overpredicted the initial reaction rates of all reactions by between 10% and 20%, this model was shown to qualitatively reproduce the behaviour of the DIPE system in response to changes in the operating pressure and the overall apolar to polar species mole ratio.

To overcome the poor kinetics of DIPE synthesis in comparison to those of MTBE or TAME synthesis, DIPE production should be performed at higher temperatures (100 – 120 °C) than in MTBE or TAME synthesis and at high pressures (> 30 bar). Unfortunately, whilst high temperature operation may favour DIPE production from a kinetic viewpoint, chemical equilibrium favours DIPE formation at low temperature. Furthermore, the maximum operating temperature is governed by the ion exchange resin catalyst which begins to deactivate by thermal decomposition at temperatures greater than 120 °C. Pressure increases both the formation rates of IPA and DIPE and, by solubilising additional propylene in the liquid phase, may force the system into the more active Type II mechanistic regime. Some of the equilibrium limitations inherent to DIPE synthesis at higher temperatures may be overcome by producing IPA in a first reactor and then using catalytic distillation to produce DIPE from the IPA. Alternatively, DIPE may be synthesised in a one-step or two-step fixed bed process.

Contents

List of Figures

List of Tables

Nomenclature

Abbreviations

A15	Amberlyst 15
A35	Amberlyst 35
A36	Amberlyst 36
CSTR	continuous stirred tank reactor
D-ASP	Degussa Deloxan ASP catalyst
DIPE	diisopropyl ether
ETBE	ethyl tert-butyl ether (tert-butyl ethyl ether)
FID	flame ionisation detector
GC	gas chromatograph
H-Y	zeolite Y in the hydrogen form
IG	ideal gas
IGM	ideal gas mixture
IPA	isopropanol (2-propanol)
LHSV	liquid hourly space velocity
MS	mass spectrometer
MTBE	methy tert-butyl ether (methyl t-butyl ether)
PR	Peng-Robinson
PRSV	Peng-Robinson-Stryjek-Vera
RVP	Reid vapour pressure

TAME	tertiary amyl methyl ether (methyl tert-pentyl ether)
TBA	tert-butyl alcohol
TCD	thermal conductivity detector
UNIFAC	UNIQUAC Functional group Activity Coefficient model
UNIQUAC	UNIversity QUAsi Chemical Activity Coefficient model
WHSV	weight hourly space velocity
WS	Wong-Sandler
WS-PRSV	PRSV equation of state with WS mixing rule
ID	inner diameter
MHSV	mass hourly space velocity
TAEE	tertiary amyl ethyl ether (ethyl tert-pentyl ether)

General

a	parameter in PR and PRSV equations of state
	parameter in Wagner equation
a_i	activity of species i
a_{mn}	functional group energy of interaction parameter
a_p	catalyst surface area per bed volume
A	parameter in PRSV equation of state
	kinetic pre-exponential factor
	parameter in Antoine equation
A^E	excess Helmholtz free energy
b	parameter in PR and PRSV equations of state
	parameter in Wagner equation
B	parameter in PRSV equation of state
	parameter in Antoine equation
c	parameter in Wagner equation
$c_1, c_2, \ldots$	constants
C	constant in Wong-Sandler mixing rule ($C = -0.623225$ for PRSV)

	parameter in Antoine equation
C_i	concentration of species i
$C_{m,i}$	catalyst saturation loading of species i
$calc$	calculated data point
C_p	heat capacity
d	parameter in Wagner equation
d_p	catalyst particle diameter
D_e	effective diffusivity
e_i	extent of reaction i
eq	equivalent, a mole of active sites
$error$	sum of relative square deviations
exp	experimental data point
E_a	activation energy
f	fraction of collisions with energy greater than E_a
f_i	fugacity of species i
f_e	wetting coefficient
F	total number of moles in system
Fr	Froude number
g	gravitational acceleration
	objective function in successive substitution algorithm
G	Gibbs free energy
	superficial mass velocity
H	enthalpy
H_i	Henry constant for component i
$\Delta H_{rxn,i}$	heat of reaction of reaction i
k	Boltzmann constant
	number of active sites involved in IPA dehydration mechanism
k_1	rate constant for propylene hydration

k_2	rate constant for IPA alkylation
k_3	rate constant for bimolecular IPA dehydration
k_{ij}	binary interaction parameter between species i and j
k_m	mechanistic acceleration parameter
k_r	kinetic rate constant
K_a	activity-based chemical equilibrium constant
K_c	concentration-based chemical equilibrium constant
K_i	species vapour-liquid equilibrium ratio
K_p	partial pressure-based chemical equilibrium constant
l	empirical parameter in UNIFAC activity coefficient model
L	total number of moles in liquid phase
$\mathfrak{M}$	total number of reactions occurring in system
m	number of active sites in IPA alkylation mechanism
m_{cat}	mass of catalyst
M	mass
	molecular weight
n	number of active sites in propylene hydration mechanism
	number of components in system
	number of functional groups
N	total moles in system
	total number of data points
N_D	number of adsorption data points
$ObjF$	objective function
p	partial pressure
P	pressure
P^{vap}	vapour pressure
q	measure of molecular van der Waals surface area
Q	functional group surface area parameter

r	reaction rate
r_1	rate of propylene hydration
r_2	rate of IPA alkylation
r_3	rate of bimolecular IPA dehydration
r_i	measure of molecular van der Waals volume of species i
	radius of molecule i
r_{obs}	observed rate of reaction
R_i	functional group volume parameter
R	universal gas constant
R_1	ratio of transition from Type I to Type II mechanism
R_2	ratio of transition from Type II to Type III mechanism
Re	Reynolds number
S	entropy
$SSRR$	sum of squared relative residuals
t	time
T	temperature
u	superficial velocity
$v_k^{(i)}$	number of functional groups of type k in molecule i
V	volume
	total number of moles in vapour phase
We	Weber number
x	species mole fraction
X	mole fraction of functional group in relevant phase
y	species mole fraction in vapour phase
z	empirical parameter in UNIFAC model (z=10)
	species mole fraction in total system
Z	compressibility
Z_{ij}	frequency of collision between molecules of species i and j

Greek

α	parameter in PR and PRSV equations of state
	NRTL excess Helmholtz free energy parameter
α_i	arbitrary independent variable
γ	liquid phase activity coefficient
ϵ	catalyst bed void fraction
κ	parameter in PR and PRSV equations of state
κ_o	pure component parameter in PRSV equation of state
κ_1	pure component parameter in PRSV equation of state
λ	thermal conductivity
μ	viscosity
ρ	density
ω	accentric factor
ϕ	fugacity coefficient
ν	stoichiometric coefficient
σ	surface tension
	standard deviation
τ	NRTL excess Helmholtz free energy parameter
	parameter in Wagner equation ($\tau = 1 - T_r$)
Φ	segment fraction
θ	area fraction
Δ	change in property
Γ	group residual activity coefficient
Ω	arbitrary dependent variable
Θ	functional group area fraction

Ψ_{km}	functional group interaction parameter between groups k and m
Φ	Weisz-Prater modulus

Superscripts

$\alpha, \beta, \gamma, ...$	exponents in power rate law
C	combinatorial
calc	calculated property
exp	experimental property
$I, II, III, ...$	phase number
IG	ideal gas
IGM	ideal gas mixture
IM	ideal mixture
k	iteration index
L	liquid
old	previous iteration value
new	current iteration value
R	residual
theo	theoretical property
V	vapour
vap	vapour pressure / saturation pressure
$\bullet$	pure component property
$*$	partial property
^{o}	standard property
$\bar{}$	molar property
$\vec{}$	vector property

Subscripts

$1, 2, 3, ...$	species index
ads	adsorption property
$bulk$	bulk phase property
bp	boiling point
c	critical property
cat	catalyst property
eqm	equilibrium property
f	fluid phase within catalyst
i	i^{th} species
	i^{th} data point
j	j^{th} species
k	functional group number
L	liquid phase
m	m^{th} functional group number
mix	mixture property
p	catalyst pellet property
rxn	reaction property
R	reduced property, e.g. $T_R = \frac{T}{T_c}$
s	surface
tot	total system property

Publications to date

Journal publications

F. Heese, M.E. Dry and K.P. Möller. **The reaction pathway and rate acceleration in the single stage synthesis of diisopropyl ether (DIPE) from propylene and water.** Accepted by *Catalysis Today*, 1998.

Conference presentations (oral)

F. Heese, M.E. Dry and K.P. Möller. **Diisopropyl ether - An alternative octane enhancer for lead-free petrol.** *1st Conference of the Indo-Pacific Catalysis Association*, Cape Town, South Africa, 1998.

F. Heese, M.E. Dry and K.P. Möller. **Single stage production of diisopropyl ether from propylene and water.** *AIChE Annual Meeting*, Los Angeles, United States of America, 1997.

F. Heese, M.E. Dry and K.P. Möller. **Diisopropyl ether - an exciting alternative octane enhancer for lead-free petrol.** *8th National Meeting of the South African Institute of Chemical Engineers*, Cape Town, South Africa, 1997.

F. Heese, M.E. Dry and K.P. Möller. **Single stage synthesis of diisopropyl ether from water and propylene.** *National Conference on Catalysis - Catalysis Society of South Africa*, Midrand, South Africa, 1996.

Conference presentations (poster)

F. Heese and M.E. Dry. **Single stage diisopropyl ether synthesis**. *Chemical Engineering R & D - South African Institute of Chemical Engineers*, Cape Town, South Africa, 1995.

Chapter 1

Introduction

1.1 Background

Increasing concerns regarding urban air pollution caused by automobile exhaust emissions have made it necessary to develop strategies designed to improve local air quality. The approaches taken include the development of novel fuels and novel fuel technologies, modifications to existing automotive engine technology and changes in the physical make-up of modern fuels.

Considerable effort has been expended on the development of novel fuels and fuel technologies to cater for the transportation needs of the future [1]. A multitude of options have been considered, including liquefied petroleum gas, fuel cells, compressed natural gas, solar energy, electrically powered vehicles, biofuels and hydrogen. Even though great strides have been made and novel fuel technologies are seeing applications in certain niche markets, in the foreseeable future the gasoline-based internal combustion engine will remain the dominant technology.

Improvements in the exhaust emissions of gasoline-powered vehicles have taken one of two major routes over the past three decades: an improvement in automobile fuel economy and a post-combustion clean-up of exhaust gases. The most obvious method to

reduce exhaust emissions is through greater fuel economy - quite simply, decreased fuel usage translates directly to decreased exhaust emissions. Following the oil crises of the 1970's and the governmental regulations stemming from them, there has been a dramatic improvement in automotive fuel efficiency, see Figure 1.1 [2]. However, in recent years fuel economy has once again worsened and is expected to decrease even further as the current world-wide trend towards larger utility vehicles continues.

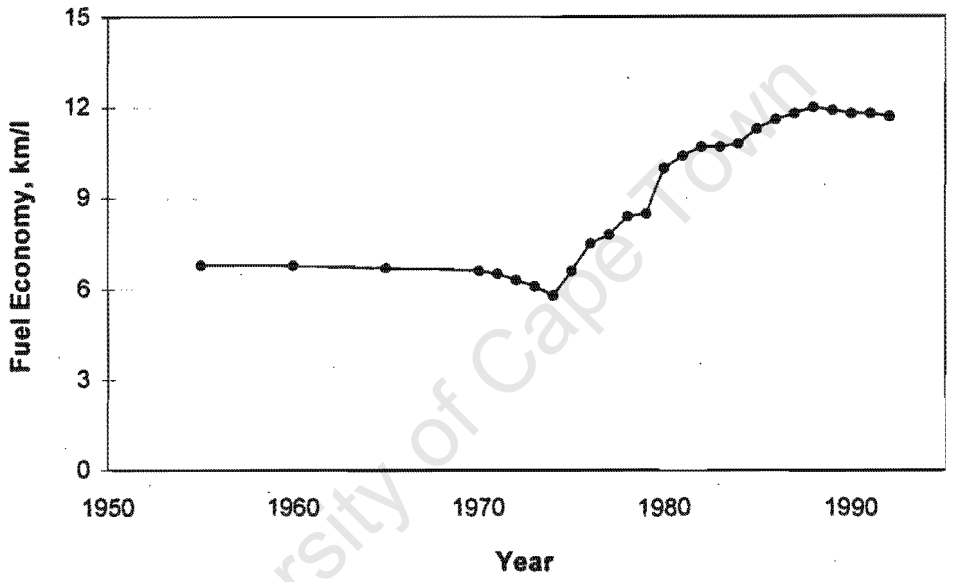

Figure 1.1: Average fuel economy of new automobiles

The cornerstone of emission control, though, has been the post-combustion clean-up of exhaust gases. This has been achieved using the three-way catalytic converter, so-called since it destroys three of the major harmful emission products: carbon monoxide (CO), nitrous oxides (NO_x) and unburnt hydrocarbons (HC). Installation of a catalytic converter typically reduces automobile emissions of these gases by at least 80% to 90% [2]. In the western world, over 80% of all automobiles are now equipped with catalytic converters.

Whilst a substantial effort has been made to improve existing combustion technology

and to develop novel fuel technology, scant attention has been paid to the formulation of common automobile fuel. Only recently, has an awareness of the impact of the proper tailoring of fuel composition evolved. This heightened awareness could not have come at a more crucial time. No innovations in combustion technology have taken place over the last few years, most motor vehicles are now equipped with catalytic converters and no improvements are taking place in fuel efficiency. Any combustion technological improvements that are made now, will only result in apparent changes once the existing motor vehicle fleet has been substantially replaced; a time period accepted to approach ten years [1]. Novel fuels and associated technologies, will, for the same reason, take at least as long to show any benefit. Consequently, negligible air quality improvements will result from these sources in the near future. On the other hand, beneficial changes in composition of the current fuels can be expected to have an impact almost immediately.

Studies have shown clearly that fuel composition significantly affects exhaust emissions. Some of the findings of the Auto/Oil Air Quality Improvement Research Program (AQIRP), a joint, comprehensive study by automobile and petroleum companies undertaken in 1989, are shown in Table 1.1 [1, 2, 3].

Beneficial changes in exhaust emissions can be achieved by decreasing the olefin and aromatic content of fuels and blending oxygenates such as methyl tert-butyl ether (MTBE) into fuel. Interestingly, reductions in the sulphur content of fuel not only affect sulphur dioxide emissions, but also result in decreases in HC, CO and NO_x emissions. Reducing the Reid vapour pressure (the vapour pressure at 38°C, RVP) and the T_{90} (the temperature at which 90% of the fuel evaporates) of a fuel also lowers harmful emissions. A number of these changes do result in increased emissions of certain targeted toxic species (formaldehyde and acetaldehyde), but substantial reductions of these can be attained by using a catalytic converter. The formation of ozone, not strictly speaking an exhaust emission but caused by the interaction of NO_x and HC emissions in the presence of sunlight, can be reduced by lowering the RVP, the T_{90} and the olefin content of fuel.

Table 1.1: Effect of fuel composition change on automobile exhaust emmissions

	Change		Change in exhaust emissions, %				
Fuel parameter	from	to	HC	CO	NO_x	ozone	toxics*
aromatics, %	45	25	−6.5	−13.3	=	=	− = ++
MTBE, %	0	15	−5.5	−11.1	=	=	== + =
olefins, %	20	5	+5.8	=	−6.1	−10	= − ==
T_{90}, °C	182	138	−21.7	=	+4.9	−10	− − −−
sulphur, ppm	450	50	−16.1	−12.9	−9.0	*na*	*na*
RVP, kPa	60	53	−4.5	−9.1	=	−	*na*

* Benzene, butadiene, formaldehyde, acetaldehyde, in this order

Note: = : no statistically relevant change

− : decrease

+ : increase

na : no available data

Based on findings such as these, legislation and quality standards have been introduced in a number of countries to regulate the composition of automobile fuel. Best known are the 1990 Amendments to the US Clean Air Act of 1970 (CAA) and the "Cahier des Charges Qualité des Constructeurs Français" guidelines (CCQCF) from France. The main points to emerge were:

- minimum fuel oxygen contents,
- limitations on aromatics and olefin levels,
- sulphur content restrictions and
- maximum RVP specifications.

Probably the most important feature of a fuel is its octane number. This number represents the combustion characteristics of a fuel; essentially, the higher the octane number the more controlled a fuel's burning. Prior to the introduction of the catalytic converter,

heavy-metal octane enhancers such as tetraethyl lead (TEL) or methylcyclopentadienyl-manganese tricarbonyl (MMT) were blended into fuel to increase the octane number. However, even small amounts of the heavy metals contained in TEL or MMT permanently poisoned the catalytic converter and hence alternative methods to increase the octane number had to be found. This was done by a combination of:

1. alkylation of light olefins (e.g. propylene and isobutene) with isobutane,
2. alkylation of aromatics (e.g. benzene) with light olefins,
3. dimerisation of light olefins to produce polygasoline and
4. oxygenation of fuel by blending in alcohols and ethers.

However, the introduction of legislation such as the CAA or the CCQCF has sparked renewed debate as to precisely which octane enhancement strategy to follow.

1.2 Alternative octane enhancement strategies

In the US market, currently almost 30% of all fuel sold falls within the guidelines of the CAA [4], so-called reformulated gasoline. This fraction is expected to increase to 70% by the year 2000 [2]. With specifically the aromatic and to a lesser extent the olefinic content of fuel being restricted by legislation, alkylation and oxygenation are going to become increasingly important in the octane enhancing strategy of the refiner.

Additional octane enhancing blending agents have to be found to take the place of aromatics and olefinic oligomers. While it is not economical to transform the linear alkanes in the gasoline pool to higher octane product, there are sufficient reactive olefins available from the FCC unit on the refinery to satisfy both octane and oxygenate demand. Presently, most C_3 and C_4 olefins are removed from the gasoline pool and re-enter it as

alkylate, oxygenate or polygasoline product. In spite of the removal of the C_3 and C_4 fractions, a significant portion of gasoline is still olefinic though, see Figure 1.2 [3, 5].

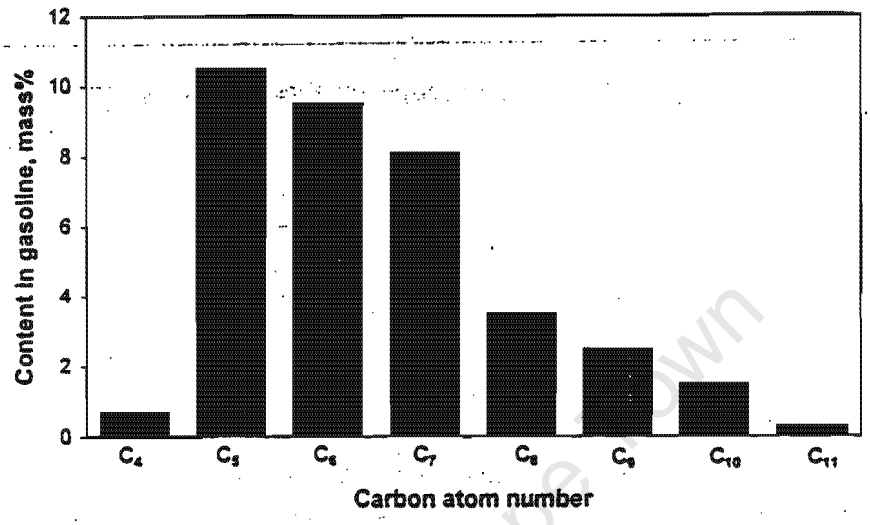

Figure 1.2: The olefin content of typical FCC gasoline - by carbon number.

Currently most of the C_5 and C_6 olefins that are produced in the FCC units are left in the gasoline pool. One of the solutions to further increase octane numbers and reduce the RVP of fuel is to reduce the quantity (typically about 20% by mass of gasoline) of this low octane, high RVP olefinic product and to exchange it for high octane, low RVP alkylate, i.e. also utilise the C_5 and heavier olefin fractions for alkylation [3, 6].

Alkylate, however, does not contain any oxygen, a requirement under new legislation, and thus oxygenated blending agents also have to be used [7]. The oxygenates which have shown the most promise as octane enhancing agents are alcohols and ethers. The production of ethers and alcohols other than methanol and ethanol competes for the same light olefins used in the alkylation processes, i.e. the C_3 to C_5 olefins. Any oxygenate blending agent would thus also have to fulfil an octane enhancing role. The properties of currently used oxygenates, alkylate products and polymeric product are shown in Table 1.2 [3, 6, 8, 9, 10, 11, 12].

Table 1.2: Properties of common octane enhancing agents

Octane enhancer	Octane number $\frac{1}{2}(RON + MON)^*$	Blending RVP kPa	O_2 content $mass\%$	Water solubility
Alkylate				
propylene	89	28	0	low
isobutylene	97	7	0	low
Dimers				
propylene	90	28	0	low
isobutylene	101	7	0	low
Alcohols				
methanol	120	414	50	high
ethanol	114	124	35	high
IPA	109	97	27	high
t-butyl alcohol	100	69	22	high
Ethers				
MTBE	109	56	18	low
ETBE	110	28	16	low
TAME	105	14	16	low
DIPE	105	28	16	low

* RON Research octane number
MON Motor octane number

Alcohols, whilst having higher octane numbers and being less expensive to produce than ethers, have the disadvantage that they have a high blending Reid vapour pressure and are highly water soluble. Furthermore, their use tends to result in greater NO_x emissions and increased engine corrosion [2]. Ethers on the other hand have shown excellent combustion properties, have very low water solubility and do not affect automobile driveability [12, 13]. Initial fears that explosive peroxides could form have been eliminated with the inclusion of small amounts of inhibitors which prevent ether decomposition without affecting exhaust emissions [10]. Also, ethers are considered to be non-toxic [10], though some equivocal evidence of carcinogenicity has recently emerged from animal studies [14].

Consequently, the oxygenate of choice has been an ether, methyl tert-butyl ether (MTBE). It has been blended into fuel as an oxygenating and octane enhancing agent in contents as high as 15% [13]. The production of MTBE has increased dramatically since the first commercial plant, with a capacity of 60000 tons/year, was built in Italy in 1973. By the year 2000, MTBE production is expected to exceed $30 \cdot 10^6$ tons/year [13].

All the current industrially significant ethers are based on the reaction of C_1 to C_3 alcohols with C_4 or C_5 tertiary olefins over ion-exchange resins at moderate temperatures and pressures. Of the 120 etherification plants in commercial operation at the end of 1996, 91 were based on catalytic distillation, see Figure 1.3, and the remainder on fixed-bed technology [15, 16], see Figure 1.4. Incidentally, MTBE production was the first commercial application of catalytic distillation [17], where conversions of isobutylene and selectivities to MTBE greater than 99% are realised [13].

In recent years, MTBE production has had the upper hand due to the low cost of methanol and the availability of isobutylene [10, 12]. Process improvements have, however, allowed other tertiary ethers such as ethyl tert-butyl ether (ETBE) and tertiary amyl methyl ether (TAME) to compete economically with MTBE.

The primary refinery source of the C_4 and C_5 olefins is the FCC unit and, while it is possible to increase the amount of these olefins produced by changing operating conditions and using a different catalyst, it is unlikely that the full olefin demand for etherification needs will be met in the near future [3, 5]. Consequently, interest is increasingly turning to the conversion of even heavier olefins (C_6 or C_7) to ethers, e.g. the NExTAME process [18]. However, if one considers that propylene constitutes the largest light olefin fraction produced in an FCC unit and that currently almost half of all propylene is used to make either propylene alkylate or polygasoline [9], one could also consider the option of producing diisopropyl ether (DIPE) from propylene and water.

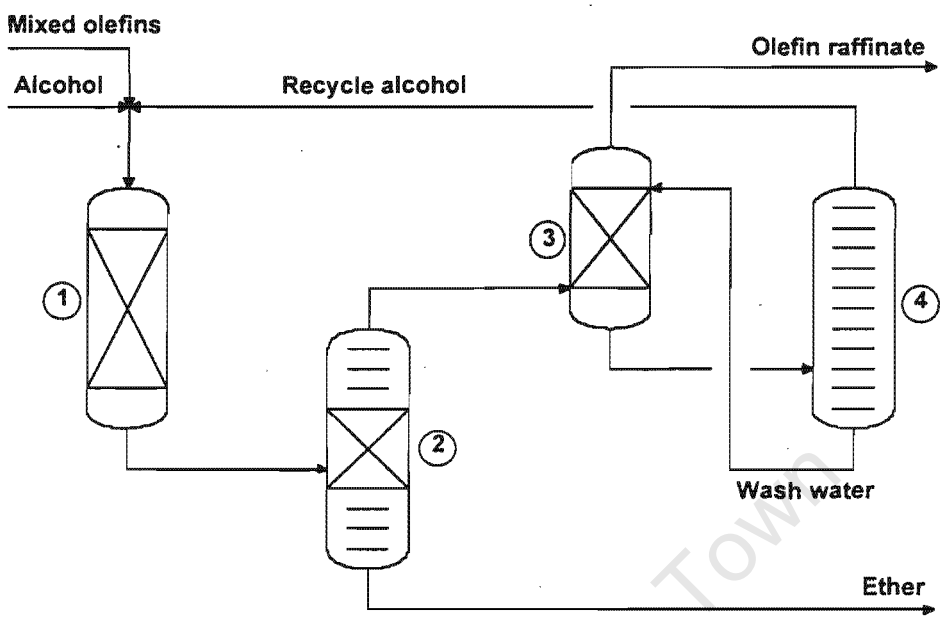

Figure 1.3: Commercial catalytic distillation process for the production of octane enhancing ethers. (1) boiling-point reactor, (2) catalytic distillation column, (3) alcohol extraction column and (4) alcohol and water recovery column.

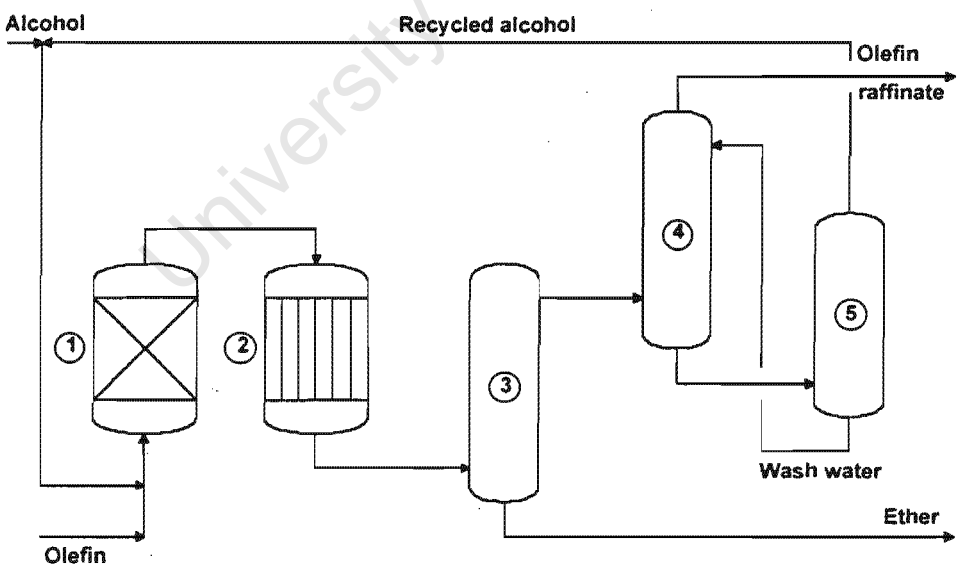

Figure 1.4: Commercial fixed-bed process for the production of octane enhancing ethers. (1) Adiabatic reactor, (2) isothermal tubular reactor, (3) ether extraction column, (4) alcohol removal tower and (5) alcohol-water fractionator.

1.3 DIPE synthesis

As the major by-product of isopropanol (IPA) manufacture, excess DIPE has been used in fuel in limited quantities for many years [10, 19]. Large-scale production of DIPE specifically for fuel oxygenation, however, necessarily means either diverting propylene from some other use or generating additional propylene.

World-wide propylene production reached 40 million metric tons in 1996. Of this, 70% was derived as a by-product of ethylene production, refineries contributed an additional 28% and propane dehydrogenation accounted for the remaining 2% [20]. Overall, 48% of propylene was consumed in polypropylene synthesis and only 4% found its way into fuel. Propylene utilisation in a refinery, however, differed significantly from this pattern, see Figure 1.5 [2, 9, 20, 21].

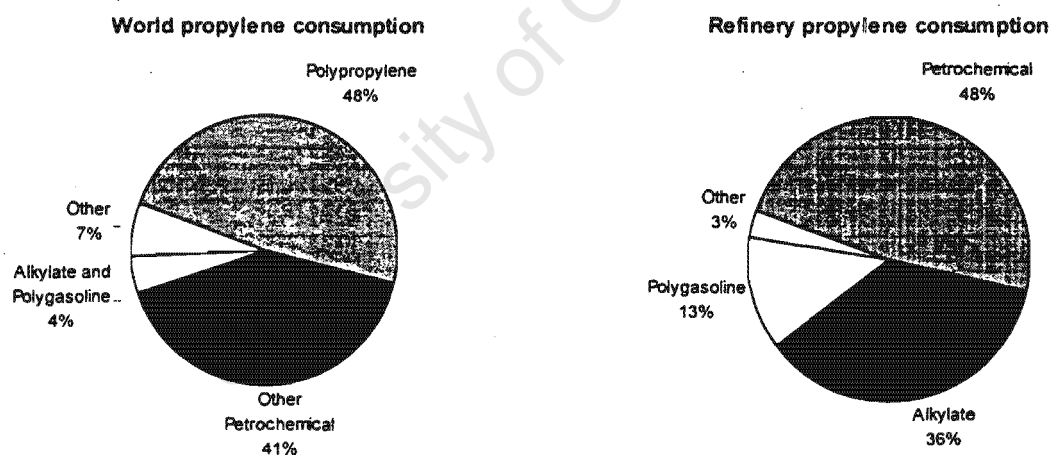

Figure 1.5: Comparison of propylene consumption: world-wide and on the refinery

In the typical US refinery 49% of propylene produced found its way into fuel as either polygasoline or alkylate whilst 48% was put to petrochemical use. A large portion of refinery propylene thus finds its way back into the fuel pool. Compared to the dimers and alkylation products of isobutylene and isoamylene, see Figure 1.6, the products of

propylene have poor fuel blending properties [6, 8, 11]. Propylene makes the lowest octane alkylate product and consumes the largest amount of isobutane per barrel of fuel alkylate. Propylene dimer also has the lowest octane number and has a significantly higher RVP in comparison to the dimers of isobutylene and isoamylene. The advantages of DIPE production over propylene alkylate or propylene dimer production are three-fold: firstly, DIPE has superior fuel blending properties, see Table 1.2, secondly, it contributes to the fuel oxygen pool and, thirdly, its production does not require isobutane. Accordingly, it would be advantageous to free alkylation and dimerisation capacity for isobutylene and/or isoamylene by redirecting propylene to DIPE production [10].

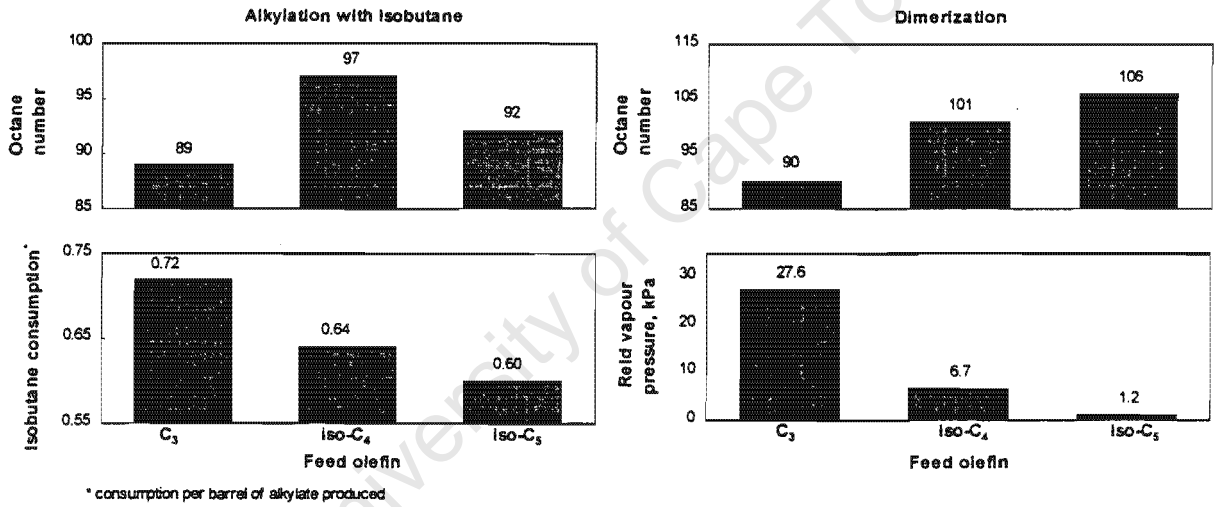

Figure 1.6: Properties of alkylate and dimeric product derived from light olefins

Extensive tests have shown DIPE to have similar emission, combustion and driveability properties to the other ethers [8, 9, 10, 11]. In addition, DIPE has the advantage that it can be produced directly from water and propylene, not requiring the purchase of alcohol from an external source as for the other ethers. Its production is thus not subject to fluctuations in alcohol prices and it can be made entirely in-house. In addition, as mentioned previously, if current trends continue, the demand for isobutylene and isoamylene to produce ETBE, MTBE and TAME will outstrip the supply of these olefins

in the near future [3, 5]. The expected oxygenate shortfall can be made up with DIPE production, since no such shortages are to be expected with propylene.

Large-scale DIPE production is a novel process. It has thus far only been produced as a by-product of IPA manufacture [10, 11, 19, 22, 23, 24, 25]. Indeed, the first licensed DIPE process was simply an extension of existing propylene hydration technology [26], see Figure 1.7. In the first reactor the IPA intermediate was synthesised from propylene and water and then, in a second reactor, DIPE was produced from propylene and IPA.

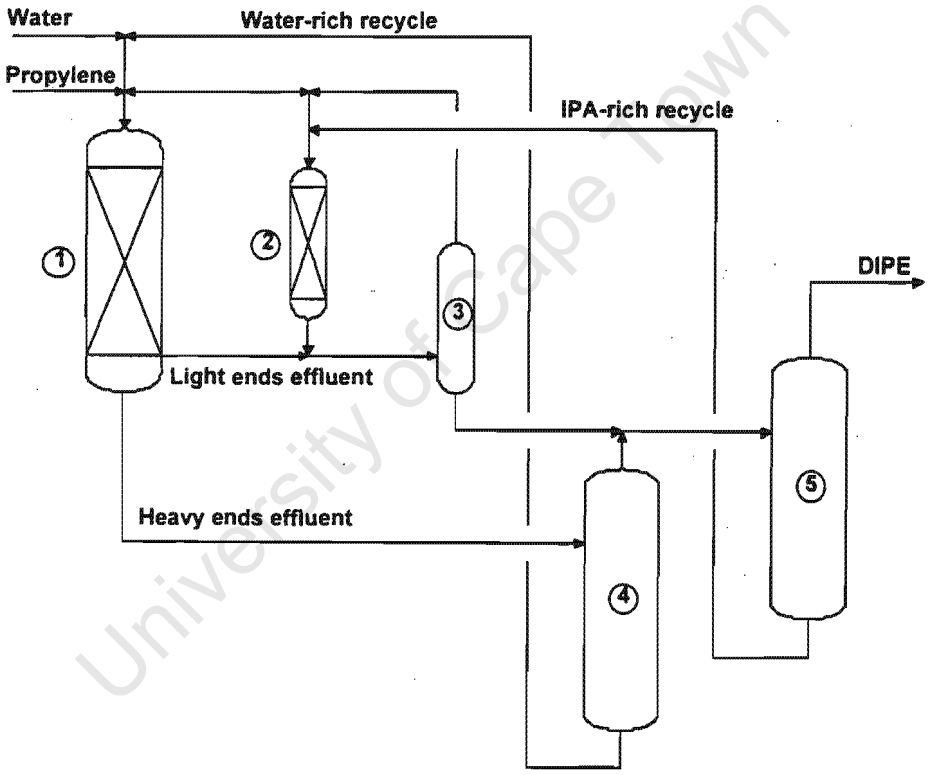

Figure 1.7: Two-stage DIPE process. (1) IPA reactor, (2) DIPE reactor, (3) light ends recovery, (4) azeotrope column and (5) DIPE-IPA splitter

In recent years, though, a number of companies such as UOP, Mobil and Texaco have licensed more economical DIPE processes (processes practically identical to those used for production of the other ethers), where the hydration and etherification reactions take place within a single reactor [27], within two reactors [28, 29] or which utilise catalytic

distillation technology [26]. The feed to most of these processes is simply propylene and water, though Texaco does offer processes using hydrogen and excess acetone from phenol synthesis as the reactants [30, 31]. The first large-scale DIPE plant, based on the single-stage UOP process, was expected to be commissioned in 1998.

With the exception of the acetone hydrogenation process which uses zeolites in the etherification step, all other processes utilise ion-exchange resin catalysts and operate at high pressures and low temperatures. Selectivities to DIPE are typically greater than 98% [8, 9]. Aside from IPA, the major by-products are the oligomers of propylene, though these can virtually be eliminated by judicious choice of operating conditions.

Currently, though, economics do not favour DIPE synthesis. Based on 1996 methanol prices, the cost of MTBE production has been variously quoted as lying between 0.72 \$/gallon and 0.84 \$/gallon [8, 4]. In comparison, an economic analysis of the one-stage DIPE process of UOP predicted DIPE production costs of 0.98 \$/gallon [8, 19], 17% to 36% more expensive. The cost of DIPE production is not expected to become cheaper than the other ethers unless there are dramatic methanol or ethanol price increases. Furthermore, in many markets, e.g. the European and Japanese, propylene is in short supply, practically the entire production being consumed by the petrochemical industry. In this scenario, DIPE production is not feasible. However, economically its production does become advantageous where propylene is used to produce polygasoline or alkylate, where alkylation capacity is limited and where isobutane or MTBE prices are high.

One such region is the South African market. To comply with changing overseas technology requirements, South Africa introduced lead-free gasoline in 1995. Currently, MTBE is being imported to satisfy the oxygenate demand, but as the demand for unleaded fuel grows, it will become more economical to erect local etherification plants. The Fischer-Tropsch process produces large amounts of propylene, most of which is returned into the fuel pool as alkylate or polygasoline. It would thus make sense to utilise this abundance of propylene for DIPE production, especially since there is a scarcity of the tertiary C_4

and C_5 olefins and a limited supply of methanol.

Unless there are dramatic improvements in DIPE production costs, it is unlikely to become a world-scale chemical and rival MTBE as an oxygenate and octane enhancer. Rather, it could find a niche in localised production where it could be used in concert with the other ethers for fuel oxygenation.

1.4 Objectives of research

Ultimately, the aim of any catalytic industrial process is to produce the desired product as efficiently as possible. This not only involves maximising the catalytic activity but also the selectivity to the desired product. In order to achieve this goal a comprehensive understanding is required of each and every step in the reaction process. This involves not only a knowledge of the effect of process parameters, but also an understanding of the thermodynamics, the mechanisms and the kinetics of the system.

In spite of the increased industrial attention DIPE has received recently, limited data on the process parameters, kinetics and thermodynamics have been published in the open literature. The objective of this study was thus to investigate the single-stage behaviour of DIPE synthesis from a feed of propylene and water, where both the hydration reaction to form IPA and the etherification reaction to form DIPE take place within the same reactor over an acidic ion exchange resin catalyst, Amberlyst 15. The following factors will be examined in greater detail:

- A thermodynamic analysis of the DIPE system focussing in particular on the chemical and phase equilibrium behaviour.
- The effect of process parameters on DIPE synthesis with a view to determining the optimal synthesis conditions.

- The mechanism of DIPE synthesis over an ion-exchange resin catalyst.
- The kinetics of DIPE synthesis over an ion-exchange resin catalyst.
- Formulation of an all-encompassing reactor model, that incorporates the phase, mechanistic and kinetic behaviour of the system.

Chapter 2

Thermodynamics of DIPE synthesis

2.1 Introduction

2.1.1 Phase equilibrium thermodynamics

When modelling any system in which phase separation occurs, it is important to have an accurate method of calculating the amount of each phase present and the concentrations of each component in every phase

The most accurate method to determine the phase or vapour-liquid behaviour of a system is from experimental data measured at the temperature and pressure in question. However, measurement of vapour-liquid equilibria generally requires highly sophisticated equipment, making this approach unfeasible for the majority of projects and necessitating the use of literature data. Failing literature data, the remaining option is to predict phase equilibrium. Since minimal multicomponent vapour-liquid data are available, prediction of such equilibria should preferentially be based upon binary mixing data of the species in the system which, through the use of applicable models, is extended to the multicomponent system at the conditions of interest.

It will be shown in Chapter 3, that the octane enhancer DIPE can be synthesised

at high pressure (20 - 100 bar) and moderate temperature (80 - 140°C) from water and propylene via the intermediate IPA. The DIPE system is a quaternary system containing: water, propylene, the intermediate IPA and the desired product DIPE. These four compounds form a highly non-ideal system covering a range of polarities from apolar propylene to highly polar water; propylene is super-critical at temperatures above 92°C and water is only partially miscible with both propylene and DIPE.

This system can form up to three fluid phases - a vapour phase, an aqueous liquid phase and a hydrocarbon-rich liquid phase. Due to a lack of experimental multicomponent data, determination of phase equilibrium in the DIPE system has to be predicted by models based on binary vapour-liquid equilibrium data. A judicious choice of such a thermodynamic model is required to extend the binary experimental data to the multicomponent system at the temperature and pressure under consideration.

Considering the amount of interest shown in tertiary ethers as octane enhancers in recent years, it is surprising that almost no information on the vapour-liquid behaviour of these systems has been published. But, since all the traditional ethers are synthesised either in a purely vapour environment at low pressure, or at high pressure in a completely liquid environment, the problem of phase separation never occurred. Those authors who have considered thermodynamic non-idealities in their systems, have only considered the non-ideal liquid-phase behaviour of ether synthesis and have modelled this with correlations such as UNIFAC or UNIQUAC [32, 33, 34, 35]. In none of these studies was a vapour phase present in the system.

One of the few authors to have considered the issue of vapour-liquid phase equilibrium in an olefin-water-alcohol-ether system was Cope [36]. Whilst the predictions of chemical equilibrium from the model proposed by the author have proven to be fairly accurate, the method of determining phase equilibrium is not overly useful for determining the liquid-phase composition, since it was assumed that the concentration of olefin in the liquid phase was negligible.

An improved method of predicting phase equilibrium thus had to be found. It is especially important to utilise a model which can accurately represent the system at its least ideal state, i.e. being able to predict the phase compositions of the highly asymmetric water-propylene mixture. The modern approach to solving problems of this nature is through an equation of state which can represent the pure components accurately. To compensate for mixture non-idealities use is made of so-called mixing rules, which usually contain empirical mixing parameters obtained from the regression of binary experimental data.

Many authors have tackled the water-light hydrocarbon problem and a variety of mixing models have been proposed to correlate these. Two of the more recently developed, for example, are those of Carroll and Mather [37] and Economou and Tsonopoulos [38] which deal mainly with water-alkane systems. These types of models are, however, typically only specific to a certain system and are thus not ordinarily applicable to systems different from the ones for which they were developed. Possibly less accurate, but more useful, are general mixing rules such as the ones of Wyczesany [39] and Wong and Sandler [40] which apply to practically any given system.

Wyczesany [39] modelled the vapour-liquid behaviour of the water-propane-propylene-IPA system. A novel mixing rule was proposed, which was to be used with the Peng-Robinson-Stryjek-Vera (PRSV) equation of state [41, 42]. This model appeared to correlate the difficult water-propylene and water-IPA systems. Unfortunately, DIPE was not included in the study, nor was the extrapolation ability of the mixing rule to different temperatures and pressures shown. In 1992 Wong and Sandler [40] introduced a theoretically correct mixing rule which has since been shown [43] to be able to correlate even highly non-ideal systems over large ranges of temperature and pressure. However, its ability to model the difficult water-propylene system has yet to be demonstrated.

The four compounds in the DIPE system form six binary mixtures: water-propylene, water-IPA, water-DIPE, propylene-IPA, propylene-DIPE and IPA-DIPE. For two of these

binaries (water-propylene and water-IPA) experimental data has been published at the reaction conditions for DIPE synthesis of 80 to 140 °C and 20 to 100 bar. For three of the remaining binaries experimental data has only been published at a pressure of 1 atm whilst for the propylene-DIPE system, no experimental data has been published at all. For the three binaries in the DIPE system measured at atmospheric pressure, one thus has to make use of a mixing rule and an applicable equation of state capable of extrapolating the data from the conditions at which they were measured to the conditions at which the reactions occurred. The only option for the calculation of the remaining binary is to predict the phase equilibrium.

Predicting phase equilibrium for many mixtures remains problematic. However, predictive liquid-phase activity coefficient models such as UNIFAC have been shown to be accurate when dealing with nonpolar systems of hydrocarbons [44, 45] at low pressure. Fortunately, the propylene-DIPE binary consists of the two least polar compounds, i.e. one can expect it to be the most ideal of the six binaries. At low pressure and temperatures below the critical temperature of propylene, UNIFAC should thus be able to give a reasonably good representation of the liquid mixing behaviour. At these conditions the vapour phase can be considered practically ideal. This allows the calculation of low pressure "pseudo-experimental" data from which mixing parameters can be regressed. As in the case of the three binaries measured at atmospheric pressure, as applicable mixing still has to be used to extrapolate this "data" to high pressure and temperature.

Under the experimental conditions reviewed in this project, the liquid-liquid phase split was never observed to occur - IPA acted as a mutual solvent - and so, to simplify the modelling, the phase equilibrium problem was treated solely as a vapour-liquid one instead of a vapour-liquid-liquid one. The multicomponent phase equilibrium of the DIPE system will be modelled by one of three models. The mixing rules of Wyczesany [39] and Wong and Sandler [40, 43] together with an applicable equation of state such as PRSV [41] will be examined for their ability to fit pure and binary experimental data and to extrapolate

them to reaction conditions. Also, the UNIFAC activity coefficient correlation will be used to predict the propylene-DIPE binary for which no literature data is available.

2.1.2 Simultaneous chemical reaction and phase equilibrium in the DIPE system

When a system is at chemical equilibrium, every reaction taking place within the system must itself be at equilibrium. In the DIPE system the major reactions are the hydration of propylene and the subsequent etherification of IPA to form the title ether. Chemical reaction equilibrium in this system can consequently be classified broadly into hydration equilibrium and etherification equilibrium. The former having been studied extensively by a number of authors, whilst practically no information is available for the latter.

2.1.2.1 Propylene hydration

Some of the earliest work undertaken in the study of propylene hydration was that of Majewski and Marek [46]. Extensive liquid- and vapour-phase reaction equilibrium measurements were performed at temperatures between 160°C and 290°C and pressures from 95 to 503 bar. This was followed by a thermodynamic analysis of the reaction. The principal reaction was that between propylene and water to form IPA. As one would expect from an exothermic reaction accompanied by a contraction in the number of moles, it was found that high pressures and low temperatures favoured IPA yields. Limited amounts of side-reactions were reported: at temperatures below 210 °C the major by-product was DIPE and above 210 °C the dominant side reaction was propylene oligomerisation. The authors were unable to quantitatively assess the extent to which these side reactions had occurred. In spite of the significant scatter which is evident in the data and the occurrence of the abovementioned side reactions, the authors were still able to correlate the equilibrium constants and calculate the free energy change for the liquid phase reaction. Unfortunately, the equilibrium data was reported in terms of the liquid-phase

concentration-based equilibrium constant, K_c, which makes further use and extrapolation to different systems difficult without extensive recalculations using thermodynamic models such as those being investigated in this study.

Petrus et al. [47] also reported chemical equilibrium for propylene hydration data in terms of a concentration-based equilibrium coefficient. In this case chemical equilibrium was measured in a highly dilute aqueous phase at a pressure of 90 bar and temperatures between 100°C and 140°C. The equilibrium constants were thus reported independent of the water concentration, which being in large excess, was considered to be constant. Once again, it is difficult use this data without extensive recalculation.

A number of authors [22, 48, 49] have reported propylene hydration chemical equilibrium measurements in terms of the fractional conversion of propylene at a given temperature and pressure. However, since neither phase compositions nor initial concentrations are stated it is not possible to determine the equilibrium constant. Without this knowledge, this data is essentially unusable.

In his review on hydration and hydrolysis reactions by solid acids, Izumi [50] gives an empirical correlation of the partial pressure based equilibrium constant, K_p, for propylene hydration which was obtained from regression of the experimental equilibrium data of Stanley et al. [51] and Schiffler et al. [52]. It is important to note, that whilst no range of applicability is given for the correlation, extrapolation outside of the measured ranges by empirical correlations can be highly inaccurate and should be avoided. In this case, the "safe" range can be assumed to be 115°C to 275°C.

In light of all the above experimental measurements, extrapolation and especially prediction still remain a problem. This is particularly so, since a variety of different equilibrium constants are used to report data. One study which attempted a predictive calculation of chemical equilibrium was that of Cope. [53].

Cope and co-workers [36, 53, 54] performed extensive thermodynamic measurements

and predictive calculations in the hydration of the lower olefins. In the first paper of the series [53] two important points emerged:

1. When measuring hydration equilibrium it is vital to include the possibility of ether formation. If it cannot be shown conclusively that ether formation is not a factor and this is then not factored into the calculations, any equilibrium data must be seriously questioned.

2. The large mixing non-idealities in the olefin-water-alcohol system cause significant errors when predicting chemical equilibrium by conventional predictive mixing rules. This can be overcome through the use of reliable vapour-liquid equilibrium data to allow calculation of the mixing non-idealities at the conditions in question.

Following these guidelines, it was shown that chemical equilibrium in ethylene [55], propylene [54] and butylene [36] hydration could be predicted with high accuracy. The data from the studies of Majewski and Marek [46], Stanley et al. [51] and Schiffler et al. [52] together with the chemical equilibrium correlations of Izumi [50] and Cope [54] are shown in Figure 2.1.

Unfortunately, in view of the simplifying assumptions made in the calculation of chemical equilibrium, the method of Cope cannot be used for low temperature / high pressure predictions. The most important assumptions in the method were those of the Lewis-Randall rule for the gas phase and the insolubility of the olefin in the aqueous phase. Whilst the former assumption is not critical, the second one only holds with reasonable accuracy at high temperature where the extent of IPA formation is limited. At high pressure and low temperature, the equilibrium is shifted significantly towards alcohol formation. A significant portion of the liquid phase is thus alcohol and the solubility of the olefin therefore increases dramatically. Any model used to account for simultaneous hydration reaction and phase equilibrium would also need to account for olefin solubility in the liquid phase.

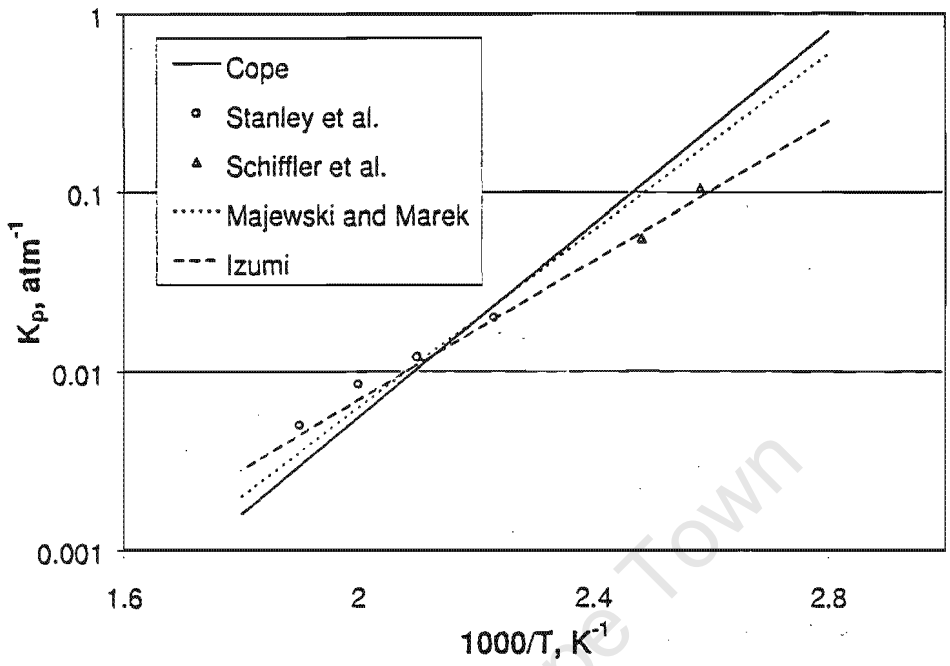

Figure 2.1: Literature chemical equilibrium data and correlations (see Section 2.2.5 for the definition of K_p)

2.1.2.2 Diisopropyl ether synthesis

The only known study of the chemical equilibrium of DIPE formation is that of Petrus et al. [47]. As for the work on propylene hydration by the same authors, chemical equilibrium was measured in a highly dilute aqueous phase at 90 bar, between 100°C and 140°C. As already mentioned, the concentration-based chemical equilibrium constant was reported independent of the water concentration, which was in large excess and thus considered to be constant during reaction. This method of reporting the equilibrium constant, unfortunately, makes it very difficult to transfer it to other systems as it becomes a strong function of the propylene to water ratio due to large mixing non-idealities.

Cope [36] in his study on the prediction of hydration equilibria, briefly touched upon the subject of DIPE formation and the importance of considering it in chemical equilibrium calculations. These predictions, however, were limited to the vapour phase at

high temperature and pressure, and as such cannot be compared to the results of Petrus et al. [47]. Also, as noted before, the method used to determine the chemical equilibrium phase compositions could not be used in the present system since propylene was considered insoluble in the liquid phase.

Significant effort has been spent on the calculation of chemical reaction equilibria in the liquid phase synthesis of the traditional octane enhancing ethers. The equilibria of isopropyl tert-butyl ether [56], TAEE [57], MTBE [32, 58, 59] and ETBE [58, 60, 61] have all been considered. In every case, however, the basic method of determining the equilibrium distribution was identical, being based either on the UNIFAC or UNIQUAC activity coefficient models. This method works particularly well for these systems since:

- the systems are purely organic with a limited range of polarities and consequently relatively small mixing non-idealities
- all compounds are sub-critical at synthesis conditions and
- the systems are purely liquid phase

In the case of single-stage DIPE synthesis none of the above statements holds due to the presence of water, super-critical propylene and vapour-liquid phase separation. This method can thus not be applied, and a model is needed to correlate the phase thermodynamics of the DIPE system. The PRSV equation of state together with either the Wyczesany or the Wong-Sandler mixing rule will be examined for their ability to calculate and/or predict chemical equilibrium in the DIPE system.

2.2 Thermodynamic theory

2.2.1 Pure component thermodynamics

2.2.1.1 Pure component properties

Generally, the best way to determine pure component properties is from high quality experimental data or, failing that, from thermodynamic compilations based on experimental results. Due to the almost infinite variety of compounds and the large number of thermodynamic properties, it is clearly not practical to determine experimentally all the properties of every species. Attempts have thus been made to reduce the required set of data to a minimum, from which the remainder of the thermodynamic properties of a pure compound can be predicted using the relevant thermodynamic theory. Typically, attempts are made to determine the properties of a fluid from a small subset of properties, these being the critical temperature, pressure and volume, the accentric factor, the enthalpy and Gibbs free energy of formation and heat capacity data. This is usually sufficient to predict the majority of properties of a pure fluid accurately. Data of this sort can be found in a variety of thermodynamic property databases [44, 45, 62, 63, 64, 65]. The thermodynamic property source which was used throughout this project was *Physical and Thermodynamic Properties of Pure Fluids* by Daubert and Danner [62], since all literature data sources had been reported, analysed and evaluated. For comparison purposes, data from the other sources mentioned above have also been included. The pure component properties for the DIPE system are given in Appendix A.

The most commonly used method to determine the pressure, temperature and volume behaviour of a species is through the use of an equation of state. The first such was the ideal gas equation of state

$$PV = NRT \tag{2.1}$$

which as the name suggests, only applies to the hypothetical ideal gas. As a rule, real

compounds, do not usually behave as ideal gases and thus more complex equations of state have to be employed. The use of a single equation of state to reproduce thermodynamic properties of real compounds and mixtures (in vapour, liquid or solid phases) has been the goal of thermodynamicists for over a century. Since van der Waal introduced his equation of state in 1873, literally hundreds of such equations have been proposed. The most popular of these for engineering design predictions are the cubic equations of state, owing to their accuracy and algebraic simplicity. These equations of state predict *fluid* behaviour not from experimental data, but from critical properties. One of the most popular cubic equations of state is the Peng-Robinson (PR) equation of state.

2.2.1.2 The Peng-Robinson equation of state

The Peng-Robinson (PR) equation of state, a derivative of the van der Waals equation, was proposed by Peng and Robinson in 1976 [66] as a volumetric equation of state capable of accurately predicting changes in a fluids' internal energy, enthalpy and entropy. It is a semi-empirical, cubic equation of state intended mainly for hydrocarbons and other non-polar species. The general form of the equation is

$$P = \frac{RT}{\overline{V} - b} - \frac{a(T)}{\overline{V}(\overline{V} + b) + b(\overline{V} - b)} \tag{2.2}$$

where

$$a(T) = 0.45724 \frac{R^2 T_c^2}{P_c} \left[1 + \kappa \left(1 - \sqrt{\frac{T}{T_c}} \right) \right]^2 \tag{2.3}$$

$$b = 0.07780 \frac{RT_c}{P_c} \tag{2.4}$$

$$\kappa = 0.37464 + 1.54226\omega - 0.26992\omega^2 \tag{2.5}$$

For each pure component the PR equation requires the critical temperature and pressure, T_c and P_c, as well as an additional parameter, the accentric factor ω. These have been determined for a large variety of compounds by many authors.

As mentioned, however, the PR equation was originally intended to handle nonpolar and slightly polar compounds only. Recent modifications to the PR equation of state have, however, dealt with problems involved in the computation of the properties of polar species. One of these modifications is the PRSV equation of state [41, 42].

2.2.1.3 The Stryjek-Vera improvements on the Peng-Robinson equation of state

The Peng-Robinson-Stryjek-Vera (PRSV) equation of state is a semi-empirical, cubic equation of state which can be used with reasonable accuracy for *both* polar and non-polar components. It extends the range of applicability of the PR equation of state by including an additional parameter for the calculation of the temperature dependent term. The PRSV equation is especially useful for the computation of vapour-liquid equilibria in super-critical and high pressure regions and for the computation of the properties of polar species.

Basically, the PRSV equation of state has the same form proposed by the PR equation, namely

$$P = \frac{RT}{\overline{V} - b} - \frac{a(T)}{\overline{V}(\overline{V} + b) + b(\overline{V} - b)} \tag{2.6}$$

Once again, a and b are given by

$$a(T) = 0.457235 \frac{R^2 T_c^2}{P_c} \alpha(T) \tag{2.7}$$

$$b = 0.077796 \frac{RT_c}{P_c} \tag{2.8}$$

The difference in the PRSV equation lies in the evaluation of the temperature dependent term, $\alpha(T)$, where an additional empirical pure-component parameter, κ_1, is introduced for greater accuracy.

$$\alpha(T) = \left[1 + \kappa \left(1 - T_R^{\frac{1}{2}}\right)^2\right] \tag{2.9}$$

$$T_R = \frac{T}{T_c} \tag{2.10}$$

$$\kappa = \kappa_o + \kappa_1 \left(1 + T_R^{\frac{1}{2}}\right)(0.7 - T_R) \tag{2.11}$$

and

$$\kappa_o = 0.378893 + 1.489715\omega - 0.171318\omega^2 + 0.019655\omega^3 \tag{2.12}$$

As for the other parameters, the value of κ_1 is specific to each component. Stryjek & Vera [42] have determined the value of this parameter for a number of pure compounds from regression of vapour pressure data. It has been shown [42] that whilst the PR equation predicts pure component vapour pressures for polar compounds with an average error of $\pm 10\%$ compared to experimental data, the modification introduced above reduces the error in vapour pressure prediction to within $\pm 1\%$. The improvements in pure component predictions for oxygen and water are shown graphically in Figure 2.2 [42].

2.2.1.4 The pure component fugacity

Fugacity is one of the most important thermodynamic functions. The fugacity function is used because its relationship to the Gibbs free energy simplifies phase and chemical equilibrium calculations. Formally, for a pure compound, i, the fugacity, $f_i^\bullet$, is defined as

$$f_i^\bullet(T,P) = P \exp\left\{\frac{\overline{G}_i^\bullet(T,P) - \overline{G}_i^{IG}(T,P)}{RT}\right\} \tag{2.13}$$

where the superscript IG refers to Ideal Gas and R is the gas constant. This can be shown to equal

$$f_i^\bullet(T,P) = P \exp\left\{\frac{1}{RT}\int_0^P \left(\overline{V}_i - \frac{RT}{P}\right) dP\right\} \tag{2.14}$$

such that $f_i^\bullet \to P$ as $P \to 0$.

As always, the simplest method to solve for the pure compound liquid- or vapour-phase fugacity is from experimental data. However, these are not always available at the

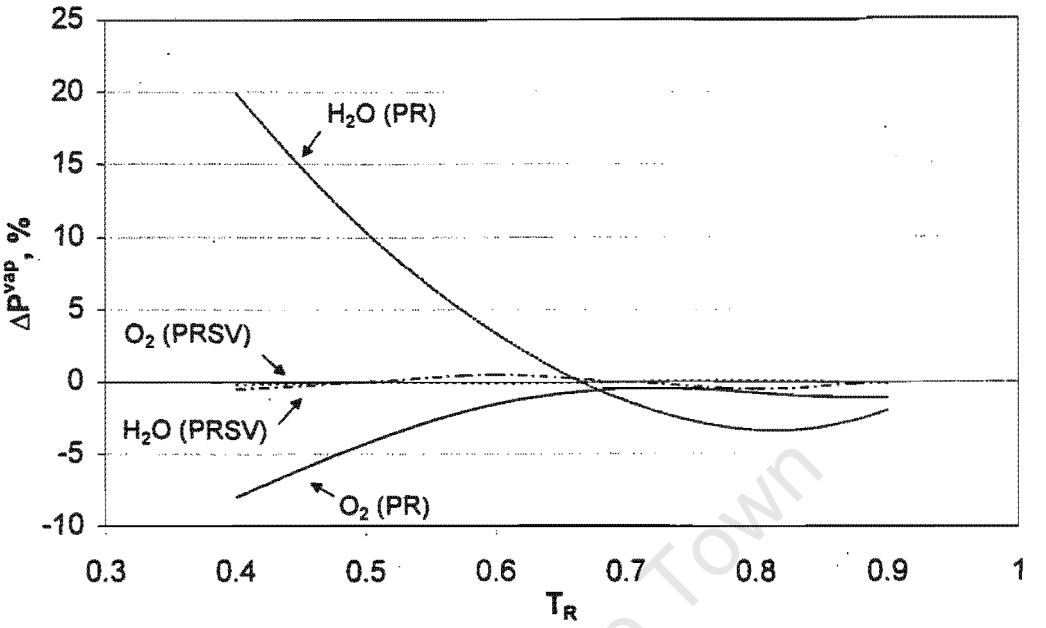

Figure 2.2: Percent deviations in the vapour pressure of oxygen and water calculated by the Peng-Robinson (PR) and the Peng-Robinson-Stryjek-Vera (PRSV) equations of state.

required conditions and thus a number of alternative methods are used. In general, the most accurate method to solve for the pure compound liquid- or vapour-phase fugacity is through the use of an applicable equation of state which can represent the pure component vapour pressure data accurately. One starts from the thermodynamic relationship of Eq. 2.14. If one now introduces the phase compressibility, Z_i, to account for deviations from ideal gas behaviour, such that

$$Z_i = \frac{P\overline{V}_i}{RT} \tag{2.15}$$

and one changes integration variables, since most equations of state are pressure explicit, then

$$\ln \frac{f_i^{\bullet}(T,P)}{P} = \frac{1}{RT} \int_{\overline{V}_i=\infty}^{\overline{V}_i=\frac{Z_i RT}{P}} \left(\frac{RT}{\overline{V}_i} - P \right) d\overline{V}_i - \ln Z_i + (Z_i - 1) \tag{2.16}$$

Now, one can solve, for example, the PRSV equation of state (Eq. 2.6) for the compressibility, to give

$$Z^3 - (1-B)Z^2 + (A - 3B^2 - 2B)Z - (AB - B^2 - B^3) = 0 \tag{2.17}$$

where

$$A = \frac{aP}{R^2T^2} \qquad \text{and} \qquad B = \frac{Pb}{RT} \tag{2.18}$$

The smallest real root of this equation, Z^L, is the high density root and is used for the liquid phase, whilst the largest real root, Z^V, is the low density root and should correspondingly be used for the vapour phase. The pressure explicit form of the PRSV equation of state together with the relevant value of the phase compressibility can now be substituted into Eq. 2.16 to solve for the species fugacity of the pure compound.

The pure component fugacity coefficient is now defined as the ratio of the species fugacity, $f_i^\bullet$, to the system pressure, P, i.e.

$$\phi_i = \frac{f_i^\bullet}{P} \tag{2.19}$$

which is purely a measure of a species deviation from ideal gas behaviour. Clearly, if a species is an ideal gas, then $\phi_i \rightarrow 1$. The further ϕ_i deviates from unity, the less ideal the species.

2.2.2 Mixture thermodynamics

2.2.2.1 Introduction

In mixture thermodynamics one not only deals with pure component non-idealities, but also with non-idealities caused by interactions between the compounds in the mixture. Thus even though the species in a mixture would in the pure form behave in a given way, in a mixture they may behave completely differently. To account for these differences from ideal mixing behaviour, a quantity analogous to the pure component fugacity has been introduced. This quantity is called the partial molar fugacity.

2.2.2.2 Partial molar fugacity

The partial molar fugacity of a species in a mixture, with reference to the *I*deal *G*as *M*ixture, can now be introduced as

$$f_i^*(T,P,x_i) = x_i P \exp\left\{\frac{\overline{G}_i^*(T,P,x_i) - \overline{G}_i^{IGM}(T,P,x_i)}{RT}\right\} \tag{2.20}$$

It is most conveniently obtained from an equation of state capable of describing all the pure components in the mixture in conjunction with a mixing rule which accommodates any mixing non-idealities. The latter is, however, where the major difficulty in phase equilibrium calculations lies. Whilst describing pure component behaviour is reasonably straightforward, obtaining a good description of the mixing behaviour is extremely difficult, especially in highly non-ideal systems and in the liquid phase. If, however, one has an equation of state capable of describing the mixture, reformulation of Eq. 2.14, analogously to Section 2.2.1.4, gives

$$f_i^* = x_i P \exp\left\{\frac{1}{RT}\int_{\overline{V}_i=\infty}^{\overline{V}_i=\frac{Z_i RT}{P}}\left[\frac{RT}{\overline{V}} - N\left(\frac{\partial P}{\partial N_i}\right)_{T,V,N_{j\neq i}}\right]d\overline{V} - \ln Z\right\} \tag{2.21}$$

One can now substitute the pressure explicit form of the equation of state and solve for the partial molar fugacity. This equation of state approach works particularly well for the calculation of vapour-phase partial molar fugacities since the mixing non-idealities are smaller than in the liquid phase, and are thus easier to describe. The calculation of the liquid-phase partial molar fugacity from an equation of state, as mentioned above, is often very difficult and a common approach is to define an activity coefficient, γ_i, which accounts for mixing non-idealities. It is a function of temperature, pressure and mixture composition. The activity coefficient can be calculated from a variety of mostly empirical activity coefficient models such as van Laar, UNIFAC or NRTL. Using the activity coefficient, the liquid phase partial molar fugacity can be calculated from

$$f_i^{*,L} = x_i \gamma_i f_i^{\bullet,L} \tag{2.22}$$

Two approaches are thus evident for calculating the partial molar fugacities of species in a mixture. The equation of state approach, where both vapour and liquid phases are described by an equation of state, or the equation of state-activity coefficient approach, where the liquid phase is described by an activity coefficient model and the vapour phase by an equation of state.

2.2.2.3 Partial molar fugacity calculation from the Peng-Robinson-Stryjek-Vera equation of state

To obtain the partial molar fugacity of a species in a mixture, one uses Eq. 2.21, i.e.

$$f_i^* = x_i P \exp\left\{\frac{1}{RT}\int_{\overline{V}_i=\infty}^{\overline{V}_i=\frac{Z_i RT}{P}}\left[\frac{RT}{\overline{V}} - N\left(\frac{\partial P}{\partial N_i}\right)_{T,V,N_{j\neq i}}\right]d\overline{V} - \ln Z\right\} \tag{2.23}$$

where the liquid compressibility, Z^L, is used for the liquid phase partial molar fugacity and the vapour compressibility, Z^V, is used for the vapour phase partial molar fugacity. One now has the option of either integrating numerically or obtaining an analytical solution for each mixing rule. The parameters, a and b, of the equation of state, defined by the mixing rule, are only functions of temperature, T, and the total number of moles of each species in the system, N_i, and are thus constant for the integration. If one normalises the number of moles, i.e. the total number of moles in the system, N_{tot}, is 1, then the solution to Eq. 2.21, in terms of the mixture fugacity coefficient, $\phi_i = \frac{f_i^*}{x_i \cdot P}$, can be derived to give Eq.'s 2.24 and 2.25 below. See Appendix B for the full derivation.

$$\ln\phi_i = \frac{\partial b + b}{b}(Z-1) - \ln(Z - \frac{bP}{RT}) - \frac{a}{2\sqrt{2}bRT}\ln\left[\frac{Z + (1+\sqrt{2})\frac{bP}{RT}}{Z + (1-\sqrt{2})\frac{bP}{RT}}\right]\left(\frac{\partial a}{a} - \frac{\partial b - b}{b}\right) \tag{2.24}$$

where

$$\partial a = \left(\frac{\partial a}{\partial N_i}\right)_{T,\overline{V},N_{j\neq i}} \qquad and \qquad \partial b = \left(\frac{\partial b}{\partial N_i}\right)_{T,\overline{V},N_{j\neq i}} \tag{2.25}$$

All that remains now is to determine the partial derivatives ∂a and ∂b. These quantities can either be obtained analytically by differentiating the respective mixing rule or, should

this prove difficult, can be obtained from a suitable numerical differentiation scheme, e.g. 5-point Lagrange interpolation about the point of interest. Now, the value of the partial molar fugacity can be determined for any component in a mixture, provided the equation of state can predict the pure component properties and the mixing rule can correlate the mixing non-idealities, i.e. calculate the values of a and b for the mixture, accurately.

2.2.2.4 The UNIFAC predictive activity coefficient model

As mentioned in Section 2.2.2.2, it is often difficult to describe the non-idealities inherent in liquid mixtures accurately with an equation of state and a mixing rule. Consequently, an activity coefficient is defined which accounts for the liquid non-idealities. The activity coefficient can be calculated in a variety of ways: either from experimental data, from correlations which fit experimental data such as Wilson's equation, UNIQUAC or NRTL, or it can be calculated from purely predictive activity coefficient models such as UNIFAC.

Due to the infinite number of possible mixtures, frequently few or no mixture data are at hand and it is necessary to estimate activity coefficients from some suitable correlation. The few available correlations are all essentially empirical. The most useful of these, being applicable to the widest range of mixtures and generally being the most accurate is the UNIFAC (UNIQUAC Functional Group Activity Coefficient) model.

In 1977 Fredenslund, Gmehling and Rasmussen [67] introduced a predictive activity coefficient model based on the UNIQUAC (UNIversity QUAsi Chemical) model of Abrams and Prausnitz [68] called UNIFAC. Like UNIQUAC, the UNIFAC predictive activity coefficient model is based on the solution-of-groups concept. This theory imagines a mixture as consisting of a "soup" of structural groups originating from the compounds in the mixture. The activity coefficients of the species in the mixture are then related to interactions between the structural groups in the "soup".

One thus uses experimentally obtained activity coefficients to yield a reduced set of

parameters characterising interactions between pairs of structural groups, which can then be used to predict the behaviour of unknown systems containing these same structural groups. This allows a reduction in the number of experimental phase measurements by many orders of magnitude, since a few structural units can be used to represent a large variety of molecules.

The UNIFAC model has been found to be fairly accurate for the prediction of the activity coefficients of species in mixtures of apolar hydrocarbon species. If components in the mixture are polar, the pressure is greater than about 10 bar or the reduced temperatures of any of the species in the mixture is greater than approximately 0.85, the accuracy of UNIFAC is known to deteriorate significantly [45].

In the UNIFAC model the molecular activity coefficient is separated into two parts: one part provides the contribution due to the differences in molecular size (combinatorial), and the other provides the contribution due to molecular interactions (residual), i.e.

$$\ln \gamma_i = \ln \gamma_i^C + \ln \gamma_i^R \tag{2.26}$$

where

$$\ln \gamma_i^C = \ln \frac{\Phi_i}{x_i} + \frac{z}{2} q_i \ln \frac{\theta_i}{\Phi_i} + l_i - \frac{\Phi_i}{x_i} \sum_i x_j l_j \tag{2.27}$$

and

$$\ln \gamma_i^R = \sum_{k,\, all\ groups} v_k^{(i)} \left(\ln \Gamma_k - \ln \Gamma_k^{(i)} \right) \tag{2.28}$$

also

$$l_i = \frac{z}{2} (r_i - q_i) - (r_i - 1) \qquad z = 10 \tag{2.29}$$

$$\ln \Gamma_k = Q_k \left[1 - \ln \left(\sum_m \Theta_m \Psi_m \right) - \sum_m \frac{\Theta_m \Psi_{km}}{\sum_n \Theta_n \Psi_{nm}} \right] \tag{2.30}$$

$$\theta_i = \frac{q_i x_i}{\sum_j q_j x_j} \qquad \Phi_i = \frac{r_i x_i}{\sum_j r_j x_j} \tag{2.31}$$

$$r_i = \sum_k v_k^{(i)} R_k \qquad q_i = \sum_k v_k^{(i)} Q_k \tag{2.32}$$

$$\Theta_m = \frac{Q_m X_m}{\sum_n Q_n X_n} \qquad \Psi_{mn} = \exp\left(-\frac{a_{mn}}{T}\right) \tag{2.33}$$

In these equations R_k represents the functional group volume and Q_k the functional group area whilst a_{mn} is a measure of the energy of interaction between functional groups m and n, where $a_{mn} \neq a_{nm}$. These four parameters have been measured for a large number of functional groups and are available in literature [44, 45]. The values of these parameters for the DIPE system are given in Appendix C.

When using the UNIFAC model, one first identifies the functional subgroups present in each molecule using a current list from literature. One then evaluates the r_i and q_i for each species in the mixture, where $v_k^{(i)}$ is the number of functional groups of type k in molecule i and x_i is the mole fraction of species i in the mixture. The combinatorial term of the activity coefficient, $\ln \gamma_i^C$, is now evaluated from Eq. 2.27 where the summations used for calculating θ_i, Φ_i and finally $\ln \gamma_i^C$ are over all species in the mixture.

The residual contribution, $\ln \gamma_i^R$, to the activity coefficient is calculated from Eq. 2.28, where Γ_k is the residual contribution of functional group k in the mixture and $\Gamma_k^{(i)}$ is the residual contribution of functional group k in a pure fluid of only species i. When calculating Γ_k from Eq. 2.30, X_m is the mole fraction of functional group m in the mixture of all functional groups present in the mixture and the summations are over all the functional groups in the mixture. For $\Gamma_k^{(i)}$, X_m refers only to the mole fraction of functional group m in molecule i and the summations are only over the functional groups in molecule i.

2.2.2.5 Mixing rules

There have been significant improvements in the accuracy of cubic equations of state for the prediction of pure component properties over the last two decades [43]. However, the same cannot be said for the calculation of the properties of mixtures, particularly in respect to phase separation. To extend equations of state capable of predicting the pressure, volume and temperature properties of pure fluids to being able to predict the same properties for mixtures, they must be modified to include the additional variable of mixture composition. In almost all cases [44] this is done by introducing a set of empirical mixing rules which in some way "average" pure component constants.

The mixing rules originally proposed by van der Waals for his equation of state literally averaged the pure component parameters a_i and b_i. In addition, to account for non-ideal mixing, a purely empirical so-called binary interaction parameter, k_{ij}, was introduced. This mixing rule was formulated as

$$a_{mix} = \sum_{i=1}^{n} \sum_{j=1}^{n} x_i x_j a_{ij} \tag{2.34}$$

$$b_{mix} = \sum_{i=1}^{n} x_i b_i \tag{2.35}$$

$$a_{ij} = \sqrt{a_i a_j} k_{ij} \qquad or \qquad a_{ij} = \sqrt{a_i a_j}(1 - k_{ij}) \tag{2.36}$$

The binary interaction parameter was symmetric, i.e. $k_{ij} = k_{ji}$, and the form of Eq. 2.36 stipulated that self-interaction was either unity, i.e. $k_{ii} = 1$, or zero, $k_{ii} = 0$. Furthermore, the binary interaction parameters were deemed independent of temperature, pressure and mixture composition.

The values of the binary mixing parameter were obtained from regression of experimental data for each binary pair in the mixture. However, the conventional single binary

interaction parameter mixing rule of van der Waals, though useful for nonpolar hydrocarbon mixtures and supercritical inorganic gases such as carbon dioxide has not proven to be suitable for even moderately non-ideal systems [43] containing water and apolar hydrocarbons for example.

A number of authors have since addressed the problem of improving the accuracy of mixing rules for a variety of systems. Two, which have been shown to be widely applicable, are the four-parameter mixing rules of Wyczesany [39] and Wong-Sandler [40].

2.2.2.6 The Wyczesany-Stryjek-Vera mixing rule

In the Wyczesany modification [39] to the Stryjek Vera mixing rules, the equation of state a_{mix} and b_{mix} parameters are calculated from mixing rules with a very similar form to that of van der Waal's original proposals. The only differences being that k_{ij} is no longer symmetric and that it has become a function of temperature. Thus,

$$b_{mix} = \sum_i b_i x_i \tag{2.37}$$

and

$$a_{mix} = \sum_i \sum_j x_i x_j (a_i a_j)^{\frac{1}{2}} (1 - x_i k_{ij} - x_j k_{ji}) \tag{2.38}$$

Where k_{ij} and k_{ji} are defined as

$$k_{ij} = k_{ij}^{(1)} + \frac{k_{ij}^{(2)}}{T} \tag{2.39}$$

$$k_{ji} = k_{ji}^{(1)} + \frac{k_{ji}^{(2)}}{T} \tag{2.40}$$

The four empirical parameters $k_{ij}^{(1)}$, $k_{ij}^{(2)}$, $k_{ji}^{(1)}$ and $k_{ji}^{(2)}$ are determined from regression of experimental data, where possible. If no experimental data is available for regression, UNIFAC predictions of the vapour-liquid equilibrium at low pressure, where it is supposedly exact, can be substituted as "pseudo-experimental" data. These parameters must be obtained for each binary pair in a mixture.

2.2.2.7 The Wong-Sandler mixing rule

In 1992 Wong and Sandler [40] introduced a mixing rule that provided a theoretically link between equations of state and excess-free-energy models (activity coefficient models). It allows the correlation of vapour-liquid equilibrium for a wide variety of mixtures over a large range of pressures and temperatures [43]. In the Wong-Sandler mixing rule, the basic equations for the calculation of the mixture parameters, a_{mix} and b_{mix}, in the equation of state are

$$b_{mix} = \frac{\sum_i \sum_j x_i x_j \left(b - \frac{a}{RT}\right)_{ij}}{1 - \frac{A^E}{CRT} - \sum_i x_i \frac{a_i}{RTb_i}} \tag{2.41}$$

$$\frac{a_{mix}}{b_{mix}} = \sum_i x_i \frac{a_i}{b_i} + \frac{A^E}{C} \tag{2.42}$$

where A^E is a Helmholtz excess-free-energy term, a_i and b_i are the equation of state parameters and C is a constant dependent on the equation of state selected. For the PR and PRSV equations of state, it can be shown that

$$C = \frac{1}{\sqrt{2}} \ln\left(\sqrt{2} - 1\right) = -0.623225\ldots \tag{2.43}$$

In this mixing rule, the mixing parameters are those of the excess-free-energy model, A^E, and the binary interaction parameter k_{ij}. The cross-product of Eq. 2.41 is given as

$$\left(b - \frac{a}{RT}\right)_{ij} = \frac{(b_i + b_j)}{2} - \frac{\sqrt{a_i a_j}}{RT}(1 - k_{ij}) \tag{2.44}$$

Now, an excess-free-energy model needs to be chosen. Orbey and Sandler [43] recommend using the modified NRTL form of Huron and Vidal [69].

$$\frac{A^E}{RT} = \sum_i x_i \left(\frac{\sum_j x_j G_{ji} \tau_{ji}}{\sum_k x_k G_{ki}}\right) \tag{2.45}$$

where

$$G_{ij} = b_i \exp(-\alpha_{ij}\tau_{ij}) \tag{2.46}$$

Thus, since $\alpha_{ij} = \alpha_{ji}$, this mixing rule introduces 4 parameters per binary pair in the mixture. They are the binary interaction parameter, k_{ij}, and the excess free energy parameters α_{ij}, τ_{ij} and τ_{ji}. Once again, these can either be obtained from fits to existing experimental data or they can be regressed from "pseudo-experimental" data calculated from predictive methods such as UNIFAC.

2.2.3 Phase equilibrium thermodynamics

2.2.3.1 The necessary condition of phase equilibrium

Phase equilibrium thermodynamics answers the question: If the total mole fractions in the system, z_i, the temperature, T, and the pressure, P, are known, what are the mole fractions in phase $I(x_1^I, x_2^I \ldots x_n^I)$, phase $II(x_1^{II}, x_2^{II} \ldots x_n^{II})$, phase $III(x_1^{III}, x_2^{III} \ldots x_n^{III})$, etc.? This could involve a vapour phase and a single liquid phase, two liquid phases or a complex system of a vapour phase, multiple liquid phases and even solid phases.

The ability to answer the question posed above with reasonable accuracy has gained importance in recent years due to the increasing awareness of the financial impact of the improved prediction of phase behaviour. Though phase equilibrium has been studied for a long period of time, most of the early work was driven by the petroleum industry. Consequently until lately, only systems of relatively apolar hydrocarbons and certain inorganic gases could be described accurately, and then only with semi-empirical methods.

This field of research has now advanced to the state where it is possible to calculate phase equilibrium behaviour of the majority of systems to reasonable accuracy, provided some mixture data is available. The correlation of the behaviour of many mixtures, and especially the prediction of unknown systems, though, still remain a major problem, particularly so with highly non-ideal mixtures composed of non-polar and polar species, with liquid-liquid equilibrium and with mixtures involving super-critical species.

The starting point for all phase equilibrium calculations is the necessary thermodynamic condition that the partial molar Gibbs free energy of component i in phase I, $\overline{G}_i^{*,I}$, the temperature, T, and the pressure, P, be the same in the vapour, all liquid phases and all solid phases, i.e.

$$\overline{G}_i^{*,I}(x_i^I, T, P) = \overline{G}_i^{*,II}(x_i^{II}, T, P) = \overline{G}_i^{*,III}(x_i^{III}, T, P) = \ldots \tag{2.47}$$

Practically, however, this is difficult to work with, since it does not relate directly to the compositions of the equilibrium phases. It is typical to proceed in one of two ways: either both phases are described by the fugacity, or the vapour phase is described by the fugacity and the liquid phase by an activity coefficient. The former approach is termed the phi-phi method whilst the latter is the gamma-phi method.

It can be shown from Eq. 2.47 that the necessary condition for phase equilibrium can be re-written as

$$f_i^{*,I}(x_i^I, T, P) = f_i^{*,II}(x_i^{II}, T, P) = f_i^{*,III}(x_i^{III}, T, P) = \ldots \tag{2.48}$$

This last form of the necessary condition in phase equilibrium thermodynamics is the one most commonly used in calculations. Ideally one would calculate the partial molar fugacity of each species in each phase from an equation of state. As mentioned previously though, difficulties in calculating liquid phase mixing effects led to the use of activity coefficient models. In terms of the activity coefficient, the partial molar liquid fugacity of component i in liquid phase I equals

$$f_i^{*,L,I}(T, P, x_i) = x_i^I \gamma_i^I(T, P, x_i) f_i^{\bullet,L}(T, P) \tag{2.49}$$

where $f_i^{\bullet,L}$ is the pure liquid fugacity of species i at the temperature and pressure of the mixture. Condition 2.48 now becomes

$$f_i^{*,V} = x_i^I \gamma_i^I f_i^{\bullet,L} = x_i^{II} \gamma_i^{II} f_i^{\bullet,L} = \ldots \tag{2.50}$$

where the vapour phase is described solely by the fugacity, and the liquid phase(s) are described by the activity coefficient.

2.2.3.2 Pure component phase equilibrium

The simplest form of phase equilibrium occurs for pure compounds during phase transitions between vapour, liquid and solid forms. Of these, the one of most concern is the vapour-liquid phase transition, i.e. the question of vapour pressure. A number of semi-theoretical and empirical correlations exist for the calculation of this quantity. The most common of these are the Antoine equation and the Wagner equation.

A simple modification of the Clapeyron equation which has been widely used to calculate vapour pressure is the Antoine equation

$$\ln P^{vap} = A - \frac{B}{T + C} \tag{2.51}$$

The parameters A, B and C are obtained from regression of experimental vapour pressure data and are available in literature for a wide range of species. The applicable temperature range of the equation is not very large; extrapolation beyond the applicable temperature limits often leads to nonsensical results.

More useful than the Antoine equation, being applicable over a wider range of temperatures and generally being more accurate is the Wagner equation. In reduced vapour pressure form, this is

$$\ln P_r^{vap} = \frac{a\tau + b\tau^{1.5} + c\tau^3 + d\tau^6}{T_r} \tag{2.52}$$

where $\tau = 1 - T_r$. As for the Antoine equation, the parameters a, b, c and d are obtained from regression of experimental data.

If, for a pure compound, one lacks the parameters for either of the above equations, then another common method employed to calculate the vapour pressure is through the use of an equation of state, such as PRSV. All that has to be done in this case, is to find, usually by iteration, the temperature at which the pure liquid and pure vapour fugacities are equal.

2.2.3.3 The flash calculation

The most common problem in vapour-liquid thermodynamics is the flash problem, dealing with a vapour phase and a single liquid phase. Here the temperature, pressure and the feed composition of the system are known and one wishes to calculate the liquid and vapour mole fractions as well as the total amount of liquid and vapour present in the system. If the liquid and vapour phases are denoted by the superscripts L and V respectively, then the necessary condition for phase equilibrium becomes

$$f_i^{*,V}(T, P, x_i^V) = f_i^{*,L}(T, P, x_i^L) = x_i^L \gamma_i f_i^{\bullet L} \tag{2.53}$$

In an isothermal and isobaric liquid-vapour phase problem, the variables which specify the system are the temperature, T, the pressure, P, and the amount of each component in the feed, F_i. The unknowns are the total moles of liquid and vapour, L and V, and the liquid- and vapour-phase mole fractions of each species, x_i and y_i. This gives a total of $2n + 2$ unknown variables to be found, n being the number of components. Clearly, one needs $2n + 2$ equations.

One starts with the necessary condition of phase equilibrium thermodynamics, reformulated for a single liquid and vapour phase

$$f_i^{*,V}(T, P, y_i) = f_i^{*,L}(T, P, x_i) \tag{2.54}$$

Typically, this is rewritten as a set of n equations in terms of the "equilibrium ratio", K_i, and the equilibrium mole fractions, x_i and y_i, such that

$$K_i = \frac{y_i}{x_i} \tag{2.55}$$

By conservation of mass during a phase split, the sum of the amount of component i in the vapour phase, Vy_i, and the amount of component i in the liquid phase, Lx_i, must equal the initial amount of i, F_i. This leads to another set of n equations

$$F_i = Vy_i + Lx_i \tag{2.56}$$

Furthermore, conservation of total mass requires

$$L + V = \sum_i F_i \tag{2.57}$$

and, clearly, the mole fractions in each phase must sum to unity. This last condition is usually rewritten as

$$\sum_i (y_i - x_i) = 0 \tag{2.58}$$

Equations 2.55 to 2.58 complete a set of $2n + 2$ non-linear equations. Isothermal and isobaric vapour-liquid equilibrium problems can now be solved using this set of equations, if the feed composition, the temperature and pressure are known. A common method of solution for a two-phase vapour-liquid calculation, for a given set of T and P, is the successive substitution method.

2.2.3.4 The bubble point pressure calculation

The bubble point pressure of a mixture is defined as the pressure at which the first bubbles of vapour form at the given temperature. This problem is very similar in nature to that of the flash calculation. In this case the temperature, T, the liquid phase mole fractions, x_i, and the total amounts of liquid, $L = F$, and vapour, $V = 0$, are known. The vapour phase mole fractions at the bubble point, y_i, and the pressure, P, are unknown. This problem is solved by successive substitution in the same way as the flash calculation, except that Eq. 2.58 becomes

$$1 - \sum_i K_i x_i = 0 \tag{2.59}$$

2.2.3.5 Successive substitution

Successive substitution is a very simple and in this case useful technique to solve systems of non-linear equations. For vapour-liquid flash calculations, Eq.'s 2.55 to 2.58 are rewritten

such that

$$L + V - F = 0 \tag{2.60}$$

$$x_i = \frac{F_i}{L + VK_i} \qquad i = 1 \ldots n \tag{2.61}$$

$$y_i = K_i x_i \qquad i = 1 \ldots n \tag{2.62}$$

$$g(V) = \sum_i^n \frac{F_i(K_i - 1)}{L + VK_i} = 0 \tag{2.63}$$

An initial guess for K_i (usually the ideal mixture K_i) and then L is made. The amount of vapour phase V as well as the vapour- and liquid-phase mole fractions, x_i and y_i, are then calculated from the initial guesses using Eq.'s 2.60 to 2.62. Eq.'s 2.60 to 2.62 are then solved iteratively for the correct value of L, given the guessed K_i. From the iterated value of L, the liquid and vapour phase fugacities and the new values of K_i are generated. According to Heidemann [70] the key step in this iterative scheme is the re-evaluation of K_i. In the successive substitution method, the new value of K_i is calculated from

$$K_i^{new} = K_i^{old} \left(\frac{f_i^{*,L}}{f_i^{*,V}} \right)^{old} \tag{2.64}$$

At convergence one satisfies the necessary criterion of phase equilibrium thermodynamics, Eq. 2.48, such that

$$\sum_i \left[\ln \left(\frac{f_i^{*,L}}{f_i^{*,V}} \right) \right] \leq 10^{-12} \tag{2.65}$$

This method can be used to solve for the vapour-liquid equilibrium of most systems. The complete algorithm used for the isothermal flash calculation is shown in Figure 2.3.

2.2.4 Chemical equilibrium

> "The equilibrium state of a closed system is that state for which the total Gibbs energy is a minimum with respect to all possible changes at the given temperature and pressure." - Smith and van Ness [71].

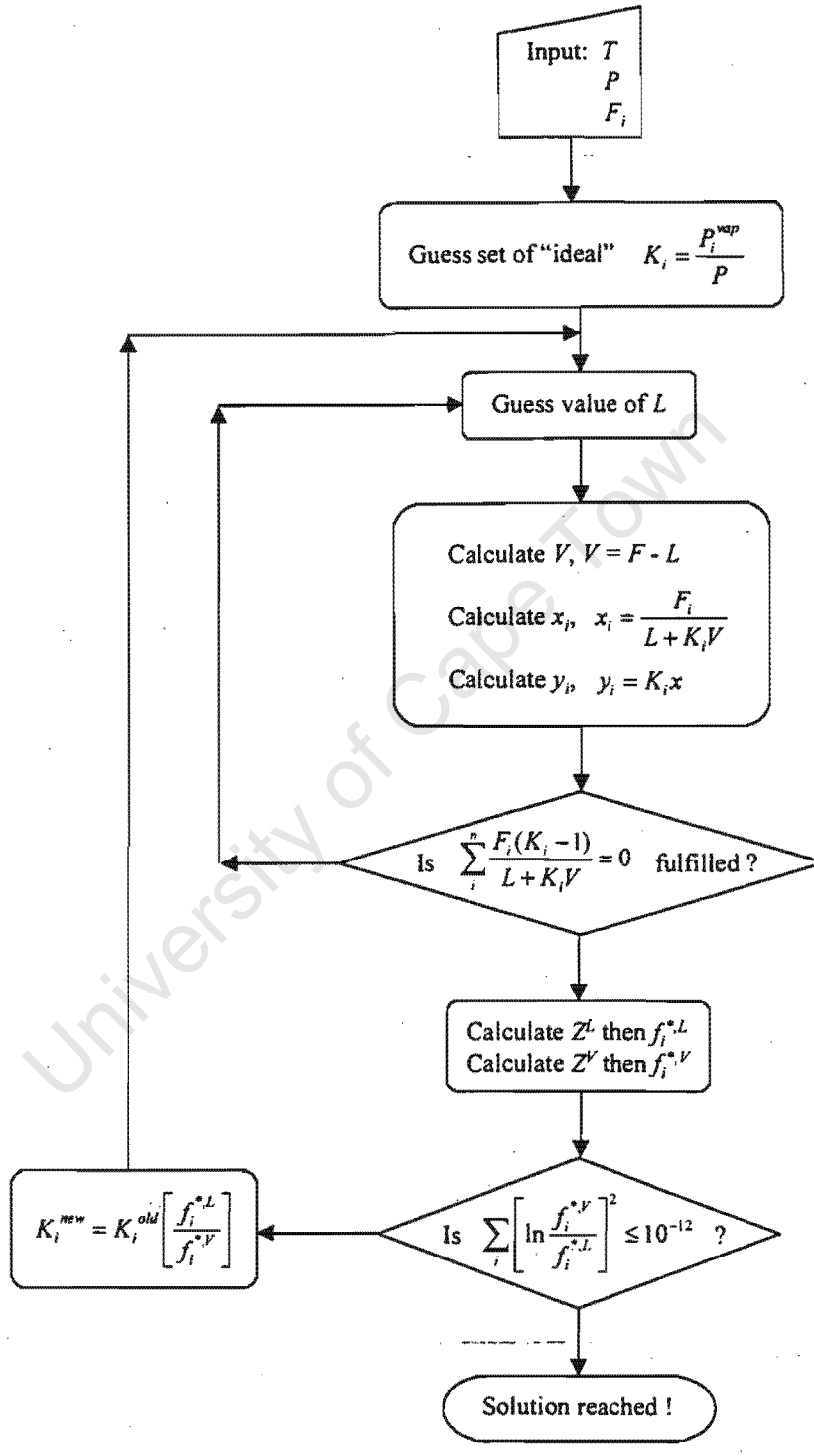

Figure 2.3: Computational algorithm for the isothermal flash calculation

For chemical reaction in a single-phase, single-reaction system this criterion translates to

$$\sum_i \nu_i \overline{G}_i^* = 0 \tag{2.66}$$

Naturally, this criterion remains the same for multiple reactions. This means that for $\mathfrak{M}$ reactions Eq. 2.66 must be satisfied for each reaction j

$$\sum_i \nu_{ij} \overline{G}_i^* = 0 \qquad j = 1, 2 \ldots \mathfrak{M} \tag{2.67}$$

Now, the partial molar Gibbs free energy, $\overline{G}_i(T, P, x_i)$, of any species i can be defined by

$$\begin{aligned} \overline{G}_i^*(T, P, x_i) &= \overline{G}_i^\circ(T, P, x_i^\circ) + \left[\overline{G}_i^*(T, P, x_i) - \overline{G}_i^\circ(T, P, x_i^\circ)\right] \\ &= \overline{G}_i^\circ(T, P, x_i^\circ) + RT \ln \left[\frac{f_i^*(T, P, x_i)}{f_i^\circ(T, P, x_i^\circ)}\right] \\ &= \overline{G}_i^\circ(T, P, x_i^\circ) + RT \ln a_i \end{aligned} \tag{2.68}$$

where the activity, a_i, of species i is defined as the ratio of the partial molar species fugacity in the mixture, f_i^*, to the partial molar species fugacity at the *standard state*, f_i°. The choice of standard state is arbitrary, though for convenience one usually chooses the standard state as the pure species, $x_i^\circ = 1$, at the temperature of interest, T, and a pressure, P, of 1 atm. In this case the standard partial molar Gibbs energy of formation, $\overline{G}_i^\circ(T, P, x_i^\circ)$, is equivalent to the pure molar Gibbs free energy, $\overline{G}_i^\bullet(T, P)$, at the same temperature and pressure.

Substitution of Eq. 2.68 into Eq. 2.67 now gives

$$\frac{-\sum_i \nu_{ij} \overline{G}_i^\bullet(T, P = 1\,atm)}{RT} = \ln \left\{ \prod_i (a_i)^{\nu_{ij}} \right\} \qquad j = 1, 2 \ldots \mathfrak{M} \tag{2.69}$$

The numerator of the LHS of Eq. 2.69 is usually referred to as the standard molar Gibbs energy of reaction, $\Delta \overline{G}_{rxn,j}^\circ(T)$, for reaction j at temperature T. Typically, one now also

introduces a *chemical equilibrium constant*, K_a, which for each specific reaction j is a function of temperature *only*, defined by

$$K_{a,j}(T) = \exp\left(-\frac{\Delta\overline{G}^{\circ}_{rxn,j}}{RT}\right) = \prod_i (a_i)^{\nu_{ij}} \qquad j = 1, 2 \ldots \mathfrak{M} \tag{2.70}$$

For many compounds the pure component Gibbs free energy of formation can be obtained from literature at the standard conditions of $T = 25°C$ and $P = 1\,atm$, e.g. Coulson et al. [63] or Daubert and Danner [62]. This makes calculation of the chemical equilibrium constant at the standard conditions trivial. If, however, one wishes to determine the chemical equilibrium constant at a temperature other than the standard temperature then one must either obtain pure component Gibbs free energy of formation data at the temperature of interest or the chemical equilibrium constant can be obtained using the van't Hoff equation,

$$\left(\frac{\partial \ln K_a(T)}{\partial T}\right)_P = -\frac{1}{R}\frac{\partial}{\partial T}\left[\frac{\sum_i \nu_i \overline{G}^{\bullet}_{f,i}(T)}{T}\right] = \ldots = \frac{1}{RT^2}\sum_i \nu_i \overline{H}^{\bullet}_{f,i}(T) = \frac{\Delta\overline{H}^{\circ}_{rxn}(T)}{RT^2} \tag{2.71}$$

thus

$$\ln\frac{K_a(T_2)}{K_a(T_1)} = \int_{T_1}^{T_2} \frac{\Delta\overline{H}^{\circ}_{rxn}(T)}{RT^2}dT \tag{2.72}$$

The standard molar heat of reaction, $\Delta\overline{H}^{\circ}_{rxn}(T)$, at any temperature can be obtained from

$$\begin{aligned}
\Delta\overline{H}^{\circ}_{rxn}(T) &= \sum_i \nu_i \overline{H}^{\bullet}_i(T) \\
&= \sum_i \nu_i \left[\overline{H}^{\bullet}_i(T = 25°C) + \int_{T=25°C}^{T} Cp^{\bullet}_i(T')dT'\right] \\
&= \Delta\overline{H}^{\circ}_{rxn}(T = 25°C) + \sum_i \nu_i \int_{T=25°C}^{T} Cp^{\bullet}_i(T')dT'
\end{aligned} \tag{2.73}$$

So, given the standard Gibbs energy of reaction, the standard heat of reaction and the heat capacity as a function of temperature for every component in a reaction, one can calculate the chemical equilibrium constant for that specific reaction at any temperature, using Eq.'s 2.72 and 2.73. Solutions to Eq. 2.72 for different forms of heat capacity, C_p, as a function of temperature are given in Appendix D.

Ultimately, the aim of any chemical reaction equilibrium calculation is to determine the concentration of each species taking part in the reaction at chemical equilibrium. This is a fairly trivial exercise using Eq. 2.70 in the case of an ideal gas, where the fugacity reduces to the partial pressure. However, in the case of non-ideal systems, especially those with multiple phases, this can become very complex.

2.2.5 Other forms of the chemical equilibrium constant

The chemical equilibrium constant introduced here is, for obvious reasons, known as the activity-based chemical equilibrium constant. This is the most useful equilibrium constant since its value is dependent only on temperature, i.e. it is independent of phase, pressure, mixing effects, departures from ideality etc. Unfortunately, this form of the chemical equilibrium constant is not in common use, due to the perceived difficulty in the calculation of the activities of the individual species.

Two other forms of the equilibrium constant that are in common use are the so-called concentration-based equilibrium constant, K_c, and the partial-pressure based equilibrium constant, K_p. The former is typically used for liquid phase reactions whilst the latter is used for vapour phase reactions. As opposed to the activity-based chemical equilibrium constant, the values of these constants are not only functions of temperature but also of phase, pressure, mixing behaviour etc. Respectively, these constants are defined as

$$K_c = \prod_i \left(\frac{C_i}{C_{tot}} \right)^{\nu_i} \tag{2.74}$$

and

$$K_p = \prod_i \left(\frac{p_i}{P_{tot}} \right)^{\nu_i} \tag{2.75}$$

Interconversion, between these constants and the activity-based chemical equilibrium constant relies on the use of a method to calculate the activity of each species in the equilibrium mixture. Here, analogously to vapour-liquid equilibrium calculations, one can make use of an equation of state based model, such as the PRSV equation used in conjunction with the Wong-Sandler mixing rule described in Section 2.2.2.7 above. However, besides the inaccuracy in the experimental measurement of the equilibrium constant, the value of K_a so calculated, may depend strongly on the model used for calculating species activity.

2.2.6 Simultaneous chemical reaction and phase equilibrium

The conditions for equilibrium when chemical reaction and phase equilibrium occur simultaneously are that each species must be in phase equilibrium amongst all phases

$$\overline{G}_i^{*,I}(x_i^I, T, P) = \overline{G}_i^{*,II}(x_i^{II}, T, P) = \overline{G}_i^{*,III}(x_i^{III}, T, P) = \ldots \tag{2.76}$$

that each chemical reaction, j, must be in chemical equilibrium in each phase

$$\sum_i \nu_{ij} \overline{G}_i^* = 0 \qquad j = 1, 2 \ldots \mathfrak{M} \tag{2.77}$$

and that the stoichiometric and state variable constraints on the system are satisfied. Clearly, the equality of partial molar Gibbs free energy, Eq. 2.76, of each species in every phase at equilibrium ensures that if the chemical equilibrium criterion is satisfied in any one phase, it will be satisfied in all phases. Analogously to phase equilibrium thermodynamics (Section 2.2.3.1), it is thus only necessary to seek a solution for which

$$f_i^I(x_i^I, T, P) = f_i^{II}(x_i^{II}, T, P) = f_i^{III}(x_i^{III}, T, P) = \ldots \tag{2.78}$$

and for which

$$K_{a,j} = \prod_i (a_i)^{\nu_{i,j}} \qquad j = 1, 2 \ldots \mathfrak{M} \tag{2.79}$$

is satisfied in any one phase.

The problem of determining the mole fractions of each species in every phase in simultaneous phase and chemical reaction equilibrium, now simply becomes one in which the phase equilibrium calculation is nested within a chemical equilibrium calculation, or vice versa. An algorithm used for determining simultaneous phase and chemical equilibrium is shown in Figure 2.4.

2.3 Thermodynamic analysis of the DIPE system

2.3.1 Phase equilibrium in the DIPE system

2.3.1.1 Vapour pressure correlation

An important factor in the selection of the equation of state to use for vapour-liquid phase calculations in the DIPE system is its ability to predict the pure component properties, especially the vapour pressure, accurately over the entire range of pressures and temperatures of interest ($80 - 140\,°C$ and $20 - 100\,bar$). If the equation of state is unable to correlate these accurately, the chances that it will be able to give an accurate representation of the partial molar fugacity of a species in an asymmetric mixture are remote.

The accuracy of the PRSV equation of state predictions of the pure compound vapour pressure for the components in the DIPE system were compared to experimental data and with two popular vapour pressure correlations: the Antoine equation and the Wagner equation. The results are given in Table 2.1. The pure component physical parameters

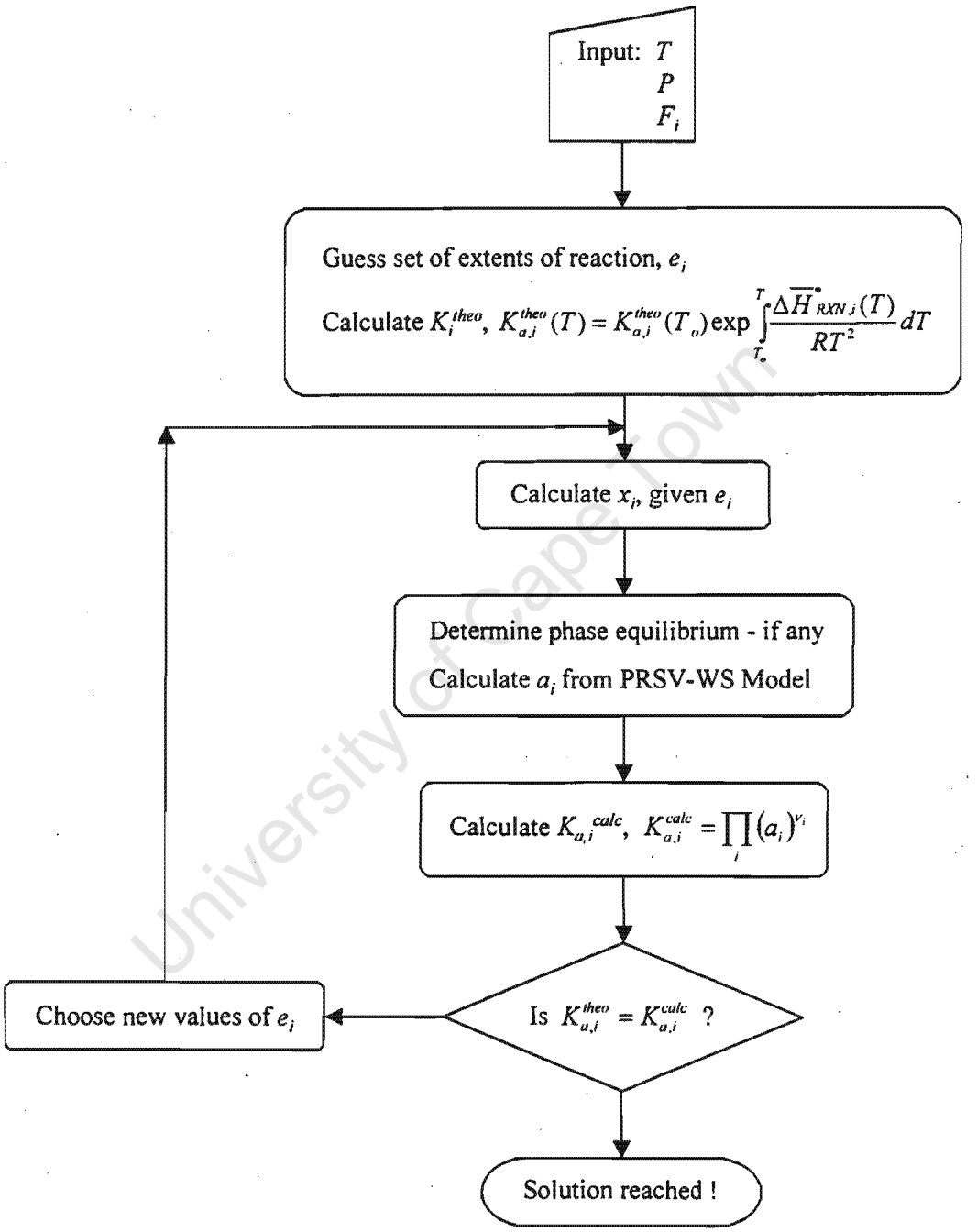

Figure 2.4: Computational algorithm for the simultaneous chemical and phase equilibrium calculation

Table 2.1: Accuracy of pure component vapour pressure predictions from the Peng-Robinson-Stryjek-Vera equation of state compared to literature data and popular vapour pressure correlations.

Component	Vapour Pressure Correlation					
	Antoine Equation		Wagner Equation		PRSV Equation	
	Range [°C]	Error%*	Range [°C]	Error%*	Range [°C]**	Error%*
Water[1]	11 to 168	1.64	2 to 374	0.14	1 to 350	0.12
Propylene[2]	−113 to −33	1.40	−133 to 92	0.80	−133 to 92	0.90
IPA[2]	0 to 111	2.23	−23 to 235	1.94	52 to 89	1.67
DIPE[3]	−24 to 91	3.30	24 to 227	1.52	12 to 92	0.14

*Error [%] $= \frac{1}{N} \sum_{i}^{N} \left| \frac{\exp_i - calc_i}{\exp_i} \right|$

**PRSV equation of state parameters fit to this temperature range. Range of applicability is considerably larger

[1] Rogers and Mayhew [72], [2] Perry and Green [64], [3] Ambrose et al. [73]

used in the above correlations are given in Appendix A. Vapour pressures calculated using the PRSV equation are given in Figure A.1, Appendix A.

The PRSV equation of state is able to correlate the experimental vapour pressure data at least as good, if not better, than either of the two empirical models with an accuracy comparable to the accuracy of measurement of the experimental data. Over the investigated temperature range, it was more accurate than the Antoine equation for every compound, and more accurate than the Wagner equation for every compound other than propylene. The PRSV equation can thus be considered able to correlate the pure component properties of both polar and apolar species.

2.3.1.2 Regression of parameters for the Wong-Sandler mixing rule

Since the Wong-Sandler mixing rule has been developed only recently, no values of the four mixing parameters (τ_{ij}, τ_{ji}, α_{ij}, k_{ij}) in the model have been published for any of the binaries in the water-propylene-IPA-DIPE system. Consequently, for the mixing

rule to be implemented in the calculation of phase equilibria, the values of the binary mixing parameters needed to be regressed from experimental data. Values of the binary mixing parameters for the PRSV equation of state with the Wyczesany mixing rule for certain of the two-component systems have been published [39] and thus do not need to be determined from regression.

Two optimization routines were used to determine the four mixing parameters. The first was the simplex method of Nelder and Mead [74]. It is a variation of the "Sequential Simplex" method of Spendley, Hext and Himsworth [75] which allows the geometric figure, the "simplex", of the original method to expand and contract continuously. It tends to be more computationally intensive than other methods, however, it is very "robust" and generally ensures a solution will be found.

The second optimization routine used was the unconstrained so-called BFGS method developed independently by Broyden [76], Fletcher [77], Goldfarb [78] and Shanno [79]. This is a secant method which employs an update procedure that retains the symmetric, positive definite nature of the Hessian matrix. It has been found to use significantly less function calls than most other optimization procedures on various testing algorithms [80] and should thus be a rapid regression method.

Traditionally, mixing parameters are fitted to binary experimental data using an objective function calculated from the sum of the squares of the relative errors of the bubble point pressure and the vapour-phase mole fractions. This works particularly well if the two components in a binary mixture have similar boiling points, for then a vapour and liquid coexist over only a small range of temperatures and pressures. Now, should the initial guess of the mixing parameters be poor, only a single phase may be predicted (either liquid or vapour). In such a case all optimization methods would fail. It is thus safer to fix the temperature and liquid-phase compositions and then calculate the bubble pressure, which always exists. Once the bubble pressure is known, the associated vapour phase mole fraction can be calculated. One thus fits data based on the accuracy of predic-

tion of the bubble pressure and the vapour phase mole fractions, even though an accurate correlation based on the vapour and liquid phase mole fractions is in fact required.

This method was used for the three binaries with compounds of relatively similar vapour pressures (i.e. water-IPA, water-DIPE and IPA-DIPE). The objective function was defined as

$$ObjF = \sum_{all\ data\ points} \left[\left(\frac{P_i^{\exp} - P_i^{calc}}{P_i^{\exp}} \right)^2 + \left(\frac{y_i^{\exp} - y_i^{calc}}{y_i^{\exp}} \right)^2 \right] \tag{2.80}$$

However, for those binaries containing propylene, where the widely differing vapour pressures ensured a vapour-liquid equilibrium for even very poor guesses of the mixing parameters, parameters were fit by minimising the sum of the squares of the relative errors of the vapour phase mole fraction of the less volatile component and the liquid phase mole fraction of propylene. This approach ensured that the mole fractions in both phases were correlated as accurately as possible at a given temperature and pressure. This objective function was defined as

$$ObjF = \sum_{all\ data\ points} \left[\left(\frac{x_i^{\exp} - x_i^{calc}}{x_i^{\exp}} \right)^2 + \left(\frac{y_i^{\exp} - y_i^{calc}}{y_i^{\exp}} \right)^2 \right] \tag{2.81}$$

Orbey and Sandler [43] recommend setting the value of α_{ij} to 0.1 and k_{ij} to 0.0. They found that this choice of parameters still allowed the correlation of a wide range of non-ideal systems. Fixing these parameters reduced the problem to a two-parameter model and greatly simplified regression. This modification was used as the starting point for all regressions involving the Wong-Sandler mixing rule. However, it quickly became clear that considerably better agreement could be obtained with experimental data when all four parameters were regressed simultaneously, particularly for the highly nonideal systems of water-propylene and water-DIPE. Consequently, all binaries were regressed with four parameters.

Because four-parameter functions can be very complex, possibly with multiple local minima, to ensure that the global optimum was found, a variety of initial guesses for

the optimization routines were chosen randomly within a pre-defined space. The initial guesses for the parameters were varied between the bounds -10 and 10 to try to ensure that all "minima" were found. Also, the surface was examined visually by keeping two of the parameters constant and generating surface plots of the objective function resulting from changes in the remaining two. Examples of such surface plots, generated for the water-IPA system with constant α_{ij} and k_{ij} are shown in Figures 2.5 and 2.6.

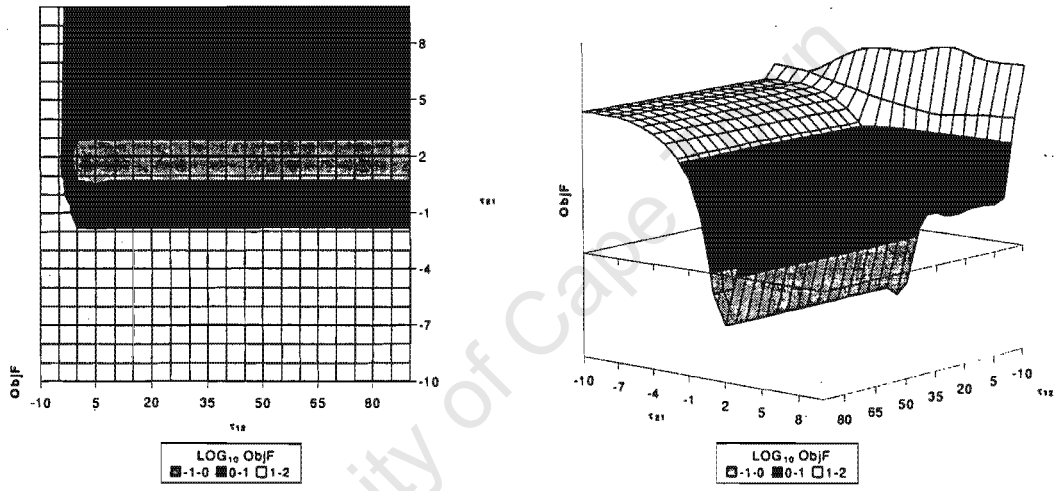

Figure 2.5: Surface plot of objective function for constant values of $\alpha_{ij} = 0.6024$ and $k_{ij} = 0.0462$

For any choice of constant parameters, only one minimum was found by visual inspection within the resulting surface. Also, starting from random points within the [-10, 10] space always resulted in the same minimum point being found. This was the same for all binaries. It is thus believed that there were no local minima resulting from the mixing rule formulation and that the only optimum was the global minimum.

For all binaries examined here, it was found that whilst the values of τ_{ij}, α_{ij} and k_{ij} were determined with relative ease, the Nelder-Mead optimization routine had problems fixing the value of τ_{ji}, regardless of the initial guess. This was because the "surface" of the objective function was a flat "plane" with a single steep-sided, extremely flat-bottomed

"valley", a two-dimensional representation of which, for fixed α_{ij} and k_{ij}, is shown in Figure 2.5. In all cases the "valley" was in the direction of the parameter τ_{ji}, and thus, even though the Nelder-Mead routine was able to locate the "valley", it was not able to move along it to find the minimum point. On a global scale the objective function does not appear to be sensitive to the parameter . However, one cannot discount it, as on a local scale, as shown in Figure 2.6, the parameter has a strong impact. For example, in the immediate vicinity of the minimum of the water-IPA system, varying τ_{ji} from 0.8 to 1.5, keeping all other parameters constant, changes the value of the objective function by three orders of magnitude.

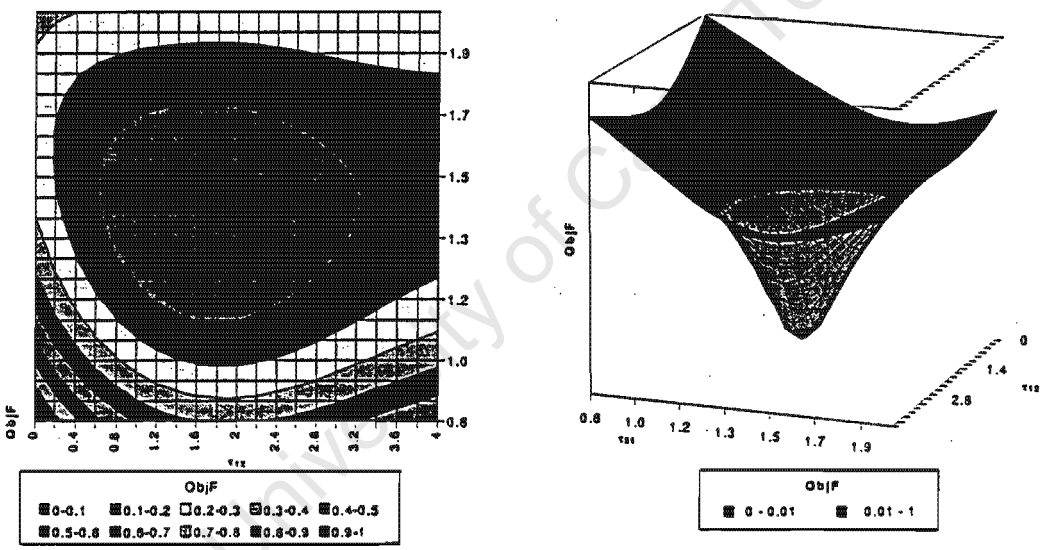

Figure 2.6: "Zoomed-in" surface plot of objective function of the water-isopropanol system for constant values of the parameters $\alpha_{ij} = 0.6024$ and $k_{ij} = 0.0462$

The BFGS routine on the other hand, if given a reasonable initial guess would always find *the* minimum. However, a poor initial guess would generally result in the method failing. If the routine was started in a region far from the optimum set of parameters, then it would often make too large step changes, resulting in single-phase predictions for the system. The problem was then, for BFGS, to find a "good" set of initial guesses for the parameters. What was ultimately employed, was a few initial iterations of the

Nelder-Mead routine, started from some random point, to fix the locality of the optimum with low accuracy. Once the region of the optimum had been found, BFGS was then used to pinpoint the actual minimum.

Where possible, the mixing parameters were regressed from experimental data measured at the conditions at which DIPE synthesis occurs. Unfortunately, experimental data was not always available in the region of interest and the parameters had to be fit at conditions far from the relevant temperatures and pressures. Also, the mixing parameters of the propylene-DIPE system had to be regressed from vapour-liquid equilibrium data, predicted by the UNIFAC model, since no experimental data was available. The conditions and the number of data points used for the regression of each set of parameters are given in Table 2.2. The values of the Wong-Sandler mixing parameters and the average absolute relative correlation deviations are shown in Table 2.3. All pure component parameters and mixing parameters used in the calculations are given in Appendix A and in Appendix C.

Table 2.2: Conditions used for fitting binary mixing parameters

Binary Mixture	Conditions of Fit			
	NDP*	$T[°C]$	$P[bar]$	References
Water-Propylene	38	38 - 138	2 - 103	1 - 3
Water-IPA	53	150 - 250	5 - 65	4 - 8
Water-DIPE	19	68 - 100	1	9, 10
Propylene-IPA	8	97	5 - 41	11
Propylene-DIPE**	11	-45 - 60	1	-
IPA-DIPE	55	66 - 82	1	10, 12, 13

* Number of experimental data points

** No experimental data - parameters fit to x-y predictions of UNIFAC with PRSV at 1.013 bar

1. Li and McKetta [81], 2. McAuliffe [82], 3. Purlee and Taft [83], 4. Barr-David and Dodge [84], 5. Udovenko and Mazanko [85], 6. International Critical Tables [86], 7. Brunjes and Bogart [87], 8. Wilson and Simons [88], 9. Hunsmann and Simmrock [89], 10. Yorizane, Yoshimura and Yamamoto [90], 11. Zabaloy, Mabe, Bottini and Brignole [91], 12. Verhoeye [92], 13. Miller and Bliss [93]

In all cases the Wong-Sandler mixing rule was able to correlate the experimental data

Table 2.3: Regressed mixing parameters for Wong-Sandler mixing rule

Binary Mixture	Binary Interaction Parameters				Average Deviation*	
	τ_{ij}	τ_{ji}	α [K]	k_{ij}	x or P [%]	y [%]
Water-Propylene[a]	4.6318	6.1483	0.3941	0.5823	8.2	5.4
Water-IPA[b]	1.4629	1.3404	0.6024	0.0462	2.8	1.4
Water-DIPE[b]	3.6547	4.6947	0.7848	0.8488	9.3	7.6
Propylene-IPA[a]	0.7197	0.2798	0.1559	0.1404	1.3	0.7
Propylene-DIPE[c]	-0.1329	-0.2996	0.0041	0.1428	1.2	0.1
IPA-DIPE[b]	-0.1537	2.0058	1.3750	0.4069	1.3	3.6

* average deviation $= \frac{1}{N}\sum_i \left|\frac{(\exp_i - calc_i)}{\exp_i}\right|$

[a] parameters fitted to literature x - y data

[b] parameters fitted to literature P - y data

[c] parameters fitted to x - y data predicted from UNIFAC with PRSV at 1.013 bar

with an average absolute relative deviation better than 10%. As one would expect, the absolute average deviation became smaller the more ideal the mixture became. It was largest for the water-DIPE mixture, where liquid-liquid as well as liquid-vapour phase splits can occur at the temperature and pressure of the experimental data. The next largest deviations occurred for the water-propylene binary, a mixture of a nonpolar, supercritical olefin and a polar inorganic species. The smallest deviations occurred for the totally organic systems of IPA-DIPE and IPA-propylene. The relevance of the error for the propylene-DIPE system and the water-DIPE system are unknown in light of the lack of experimental data for the former and the crossing of the liquid-liquid phase boundary by the same set of mixing parameters for the latter.

The water-DIPE data should only be used if one is certain that there is no phase split in the region of interest. Ideally, one would fit each phase of the water-DIPE data separately and then use an appropriate liquid-liquid phase model to correlate the mixing non-idealities. However, as mentioned in Section 2.1.1, a liquid-liquid phase split was

never observed, and consequently the aqueous and hydrocarbon-rich liquid data for this binary have been lumped together. The Wong-Sandler mixing rule is still able to represent the experimental data, though as can be seen, at a lower accuracy than for any of the other binaries.

Interestingly, the binary interaction parameters, the k_{ij}'s, seem to mirror the non-ideality of the mixture. The largest k_{ij}'s are those of the water-propylene and water-DIPE systems - the binaries one would expect to be the least ideal, whilst the more symmetric propylene-IPA and propylene-DIPE binaries have small values of the binary interaction parameter. Water-IPA, though, has the smallest binary interaction parameter even though one would expect significant mixing nonidealities due to the high polarity of both molecules. This ordering of the binary interaction parameters may be purely coincidental, though, in light of the presence of three other empirical mixing parameters.

2.3.1.3 Comparison of the Wong-Sandler and Wyczesany mixing rules

The binary predictions of the Wong-Sandler mixing rule used in conjunction with the PRSV equation of state were compared to the predictions of the Wyczesany mixing rule also used with the PRSV equation of state. The binary mixing parameters of the Wyczesany mixing rule did not have to be determined by regression of experimental data as those of the Wong-Sandler rule had to, since they had already been measured for the relevant binaries in the DIPE system [39].

Wyczesany [39] showed that his mixing rule was capable of accurately correlating experimental data in the water-propylene-propane-IPA system with accuracies of the order of 5%. However, the data was fit to a narrow range of temperatures and pressures, corresponding to those at which propylene is hydrated industrially, between $104 - 137\,^{\circ}C$ and $35 - 103$ bar. At different temperatures and pressures from those at which the parameters were fit, this mixing rule may show significant deviations. For the comparison of the

mixing rules in Table 2.4, the parameters of the Wong-Sandler mixing rule were fit for the water-IPA and the water-propylene system **at the same** temperature and pressure as those at which Wyczesany fitted his parameters. Only these two sets of binary data could be shown, since no experimental data exists for a range of temperatures and pressure for any of the other four binaries in the system.

Table 2.4: Comparison of Wyczesany and Wong-Sandler mixing rules

Binary System	Conditions		Wyczesany Mixing Rule		Wong-Sandler Mixing Rule	
	T range [°C]	P range [bar]	x-error [%]	y-error [%]	x-error [%]	y-error [%]
Water-Propylene[1]	37.8	3.4 - 15.5	38.7	20.4	4.3	11.9
	71.1	5.2 - 29.3	3.9	19.1	5.7	3.4
	104.4**	10.3 - 103.4	11.8	35.9	6.8	5.0
	137.8	20.7 - 103.4	2.3	52.4	13.2	2.6
Water-IPA[2]	30	0.04 - 0.08	194.6	43.2	51.6	27.4
	82.3 - 100.0	1.01	36.8	5.8	17.4	10.4
	122.7 - 144.6	4.1	16.3	5.6	8.3	5.9
	150**	5.0 - 8.6	10.6	5.3	3.5	1.3
	200	15.7 - 26.1	9.4	2.3	2.5	0.7
	250	43.1 - 64.9	11.3	2.9	3.9	2.1

* average deviation $= \frac{1}{N}\sum_i \left|\frac{(\exp_i - calc_i)}{\exp_i}\right|$

**Conditions at which the parameters for the Wong-Sandler mixing rule were fit for comparison purposes

[1] Li and McKetta [81]

[2] Barr-David and Dodge [84], Udovenko and Mazanko [85]

Table 2.4 clearly shows that the Wong-Sandler mixing rule is not only better able to correlate the experimental data at the actual regression conditions than the Wyzcesany mixing rule, but is also better able to extrapolate to conditions far from the conditions at which the data were regressed. This is important for those systems where data is only available at 1 atmosphere. For the water-propylene data with mixing parameters regressed

at 104°C, the Wong-Sandler mixing rule is still able to predict phase data at 38°C (crossing the critical temperature) with an overall accuracy better than 10%. The mixing rule of Wyczesany is only able to predict the same data to an accuracy of approximately 25%. The same results are obtained for the water-IPA system for moderate extrapolations. However, it is obvious that even the Wong-Sandler mixing rule cannot extrapolate over too large ranges. When predicting water-IPA data at very low pressures (≈0.05 bar), it is only able to correlate data with an accuracy of the order of 30% with parameters fit to about 2% accuracy at 5 bar.

For interest, the predictive ability of the unmodified UNIFAC method for the liquid phase used in conjunction with the PRSV equation of state was examined for applicability to polar-apolar systems. It was found that UNIFAC over-predicted the propylene solubility in the aqueous liquid phase at 50 bar and 120 °C by over 1000%. Using UNIFAC a liquid phase propylene mole fraction of $1.19 \cdot 10^{-2}$ was predicted as opposed to the actual value of $1.14 \cdot 10^{-3}$. The accuracy of this prediction can be increased if one uses one of the recently developed modifications to the original UNIFAC model, such as the modifications of Larsen et al. [94]. However, the use of mixing rules with regressed parameters (where possible) remains more accurate.

A detailed discussion of the correlation of the models for each of the binary mixtures follows:

1. **Propylene-Water:** As was mentioned earlier, this is likely the most non-ideal system, being a mixture of an apolar, super-critical hydrocarbon and polar water. Even though this system is theoretically capable of forming a second propylene-rich liquid phase, this is only possible at temperatures and pressures which were not considered in this study. The model predictions of the propylene fraction in the liquid phase and the water fraction in the vapour phase are shown in Figures 2.7 and 2.8 respectively (the data at 138 °C was omitted for clarity). The parameters

of Wyczesany were reportedly [39] fitted over quite a narrow range of temperatures, 104 °C to 137 °C, and pressures, 35 to 103 bar, for the liquid phase only. The parameters used for the Wong-Sandler rule were fit over all the data points for both phases. Whilst the Wyczesany mixing rule with the PRSV equation of state predicts the liquid phase concentration very well at high temperature and pressure, it cannot do so for the liquid phase at low temperature (38 °C). Also, the Wyczesany mixing rule fails to predict the vapour phase fraction well at any temperature and pressure. The Wong-Sandler rule on the other hand predicts both the vapour- and the liquid-phase concentration accurately over the entire range of temperature and pressure. Even though this system is highly asymmetric, average deviations of only 8% for the liquid phase mole fraction and 5% for the vapour phase mole fraction were obtained.

2. **IPA-Water:** This is the only other binary system for which vapour-liquid equilibrium data exists for a wide range of temperatures and pressures. The correlation of the two mixing rules together with the PRSV equation of state is shown in Figure 2.9. As was the case for the propylene-water binary, the Wyczesany mixing rule is less capable of correlation over large ranges of temperature and pressure than the Wong-Sandler mixing rule. For both mixing rules deviations were smaller than for the propylene-water mixture due to the greater ideality of the binary.

3. **DIPE-Water:** The fit of the Wong-Sandler model to the experimental data is shown in Figure 2.10. The DIPE-water binary was one of the more problematic to model. This binary system could form up to three distinct phases: a vapour phase, an aqueous phase and a hydrocarbon-rich phase. To prevent the vapour-liquid equilibrium model from becoming overly complex it was decided to model this binary as though it did not undergo a liquid-liquid phase split. Whilst it is acknowledged that this is a poor assumption, it was considered acceptable in the present system, since the liquid-liquid phase split was never observed to occur

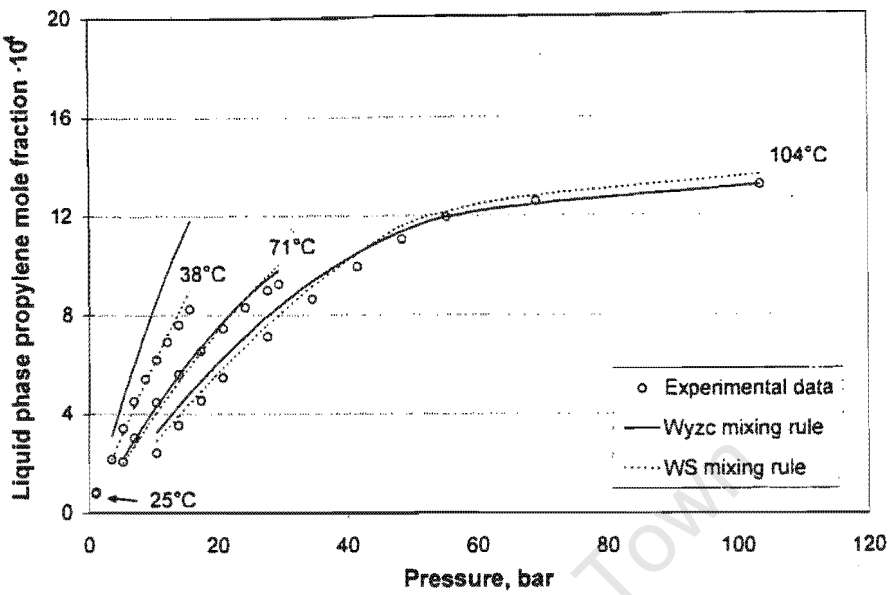

Figure 2.7: Comparison of the liquid-phase propylene mole fraction predictions of the PRSV equation of state with the Wong-Sandler (WS) or Wyzcesany (Wyzc) mixing rules to experimental data of the propylene-water binary.

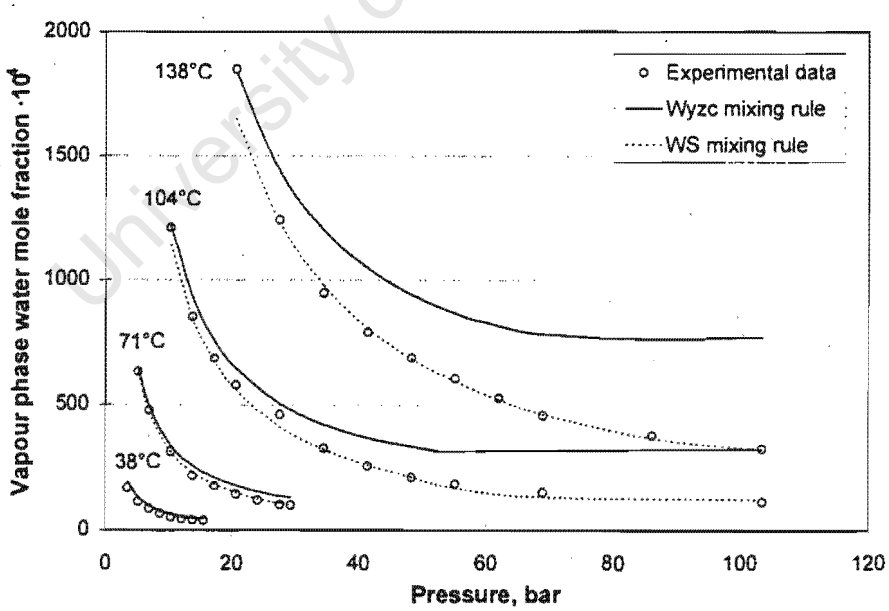

Figure 2.8: Comparison of the vapour-phase water mole fraction predictions of the PRSV equation of state with the Wong-Sandler (WS) or Wyzcesany (Wyzc) mixing rules to experimental data of the propylene-water binary.

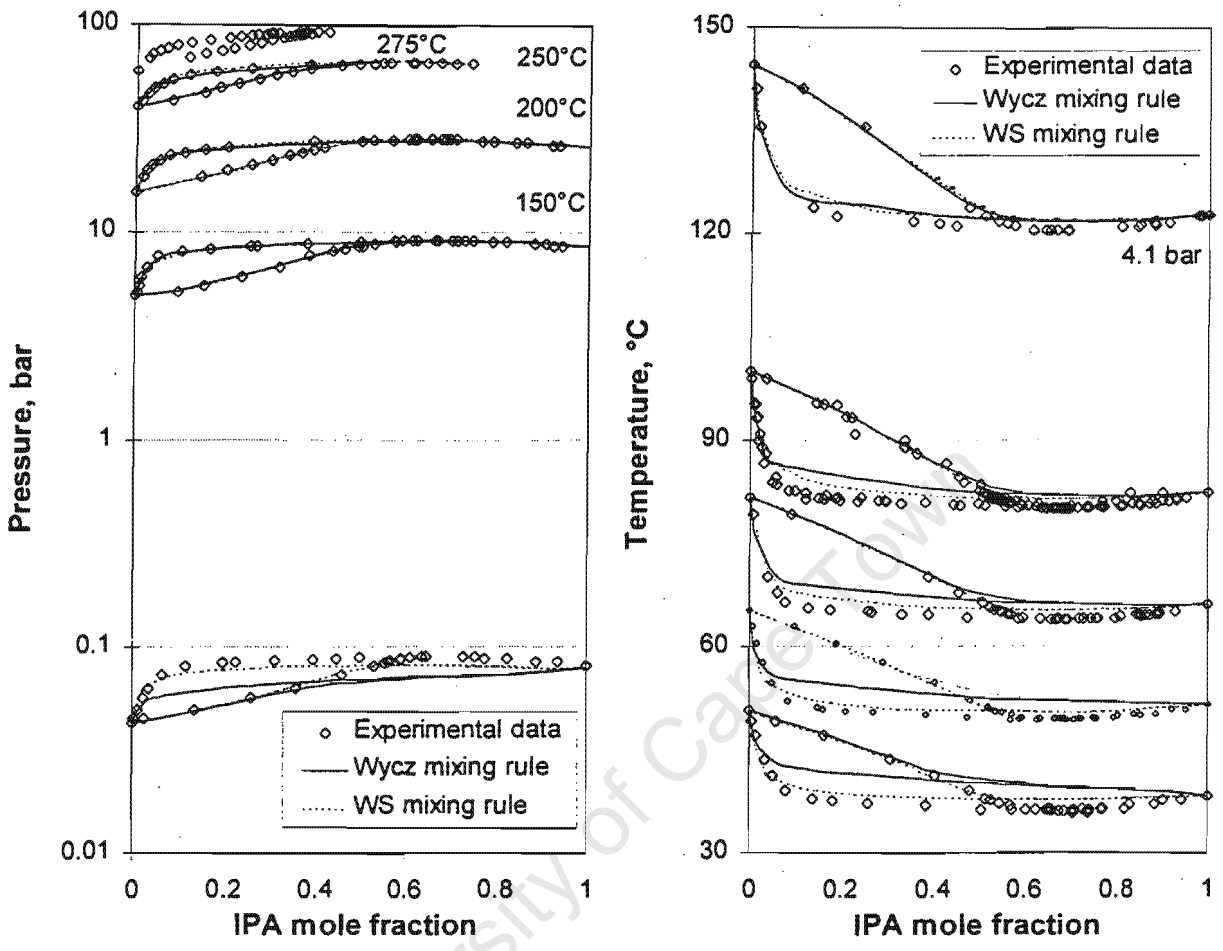

Figure 2.9: Comparison of the vapour-liquid mole fraction predictions of the PRSV equation of state with the Wong-Sandler (WS) or Wyzcesany (Wyzc) mixing rules to experimental data of the IPA-water binary.

under the experimental conditions examined in this study. It was found that the model could simultaneously correlate the mixing non-idealities of both liquid phases lumped together with no great loss in predictive accuracy. No comparison between the Wong-Sandler mixing rule and the Wyczesany mixing rule was possible for this or any other binary in which DIPE occurred, since the presence of ether was not considered in the system of Wyczesany [39] and, accordingly, no binary mixing parameters were regressed.

4. **Propylene-IPA:** Both the Wong-Sandler and the Wyczesany mixing rules were able to correlate the vapour-phase mole fractions with a high degree of accuracy. However, as was the case for the propylene-water and IPA-water binaries, the Wong-Sandler mixing rule was considerably better at predicting the liquid-phase mole fractions than the Wyczesany mixing rule over the temperature and pressure range for which experimental data had been measured (Figure 2.11). As compared to the previous water-organic binaries, vapour-liquid correlation in this system was significantly improved due to the greater ideality of the purely organic species mixture.

5. **Propylene-DIPE:** This was the only binary pair in the DIPE system for which no experimental data was available. However, as mentioned earlier, this system can be considered the most ideal of all the binaries since both compounds are organic and neither is strongly polar. This meant that vapour-liquid predictions from a model such as UNIFAC could be expected to be quite accurate, provided the temperature was below the super-critical temperature of propylene and the pressure was below 10 bar [45]. So-called "pseudo-experimental" data were predicted using the UNIFAC activity coefficient correlation and the PRSV equation of state, from which the Wong-Sandler mixing parameters were regressed. Since it had been shown that the Wong-Sandler mixing rule was capable of extrapolating non-ideal behaviour over large temperature and pressure ranges with no great loss in accuracy, parameters regressed at these conditions could be used to predict vapour-liquid equilibrium at DIPE synthesis conditions (120 °C and 50 bar). The UNIFAC-PRSV prediction and the Wong-Sandler correlation to this "data" are shown in Figure 2.12. Hardly surprisingly, the Wong-Sandler mixing rule predicted the pseudo-experimental data with a high degree of accuracy.

6. **IPA-DIPE:** The fit of the Wong-Sandler model to the binary data is shown in Figure 2.13. As is to be expected for a hydrocarbon-hydrocarbon system, the model fits the experimental data very well.

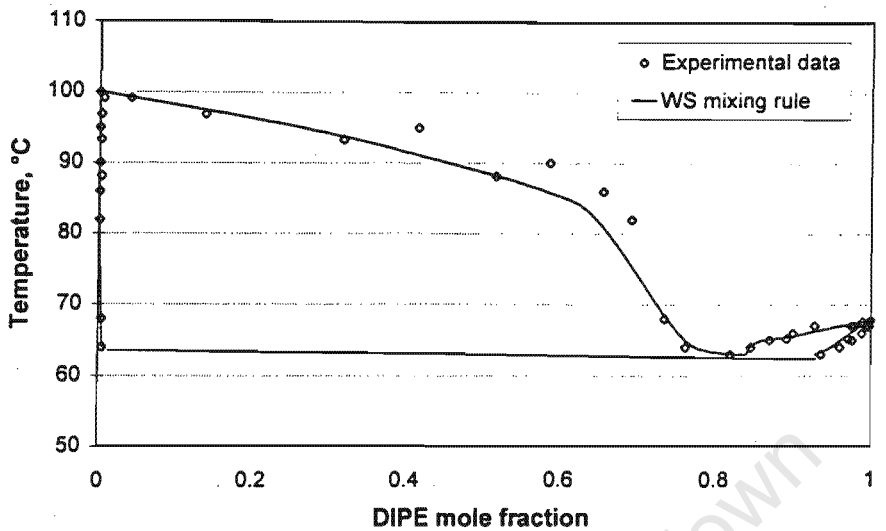

Figure 2.10: Comparison of the vapour-liquid mole fraction predictions of the PRSV equation of state with the Wong-Sandler (WS) mixing rule to experimental data of the DIPE-water binary.

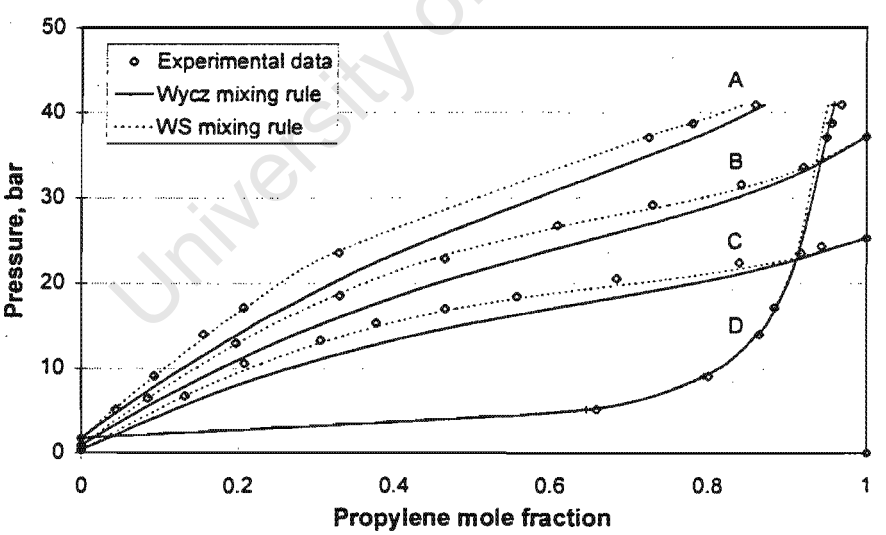

Figure 2.11: Comparison of the vapour-liquid mole fraction predictions of the PRSV equation of state with the Wong-Sandler (WS) or Wyzcesany (Wyzc) mixing rules to experimental data of the propylene-IPA binary. (A) Liquid phase, 97°C, (B) liquid phase, 80°C, (C) liquid phase, 60°C, (D) vapour phase, 97°C.

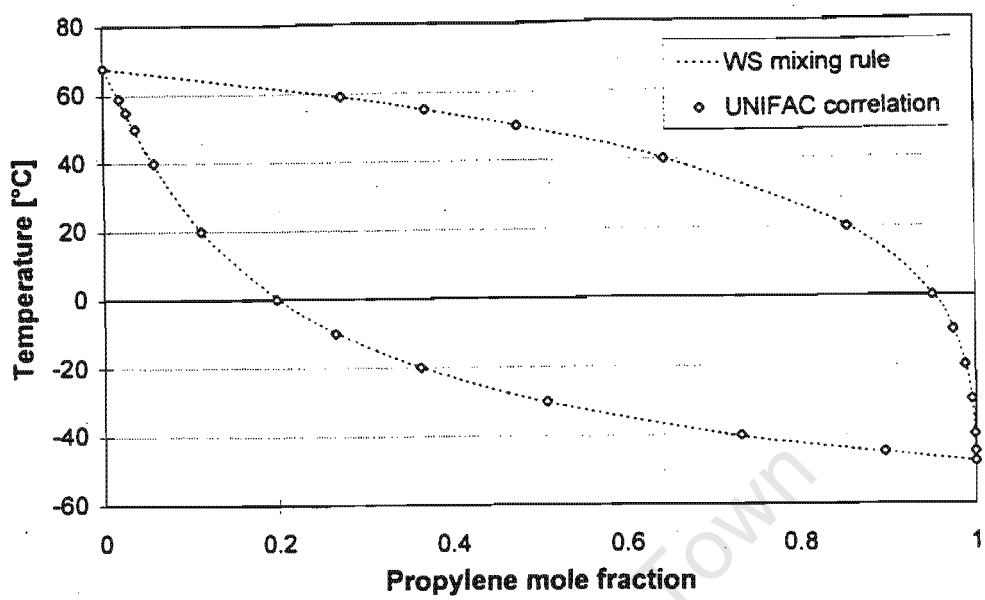

Figure 2.12: Correlation of the PRSV equation of state with the Wong-Sandler mixing rule (WS) to predictions of UNIFAC with the PRSV equation of state for the propylene-DIPE binary.

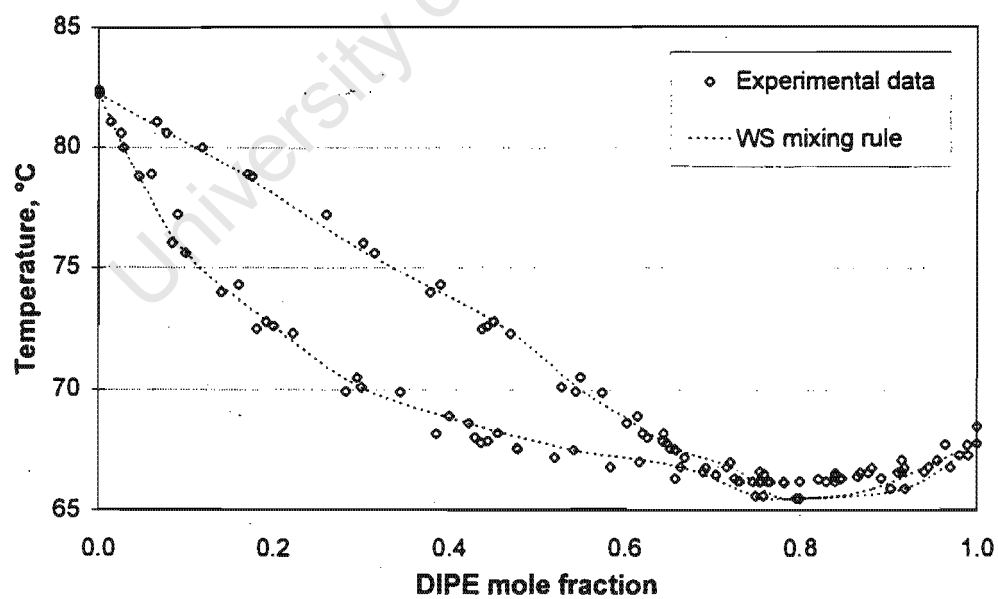

Figure 2.13: Comparison of the vapour-liquid mole fraction predictions of the PRSV equation of state with the Wong-Sandler (WS) mixing rule to experimental data of the IPA–DIPE binary.

2.3.2 Simultaneous chemical and phase equilibrium in the DIPE system

Chemical reaction equilibrium in the DIPE system was predicted using the theory of Section 2.2.4. Considering only the hydration and etherification reactions and ignoring any side reactions such as oligomerisation, only three chemical equilibrium reactions need be considered. These are the reaction of water (W) with propylene (P) to form IPA (A), the alkylation of IPA with propylene to form DIPE (E) and the bimolecular dehydration of IPA to form ether and water, i.e.

$$\begin{aligned} 1.\quad & P + W \iff A \\ 2.\quad & P + A \iff E \\ 3.\quad & A + A \iff E + W \end{aligned} \tag{2.82}$$

The equilibrium constants in terms of activities, for these reactions, can now be defined according to Eq. 2.70 as

$$K_{a,1} = \frac{a_A}{a_P a_W} \tag{2.83}$$

$$K_{a,2} = \frac{a_E}{a_P a_A} \tag{2.84}$$

$$K_{a,3} = \frac{a_E a_W}{a_A^2} \tag{2.85}$$

Only two of these equilibrium constants need be determined for calculations since

$$K_{a,1} K_{a,3} = K_{a,2} \tag{2.86}$$

From Eq. 2.72 the values of the chemical equilibrium constants could be calculated for a range of temperatures. It was found that the theoretical predictions of the chemical

equilibrium constant for hydration, $K_{a,1}$, varied significantly depending on which thermophysical database was used. Three of the databases gave very similar values for the equilibrium constant, whilst the values calculated from the data of Sandler [45] deviated substantially. The greatest difference in the databases lay in the value of the Gibbs free energy of formation for IPA. Whilst Daubert and Danner [62], Coulson et al. [63] and Stull et al. [65] gave a value of -173.5 $kJ/mol \pm 0.1\%$ and obtained their data from a large variety of sources, Sandler [45] reported a value of $-159.9\, kJ/mol$.

To determine the extent to which the WS-PRSV vapour-liquid equilibrium model could be used for the multi-component system, experimental chemical equilibrium data from literature in the form of concentration- or partial pressure-based equilibrium constants for both the hydration and etherification reactions was recalculated in terms of activities by the model. The theoretical chemical equilibrium constant calculations from the different property databases along with the recalculated values of the chemical equilibrium constants from literature are shown in Figure 2.14 and Figure 2.15.

As mentioned previously, the value of the chemical equilibrium constant for hydration predicted from thermophysical data varies depending on the data source used. However, since the chemical equilibrium predictions from three of the sources [62, 63, 65] almost coincided and agreed well with literature, one can accept that the pure component properties from Sandler [45], in particular the reported value of the Gibbs free energy of formation for IPA are incorrect. One cannot discriminate between the other three sets of thermophysical data.

It can be seen that the values of the chemical equilibrium constant predicted from theory and the recalculations of the experimental data of Cope [36], Izumi [50], Majewski and Marek [46], Petrus et al. [47], Schiffler et al. [52] and Stanley et al. [51] using the WS-PRSV model give excellent agreement. The equilibrium correlation of Izumi [50] can be seen to deviate substantially from both the experimental data and the theoretical predictions for temperatures above 280 °C and below 80 °C. However, as mentioned pre-

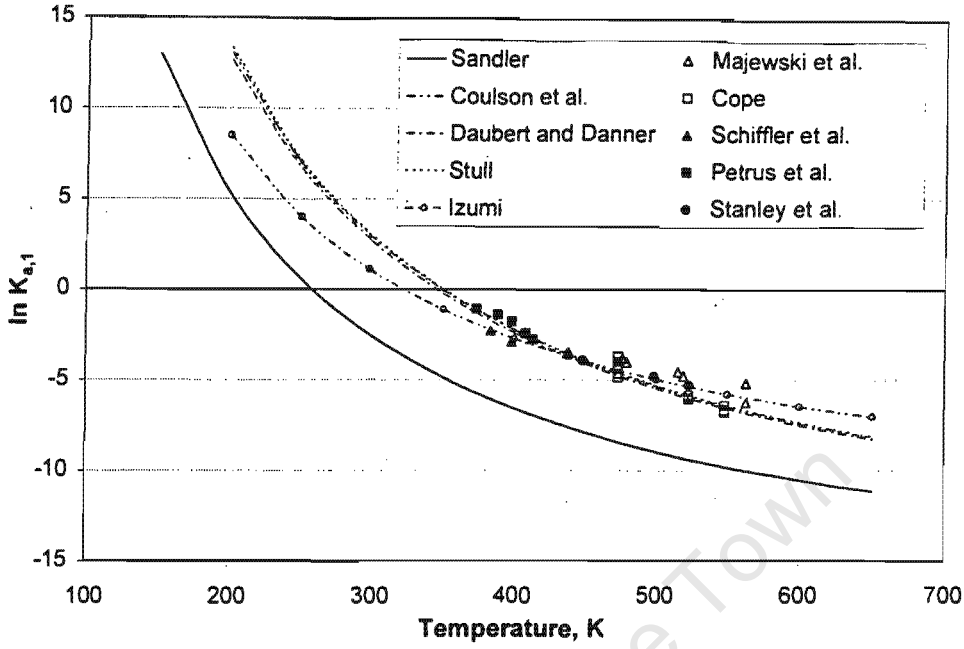

Figure 2.14: Comparison of literature and theoretical chemical equilibrium for the hydration of propylene.

viously, one must bear in mind that this correlation was purely an empirical fit to limited experimental data and should not be used outside of the range of data to which it was fit, i.e. between 115°C and 275°C.

As for hydration chemical equilibrium, recalculation of etherification experimental equilibrium data from Petrus et al. [47] and Cope [36] using the Wong-Sandler mixing rule together with the PRSV equation of state resulted in excellent agreement with theoretical equilibrium predictions. Once again, theoretical predictions using data from different thermophysical data sources gave slightly different predictions for the chemical equilibrium constant. This time, however, the deviation between the three sets of predictions is not so large that one can discriminate, especially in view of the lack of experimental data and the inherent scatter. Theoretical predictions of $K_{a,1}$ and $K_{a,2}$ from the pure component data of Sandler [45] could not be calculated as the Gibbs free energy of formation of DIPE was not given.

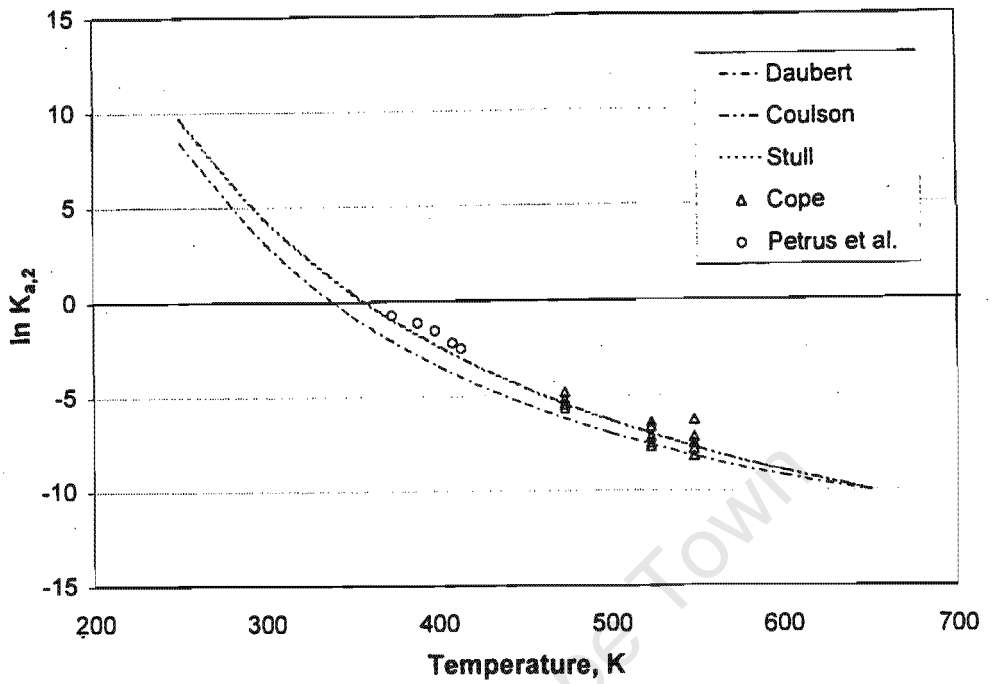

Figure 2.15: Comparison of literature and theoretical chemical equilibrium for the alkylation of propylene and isopropanol.

It is known that the natural logarithm of the chemical equilibrium constant has an almost linear dependence on the reciprocal temperature. To facilitate calculation of the value of the chemical equilibrium constants, linear fits, with a correlation coefficient of 1.000 in every case, of the chemical equilibrium constant (between 0 and 300°C) determined from the data of Daubert and Danner [62] gave the following three equations in terms of K_a,

$$K_{a,1} = \exp\left(\frac{6097}{T} - 17.76\right)$$

$$K_{a,2} = \exp\left(\frac{7992}{T} - 22.28\right) \tag{2.87}$$

$$K_{a,3} = \exp\left(\frac{1795}{T} - 4.521\right)$$

2.3.3 Error analysis of the WS-PRSV model

It was shown in Section 2.3.1.2 that the error in predicting the mole fractions of species in binary mixtures in the DIPE system ranged from 1% for the propylene-DIPE binary to 9% for the water-DIPE binary. Unfortunately, the error of the WS-PRSV model in predicting ternary or quaternary mixture behaviour could not be determined due to a lack of multicomponent vapour-liquid equilibrium data. It is known that the so-called "mixture-effect" essentially "dilutes" system non-idealities and thus predictions of multi-component systems are comparatively more accurate than the predictions of binary systems [95]. Qualitatively, this was shown by Wyczesany [39] for the water-ethylene-ethanol system where multicomponent chemical equilibrium and phase equilibrium predictions showed better correlation with experimental data than some of the binary systems. For the DIPE system, however, literature chemical equilibrium data is available and this allows a quantitative estimate of the maximum error in multicomponent system predictions.

The squared fractional error in a dependent variable Ω, which is a function of independent variables $\alpha_1 ... \alpha_m$ is given by [96]

$$\left(\frac{\Delta\Omega}{\Omega}\right)^2 = \sum_{i=1}^{m}\left[\left(\frac{\partial(\ln\Omega)}{\partial(\ln\alpha_i)}\right)^2\left(\frac{\Delta\alpha_i}{\alpha_i}\right)^2\right] \tag{2.88}$$

Now, the chemical equilibrium constant K_a is defined by

$$K_a = \prod_i (a_i)^{\nu_i} = \frac{a_1^{\nu_1} a_2^{\nu_2} ...}{a_3^{\nu_3} a_4^{\nu_4} ...} \tag{2.89}$$

such that

$$\ln K_a = \nu_1 \ln a_1 + \nu_2 \ln a_2 - \nu_3 \ln a_3 - \nu_4 \ln a_4 + ... \tag{2.90}$$

and the squares of the partial derivatives of $\ln K_a$ with respect to $\ln a_i$ are

$$\left(\frac{\partial(\ln K_a)}{\partial(\ln a_1)}\right)^2 = \nu_1^2 \tag{2.91}$$

$$\left(\frac{\partial(\ln K_a)}{\partial(\ln a_2)}\right)^2 = \nu_2^2 \tag{2.92}$$

$$\left(\frac{\partial(\ln K_a)}{\partial(\ln a_3)}\right)^2 = \nu_3^2 \tag{2.93}$$

$$\left(\frac{\partial(\ln K_a)}{\partial(\ln a_4)}\right)^2 = \nu_4^2 \tag{2.94}$$

The fractional error in the chemical equilibrium constant thus equals

$$\left(\frac{\Delta K_a}{K_a}\right)^2 = \nu_1^2\left(\frac{\Delta a_1}{a_1}\right)^2 + \nu_2^2\left(\frac{\Delta a_2}{a_2}\right)^2 + \nu_3^2\left(\frac{\Delta a_3}{a_3}\right)^2 + \nu_4^2\left(\frac{\Delta a_4}{a_4}\right)^2 \tag{2.95}$$

so that, for the three relevant reactions in the DIPE system, it can be shown that

$$\left(\frac{\Delta K_{a,1}}{K_{a,1}}\right)^2 = \left(\frac{\Delta a_P}{a_P}\right)^2 + \left(\frac{\Delta a_W}{a_W}\right)^2 + \left(\frac{\Delta a_A}{a_A}\right)^2 \tag{2.96}$$

$$\left(\frac{\Delta K_{a,2}}{K_{a,2}}\right)^2 = \left(\frac{\Delta a_P}{a_P}\right)^2 + \left(\frac{\Delta a_A}{a_A}\right)^2 + \left(\frac{\Delta a_E}{a_E}\right)^2 \tag{2.97}$$

$$\left(\frac{\Delta K_{a,3}}{K_{a,3}}\right)^2 = \left(\frac{\Delta a_E}{a_E}\right)^2 + \left(\frac{\Delta a_W}{a_W}\right)^2 + 4\left(\frac{\Delta a_A}{a_A}\right)^2 \tag{2.98}$$

Thus, if one has an estimate of the size of the error in the calculation of the chemical equilibrium constant by the WS-PRSV model, one can estimate the average size of the error in the calculation of species activity. Given literature chemical equilibrium mole fractions and applying the WS-PRSV model to calculate the activities of each of the species in the system, one can determine the value of the chemical equilibrium constant as calculated by the WS-PRSV model. Assuming that the literature mole fractions, temperature and pressure are accurate one can compare this value of the chemical equilibrium constant to the theoretical value calculated at the same temperature via the standard Gibbs free energy of reaction. This method allows an estimate of the size of the error

inherent to activity calculations by the WS-PRSV model in multicomponent mixtures in the DIPE system.

The chemical equilibrium data of Cope [36], Majewski and Marek [46], Petrus et al. [47], Schiffler et al. [52] and Stanley et al. [51] were recalculated using the model. The relative error in the calculation of the chemical equilibrium constant by the model was defined as

$$\frac{\Delta K_a}{K_a} = \frac{|K_{a,WS-PRSV} - K_{a,theo}|}{K_{a,theo}} \tag{2.99}$$

Figures 2.16 and 2.17 show the squared relative errors in the chemical equilibrium constant as a function of system temperature and pressure. The random scatter over the entire range of temperature and pressure shows that there was no systematic error in the calculation of the species activities by the WS-PRSV model, i.e. the error neither increased nor decreased in direct response to a change in one of the system parameters. It is likely that there were experimental errors inherent to the measurement of the chemical equilibrium data taken from literature, and that these errors were included in the calculation of the fractional error in the chemical equilibrium constant. However, the error in experimental measurement should be random and any significant systematic deviations of the model with temperature or pressure should be superimposed over the experimental error.

The error in individual species activity could not be calculated. However, assuming similar errors in the calculation of the activities of all species, the *average* errors in species activity could well be calculated and these, together with the average errors in the chemical equilibrium constant calculations, are shown in Table 2.5.

As mentioned above, this estimate of the accuracy of prediction of the WS-PRSV model necessarily incorporates the experimental error in determining the chemical equilibrium composition and the error in the theoretical calculation of $K_{a,i}$. This means that the average error in activity is also inflated by both the error in the experimental chem-

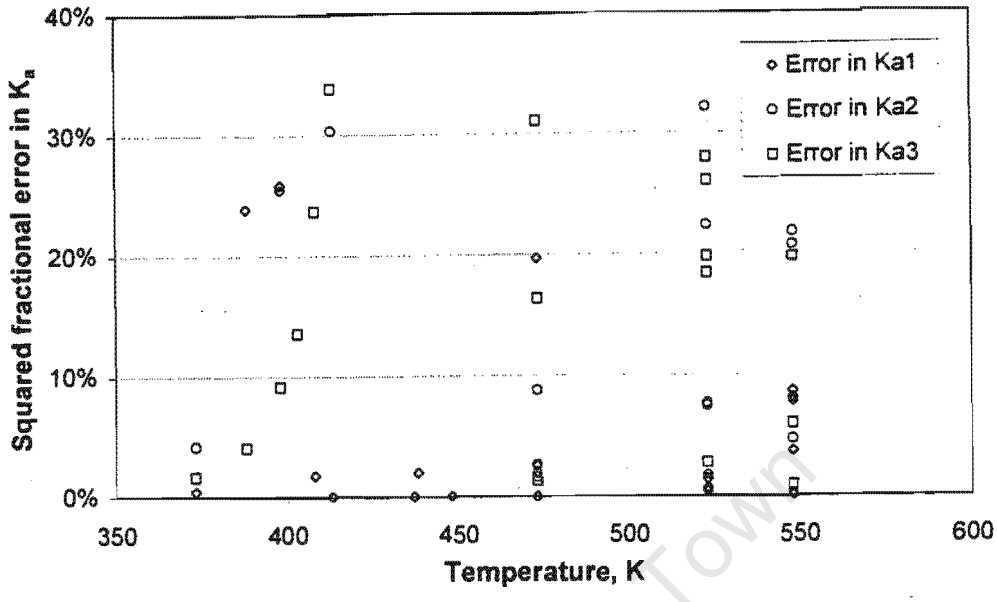

Figure 2.16: Squared fractional error in the recalculation of literature experimental chemical equilibrium data using the WS-PRSV model as compared to the theoretical value. Variation with temperature.

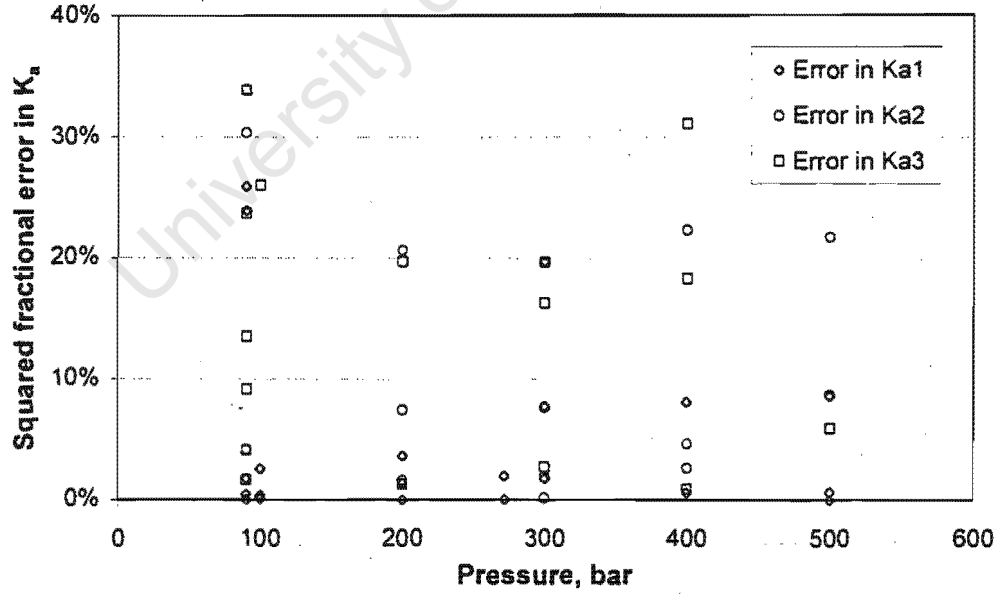

Figure 2.17: Squared fractional error in the recalculation of literature experimental chemical equilibrium data using the WS-PRSV model as compared to the theoretical value. Variation with pressure.

Table 2.5: Average error in prediction of chemical equilibrium constant and species activity using the WS-PRSV model

Reaction	Average error in $K_{a,i}$	Average error in a_i
1	7.0%	4.0%
2	10.1%	5.9%
3	12.6%	5.1%

ical equilibrium composition obtained from literature and by the error in the theoretical calculation of $K_{a,i}$. Nevertheless, at least over the temperature and pressure range of the literature data ($95 - 275\,°C$ and $90 - 500\,bar$) it can be assumed that the WS-PRSV model calculates activities, and thus also vapour-liquid equilibrium mole fractions with an accuracy better than 6%.

Given accurate chemical equilibrium mole fractions, temperatures and pressures, the value of the activity based chemical equilibrium constant can be calculated with an error smaller than 13%, relative to literature predictions, by the WS-PRSV model. It thus not only predicts binary mixing behaviour accurately but also predicts multicomponent mixing behaviour accurately.

2.3.4 Range of applicability of the WS-PRSV model

While most models are only valid over the range of conditions where parameters were estimated and any extrapolation outside these regions is risky, it has been demonstrated that the WS-PRSV model is quite capable of extrapolation over large ranges of temperature and pressure without great losses in accuracy. Restrictions do however, exist. A number of assumptions were made in deriving the WS-PRSV model. The most important of these were that the system never forms a second liquid phase and that the "pseudo-experimental" data used for estimating the propylene-DIPE binary interaction parameters represents the real binary mixture accurately.

Besides the fact that very limited liquid-liquid phase data was available, it was decided to model the system as a purely vapour-liquid one to facilitate the calculation of phase equilibrium and to improve the accuracy of prediction. It is known, however, that both the water-propylene [81] and the water-DIPE [89, 90] binary mixtures can form two liquid phases. Liquid-liquid phase separation only occurs in the water-propylene binary at sub-critical temperatures (i.e. below 92 °C) and only occurs in water-DIPE mixtures if no co-solvent is present. In this study the temperature was always greater than the critical temperature of propylene and, whenever water and DIPE were present in a mixture to any significant extent, a co-solvent (in this case IPA) was also present. In another system, should this not be the case, the model may not strictly apply.

No experimental vapour-liquid equilibrium data was found in literature for the propylene-DIPE binary. So that the model could be used for mixtures in which both of these components were present, it was necessary to estimate the values of the binary interaction parameters from predicted vapour-liquid equilibrium data. As has been described previously (Section 2.3.1.3), the UNIFAC activity coefficient correlation was used to estimate the liquid phase interactions. The pressure chosen for calculation of the pseudo-experimental data was 1 atm, so the vapour phase was be assumed to be ideal. While this mixture can be expected to show minimal deviations from ideal mixing behaviour as both compounds are organic and neither is strongly polar, experimental data would nonetheless be required to prove this.

An additional limitation must be placed on the model. It has been observed by Berecz and Balla-Achs [97] that propylene hydrates form at temperatures below 10 °C. This phenomenon, naturally, has not been incorporated into the model. Any use of the model for mostly propylene-water systems at temperatures below 10°C could thus lead to highly inaccurate calculations.

In summary, the WS-PRSV model can thus be used with confidence for the DIPE system unless:

- the temperature is below 10°C in systems where propylene and water predominate,
- no co-solvent is present in systems where water and propylene, water and DIPE or water, propylene and DIPE occur simultaneously,
- the temperature is less than 92 °C if no co-solvent is present in a system where water and propylene predominate.

Barring any of the above situations, errors in the multi-component prediction of the species activity, as shown in Section 2.3.3, and consequently in species mole fraction for the DIPE system can be expected to be smaller than 6% over temperature and pressure ranges of $10 - 250\,°C$ and $1 - 500$ bar.

2.3.5 Phase and yield predictions for system parameters

Using the WS-PRSV model and the algorithm described in Section 2.4, one can now predict the equilibrium yield of DIPE and the equilibrium phase distribution for any given set of temperature, pressure and propylene to water ratio. The resulting yield and phase equilibrium predictions are shown in Figures 2.18 and 2.19 respectively for temperatures between 0 and 300 °C and pressures between 1 and 300 bar at a propylene to water ratio of 2 : 1, stoichiometric for DIPE formation. The mole fraction of DIPE at chemical equilibrium is shown as a function of temperature and propylene to water ratio at a pressure of 50 bar in Figure 2.20. Selected values of the DIPE yield, the molar distributions and the liquid phase mole fraction are given in Appendix E.

The DIPE yield is strongly affected by the reaction pressure and temperature. The synthesis of IPA and DIPE involves a contraction in the number of moles in the system. Hence, at low pressure the reactants propylene and water are thermodynamically favoured, whilst at high pressure the reaction products IPA and especially DIPE are favoured. The

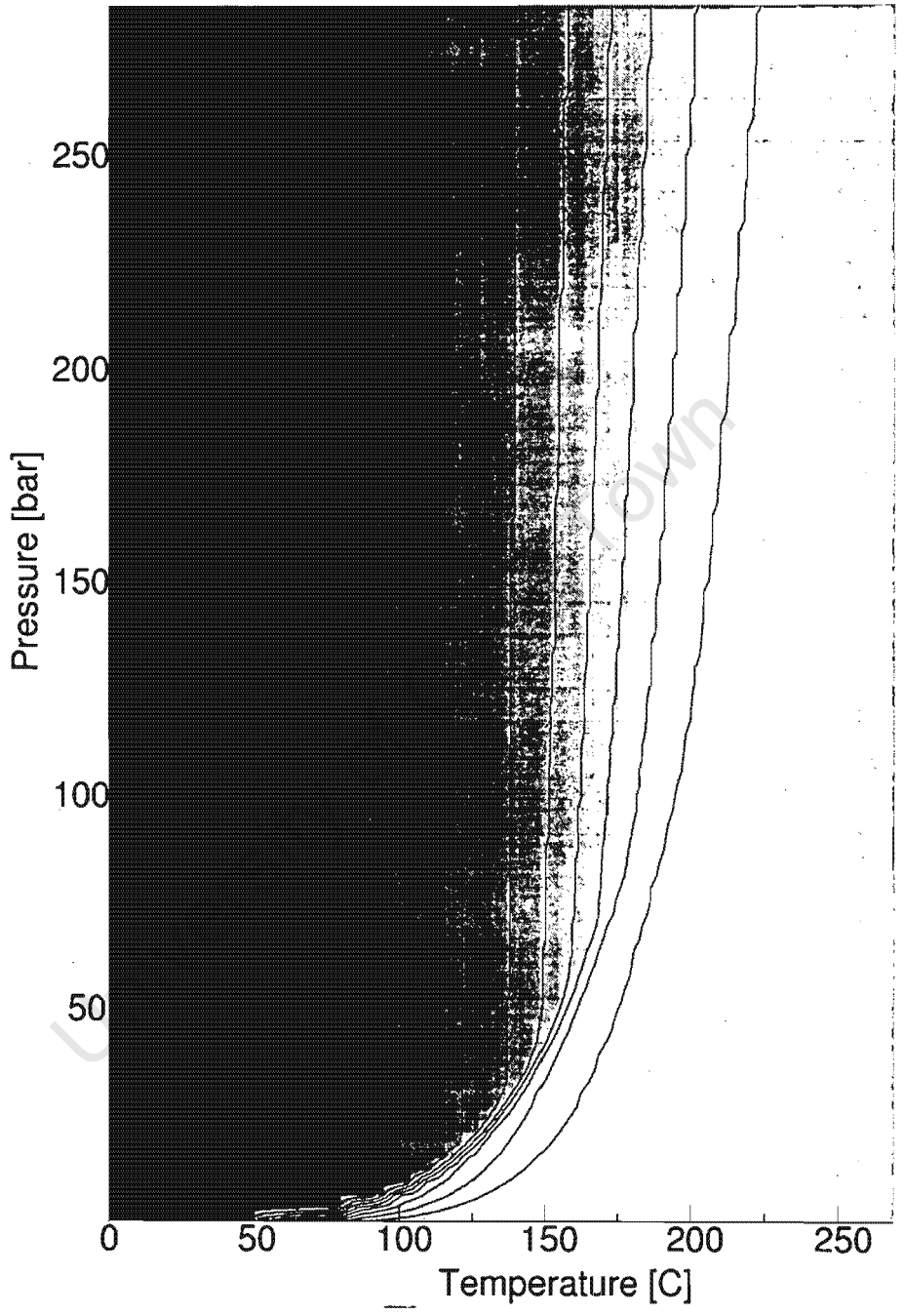

Figure 2.18: Predicted diisopropyl ether yield at chemical and phase equilibrium. Lightest grey represents 0% yield, graduations increase in 10% increments up to almost 100% DIPE yield at darkest shading.

Figure 2.19: Predicted phase conditions of diisopropyl ether synthesis at chemical and phase equilibrium. Lightest grey represents 0% liquid, graduations increase in 10% increments up to almost pure liquid at darkest shading.

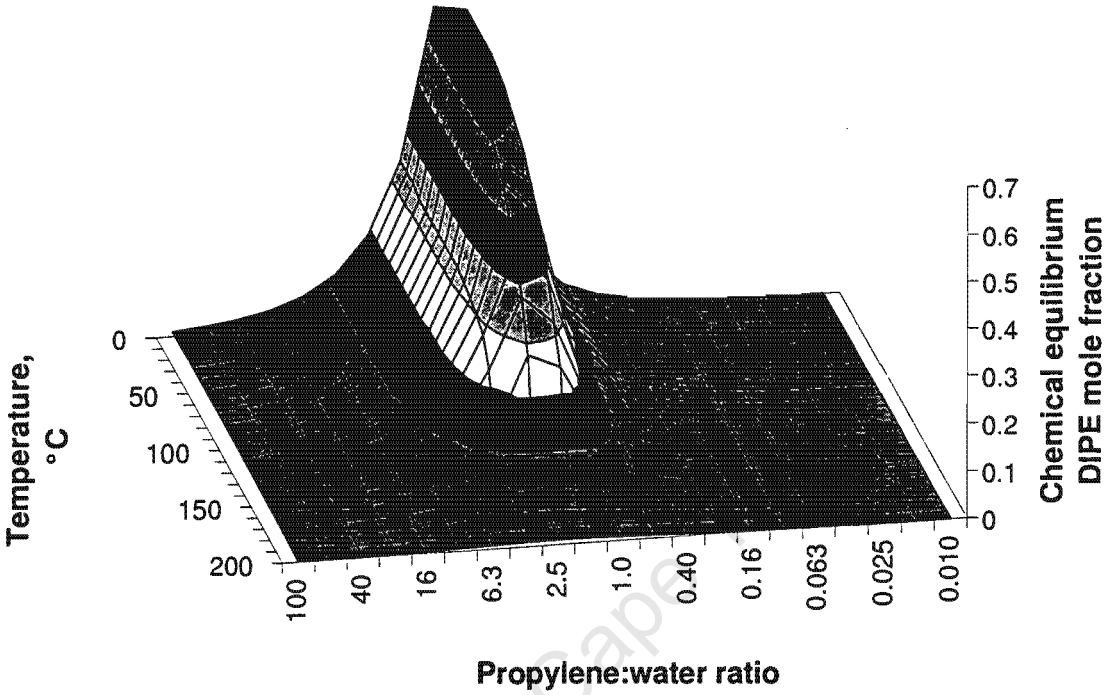

Figure 2.20: Predicted DIPE mole fraction at chemical equilibrium for changing propylene to water mole ratio and system temperature at a pressure of 50 bar.

hydration and etherification reactions are exothermic. Consequently, high temperatures favour propylene and water, whilst low temperatures favour IPA and DIPE formation.

As expected, at low temperature and high pressure the equilibrium DIPE system is practically pure liquid, as these conditions favour product formation (IPA and DIPE formation). The opposite is true at high temperature and low pressure. Interestingly, one can observe retrograde behaviour in the DIPE system. At a temperature of 100 °C, for example, pressures below 7 bar ensure the system is completely vapour phase. As the pressure is increased beyond this value, liquid begins to appear until, at 10 bar, the system is practically pure liquid phase. However, once the pressure exceeds 77 bar, vapour begins to appear once more. This type of behaviour has been observed before in even very simple systems such as ethane-heptane [45]. Whether, in this case, the retrograde behaviour

is an artefact of the model or represents real behaviour is not known, and would require additional experimental data to confirm.

The greatest yield of DIPE relative to the total number of moles in the system is always obtained at the stoichiometric ratio for DIPE formation, i.e. a propylene:water ratio of 2 : 1. Any overall system propylene:water ratio above or below this ratio results in a significant decrease in the equilibrium DIPE yield.

2.3.6 Predictions of the heat of reaction using the WS-PRSV model

The heat of reaction of a particular reaction in the ideal gas phase at a given temperature need not be the same as the heat of reaction of the same reaction in a non-ideal mixture, especially if the reaction takes place in a different phase. Solá et al. [33] studied the initial heat of reaction of MTBE in the liquid phase and obtained a reaction enthalpy of -34 kJ mol^{-1} for reaction between methanol and isobutylene at 25 °C and 10 bar. In comparison, the ideal gas heat of reaction for the reaction between methanol and isobutylene at 25 °C is -39 kJ mol^{-1}. No studies examining different molar compositions or examining any of the reactions occurring in the DIPE system were found in the literature.

The heats of reaction of the three reactions presumed to occur in the DIPE system can be calculated from the partial molar enthalpies of the species taking part in the reaction from

$$\Delta\overline{H}^*_{rxn,1} = \overline{H}^*_A(T,P,x_i) - \overline{H}^*_P(T,P,x_i) - \overline{H}^*_W(T,P,x_i) \tag{2.100}$$

$$\Delta\overline{H}^*_{rxn,2} = \overline{H}^*_E(T,P,x_i) - \overline{H}^*_P(T,P,x_i) - \overline{H}^*_A(T,P,x_i) \tag{2.101}$$

$$\Delta\overline{H}^*_{rxn,3} = \overline{H}^*_E(T,P,x_i) + \overline{H}^*_W(T,P,x_i) - 2\overline{H}^*_A(T,P,x_i) \tag{2.102}$$

Now, it has been shown [45] that the partial molar enthalpy of a component in a mixture is related to its partial molar fugacity, its mole fraction, its partial molar ideal gas mixture enthalpy and the system pressure and temperature by

$$\left(\frac{\partial \ln\left(\frac{f_i^*}{x_i P}\right)}{\partial T}\right)_{P,x_i} = -\frac{\overline{H}_i^* - \overline{H}_i^{*,IGM}}{RT^2} \tag{2.103}$$

thus

$$\overline{H}_i^* = \overline{H}_i^{*,IGM} - RT^2 \left(\frac{\partial \ln\left(\frac{f_i^*}{x_i P}\right)}{\partial T}\right)_{P,x_i} \tag{2.104}$$

The partial molar enthalpy of each species in an ideal gas mixture is equivalent to the molar enthalpy of the ideal gas of that species and may be calculated from correlations given in literature [62], whilst the partial derivative term can be obtained from any phase equilibrium model which applies at the temperature, pressure and phase of interest. In the present system, the partial derivative term may thus be obtained from the WS-PRSV model. The heat of reaction for the three reactions presumed to occur in the DIPE system are given in Table 2.6 for ideal gas and liquid phase reactions at various temperatures. Figure 2.21 shows the heat of reaction for the three reactions as a function of the approach to chemical equilibrium in the DIPE system starting from a feed of propylene and water in a 2:1 molar ratio at a temperature of 120 °C and 50 bar.

Table 2.6: The heat of reaction of propylene hydration, IPA alkylation and bimolecular dehydration of IPA under ideal gas (IG) conditions and at initial and chemical equilibrium process conditions

	Heat of reaction, kJ mol^{-1}				
Reaction	IG, 25 °C	IG, 120 °C	2:1*, 100 °C	2:1*, 120 °C	2:1*, 140 °C
Propylene hydration	-47.7	-50.8	-53.9	-34.5	-31.0
IPA alkylation	-64.8	-65.8	-92.1	-79.1	-77.9
IPA dehydration	-17.1	-15.0	-38.2	-44.6	-46.9

* At a pressure of 50bar and a propylene:water molar ratio of 2:1, liquid phase reaction

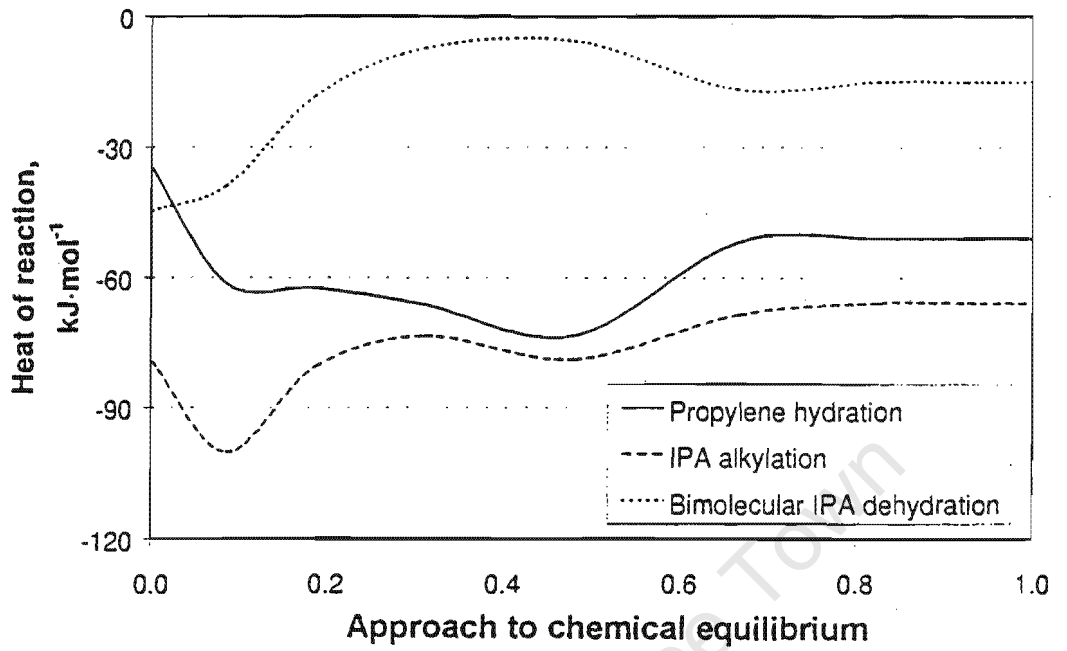

Figure 2.21: The heat of reaction of propylene hydration, IPA alkylation and bimolecular IPA dehydration as a function of the approach to chemical equilibrium in the DIPE system, starting from a feed of propylene and water in a 2:1 mole ratio at a temperature of 120 °C and 50 bar.

Regardless of the phase in which the reaction is taking place, all three reactions are exothermic. The heat of reaction is not a strong function of temperature for the ideal gas. For the high pressure liquid phase reaction, on the other hand, it is very sensitive to temperature. The reaction enthalpy of the propylene hydration reaction, for example, increases from -53.9kJ mol^{-1} at 100 °C to -31.0kJ mol^{-1} at 140 °C. The heat of reaction was also found to be a strong function of the mixture composition due to the large thermodynamic non-idealities in the asymmetric liquid phase. As one approaches chemical equilibrium starting from a mixture of propylene and water in a 2 : 1 molar ratio at 120 °C and 50 bar, the heat of reaction of the propylene hydration reaction varies between -34.5kJ mol^{-1} and -73.4kJ mol^{-1} before stabilising at -50.9kJ mol^{-1} at chemical equilibrium (see Figure 2.21). These strong variations with temperature would obviously have to be accounted for in any reactor design.

Chapter 3

Catalytic DIPE synthesis

3.1 Introduction

3.1.1 Background

Since DIPE is a symmetric dialkyl ether it possesses the unique property, in contrast to the other octane enhancing ethers, that it can be synthesised directly from only an olefin and water. The reactions first to produce the alcohol (IPA) and then, in a further reaction step, to produce DIPE are acid catalysed and can, with the correct tailoring of process conditions, be made to occur within one catalyst bed. To take advantage of this property of DIPE one thus needs to find a catalyst capable of promoting both the hydration and the etherification reactions.

Conventionally, the hydration of propylene to IPA was carried out in a two-step process, the so-called indirect hydration process. In the first step propylene was dissolved in concentrated sulphuric acid which led to the formation of propylene monosulphate. In a second step excess water was added to the acid mixture to hydrolyse the sulphate, yielding IPA. This process had several serious drawbacks, the most pronounced being the corrosive nature of the homogeneous catalyst and the high cost of sulphuric acid recovery. These drawbacks were circumvented by the development of the direct hydration

of propylene over solid acid catalysts. Initially phosphoric acid on a porous support was used, but its lack of stability in aqueous media led to acidic ion exchange resin catalysts taking over as the catalyst of choice [47]. Figure 3.1 illustrates the reactions occurring in each process.

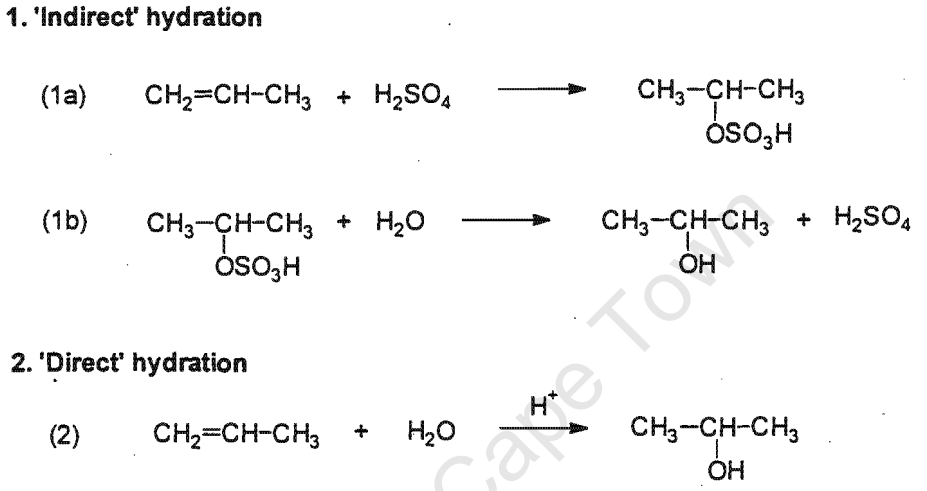

Figure 3.1: Indirect and direct hydration reactions of propylene

As previously stated in Section 1.3 very little process information is available in the open literature on DIPE synthesis though one would expect similar synthesis conditions as for the other octane enhancing ethers. The desired reaction is the ether formation reaction, i.e. the alkylation of the alcohol with the olefin which, in the case of MTBE for example, would be the reaction of methanol with isobutylene (Figure 3.2). As for the hydration reaction, it has been found that acidic ion exchange resins catalyse the alkylation reaction very efficiently. MTBE, ETBE and TAME are currently all synthesised exclusively over ion exchange resins.

Due to the industrial importance of hydration and etherification reactions, considerable research has been conducted into developing improved catalysts. Besides ion exchange resins, this has covered both homogeneous catalysts such as sulphuric and paratoluene sulphonic acid as well as heterogeneous catalysts such as zeolites and supported heteropoly

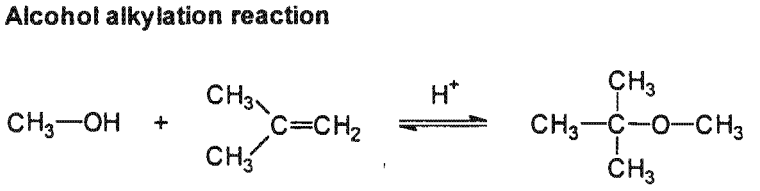

Figure 3.2: Alkylation of methanol with isobutylene to produce MTBE

acids (see Table 3.1). Although it has been demonstrated that some of these novel catalysts outperform conventional catalytic ion exchange resins in certain aspects, to date no catalyst has been developed which improves upon the combined selectivity, activity and lifetime performance of acidic ion exchange resin catalysts. Acidic ion exchange resins are thus the logical choice to perform the simultaneous hydration and etherification reactions required to produce DIPE from a feed of propylene and water within a single catalyst bed.

3.1.2 Ion exchange resins as solid acid catalysts

3.1.2.1 Background and catalytic applications of ion exchange resin catalysts

The industrial use of ion exchange resins covers a wide field and involves applications in the conversion and concentration of ionic species, purification and deionization, fractionation by ion exchange chromatography and of course in catalysis. The first practical applications and plant scale processes using ion exchange resins as catalysts were developed by I.G. Farben during World War II [111]. Today probably the largest consumer of ion exchange resins as catalysts is the petroleum refining industry.

Ion exchange resins can be functionalised in a number of ways, resulting in catalysts ranging from strongly basic to strongly acidic. The most common, however, is the strongly acidic sulphonic ion exchange resin catalyst. Acidic ion exchange resin catalysts are often used to promote chemical reactions normally catalysed by mineral acids and are

Table 3.1: Catalysts other than ion exchange resins studied for applicability in hydration and etherification

Author	Reaction	Catalyst
Hydration Reactions		
L. Fan et al. [98]	Tertiary butyl alcohol	SiO_2-TiO_2, Na_2MoO_4 and Pd/carbon
D. Kalló and R.M. Mihályi [99]	Isobutyl alcohol	H-Clinoptilolite
E.L. Purlee et al. [100]	Isobutyl alcohol	Aqueous nitric acid
M.H.W. Sonnemans [101]	IPA	Zeolites H-Y, H-Mor, H-ZSM-5 and ASA
K. Tao et al. [102]	IPA	H-β
Etherification Reactions		
S. Ahmed et al. [103]	MTBE	H-ZSM-5
A.M. Al-Jarallah et al. [104]	MTBE	Sulphuric acid
F. Ancillotti et al. [105]	Alcohol alkylation	p-Toluene sulphonic acid
K. Chang et al. [106]	MTBE	Titanium-silicalite I, H-ZSM-5
P. Chu and G.H. Kühl [107]	MTBE	H-Y, H-ZSM-11, H-β and H-Mor
A. Nikolopoulos et al. [108]	MTBE	amorphous silica alumina and H-Y
S. Shikata et al. [109]	MTBE	Heteropolyacids on silica
M.H.W. Sonnemans [110]	Methyl isopropyl ether	H-ZSM-5

well established as economical catalysts in a wide spectrum of industrial processes. This type of resin has been, amongst others, used for alkylation, condensation, dehydration, etherification, esterification, hydration, hydrolysis, isomerisation and polymerisation reactions. Table 3.2 gives an outline of some of the reactions catalysed by ion exchange resins [112]. The table shows the type of reaction, its application and the structure of the resin used.

3.1.2.2 Structure of polymeric ion exchange resin catalysts

Ion exchange resins consist of an irregular, macromolecular three-dimensional network of hydrocarbon chains bound together by crosslinks. Most commonly, the hydrocarbon backbone is made up of styrene monomers, whilst the crosslinks consist of divinyl benzene.

Table 3.2: Applications of ion exchange resin catalysts

	Type of catalyst			
	Gel form	Macroreticular		
Type of Reaction	beads	beads	powder	**Application**
Acetal formation		x		acetals
Alkylation			x	p-alkyl phenol
Chromatography	x			fructose/glucose
Condensation	x			bisphenol A
Epoxidation	x			butyl oleate
Ester formation	x			acetic acid ethyl ester
Ester splitting		x		sorbic acid
Etherification		x		MTBE, ETBE, TAME
Hydration		x		IPA, tert-butyl alcohol
Hydrolysis	x			allyl alcohol
Oligomerisation			x	n-butene
Phenol purification		x		pure phenol
Polymerisation			x	1,3,5 trioxane
Re-esterification		x		hydroxyalkyl phosphinic ester

This structure forms the hydrocarbon matrix to which fixed ionic groups are attached. The ionic groups form the active sites of the ion exchange resin. Figure 3.3 gives a pictorial representation of acidic ion exchange resin synthesis.

While the matrix of ion exchange resins is hydrophobic, the ionic groups are hydrophilic. Both the hydrocarbon polymer and the ionic groups together are soluble in water. This solubility is removed by interconnecting the polymers with crosslinks. Even though this makes the ion exchange resin insoluble, it can still sorb solvents and expand by a swelling of the matrix. The extent of swelling is determined mainly by the polarity of the sorbing species and the degree of cross-linking.

The early ion exchange resins came in the form of solid spheres, the so-called gel

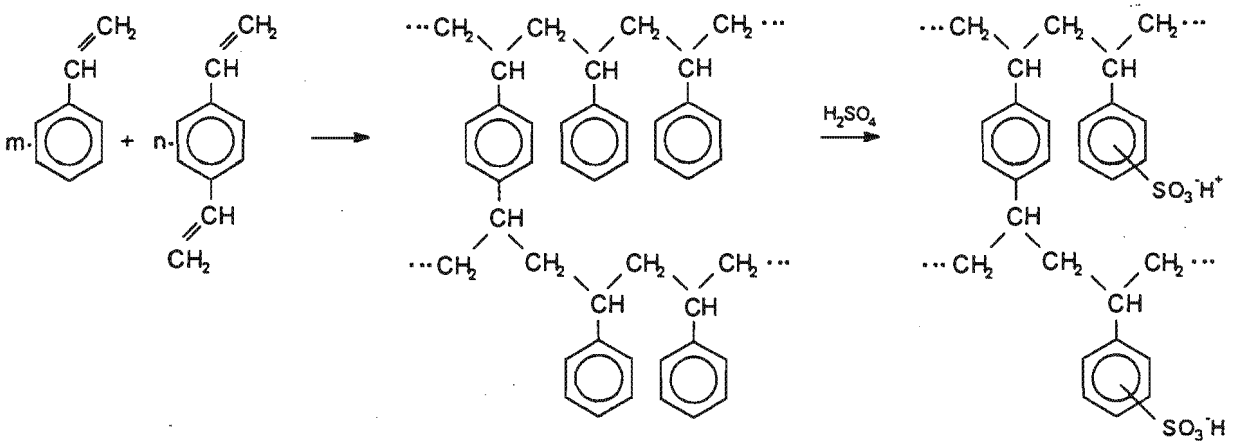

Figure 3.3: Synthesis of ion exchange resin

form. Typical catalyst bead sizes ranged from 0.3mm to 1.2mm. Only in water and polar systems, however, were functionalised gel polymers found to have catalytic efficiencies approaching those of the corresponding homogeneous catalysts [113]. In less polar media where swelling was decreased due to the poorer solvation of the polar functional group, the catalytic efficiency was diminished to far below that of the homogeneous catalyst. This deficiency of gel polymers resulted from the lack of accessibility of reactants to the interior of the catalyst particle, only the periphery of the particle being utilised. In hydration reactions, the effective thickness of this peripheral region has been estimated to be 1 μm thick, in poorly solvating organic media this shrinks to only 0.1 μm [113]. For a typical gelular bead of 0.5 mm diameter, this means that only 0.1% - 1% of the catalyst is actively involved in the reaction.

The discovery of macroreticular resins in 1957 [114] solved this problem. Macroreticular resins are composed of microgel particles (0.01 to 1.5 μm) agglomerated to form clusters (0.4 to 60 μm), see Figure 3.4 [113]. The microgel particles are identical to gel particles in all respects except their size. The clusters are connected at the interfaces so that the porous polymeric particle is constructed of two continuous phases - a continuous pore phase and a continuous gel phase. Macroporosity arises from the void spaces

between and within the clusters whilst significantly enhanced surface area arises from the exposed surface of the microgels. The surface area of macroreticular resins is typically 50 m^2/g, about 10 000 times greater than gelular resins. The large void space provides ready access for reactants to the microgels whilst the small size of the microgels leads to greater catalyst utilisation. Thus whereas gelular resins can only function effectively in a swelling medium, macroreticular resins are effective catalysts in both swelling and nonswelling solvents. Consequently, the majority of resins used as catalysts today are macroreticular in nature.

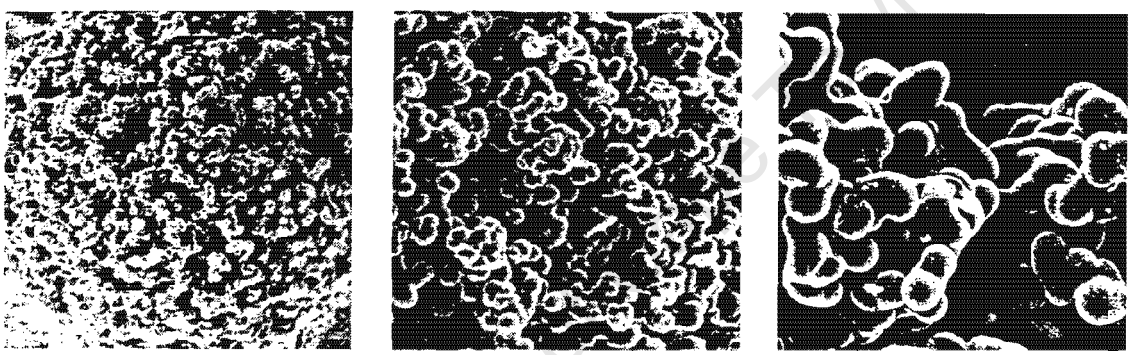

Figure 3.4: Microscopic structure of a macroreticular resin at 100X, 300X and 1000X magnification respectively

The cluster size of the microgel accounts for the visual appearance of the porous polymers. Clusters larger than 2000 Å (half the wavelength of the shortest frequency of the visible part of the electromagnetic spectrum) scatter the light waves (Mie scattering) as light passes through the porous matrix and produce opacity. Clusters smaller than 2000 Å are not of sufficient size to induce the same type of light scattering and appear translucent, from the Rayleigh scattering of photons as they pass through the alternating sequence of pores and clustered microgels. Non-porous gel resins appear transparent, as there is no internal structure of significant size to perturb the flow of photons passing through [113]. Figure 3.5 [113] shows the visual differences between a gelular resin, a macroreticular resin with small clusters and a macroreticular resin with large clusters.

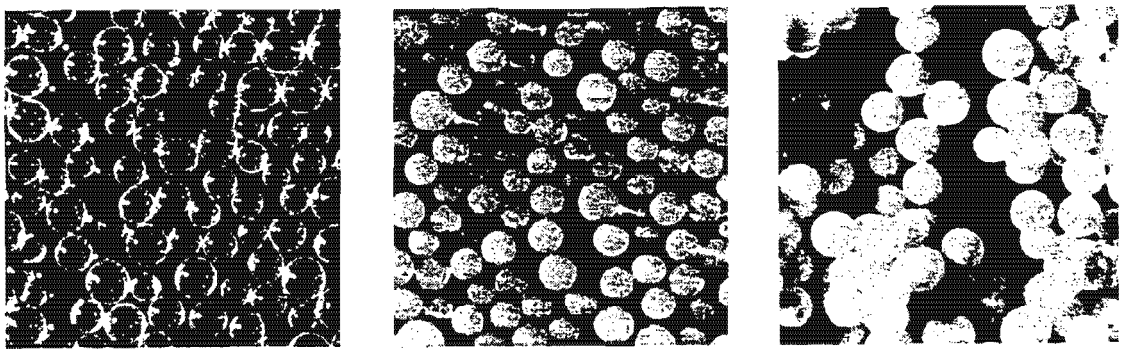

Figure 3.5: Physical appearance of a gelular resin, a macro-reticular resin with small clusters and a macro-reticular resin with large clusters

3.1.2.3 Porosity in catalytic ion exchange resins

Since both the macrostructure and the matrix of macroreticular resins are random, pore sizes are not uniform. Macroreticular polymeric catalysts have two types of pores: permanent macropores between the microgel clusters and "temporary" micropores within the microgel beads. The sizes of these pores change significantly depending on the extent of swelling.

When the resin is totally dry, the polymeric matrix is collapsed and the polystyrene chains lie as close as atomic forces will allow. In this condition, the matrix is completely impervious to any molecule incapable of acting as a swelling medium. Thus unless a reactant is itself capable of swelling the matrix, the only catalytic sites exhibiting any activity would be those on the external surface of the microgel clusters. The only pores existing in this system are the large void spaces in between the microgel clusters. Depending on the type of macroreticular catalyst, these pores may vary in size from as small as 20 Å to as large as 500000 Å [113, 115]. The pore size distribution of a typical dry, unswollen macroreticular ion exchange resin catalyst is shown in Figure 3.6 [113].

In all resins, microporosity (i.e. pore sizes below 20Å) only becomes apparent in the

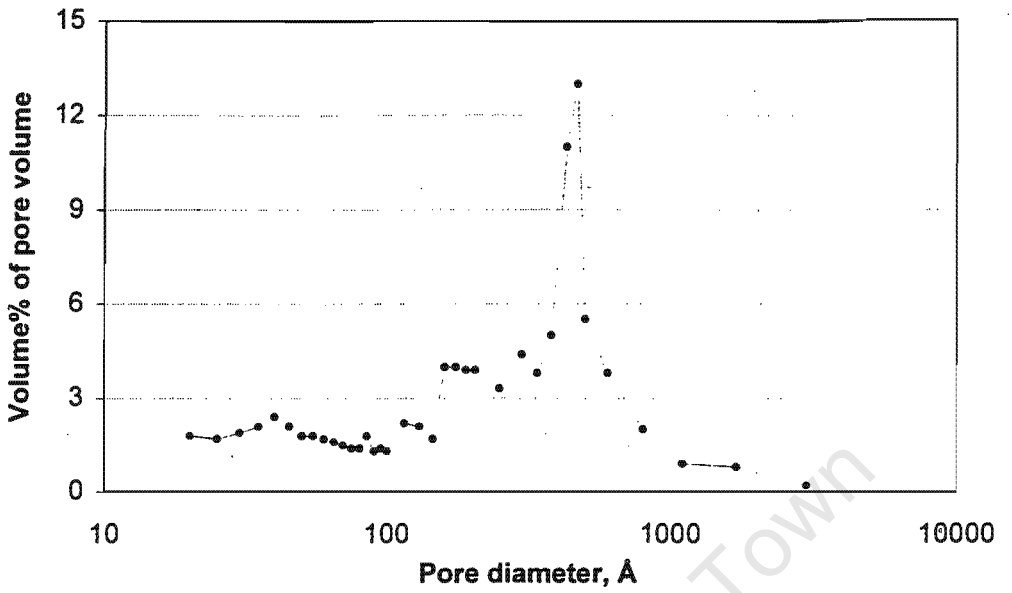

Figure 3.6: Typical pore size distribution of a dry macroreticular ion exchange resin determined by nitrogen desorption isotherm

swollen state. In swelling media the sulphonic acid groups are surrounded by solvation spheres causing the matrix to expand relative to the dry form. This opens up micropores between the polymeric hydrocarbon backbones (Figure 3.7) [115].

The sizes of these micropores are inversely proportional to the amount of crosslinking agent present in the resin. The more crosslinker in the matrix, the greater the number of connections between the polystyrene chains. This reduces the extent of swelling and also the diameters of the micropores. In gelular resins with a low to medium degree of crosslinking (2-13%) "micropores" of 5 to 40 Å diameter open up during swelling. Macroreticular resins where the degree of crosslinking is usually slightly higher (7-25%) exhibit micropores with smaller diameters, typically between 5 Å and 20 Å.

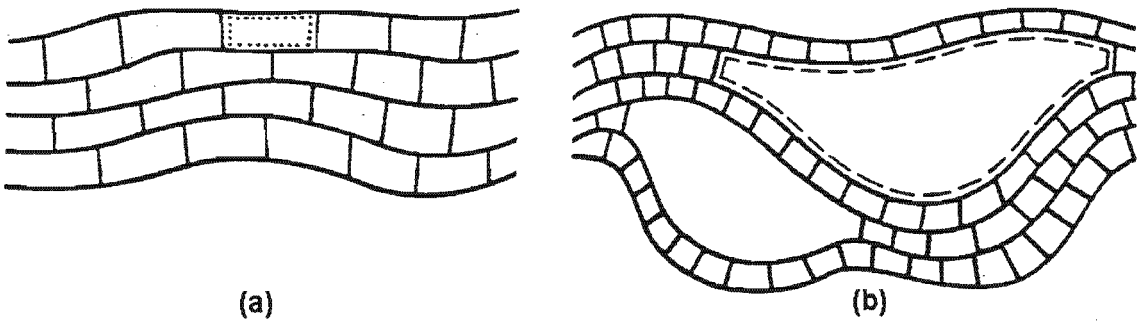

Figure 3.7: Creation of micropores by swelling of the hydrocarbon backbone by a polar solvent. (a) Unswelled matrix (b) Swelled matrix

3.1.2.4 Catalytic nature of acidic ion exchange resins

The catalytically active sites in acidic ion exchange resins are the sulphonic acid groups in the hydrogen form [116]. The nature of the catalytic action, however, has been the subject of considerable discussion in the literature since it is believed to differ significantly depending on the reaction medium. In most existing work it has been assumed that acidic resin catalysis falls into one of four categories:

1. Catalysis by fully water-swollen resins in aqueous systems
2. Catalysis in mixed water/organic solvents
3. Anhydrous catalysis where water is a product of reaction
4. Anhydrous catalysis where water is not a product of reaction

Infrared (IR) studies [117] have shown that the sulphonic acid groups in dry resins pair off by the formation of a doubly-hydrogen bonded structure. The addition of a small amount of water to the anhydrous resin leads to the break-up of this paired array as the water forms hydrogen bonds to multiple sulphonic acid groups. Three or even four groups may be involved in these highly stable complexes. Additional water breaks

up these groups and monohydrates are formed. As ever more water is added, increasing amounts of mono- and then bi-hydrates form, until eventually the sulphonic acid groups become solvated and the hydride ions delocalise. Solvation of the acid groups is believed to take place when the ratio of water to sulphonic acid groups within the resin matrix exceeds two [118]. The progressive solvation of resin is summarised in Figure 3.8.

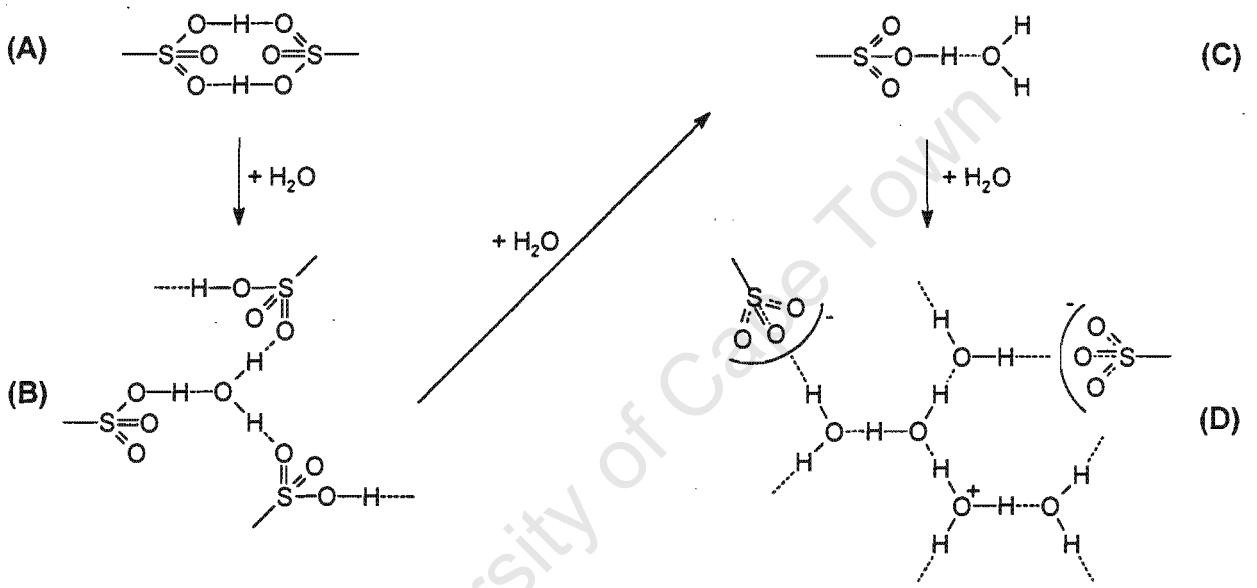

Figure 3.8: Interaction of water with the resin matrix. (A) Anhydrous pairing (B) Multiply-hydrogen bonded water (C) Monohydrated sulphonic acid groups (D) Completely solvated resin

In-situ IR studies of the dehydration of alcohols over thin polymeric films by Thornton and Gates [119] and Knözinger and Noller [120] determined that alcohols interact with the resin matrix in a similar fashion to water. All the alcohols used in these studies (methanol, ethanol, IPA, s-butyl alcohol and isobutyl alcohol) exhibited identical behaviour. A separate study on formic acid dehydration [116] showed that these resin matrix-functional group interactions were not limited to alcohols, but occurred with other polar organic species as well.

At low partial pressures alcohol was hydrogen-bonded to multiple active sites. Identically to water, alcohol molecules displayed a preference of simultaneously "bonding" to proton accepting and proton donating sites [121, 122]. As the partial pressure of alcohol was increased, the characteristic IR absorption bands for -S=O gradually disappeared, indicating the formation of highly stable hydrogen bonded alcohol-sulphonic acid structures. Once all the available -S=O groups had bonded, additional alcohol led to dissociation of the acid groups and the corresponding break-up of the strongly hydrogen bonded networks. The band indicating free -OH groups (whether from the resin or from the alcohol) was absent under all conditions, suggesting that these groups were always involved in hydrogen bonds. The progression from dry resin to dissociation by polar species is depicted graphically in Figure 3.9, using methanol as an example.

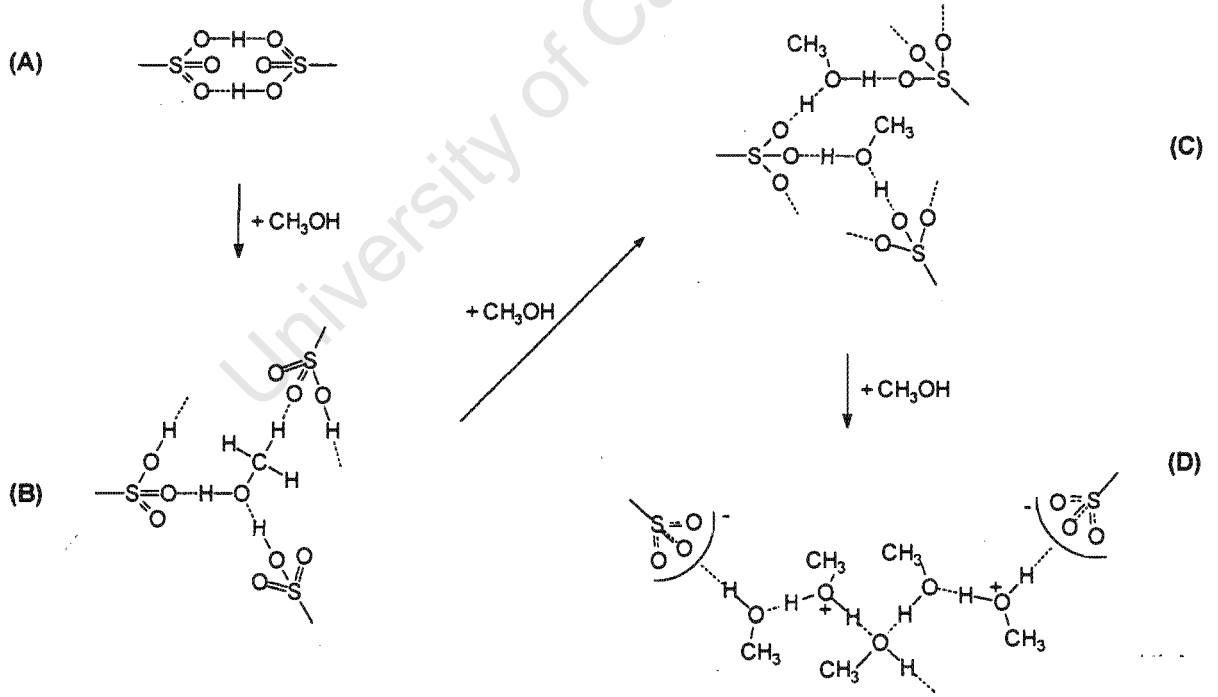

Figure 3.9: Interaction of methanol with the acidic resin matrix. (A) Anhydrous pairing (B) Multiply hydrogen-bonded alcohol (C) Strongly hydrogen bonded network (D) Dissociation of sulphonic acid groups

In nonpolar or only slightly polar media, the nature of the species-matrix interactions differs since the reaction medium can no longer swell the resin and is unable to dissociate the active sites. The reactants are believed to "bond" into a network of sulphonic groups [123]. A charge imbalance is created between the adsorbed molecules and the active sites which leads to the formation of an adsorbed carbocation phase. This charge imbalance is shared out amongst the interconnected sulphonic groups (Figure 3.10). Experimental reaction evidence indicates that up to seven sulphonic groups are involved in such complexes [119, 123]. IR studies have shown benzene, propylene and diethyl ether to adsorb in this manner.

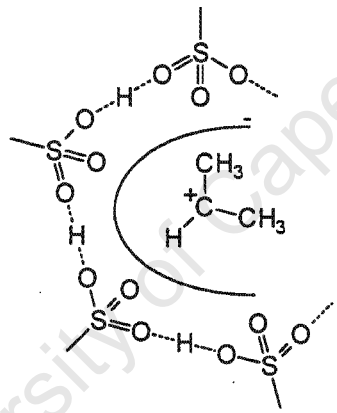

Figure 3.10: Suggested structure of propylene adsorbed onto an acidic resin

The classification of catalysis by ion exchange resins into four categories with different mechanisms needlessly complicates the picture. All polar species (be they water or organic) display essentially the same functional group interactions with the resin matrix. The nature of ion exchange resin catalysis in polar media then, can be described quite simply as the transition from catalysis by ionic -SO_3H groups (whether concerted or singly bound) to catalysis by delocalised protons and dissociated sulphonic acid sites. The change-over between the two states is dependent on the concentration of the polar species at the active sites. When the resin is in the fully solvated state, catalysis can be likened to homogeneous catalysis by mineral acids and, indeed, reactions exhibit the

same activation energies and reaction orders [124].

In nonpolar media on the other hand, this gradual transition from "ionic" to "homogeneous" catalysis does not occur. The ionic groups cannot become dissociated so the catalytically active species always remains the ionic group. In systems of mixed polar and nonpolar species the same principles apply. The more polar species preferentially adsorb on the active sites where, depending on the concentration of the polar species, they can be multiply hydrogen-bonded, be singly bonded or even solvate the sulphonic acid groups [99]. Reaction would then occur between the adsorbed polar species and the nonadsorbed nonpolar species. In such systems kinetic evidence points to the possible transport of the nonpolar species to the adsorbed polar species by surface diffusion [125] along the hydrocarbon backbone.

3.1.2.5 Deactivation of ion exchange resin catalysts

Sulphonic acid ion exchange resins can be deactivated in a number of ways. They can lose hydrogen ions (and thus catalytic activity) through ion exchange, active sites may become blocked or inaccessible by polymeric material (i.e. fouling of the active sites), the resin matrix may become decrosslinked or the resin may lose sulphonic acid groups due to excessive operating temperatures.

Feed contamination by cations may result in the partial or total displacement of the active H^+ species by ion exchange, leading to a loss in capacity and thus activity. The extent of deactivation depends on the nature of the impurity. In MTBE synthesis, for example, it was observed that a 1 g/l of resin Fe impurity led to a 30% decrease in activity [115]. In this situation the catalyst may be reactivated by strong mineral acids which displace the adsorbed inactive cationic Fe species.

In some processes, easily polymerisable material such as dienes and acetylenes react to form polymeric gum on contact with the catalyst. This blocks access to the active sites

and greatly reduces the catalytic effectiveness of the resin. A complete reactivation of the resin through washing with organic solvents is generally not possible and replacement of the resin becomes necessary [115].

Exposure of the catalyst to strong oxidizing agents such as Fe^{3+}, O_2 or peroxides results in the decrosslinkage and swelling of the resin. This affects the diffusion of reactants inside the matrix and increases the pressure drop down the resin bed. Excessive decrosslinking may even lead to the partial dissolution of the resin matrix. Decrosslinked resins are irreparably damaged.

The most common cause of resin deactivation is desulphonation due to thermal degradation. Strongly acidic polymeric resins are thermally stable up to temperatures of 120-150°C. Above this temperature a gradual loss of catalytic activity is observed which is due to the splitting-off of sulphonic acid groups from the polymer matrix. The sulphonic acid groups are lost in the endothermic reverse reaction of the sulphonation process (Figure 3.11). In an inert atmosphere this deactivation process gives sulphur trioxide, in aqueous media it gives sulphuric acid [126]. The rate of desulphonation depends mainly on the operating temperature and on the nature of the system [127]. The higher the temperature and the less inert the surrounding medium, the more rapid the desulphonation process, see Figure 3.12 [127].

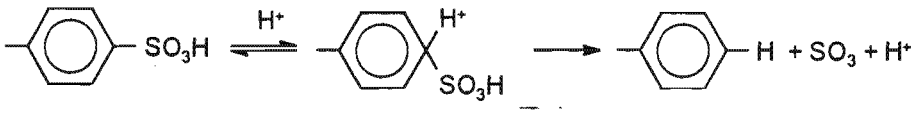

Figure 3.11: Deactivation of a polymeric resin by desulphonation

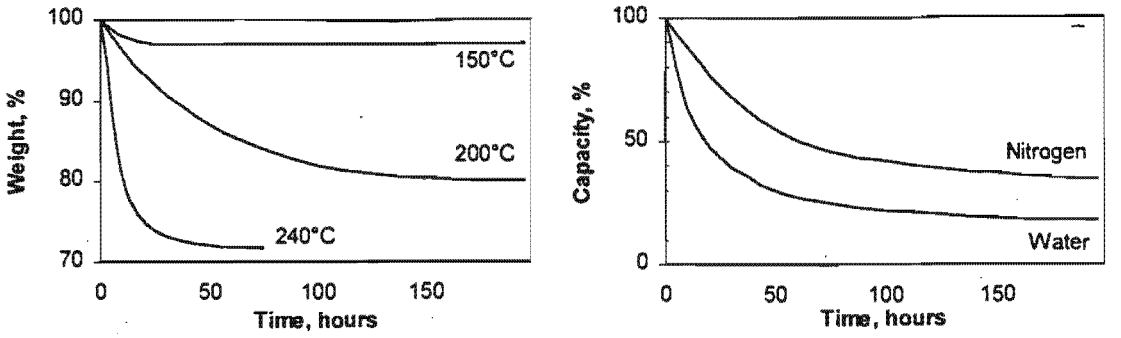

Figure 3.12: Deactivation of Amberlyst 15. Effect of temperature on weight loss and effect of operating medium on capacity loss.

3.1.3 The thermodynamics and system parameters of hydration and etherification

The equilibrium conversions of the olefins in ether synthesis at 20 bar are displayed in Figure 3.13. The data for MTBE, ETBE and TAME synthesis were obtained from the Handbook of Heterogeneous Catalysis [13] whilst the data for DIPE synthesis was calculated using the WS-PRSV model described in Section 2.3.

The equilibrium conversion towards DIPE appears to be more temperature sensitive than that of the other ethers. However, in MTBE, ETBE and TAME synthesis the system was entirely liquid phase and only the etherification reaction was considered. In calculating the equilibrium in DIPE synthesis, on the other hand, both a vapour and a liquid phase were present in the system and the propylene hydration reaction was included too. This affects the equilibrium behaviour of DIPE synthesis relative to that of the other ethers. Nevertheless, all the etherification reactions are exothermic and thermodynamically limited. The equilibrium limitations consequently increase with temperature. The same has been found of propylene hydration [49]. To take advantage of LeChatelier's principle and improve the poor thermodynamics, these reactions are thus usually carried out at high pressures and low temperatures. However, hydration and

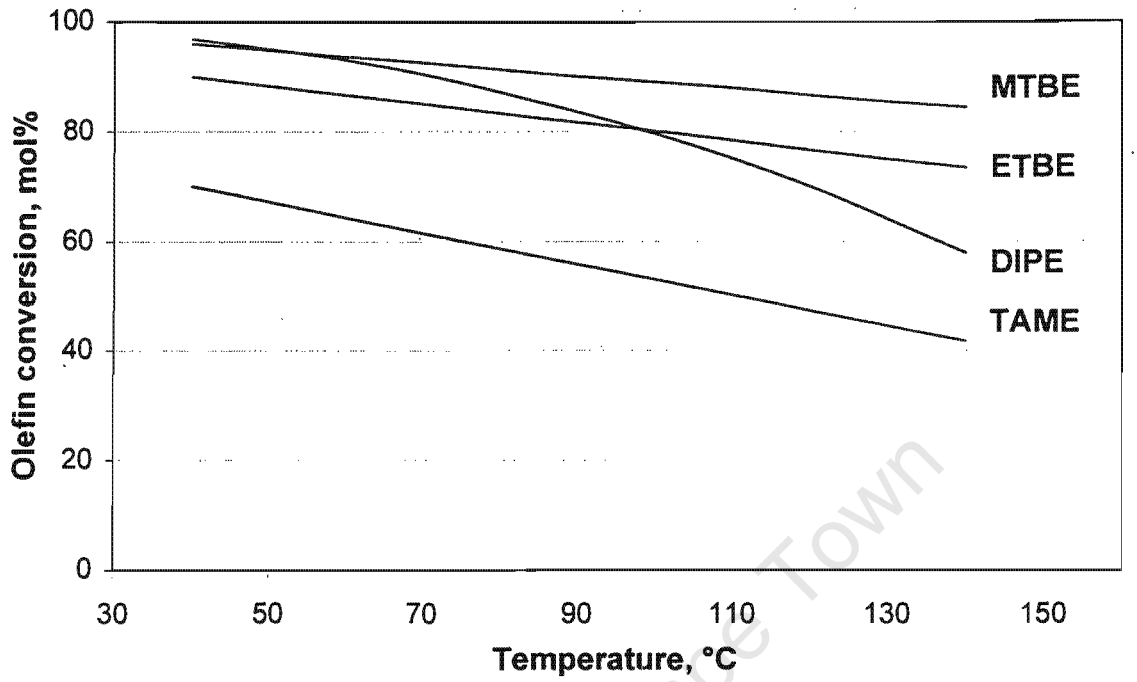

Figure 3.13: Olefin conversion in ether synthesis at chemical equilibrium. Alcohol:olefin ratio = 1:1 and pressure = 20 bar.

etherification reactions have to be separated into 2 distinct classes depending on reaction temperature:

- those where the temperature is lower than the critical temperature of the olefin, e.g. MTBE, ETBE and TAME synthesis and
- those where the temperature is greater than the critical temperature of the olefin, e.g. IPA and DIPE synthesis.

The difference between these two classes comes about as a result of the thermodynamic behaviour of the super-critical species. In sub-critical temperature operation any increase in pressure beyond that required to liquefy all components in the system results in only negligible changes in the activities of the species present in the system. Consequently, neither the rate nor the equilibrium conversion are affected by pressures beyond

the bubble point pressure of the system. In super-critical synthesis, however, pressure will always have an effect, since the super-critical species cannot be liquefied. Even if the super-critical species has dissolved almost completely in the liquid phase, its activity will continue to increase with increasing pressure and, in the case of hydration and etherification, this will result firstly in greater reaction rates and secondly will favourably affect the equilibrium conversion. The difference between the two classes is reflected in the typical reaction conditions.

Synthesis temperatures for the octane enhancing ethers derived from isobutylene and isoamylene range from 40 to 80°C [13, 128]. Since the critical temperatures of isobutylene and the isoamylenes are 145°C and 192-197°C, respectively, MTBE, ETBE and TAME are produced at sub-critical temperatures and consequently system pressures only slightly higher than the bubble pressure of the system are employed, i.e. pressures range between 7 and 20 bar. Commercial IPA production by propylene hydration on the other hand takes place at 130 to 150°C [49, 22]. This is considerably greater than the critical temperature of propylene (92°C). Thus, equilibrium conversions and rates can be enhanced by higher pressures and consequently 60-100 bar trickle-bed operation is standard. Similarly, DIPE synthesis is proposed at elevated pressures around 70 bar [8].

3.1.4 Side reactions in hydration and etherification

Selectivities greater than 95% can be achieved in hydration and etherification reactions over ion exchange resin catalysts [13, 33]. Side reactions, besides double bond shifts, do not generally play an important role in hydration and etherification as long as suitable reaction conditions are applied [129]. Still, since some side reactions such as oligomerisation can lead to a reduction in catalyst activity by fouling of the active sites and a reduction in quality by colouring the product, they should be avoided. In MTBE synthesis for example, the major side reactions are the dehydration of methanol to give dimethyl ether and water, the oligomerisation of isobutylene and the hydration of isobutylene with the

product water from methanol dehydration. These reactions are, however, not the only ones which have been observed. The observed reactions in MTBE synthesis are listed in Figure 3.14 [13]. During isobutylene hydration to give tertiary butyl alcohol the major side reaction is the formation of isobutylene oligomers [125].

The picture in IPA and DIPE synthesis is very similar to that of the synthesis of tert-butyl alcohol and MTBE. Neier and Woellner [22] report selectivities during IPA synthesis of 96%, the major by-product being DIPE. Only traces of oligomers were found to occur. During DIPE synthesis, the number of unfavourable side-reactions is reduced relative to MTBE synthesis, due to the fact that DIPE is a symmetric dialkyl ether. The bimolecular alcohol dehydration and olefin hydration reactions, respectively, would simply form DIPE or the intermediate, IPA. Accordingly, in DIPE synthesis (from water and propylene) Marker et al. [8] report process selectivities to DIPE of 98%, the remainder being oligomers. All IPA was recycled. Neglecting the reactions of the diolefins the main reactions which can be expected to occur are given in Figure 3.15.

3.1.5 Hydration and etherification mechanisms

Early work on hydration and etherification reactions over acidic ion exchange resins started out from the premise that the catalytic action occurred via a mechanism identical to that in homogeneous mineral acid catalysed systems [49, 22, 47]. It was assumed that the protons from the sulphonic acid sites were delocalised and solvated within the gel phase of the resin bead, i.e. the interior of the catalyst bead could be considered as a discrete region of homogeneous mineral acid catalysis. Fittingly, this model was termed the "pseudo-homogeneous" model. Regardless of whether the reaction was electrophilic addition as in hydration, oligomerisation or alcohol alkylation or whether the reaction was nucleophilic substitution as in the bimolecular dehydration of alcohol, the first (and rate controlling) step was, in every case, assumed to be the formation of a carbocation radical. The mechanisms assumed for the homogeneous hydration [130] and etherification

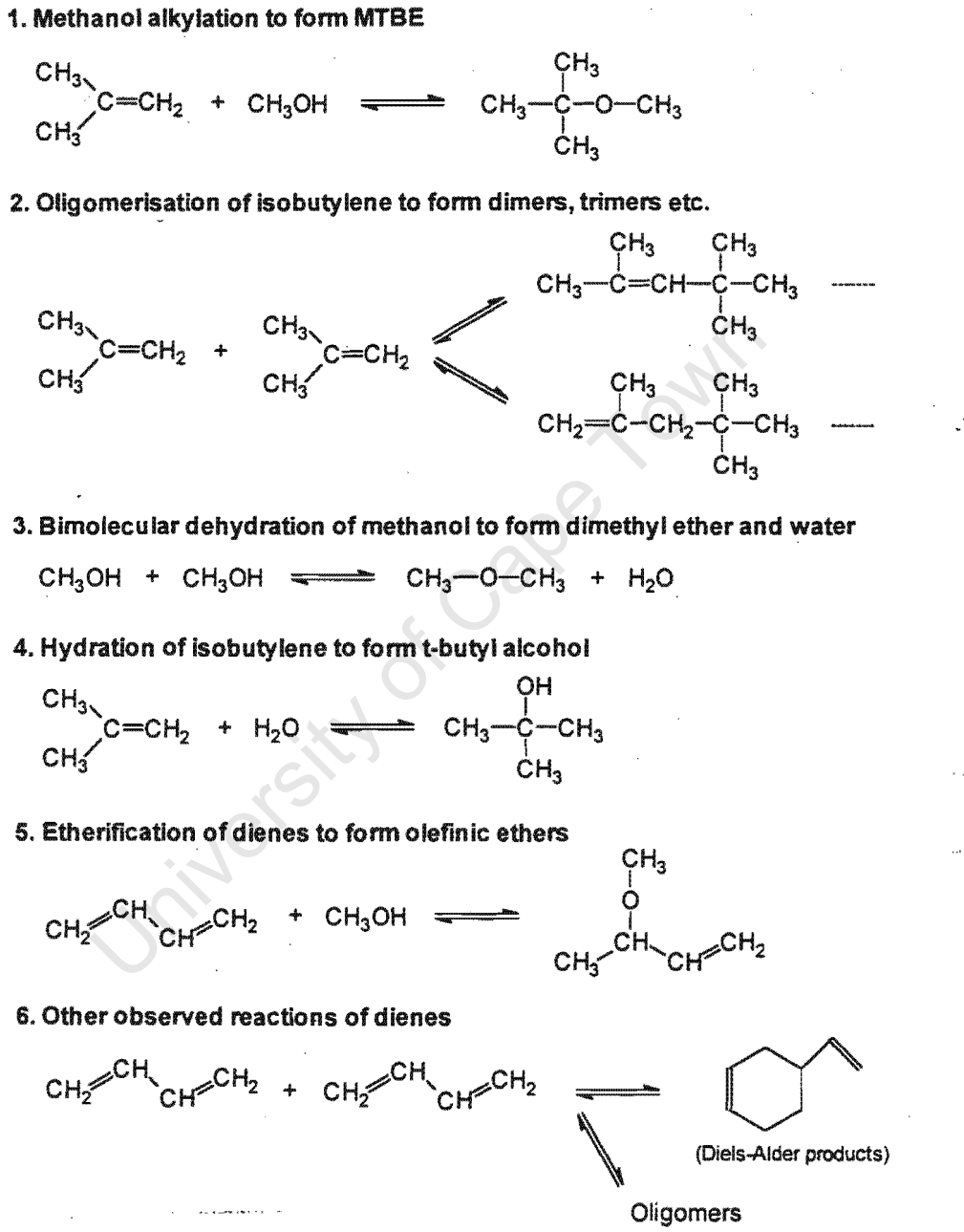

Figure 3.14: Main reactions in MTBE synthesis

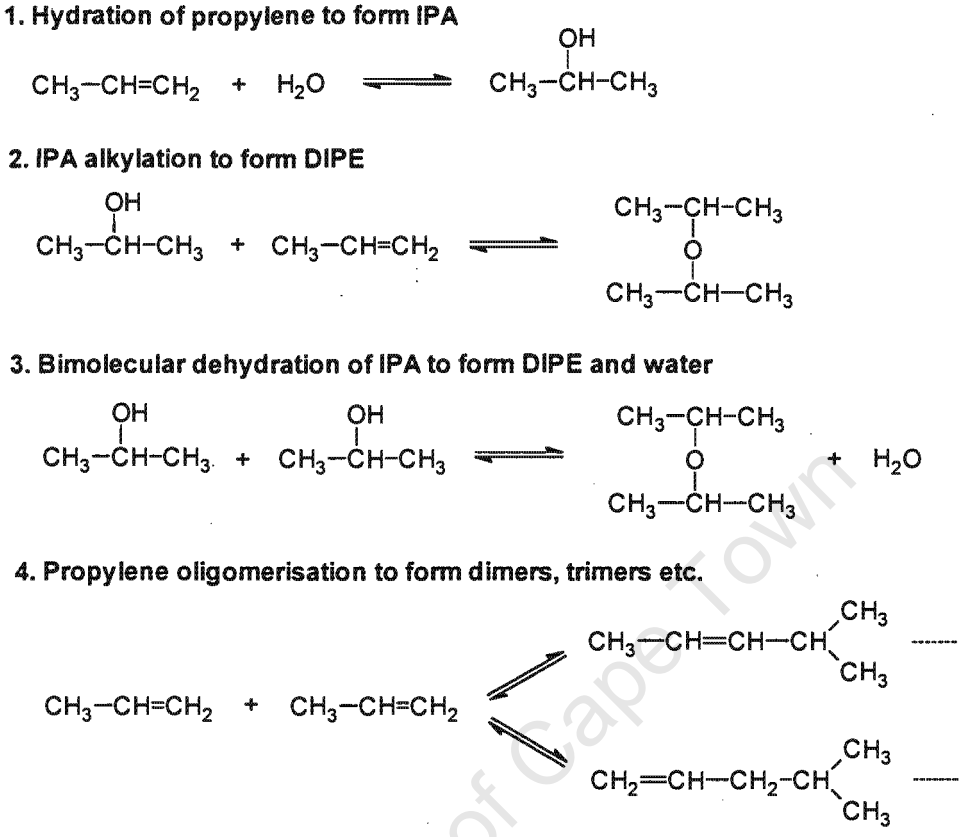

Figure 3.15: Expected reactions in DIPE synthesis

reactions [131] are shown in Figure 3.16 whilst Figure 3.17 shows the mechanism of olefin dimerisation [131] using the DIPE system as an example.

The pseudo-homogeneous model generally fit reaction data well. Ancillotti et al. [105] observed that at low isobutylene to methanol ratios the rate of MTBE formation was first order in isobutylene and zero-order in methanol. As the ratio was increased the reaction rate increased and depended on both species. At high ratios of isobutylene to methanol the situation reversed and the etherification rate became first order in methanol concentration and independent of isobutylene concentration. These observations were still consistent with pseudo-homogeneous catalysis. However, water was found to markedly inhibit the rate of reaction and variations in reaction rate at low species concentrations were observed which could not be explained by the pseudo-homogeneous theory.

1. Hydration of propylene

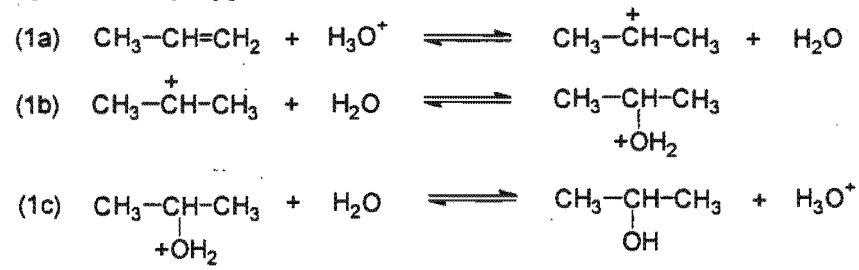

2. Alkylation of IPA

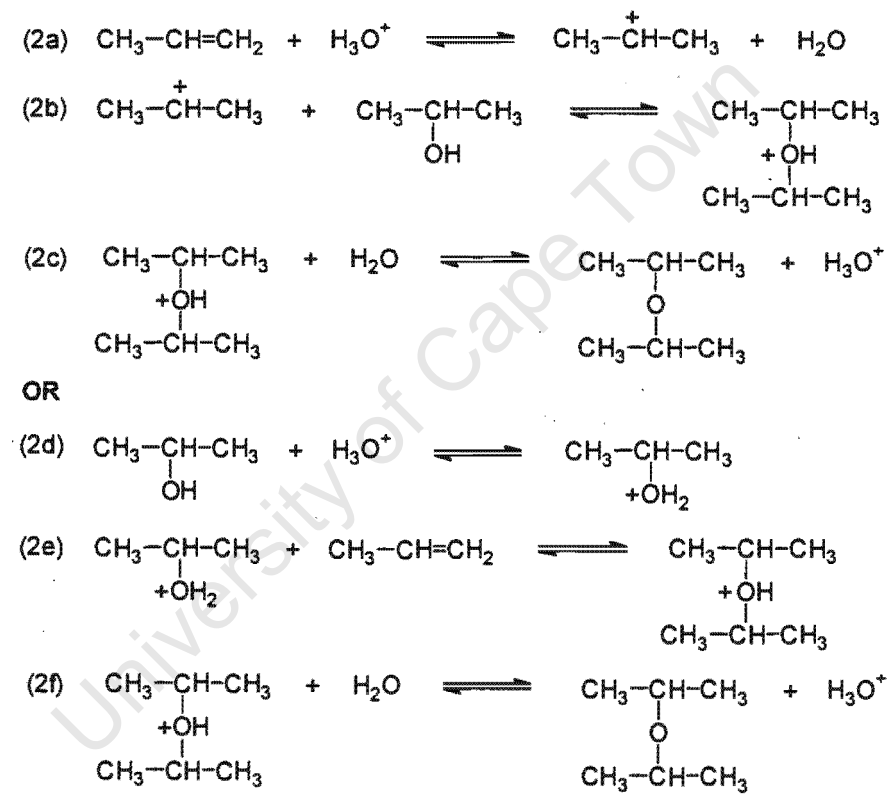

3. Bimolecular dehydration of IPA

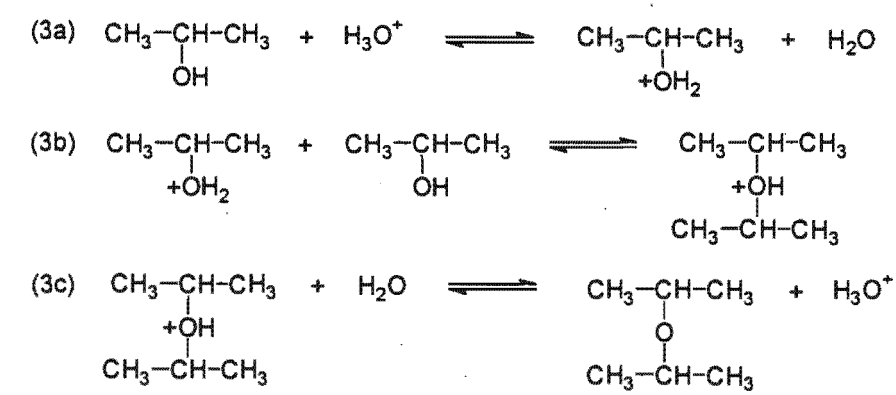

Figure 3.16: Homogeneous acid catalysed reaction mechanisms

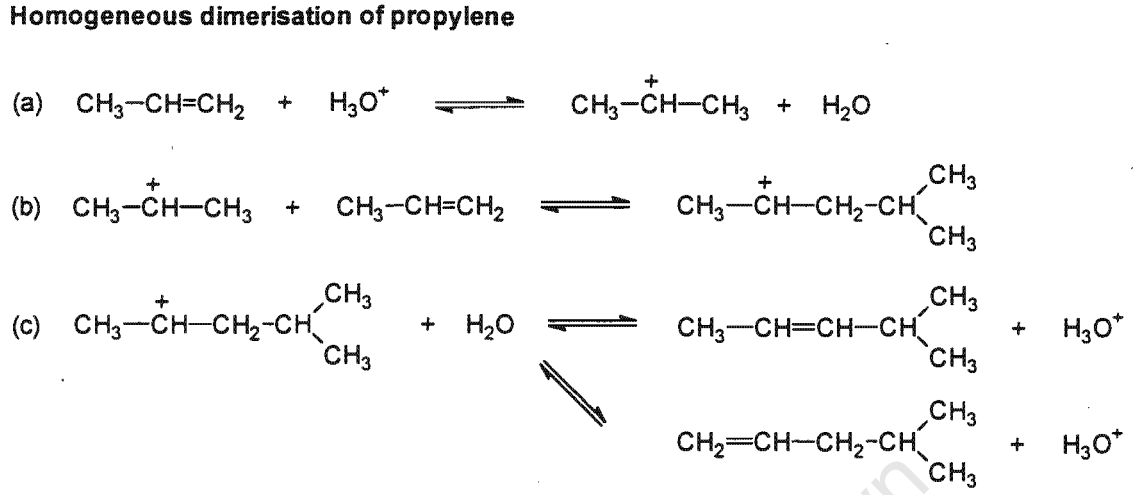

Figure 3.17: Homogeneous propylene dimerisation reaction mechanism

The first papers to tie up the sometimes contradictory experimental evidence and link it to the adsorption structures observed previously in ion exchange resins (Section 3.1.2.4) were those by Tejero et al. [132] on MTBE synthesis and Kalló and Mihályi [99] on isobutylene hydration. Tejero et al. [132] summarised literature data on the initial rate of MTBE formation, see Figure 3.18, and explained the behaviour by a progression through three regimes of catalytic action:

1. At low ratios of isobutylene to methanol, ratio $\leqslant 0.7$, the etherification reaction takes place exclusively between adsorbed methanol and isobutylene from solution. The surface reaction is the rate limiting step, occurring via a concerted proton transfer mechanism similar to that proposed by Gates and co-workers [121, 122], see Section 3.1.2.4. It is believed that three sulphonic acid groups are required to effect proton transfer and form the active cationic structure.

2. At intermediate ratios of isobutylene to methanol, $0.7 \leqslant$ ratio $\leqslant 3.5$, it was hypothesised that reaction between adsorbed methanol and adsorbed isobutylene also begins to take place. The surface reaction is the rate limiting step. Once again, it is believed that the concerted action of three active centres is required for this

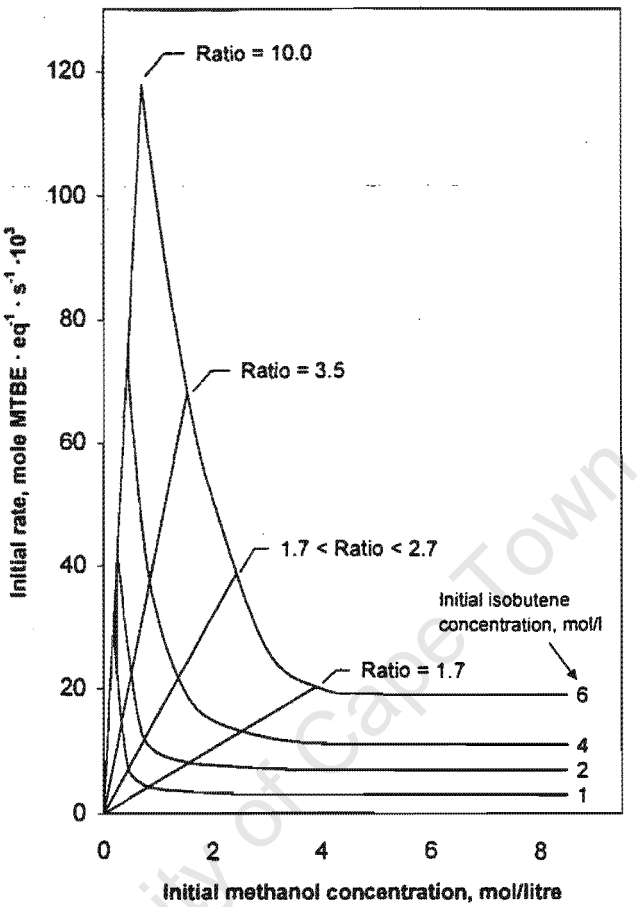

Figure 3.18: Initial rate dependence on initial methanol concentration at various isobutene contents. Ratio = isobutene / methanol, temperature 60°C over Amberlyst 15

mechanism to take place.

3. At high ratios of isobutylene to methanol, ratio $\geqslant 3.5$, the reaction medium is unable to fully swell the polymer matrix. The network of sulphonic acid groups is dense and reaction occurs almost exclusively between adsorbed phase species. This is the fastest reaction mechanism.

In contrast to Tejero et al. [132] who focussed on a system where at least some isobutylene adsorption had taken place, Kalló and Mihályi [99] worked in a system where

the overwhelming majority of active sites (>99.8%) had adsorbed the polar species, water. The greater coverage by the polar species in their system could be attributed to lower olefin to polar species ratios and to the higher polarity of water as compared to methanol - species of greater polarity will adsorb preferentially on the active sites. Reaction in this system thus occurred exclusively between the adsorbed polar species and the olefinic species from solution (regime 1 according to the Tejero et al. [132] classification).

As expected, the initial rate of isobutylene hydration was found to increase linearly with isobutylene partial pressure. However, it was found that even though all sites were occupied by water, the partial pressure of water at constant isobutylene partial pressure still had a marked effect on reaction rate, see Figure 3.19 [99]. This phenomenon was explained as follows: at low water partial pressures only one water molecule is hydrogen-bonded per active site, forming the most active complex. As the water partial pressure is raised bi-, tri- and finally polyhydrates form around the active sites. The hydrogen-bond interaction with the water molecules is shared out equally amongst ever more water molecules and the activity of the adsorbed water-active site complex decreases.

Tejero et al. [132] based their findings on a system with insufficient methanol to cause full swelling and proton delocalisation by the polar species. On the other hand, Kalló and Mihályi [99] worked in a system where minimal olefinic adsorption took place, thus they never observed a system where interaction occurred between two adsorbed phase species. The two proposed series mechanisms can, however, be combined into a single one with three distinct mechanistic regimes. The type of mechanism depends on two factors: the ratio of polar to apolar species [132] and the total amount of reactive polar species present [99].

The ratio of polar to apolar species determines whether reaction will occur between an adsorbed polar species and an apolar species from solution (slower mechanism) or between adsorbed polar and adsorbed apolar species (faster mechanism). At large polar to apolar species ratios the total amount of reactive polar species, however, determines

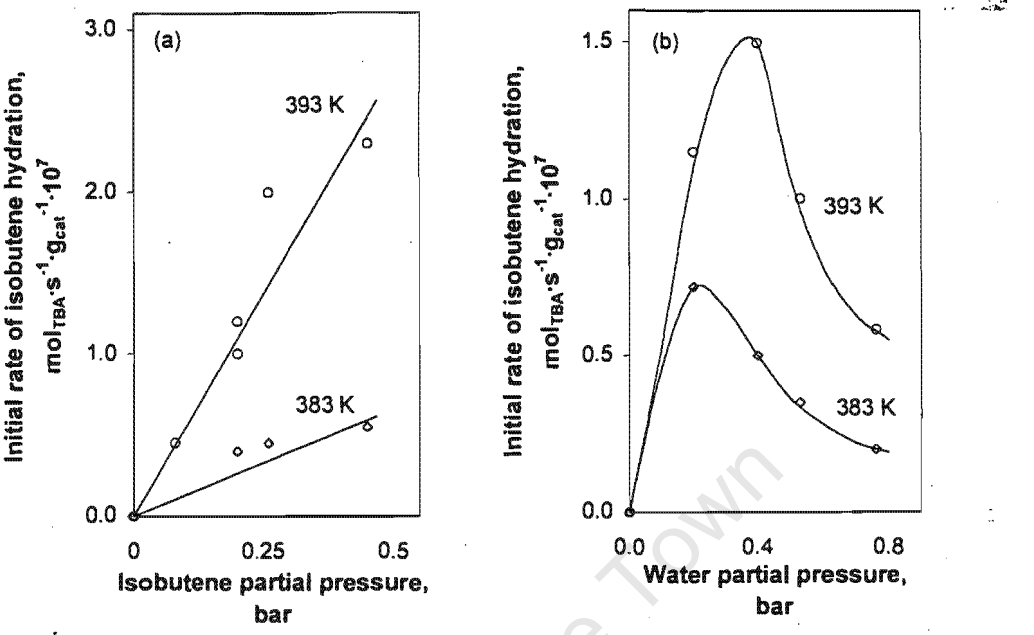

Figure 3.19: Initial rate of isobutene hydration on Varion KSM as a function of (a) isobutene partial pressure at constant water partial pressure of 0.57 bar and (b) water partial pressure at a constant isobutene partial pressure of 0.20 bar.

whether mono-adsorbed, bi-adsorbed or poly-adsorbed complexes take part in the reaction. Leaving out the transition phases between the mechanistic regimes, catalytic action in ion exchange resins can now be categorised into three classes: Type I, Type II and Type III. Catalytic activity increases from Type I to Type III.

I. At very high polar to olefinic species ratios and at high overall species concentrations, multiple polar species are hydrogen-bonded to each active site, forming polyhydrates in the case of water. Reaction takes place between adsorbed polar species and solution-phase apolar species with a single active site taking part in the reaction. This is the least active regime. This mechanism can be likened to homogeneous catalysis.

II. At intermediate ratios of polar to nonpolar species reactions between adsorbed polar

species and olefins from solution still dominate. However, in contrast to the Type I mechanism, more than one active site now takes part in the reaction in a concerted mechanism where the polar species are multiply hydrogen-bonded to a network of active sites.

III. At high ratios of apolar to polar species, reaction takes place between adsorbed polar and adsorbed apolar species. Due to the poor solvation ability of the apolar species the resin matrix is poorly swelled and active sites are at their most concentrated. Both species are multiply hydrogen-bonded to a number of active sites. This mechanism is believed to be the fastest.

3.2 Materials, apparatus and experimental procedures

3.2.1 Materials

3.2.1.1 Chemicals

The chemicals listed in Table 3.3 were used without any further purification. Deionised water with a resistivity greater than 18 $M\Omega \cdot cm^{-1}$ was supplied by a Millipore Milli-Q^{TM} Water System. All chemicals used for reaction work were filtered to sub 0.22 μm.

Acid washed sand from Aldrich was washed with deionised water until a pH of 7 was obtained. Glass beads with a diameter of 1 mm were acid washed with 1 mol / l HCl and then washed with deionised water until the pH returned to 7. Chromosorb (with a particle size of 180 - 250 μm) and silanised glass wool were supplied by Supelco.

As mentioned in Section 2.3.2 depending on the literature source used, the reported physical properties of the chemicals varied widely. The pure component properties that were used throughout the remainder of this work were those of Daubert and Danner [62], see Appendix B.

Table 3.3: Sources and purities of chemicals used in this project

Chemical	Source	Purity, mass%
Benzene	Aldrich	99.8
DIPE*,#	Merck	99.0
Hexane	Saarchem	96.0
IPA*	Saarchem	99.7
Methane*	Fedgas	>99.9
Methanol	Merck	>99
Propylene*	SASOL	>99.9

* used for reaction and/or adsorption work

stabilised with 10ppm 2,6-di-tert-butyl-4-methylphenol

3.2.1.2 Catalysts

All the catalysts used in this project are commercial catalysts. Three macroporous polystyrene divinyl benzene copolymers (Amberlyst 15 (A15), Amberlyst 35 (A35) and Amberlyst 36 (A36)) with sulphonic acid active sites containing differing amounts of divinyl benzene crosslinker and with different acid site densities were obtained from Rohm & Haas. These resins were supplied in the dry state. The macroporous organofunctional polysiloxane, Deloxan ASP (D-ASP), also with sulphonic acid groups, was obtained from Degussa, whilst the microporous zeolite H-Y (L-HY) extrudate with hydroxyl functional groups (Si-OH-Al) was obtained from Linde. The properties of the catalysts are given in Table 3.4.

3.2.2 Catalyst pretreatment, modification and characterisation

3.2.2.1 Pretreatment

The pretreatment procedure used for all the ion exchange resins was that recommended by Schumann [112]. The resin was washed with benzene to remove any monomer which remained in the catalyst matrix after synthesis. It was then rinsed with methanol to remove the benzene and partially swell the resin before it was washed with deionised

Table 3.4: Physicochemical catalyst properties

Catalyst properties, dry	A15[1,2]	A35[2,3]	A36[2,4]	D-ASP[5]	L-HY[6,7]
Lot number	443277	24035	24025	-	966084060002-5-10
Bulk density in air, kg/m^3	630	580	610	350	690
Acid site density, meq/g	4.8#	5.2#	5.5#	1.00	1.35
Crosslinker, mass%	20	20	12	-	-
Average particle size, μm	810	610	510	700	1590*
BET surface area, m^2/g	45	44	35	400	525
Max. operating temp., °C	120	130	140	>150	500

* average extrudate diameter. Extrudate length: 3.2 mm to 6.4 mm.

\# measured by titration

[1]Rohm and Haas [133], [2] Rohm and Haas [134],[3]Rohm and Haas [135], [4] Rohm and Haas [136], [5] Degussa [137], [6] Linde [138], [7] Möller [139]

water to fully swell the resin and remove the methanol. To ensure the resin was entirely in the hydrogen form it was ion-exchanged with 1 mol / l sulphuric acid. The catalyst was then dried in an oven at 120°C for 24 hours after which it was stored over silica gel until used. See Appendix F for the precise procedure. If required, the dry resin beads were sieved to various size fractions ($250 - 350\mu$m and $850 - 950\mu$m) by using metal screens. Since the commercial Y-zeolite was already in the hydrogen form, the only pretreatment required was calcination. This was done in an oven at 500°C for 18 hours under air to remove any carbonaceous material possibly present in the catalyst.

The dried catalyst was used as is for adsorption. For reaction work, the required amount of catalyst was first weighed out. The resins were then pre-swelled with methanol before being washed with water. It was necessary to swell the resin gradually as the resin beads shattered if washed with water only. The wet catalyst was then loaded into the reactor as a slurry. It was found that if dry resin was loaded into the reactor, it would crush itself on swelling and cause a high pressure drop over the reactor. Presumably this would also affect the mass transport properties and thus the performance of the catalyst, though this was never tested.

3.2.2.2 Modification of acid site density

The acid site density of Amberlyst 15 was modified by ion-exchange with NaOH. A sample of ion-exchange resin was accurately weighed out. This sample was swelled by consecutive washing with methanol and deionised water. The resin was then ion-exchanged with an amount of sodium hydroxide corresponding to the desired acid site density. It was washed with deionised water, dried and then stored as for the unmodified samples, see Section 3.2.2.1. The exact method is detailed in Appendix F.

The acid site density was determined by adding sodium hydroxide solution to a dried, weighed sample of ion-exchange resin to completely convert the catalyst to the sodium form. The excess NaOH was drained off and then neutralised by back-titration with dilute HCl. From the amount of HCl required, the acid site density could be calculated. This method was preferred to direct titration of the resin with NaOH, since the time taken to ion-exchange the resin was unknown and errors could thus easily have occurred. The entire procedure is outlined in Appendix F.

3.2.2.3 Size analysis

Resins are known to swell in polar solvents. To determine the sizes of catalyst particles in the various solutions occurring in this project, a Malvern Instruments Mastersizer S particle sizer was used. This instrument infers volume-averaged particle sizes either in air or liquid media from laser diffraction. A number of measurements were taken per sample to minimise errors.

3.2.3 Adsorption Experiments

3.2.3.1 Experimental Apparatus

The experimental apparatus used for the adsorption work is shown in Figure 3.20. It was operated in the gas phase at near-atmospheric pressure. Helium and propylene were both fed to the experimental rig through UNIT UFC-1000 mass flow controllers. Any particulates in the feed were removed by 2 μm filters installed in the feed lines. Any water in the feed gases was removed in a water trap filled with 5Å molecular sieve. Helium could either be used as a diluent by bypassing the saturator or as a carrier gas by passing it through the saturator.

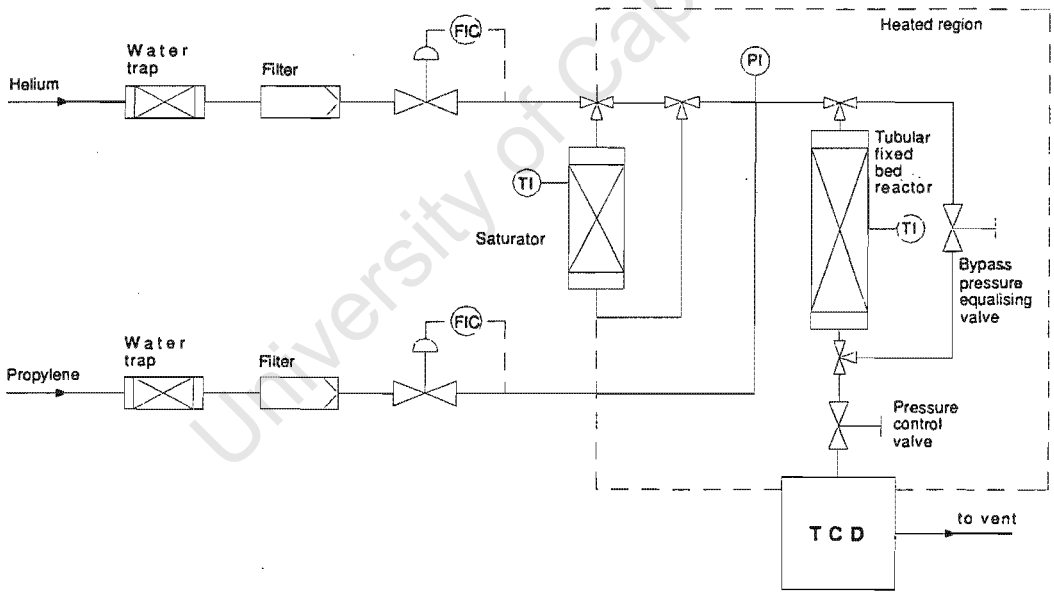

Figure 3.20: Schematic of adsorption rig

The single stage saturator was packed with chromosorb which was in contact with a liquid feed reservoir. The liquid was drawn up into the saturation zone by capillary forces. Helium was passed through this saturation zone where it picked up desorbing liquid. The

partial pressure of the liquid component in the helium exit stream was determined by the temperature of the saturation zone.

The feed streams now passed into the heated pre-reactor region, kept at a temperature greater than that in the saturator to prevent condensation in the feed lines. From here, the gas-phase feed stream, either propylene diluted with helium or helium containing evaporated liquid, passed into the reactor or flowed through the reactor bypass. To ensure the same pressure drop over the bypass as through the reactor, a pressure equalising valve was installed in the bypass. A needle valve for pressure control of the entire system was situated after the reactor. The reactor effluent now flowed through a sample valve in a TCD GC before being vented. The stream could be analysed by the TCD GC via the sample valve ($80\mu l$ samples).

3.2.3.2 The adsorption reactor

The reactor used for the adsorption work is shown schematically in Figure 3.21. The reactor was a 300mm long stainless steel tube with an 11mm ID. At the top and bottom, the reactor was attached to the rig by VCR fittings. A thermocouple was inserted midway into the catalyst bed. The reactor was heated by heating wire.

The catalyst bed was divided into three sections: a preheat and mixer section, the actual catalyst bed and a space filler section which ensured the catalyst bed was in the isothermal region of the reactor. The three zones of packing were separated by silanised glass wool.

3.2.3.3 Experimental procedure

Dry catalyst which had been pretreated as detailed in Section 3.2.2.1 was packed into the reactor. The required flow of helium was set. The temperature in the reactor, in the feed and product lines and in the saturator was set and left to stabilise for 2 hours

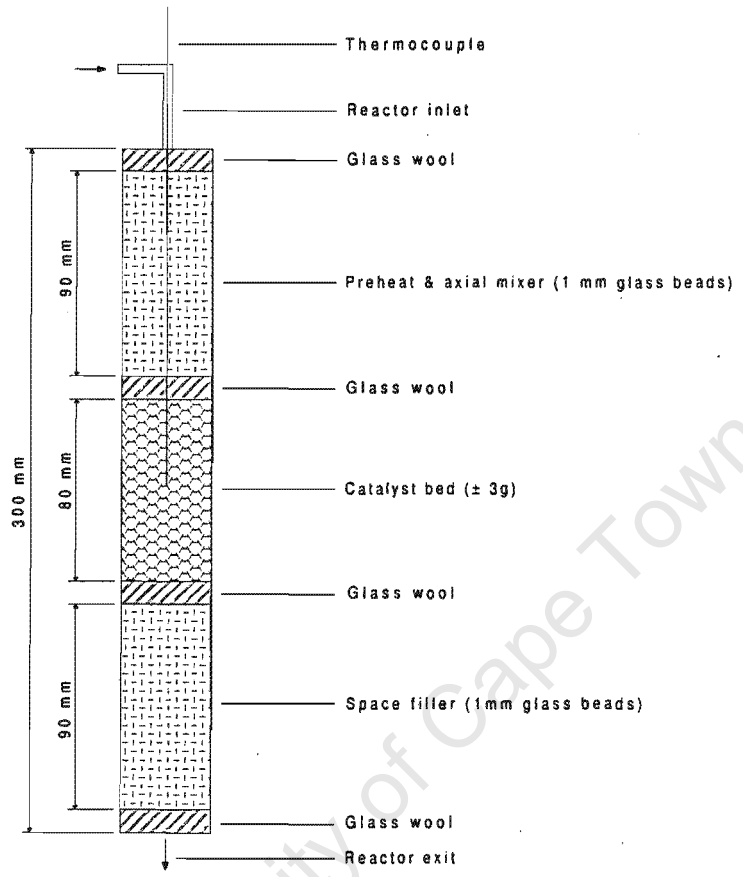

Figure 3.21: Adsorption rig reactor

under flow conditions. After stabilisation, a number of bypass analyses were performed by TCD GC to determine whether the rig had stabilised and to set the baseline. The reactor was then switched in-line. The effluent stream was sampled in approximately 10 second intervals until the GC response had returned to the baseline for an extended period of time. Appendix G shows a sample run sheet and the accompanying calculation procedures.

3.2.4 Reaction Experiments

3.2.4.1 Experimental Apparatus

The apparatus used for the experimental work is shown in Figure 3.22. The rig could operate in high-pressure (15 to 100 bar) or low-pressure mode (below 15 bar) depending on the setup being used. For high pressure operation, the bypass line around the back pressure regulator was closed, for low pressure operation the bypass was open.

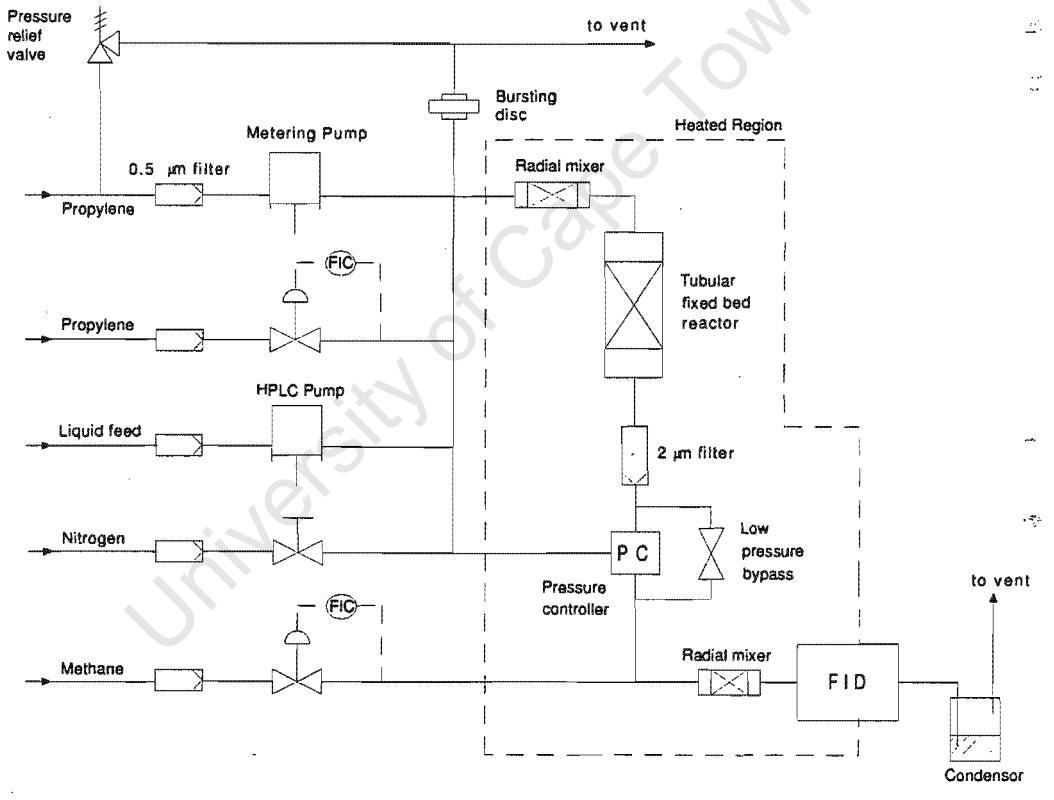

Figure 3.22: Experimental rig

Liquid reagents (either pure water, IPA and DIPE, or mixtures thereof) were fed to the reactor by a high pressure liquid chromatography pump (Hewlett-Packard Series 1100 Isocratic Pump) from a container placed 1.5m higher than the pump to prevent

vapour lock. The container was placed on a mass balance to accurately and independently determine the amount of liquid dispensed by the pump. During high pressure operation, propylene from a pressurised gas bottle was fed to the rig by a diaphragm pump (LEWA FC1). The pump head was cooled to $-3\,^{\circ}C$ by an ethylene glycol/water mixture to prevent vapour lock. For low pressure operation propylene was fed to the rig through a Brooks 5850TR mass flow controller. All feed streams passed through $0.5\,\mu m$ filters to remove any particulate matter.

The propylene and liquid feed streams were fed through heated lines to a combined radial mixer and preheater filled with 1 mm glass beads situated directly ahead of the downflow reactor. The mixer ensured that the reactants were brought close to reaction temperature and were thoroughly mixed before entering the reactor. After the reactor, the reactants passed through a $2\,\mu m$ filter which trapped any catalyst fines. Depending on the mode of operation, the reactant stream then either proceeded through the back pressure regulator (pressure maintained by nitrogen) or bypassed the back pressure regulator entirely. The products then flowed through another radial mixer, also filled with 1 mm glass beads, where the internal standard (methane) was introduced.

Methane was chosen as the internal standard for quantitative analysis since it could not be produced from the reactants over the catalysts used in this project at the operating conditions. The internal standard flow was controlled by a Brooks 5850TR mass flow controller. From the final mixer the now gas phase reactor effluent flowed via a heated line (130°C), at atmospheric pressure, through a sample valve in an FID GC. If desired, $100\mu l$ samples of the stream could be analysed by the FID GC. From the GC the stream flowed into a condensor, held at $5\,^{\circ}C$, where the liquid components were trapped. The gaseous fraction was vented.

3.2.4.2 The DIPE synthesis reactor

Figure 3.23 shows a diagram of the tubular fixed bed reactor used for all the catalytic reaction work and displays the packing order. It consisted of a stainless steel tube with an internal diameter of 22.6mm, an outer diameter of 25.6mm and a length of 330mm. The reactor was rated to a pressure of 150 bar at 25°C. To measure the axial temperature in the reactor a thermowell with an outer diameter of 6 mm and a total in-reactor length of 320mm was welded to the head piece. The maximum catalyst space was thus 123.3cm^3. The reactor operated in downflow mode. A metal distributor situated directly above the first layer of packing ensured good feed distribution to the preheat/catalyst bed. At its base the reactor was connected to the experimental rig by $\frac{1}{4}$" Swagelok fittings, at the top by an 80mm flange sealed by a PTFE gasket. The reactor was heated by heating wire.

Directly after the inlet a long preheat section was situated to ensure the reactants were at the desired reaction temperature. After the preheat came the catalyst bed. The catalyst bed was placed in the isothermal reactor zone to minimise axial temperature profiles during reaction. No dilution of the catalyst bed with inert material was necessary as the reaction rate was sufficiently low that the axial temperature profile was constant to within ±1 °C of the setpoint over the entire catalyst bed. An additional space filling section of glass beads completed the packing. Each section of packing was separated from the other by inert, silanised glass wool. The packing was supported on a perforated steel plate.

3.2.4.3 Experimental procedure

The catalyst was prepared for reaction work as detailed in Section 3.2.2.1 and loaded into the reactor. The required pressure was set and the liquid feed started. Once the pressure had attained the set value, the feed was switched off and the rig checked for leaks by observing the pressure. The liquid feed was used for pressure testing, as leaks are

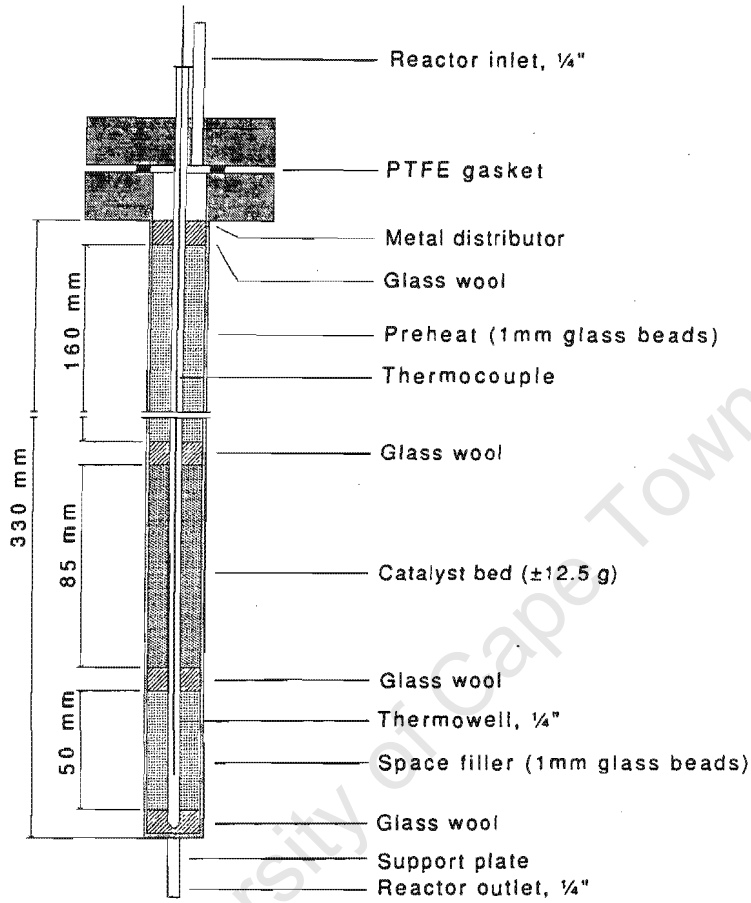

Figure 3.23: Diagram of reactor.

more apparent with liquid and because it led to a thorough wetting of the catalyst bed which results in improved liquid flow distribution and mass transfer [140].

After the pressure test, both the liquid and propylene feeds were switched on and the temperature slowly ramped (30-50 °C $\cdot hr^{-1}$) to approach the desired reaction temperature. Once the temperature had stabilised, on-line GC samples were taken every 15 minutes until the reaction was judged to have reached steady state (±3 hours). An hour after this, the liquid trapped thus far in the condensor was drained so that the steady-state liquid sample could be collected. After 2 hours of steady-state operation, during which analyses

were performed every 15 minutes, the experimental run was stopped.

The mass of liquid fed, the temperature and the pressure within the reactor were monitored throughout the run. The mass of propylene fed was determined by weighing the gas bottle before and after each run. Carbon analysis of the reactor effluent was performed on-line by FID. Water data was calculated from these chromatographic results by mass balance. Integral analysis of the steady-state liquid product was performed by manual injection of samples into a TCD, which enabled analysis of water, IPA and DIPE, to be crosscorrelated with the FID results. A sample run sheet with accompanying calculations is shown in Appendix G. Any experimental runs with carbon balances, based on the flow rate of the internal standard, poorer than 95% by mass were rejected. Experimental runs with relative standard deviations in the on-line FID results greater than 5% were also rejected.

3.2.5 Product analysis

3.2.5.1 Hydrocarbon analysis

The analysis of organic reaction products was performed on-line using a Varian 3700 GC fitted with a flame ionization detector (FID) and a 50m long, 0.2mm diameter Hewlett-Packard HP1 (crosslinked methyl silicone gum) capillary column. This allowed quantitative analysis of propylene, the reaction products IPA and DIPE, as well as of the internal standard methane. Response factors of 1.00 were used for the hydrocarbons. Factors of 0.56 and 0.85 were used for IPA and DIPE respectively. These were determined from manual injections and corresponded well with the values reported in literature [93, 141]. Peaks were identified and assigned by hand injected doping and by MS analysis. The FID settings, response factor determination and a sample integrator trace are given in Appendix H.

3.2.5.2 Water and hydrocarbon analysis

Integral analysis of the steady-state liquid product was performed by manual injection of samples into a Varian 1400 GC with a thermal conductivity detector (TCD) fitted with a 1.8m, 1/8", packed, 0.1% SP1000 Carbopack C column. During the reaction work it was predominantly used to analyse for water. Response factors for the major liquid products were determined by manual injection. For water a value of 1.26 and for DIPE a value of 0.89 was obtained relative to the response of IPA. Since only the liquid fraction was to be analysed, it was not necessary to determine the factor for the gaseous species methane and propylene. A sample output, GC settings and the response factor calculations are given in Appendix H.

3.2.5.3 Species identification

The mass spectrometer (MS) was used purely for qualitative analysis of the reaction products, and so no response factors needed to be determined. Species were assigned based on their ion fingerprint, identified from the *Eight Peak Index of Mass Spectra* [142]. The MS settings and a sample output are shown in Appendix H.

3.3 Catalytic results and discussion

3.3.1 The use of species activity

Kinetic theory maintains that for a bimolecular reaction to occur, the reacting molecules must, firstly, collide with each other and, secondly, possess sufficient energy that the minimum energy barrier for reaction, the so-called activation energy, is overcome. The rate of chemical reaction between species A and B thus depends on the frequency of these collisions and on the fraction of such collisions with energy greater than the activation

energy. The frequency of collision, in turn, depends on the velocity, the relative sizes and the molecular density of the reacting molecules. The fraction of collisions with sufficient energy for reaction depends on the magnitude of the activation energy and on the total energy contained within the system.

These concepts have been incorporated into numerous kinetic models, e.g. the so-called Simple Collision Theory (SCT) which regards reacting molecules as simple, non-interacting hard spheres. While the experimentally determined rate constants and the theoretical value of the rate constant calculated from SCT only agree for a comparatively small number of reactions, the fundamental theory underlying this model is believed to be correct [143, 144], it simply lacks the sophistication to deal with non-spherical, interacting real molecules. Consequently, the SCT model will serve for illustrative purposes to qualitatively show the validity of using activities in kinetic analyses.

Based on the SCT model, it has been shown [143, 144] that the frequency of collision, Z_{AB}, and the fraction of collisions, f, with energy greater than the activation energy can be expressed by

$$Z_{AB} = \pi (r_A + r_B)^2 \left(\frac{8kT}{\pi\mu}\right)^{\frac{1}{2}} \cdot C_A C_B \tag{3.1}$$

and

$$f = \exp\left(\frac{-E_a}{RT}\right) \tag{3.2}$$

Where r_A and r_B represent the radii of molecules A and B respectively, $\left(\frac{8kT}{\pi\mu}\right)^{\frac{1}{2}}$ represents a velocity term and C_A and C_B are molecular concentration terms; E_a is the activation energy for the reaction. The rate of the forward reaction between species A and species B can then be written as

$$rate = Z_{AB} \cdot f = \pi (r_A + r_B)^2 \left(\frac{8kT}{\pi\mu}\right)^{\frac{1}{2}} \cdot C_A C_B \cdot \exp\left(\frac{-E_a}{RT}\right) \tag{3.3}$$

This theoretical form of the rate equation is usually condensed into a form containing the so-called pre-exponential factor, A, the exponential activation energy term and the two molecular density terms, C_A and C_B. The pre-exponential factor and the activation energy terms are typically further condensed into the kinetic rate constant, k_r. The rate of a bimolecular chemical reaction thus depends on the kinetic rate constant (which is only a function of temperature for a given reaction) and on the molecular densities of the two reactants,

$$rate = A \cdot \exp\left(\frac{-E_a}{RT}\right) \cdot C_A C_B = k_r \cdot C_A C_B \tag{3.4}$$

Conventional treatment of kinetic data has been carried out in terms of this theory. The pre-exponential factor and the exponential term have been determined experimentally whilst the molecular density functions have been retained in the form of species partial pressure (vapour phase systems) or in the form of species concentrations (liquid phase systems). This approach worked extremely well if the system under consideration was essentially ideal, i.e. in vapour phase systems at low pressure and high temperature or in liquid phase systems with chemically similar species.

In non-ideal systems, however, where large deviations from ideal behaviour are experienced this method failed to account for experimental observations. This has led to rate equations for non-ideal systems being redefined in terms of the species partial molar fugacity, i.e.

$$rate = A \cdot \exp\left(\frac{-E_a}{RT}\right) \cdot f_A^* f_B^* = k_r \cdot f_A^* f_B^* \tag{3.5}$$

While this approach has been highly successful, one of the concerns of the redefinition of the rate equation in this manner, is that one apparently loses one of the tenets of kinetic theory: the fact that rate depends on the density of molecules and thus on the frequency of collisions - the molecular density term, either concentration or partial pressure, having been replaced by a thermodynamic quantity, the fugacity. However, by

using the definition of the partial molar fugacity as given by Eq. 2.20 in Section 2.2.2.2, one can rearrange the modified rate equation to obtain

$$rate = A \exp\left(\frac{-E_a}{RT}\right) \cdot \exp\left(\frac{\overline{G}_A^* - \overline{G}_A^{IGM} + \overline{G}_B^* - \overline{G}_B^{IGM}}{RT}\right) \cdot p_A p_B \tag{3.6}$$

This shows that by incorporating the fugacity instead of the partial pressure or concentration, the overall form of the rate equation is not altered substantially. The pre-exponential factor remains constant, the dependency of rate on molecular density is retained and the exponential activation energy term is unaffected. One has simply incorporated an additional concentration dependent term into the rate equation which accounts for species interactions. Intuitively this makes sense: if molecules interact, i.e. repel or attract each other due to differences in their chemical properties, then in some manner this must impact on either the frequency of collision or on the energy with which these collisions take place, or both. In either case, the rate will deviate from the ideal rate. Expressed differently, the use of fugacity instead of concentration or partial pressure is not a deviation from the principles of kinetic theory, but rather is an extension of kinetic theory to account for thermodynamic interactions between the species in the reacting medium.

In a system such as the DIPE system where more than one phase may be present, the pressure is relatively high and the temperature relatively low, where one of the components is super-critical and polarities range from highly polar water to apolar propylene, large deviations from ideality are experienced due to significant interactions between the species in the system. These interactions must be incorporated into the kinetic analysis and this can be done by the use of species fugacities or its unitless analogue, the species activity. In this project, the activities were calculated using the PRSV equation of state in conjunction with the Wong-Sandler mixing rule, as described in Section 2.3. Since thermodynamic theory maintains that the fugacity (or activity) of every species must be the same in every phase at thermodynamic phase equilibrium, the activity of the non-adsorbed species within the catalyst particles at phase equilibrium must be identical to

those of the bulk phase. This has a useful side effect, as kinetics can be related to bulk phase conditions rather than to theoretical catalyst phase conditions.

3.3.2 Internal and external transport effects

To ensure that data obtained from experiments reflect only chemical events, interphase, interparticle and intraparticle transport gradients must be minimised and all active sites should be exposed to the same reaction medium. The presence of significant temperature and concentration gradients, whether inside or outside the catalyst particles, can lead to severe deviations in catalyst performance, possibly disguising the true behaviour of the reaction(s) being studied. Similarly, due to the possible vapour-liquid nature of the DIPE system, care must be taken that all resin beads within a cross-section of the catalyst bed experience the same phase. If a portion of the catalyst bed cross-section is exposed to a different phase, desirable reactions may be retarded whilst undesired side-reactions may be promoted.

3.3.2.1 Wetting efficiency

At any temperature above the critical temperature of propylene, a vapour phase will be present in the reactor, which will thus behave as a trickle-bed. In such systems it has been observed [145] that reaction rates and selectivities vary with the amount of catalyst surface covered by the liquid phase. This effect is not so much a chemical as a physical phenomenon. Assuming phase equilibrium, the activities of all species *must* be identical in both the vapour and liquid phases. The adsorption behaviour on the catalyst and the rates of all reactions must thus necessarily be identical regardless of the reaction phase. However, the rate of physical transport to and from the catalytically active sites may vary according to the phase and reactions may consequently be retarded or accelerated. Thus, to ensure that one observes only chemical effects under identical physical conditions, it

is important that all catalysed reactions occur within the same phase. In the case of a two-phase trickle-bed system, this must necessarily be the liquid phase.

A measure of the amount of catalyst surface covered by liquid is the wetting efficiency. Generally, the greater the flow of liquid relative to the flow of gas through the catalyst bed the greater the wetting efficiency. Flooding the catalyst bed with the liquid phase prior to reaction also helps to improve catalyst wetting [140]. A correlation was developed by Mills and Dudukovic [146] (Eq. 3.7) which estimates the steady-state wetting efficiency, f_e, of a trickle bed

$$f_e = \tanh\left[0.664\,\mathrm{Re}_L^{0.333}\,Fr_L^{0.195}We_L^{-0.171}\left(\frac{a_p d_p^2}{\epsilon^2}\right)^{-0.0615}\right] \tag{3.7}$$

The greatest amount of vapour phase relative to liquid phase will be present when the system consists solely of super-critical propylene and liquid water. If any IPA or DIPE were present, the solubility of propylene would be increased and the amount of vapour phase decreased. Consequently, in the DIPE system, poor wetting is most likely to occur when only super-critical propylene and liquid-phase water are present. This system, at 120 °C and 50 bar, was examined for wetting efficiency. It was found (see Appendix I), for propylene:water ratios smaller than 5:1 one can assume the catalyst surface is completely wetted.

3.3.2.2 Mass transport limitations

External diffusion constraints have been observed over acidic ion exchange resin catalysts in both hydration and etherification reactions in continuous stirred tank reactors (CSTR) and in fixed bed reactors. In isobutylene hydration, Gupta and Douglas [125] observed external mass transfer limitations at temperatures greater than 70°C. In etherification, external mass transfer limitations were observed in CSTR experiments by Rehfinger and Hoffman [32] during MTBE synthesis in the liquid phase at 60°C and by Linnekoski and

Rihko [147] for TAME synthesis at temperatures above 80°C. In a fixed bed reactor, Fité et al. [61] observed external mass transfer constraints during ETBE synthesis at 90°C at liquid hourly space velocities (LHSV) below $60\,h^{-1}$ (corresponding to a weight hourly space velocity (WHSV) of approximately $14\,h^{-1}$). Zhang and Datta [128], on the other hand, found that external diffusion was not rate controlling during MTBE synthesis at a lower WHSV of $8\,h^{-1}$, however. the temperature was also lower, at 80°C. Panneman and Beenackers [148] observed MTBE formation rates affected by diffusion at an even lower temperature of 60°C, though they did not state whether this was as a result of internal or external limitations.

As for external diffusion control, internal diffusion limitations have also been observed in hydration and etherification. Velo et al. [149] showed that the hydration of isobutylene to tert-butyl alcohol was not internal mass transfer limited at temperatures below 60°C. Gupta and Douglas [125], though, showed that above 90°C internal mass transfer does, indeed, become a factor for this reaction. Zhang and Datta found that intraparticle diffusion effects were not significant in MTBE synthesis for temperatures below 60°C and particle sizes of 0.19 and 0.74mm. Above 60°C, internal mass transfer limitations became apparent for the larger particles. Likewise, during TAEE synthesis, Linnekoski and Rihko [147] found that at temperatures of 80°C no internal diffusion effects were apparent for catalyst particles smaller than 0.65mm. At an even higher temperature, 90°C, Fite et al. [61] showed that particles smaller than 0.2mm were required to eliminate internal diffusion effects during ETBE synthesis.

An interesting study on internal diffusion effects by Rehfinger and Hoffman [32] showed that during MTBE synthesis internal diffusion could be rate limiting down to particle sizes of 0.04mm at 60°C depending on the concentration of the polar component. At methanol concentrations above 1 mol/l methanol in n-butane and isobutylene, particle sizes below 0.8mm showed no internal diffusion limitations. At lower methanol concentrations the critical particle size became ever smaller until at 0.001 mol/l, particle sizes as low

as 0.04mm were required to exclude internal diffusion limitations. The variation with methanol concentration can be attributed to the swelling behaviour of the resin matrix. At low methanol concentrations the resin is poorly solvated, the pores are at their smallest and diffusional restrictions at their greatest. As the methanol concentration increases, the resin becomes ever more solvated and the pores increase in size, which decreases diffusional restrictions. During experimental work, care thus has to be taken that internal diffusion constraints are eliminated over the entire range of polar species concentrations studied, particularly if substantial concentration changes occur during reaction.

Both isobutylene and isoamylene hydration and etherification reactions thus have been found to be subject to external and internal mass transfer limitations at temperatures greater than 60-80°C and average catalyst particle sizes larger than about 0.6mm in polar media. The presence of internal and external transport limitations in the DIPE system was thus investigated experimentally to ensure that data obtained in this study reflected only chemical effects.

Mass transport limitations are most obvious under conditions where the reaction rate is greatest and the diffusivities of the reactants are at their smallest. If no effect is observed under these conditions, then it can safely be assumed there are no diffusion limitations at milder conditions. The catalyst in a properly wetted trickle bed reactor is covered by the liquid phase. Consequently, if there are diffusion limitations these must necessarily be of the gaseous component diffusing from the gas phase through the liquid phase to the catalytically active sites. Using the Wilke-Chang correlation (see Appendix I) it was shown that propylene diffuses approximately 20% faster through IPA than through water. Given the same reaction rate, it is thus more likely that diffusional limitations will occur during hydration than during etherification. Also, it has been shown that the maximum operating temperature at which Amberlyst 15 (the catalyst used for the majority of the experimental work) shows minimal deactivation in aqueous media is 120°C [127]. Consequently, experiments to test for mass transport limitations

were conducted at 120°C under hydration conditions at propylene to water ratios of 5:1, the limit of complete catalyst wetting. The pressure was arbitrarily chosen as 50 bar. The effect of polarity on diffusion through the catalyst was not examined as all reaction work was to be carried out under polar conditions.

To check for external diffusion limitations the WHSV was kept constant whilst the superficial mass velocity was varied (Figure 3.24). In a second set of experiments, to check for internal diffusion constraints, the catalyst loading and the WHSV were kept constant, but the size of the resin beads was varied (Figure 3.25). Three sizes of catalyst were used: as supplied commercial Amberlyst 15 with an average bead diameter of 810 μm and two sieved fractions with bead diameters of $250 - 350\,\mu$m and $850 - 950\,\mu$m. In all diffusion experiments it was ensured that water conversion was below 5%, so that the reactor could be assumed differential and chemical equilibrium would not affect the reaction rate [150].

Neither the catalyst bead diameter nor the mass flux had any effect on the hydration rate, indicating that there were no internal or external diffusion constraints at the conditions under consideration. This is hardly surprising. For reasons which will be discussed in Section 3.3.3.1, even at 120°C the initial rates of propylene hydration and etherification are about two orders of magnitude lower than the corresponding rates at which diffusional constraints are observed in isobutylene and isoamylene hydration and etherification. In MTBE synthesis for instance, Rehfinger and Hoffman [32] observed diffusional constraints for etherification rates greater than $9.6 \cdot 10^{-5}\,\mathrm{mol\,g_{cat}^{-1}\,s^{-1}}$. Gupta and Douglas [125] observed diffusional restrictions in tert-butyl alcohol synthesis starting at an hydration rate of approximately $2.8 \cdot 10^{-5}\,\mathrm{mol\,g_{cat}^{-1}\,s^{-1}}$. The initial rate of hydration in this study was $8.1 \cdot 10^{-7}\,\mathrm{mol\,g_{cat}^{-1}\,s^{-1}}$. Assuming similar reactant diffusivities, if mass transfer effects only became apparent in similar systems at rates 100 times greater, then it is unlikely that diffusion will have any noticeable effect in the DIPE system. Further confirmation of the lack of external and internal diffusion resistances can be obtained from

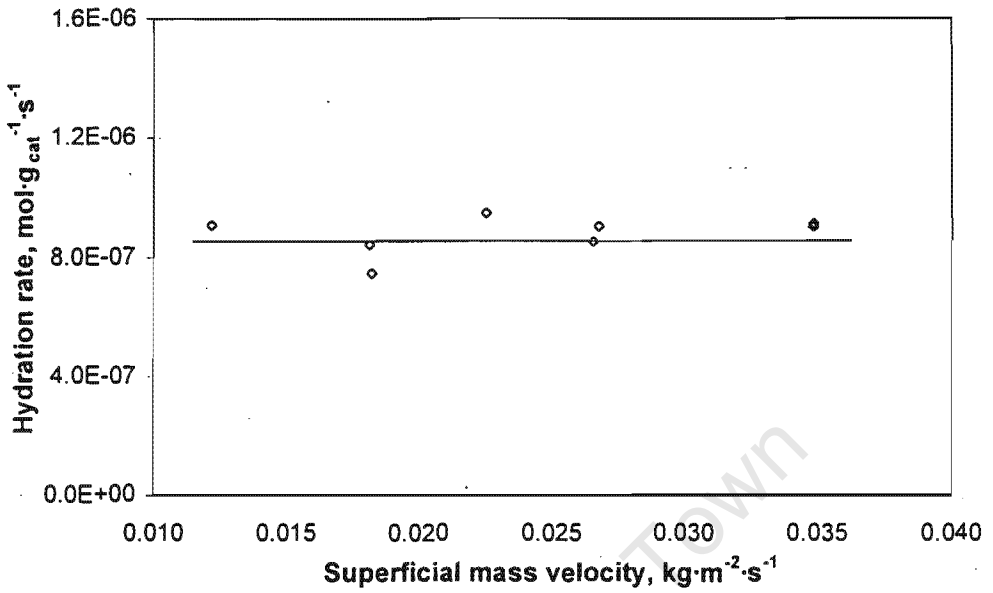

Figure 3.24: Effect of superficial mass velocity on the initial hydration rate. Temperature = 120 °C, pressure = 50 bar and WHSV = 2.0 h^{-1}.

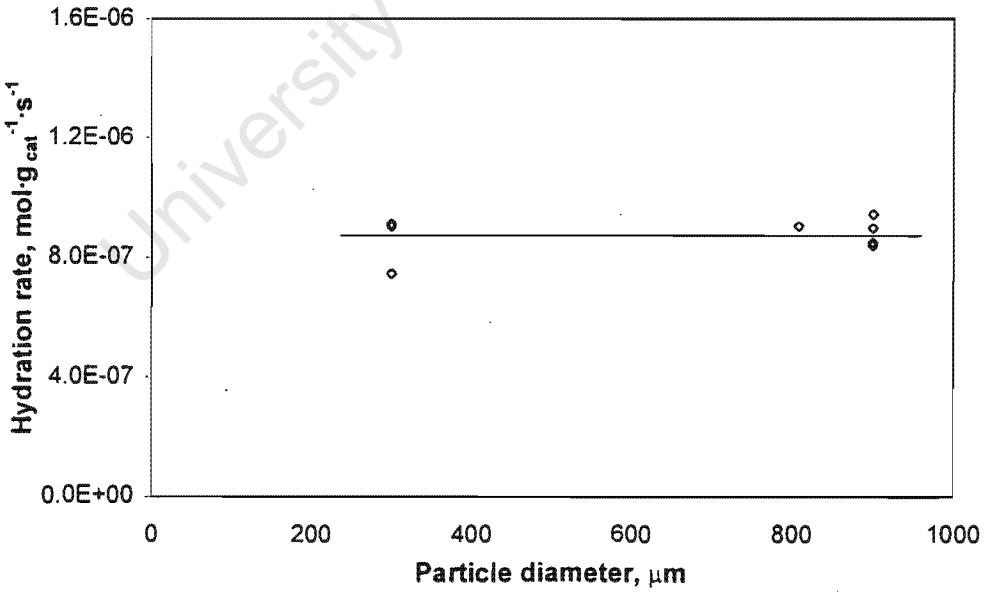

Figure 3.25: Catalyst particle size effect on initial hydration rate. Temperature = 120 °C, pressure = 50 bar and WHSV = 2.0 h^{-1}.

the Satterfield and the Weisz-Prater criteria, given by equations 3.8 and 3.9 respectively.

$$\frac{5 \cdot d_p \cdot \epsilon \cdot r_{obs}}{3 \cdot C_{eqm} \cdot D_e \cdot a_p} < 1 \tag{3.8}$$

$$\frac{\rho_{cat} \cdot r_{obs} \cdot (\frac{d_p}{6})^2}{D_e(C_{bulk} - C_{eqm})} \ll 1 \tag{3.9}$$

The Satterfield criterion [151] gives a value of 0.993 for the hydration reaction whilst a value of 0.152 is obtained for the etherification reaction (Appendix I). Even though it has been shown experimentally that the hydration reaction is not limited by mass transfer, this indicates it may, nevertheless, be on the border line between kinetic and external diffusion control. The etherification reaction may be assumed to be completely free of external mass transfer resistances.

Values of the Weisz-Prater criterion of $2.84 \cdot 10^{-3}$ and $9.24 \cdot 10^{-4}$ were obtained for the hydration and etherification reactions respectively. These values are sufficiently smaller than unity, that one can assume negligible internal diffusion effects. Indeed, Levenspiel [152] states the value of the Weisz-Prater criterion [149] need only be below 0.15 to completely discount internal diffusion effects.

3.3.2.3 Thermal gradients

The majority of authors only consider mass transport effects, but significant internal and external temperature gradients can build up in catalyst beads, which could significantly affect any subsequent kinetic evaluation. The only comprehensive study of the effect of internal and external thermal effects during hydration or etherification reactions over ion-exchange resin catalysts was that carried out by Rehfinger and Hoffman [32] in their work on MTBE synthesis. It was observed that a temperature difference as great as 10 °C can exist between the external surface of the catalyst particles and the bulk liquid under diffusion limited conditions. In the case of the DIPE system, however, the reaction rates

of both hydration and etherification are more than an order of magnitude lower than those encountered in MTBE synthesis and, as shown, none of the reactions are diffusion limited. At 120 °C and 50 bar the temperature gradient between the external catalyst surface and the bulk fluid phase estimated from the Hougen correlation [153] (see Appendix I) was found to be smaller than 0.1°C during both hydration and etherification. For all intents and purposes, the temperature of the external surface of the catalyst particles can thus be assumed to be equal to that of the bulk fluid phase.

To determine whether intraparticle temperature gradients exist, one can use the Anderson criterion [154] for spherical catalyst particles (Eq. 3.10) which is based on the assumption of an Arrhenius dependence of rate on temperature and holds even under diffusion constrained conditions

$$\frac{\Delta H_{rxn} \cdot r_{obs} \cdot d_p^2 \cdot E_a}{3 \cdot R \cdot \lambda_{cat} \cdot T_s^2} < 1 \tag{3.10}$$

Values of the Anderson criterion of $1.21 \cdot 10^{-3}$ and $1.18 \cdot 10^{-3}$ were calculated (Appendix I) for the hydration and etherification reactions respectively (at 120 °C and 50 bar). These values are sufficiently smaller than unity that one can assume negligible temperature gradients exist within the catalyst beads. This finding is in agreement with Rehfinger and Hoffman [32] who determined that the internal temperature gradients during MTBE synthesis over ion exchange resin beads were smaller than 0.4 K.

3.3.3 Effect of system parameters on DIPE synthesis

3.3.3.1 Effect of reaction temperature

The effect of reaction temperature on the initial rate of propylene hydration and etherification was investigated by varying the temperature in 10°C increments between 70 and 160°C. A pressure of 50bar was chosen for both sets of experiments. Reactants were fed in the stoichiometric ratio for DIPE synthesis, i.e. for hydration propylene and wa-

ter were fed in a 2:1 molar ratio whilst for etherification propylene and IPA were fed in a 1:1 ratio. By varying the WHSV, conversion was kept below 10% to minimise the influence of chemical equilibrium and secondary reactions on the primary reaction being studied. Indeed, only traces of DIPE and water were detected during propylene hydration and propylene etherification respectively. The reactor could be considered differential at these low conversion levels. Arrhenius type plots of the data are shown in Figures 3.26 and 3.27.

Apparent activation energies of 90.0 ± 1.6 kJmol^{-1} and 74.3 ± 1.5 kJmol^{-1} were determined from the slopes of the straight line section for propylene hydration and etherification respectively. While a major portion of the Arrhenius type plot for hydration is a straight line, it begins to deviate from the straight line relationship for temperatures above 130°C, indicative of a transition from a chemical reaction rate controlling regime to a diffusion rate controlled regime. No such diffusion limitations are evident during etherification over the temperature range studied. No side-reactions such as propylene oligomerisation were observed.

Compared to literature data for propylene hydration over ion-exchange resin catalysts (Table 3.5), the initial rate of propylene hydration over Amberlyst 15 is approximately twice as fast (on an equivalent basis) as over the intermediate macroreticular C8P resin [47] and the 50WX8 gel-type resin [155]. The apparent activation energy, E_a, of the present work is approximately 20% smaller. These large variations between different sulphonic acid ion exchange resins are, however, not uncommon. Panneman and Beenackers [148] observed variations in initial rates of MTBE formation as large as 350% between different sulphonic ion exchange resins and variations in activation energies as large as 26%. There is no reason to suppose these findings would not also apply to propylene hydration; Amberlyst 15 is apparently simply a better hydration catalyst than either of the above two ion exchange resins.

Neither initial rate of formation data nor apparent activation energy data are available

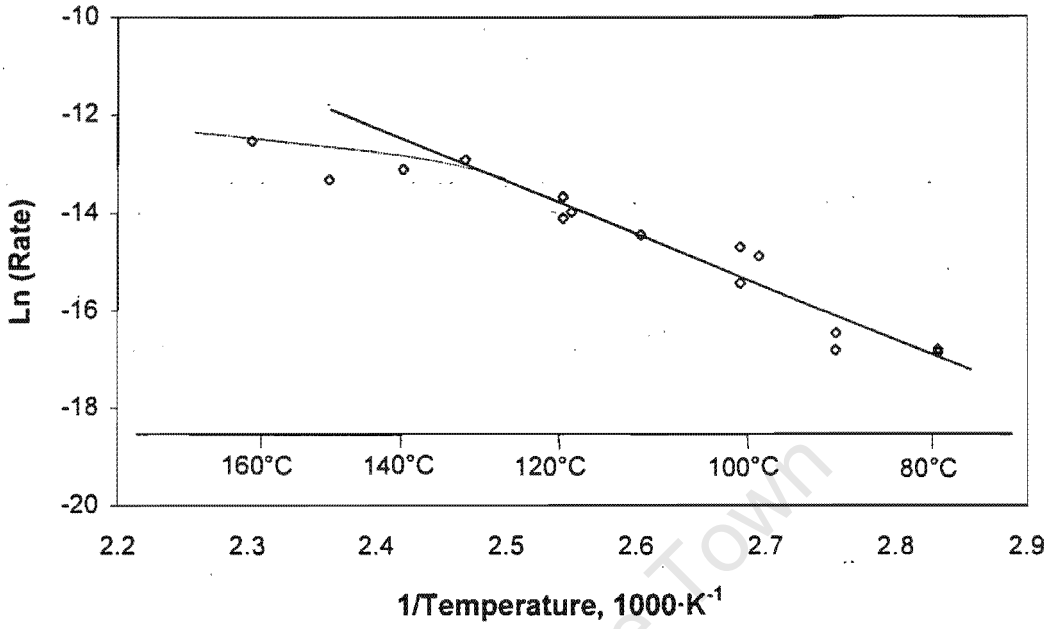

Figure 3.26: Arrhenius plot of initial propylene hydration rate in $\text{mol}_{IPA}\ \text{g}^{-1}\,\text{s}^{-1}$. Pressure $= 50\,\text{bar}$ and WHSV $= 1.4 - 5.2\,\text{h}^{-1}$

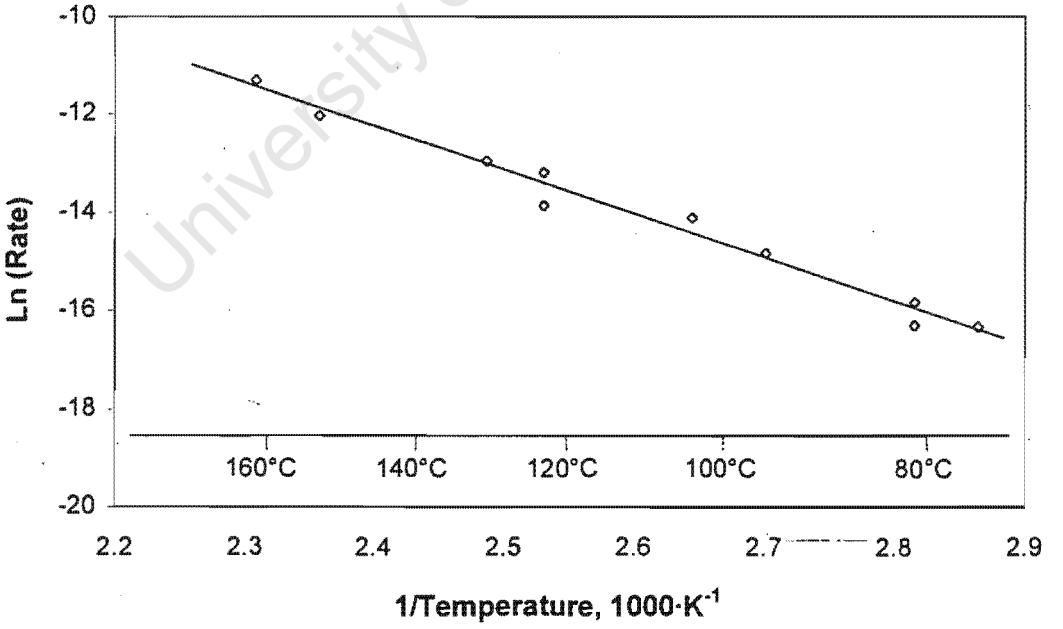

Figure 3.27: Arrhenius plot of initial etherification rate in $\text{mol}_{DIPE}\ \text{g}^{-1}\,\text{s}^{-1}$. Pressure $= 50\,\text{bar}$ and WHSV $= 2.6 - 10.5\,\text{h}^{-1}$

Table 3.5: Comparison of initial experimental propylene hydration rates from this study with experimental literature data.

	Initial rate of propylene hydration, $mol_{IPA}\, eq_{cat}^{-1}\, s^{-1\#}$		
	Present study	Petrus et al. [47]*	Hiestand [155]*
Catalyst	Amberlyst 15	C8P	50WX8
Temperature, °C			
100	$5.2 \cdot 10^{-5}$	$1.4 \cdot 10^{-5}$	$1.3 \cdot 10^{-5}$
120	$1.8 \cdot 10^{-4}$	$8.4 \cdot 10^{-5}$	$9.3 \cdot 10^{-5}$
130	$4.0 \cdot 10^{-4}$	$1.9 \cdot 10^{-4}$	$2.1 \cdot 10^{-6}$
140	$5.8 \cdot 10^{-4}$	$4.2 \cdot 10^{-4}$	$3.8 \cdot 10^{-4}$
Apparent E_a, $kJmol^{-1}$	90	109	116

* The literature values for the initial rate of propylene hydration have been adjusted to a pressure of 50bar by linear interpolation.

\# Reaction rates are quoted on an equivalent basis, i.e. $mol_{IPA} eq_{cat}^{-1} s^{-1}$, where an equivalent represents a mole of active sites.

in the literature for DIPE synthesis from propylene and IPA. The apparent activation energy for DIPE synthesis corresponds reasonably well, though, to that of other ethers over Amberlyst 15. For MTBE synthesis Gicquel and Torck [156] and Rehfinger and Hoffman [32] report values of 82.0 ± 6.7 $kJmol^{-1}$ and 86.4 ± 4.5 $kJmol^{-1}$, respectively. In ETBE synthesis Fité et al. [61] report a value of 79.3 $kJmol^{-1}$ whilst Ancillotti et al. [105] report a value of 77.7 $kJmol^{-1}$. In spite of the fact that these are apparent activation energies for the formation of different compounds, chemically similar reactions are occurring and the activation energies should thus lie in the same range. An interesting problem in DIPE synthesis, however, is that the ether can form either from the bimolecular dehydration of IPA or from the alkylation of IPA. The apparent activation energy observed here may thus be a combination of the activation energies of these two parallel reactions.

It has been shown previously that the propylene hydration rate agrees well with that from literature [47, 155]. However, the rates of formation of both IPA and DIPE are

approximately three orders of magnitude lower than the corresponding rates of products derived from isobutylene or isoamylene, see Table 3.6. While individual values in the table are not directly comparable due to the use of different acidic resin catalysts and reactant concentrations, these differences cannot account for the enormous deviations in rate.

These differences in rate are not unique to ion exchange resins. Sonnemans [110] studied the hydration of propylene and the subsequent etherification with methanol to form methyl isopropyl ether (MIPE) over H-ZSM-5. The rates of isobutylene hydration over Clinoptilolite and etherification over H-ZSM-5 have been studied by Kalló and Mihályi [99] and Chang et al. [106] respectively. Once again, it may be observed that the rate of propylene hydration is consistently lower than that for isobutylene. Furthermore, this difference in rate is not restricted to propylene. Other olefins such as ethylene and 1-butylene also exhibit low hydration and/or etherification rates.

From Table 3.6, it is apparent that reaction rates increase from ethylene, over propylene and 1-butene to isobutylene and isoamylene, which exhibit the fastest rates. Hydration and alcohol alkylation are electrophilic addition reactions whilst bimolecular dehydration is a nucleophilic substitution reaction. In these reactions a carbonium ion is the intermediate species. It is well known [131] that the reactivity and stability of carbocations increases from primary (1°) to secondary (2°) to tertiary (3°), i.e.

$$3° > 2° > 1°$$

This is in accordance with the rate data. Ethylene, which displays the slowest hydration and etherification rates gives rise to a primary carbocation. Propylene and 1-butylene, which form a secondary carbocation, exhibit faster hydration and etherification rates than ethylene, but slower than isobutylene and isoamylene which form tertiary carbocations. The rate depression is thus not a catalyst effect nor an effect of the reaction conditions, but results, rather, from the relative stability of the intermediate carbocation species.

At temperatures above 130°C the rate of propylene hydration deviates from straight

Table 3.6: The initial hydration and etherification rates of various olefins and the intermediate carbocations believed to take part in the reaction mechanism. Reaction temperature extrapolated to 60C for ion exchange resins and 120C for zeolites

Olefin	Initial rate, $mol\,eq^{-1}\,s^{-1}$	Catalyst	Intermediate carbocations#
Ethylene			
Ethanol [157]	$1.5 \cdot 10^{-7}$	Amberlyst 16	1°
Diethyl Ether [157]	$3.3 \cdot 10^{-6}$	Amberlyst 16	1°
Propylene			
IPA (this work)	$1.3 \cdot 10^{-6}$	Amberlyst 15	2°
DIPE (this work)	$3.1 \cdot 10^{-6}$	Amberlyst 15	2°
IPA [110]*	$1.7 \cdot 10^{-7}$	H-ZSM-5	2°
Methyl isopropyl ether [110]*	$2.5 \cdot 10^{-7}$	H-ZSM-5	2°
1-Butylene			
2-Butanol [158]	$2.0 \cdot 10^{-6}$	XE-307	2°
Isobutylene			
tert-Butyl alcohol [125]	$1.6 \cdot 10^{-3}$	Dowex 50W	3°
MTBE [132]	$1.9 \cdot 10^{-2}$	Amberlyst 15	3°
ETBE [105]	$1.1 \cdot 10^{-2}$	Amberlyst 15	3°
tert-Butyl alcohol [99]*	$2.9 \cdot 10^{-6}$	H-Clinoptilolite	3°
MTBE [106]*	$2.8 \cdot 10^{-4}$	H-ZSM-5	3°
Isoamylene			
tert-Amyl alcohol [157]	$1.4 \cdot 10^{-3}$	Amberlyst 16	3°
TAME [35]	$3.9 \cdot 10^{-3}$	Lewatit SPC 118	3°

* Zeolite catalyst

#1° primary carbocation; 2° secondary carbocation; 3° tertiary carbocation

line behaviour 3.26. This is typical of the transition from a reaction rate controlled regime to a mass transfer limited regime. Identical behaviour was also observed by Petrus et al. [47] at temperatures above 130°C. Interestingly, as stated in Section 3.3.2.2, a value of 0.99 was calculated for the Satterfield criterion for the propylene hydration reaction at 120 °C while a value of 0.15 was obtained for the etherification reaction at the same conditions. This indicated that the hydration reaction was most likely closer to a diffusion limited regime than the etherification reaction, identical to the situation observed here. The maximum rate of hydration which can be assumed completely free of mass transfer limitations is $2.0 \cdot 10^{-6}\,\mathrm{mol}_{IPA}\,\mathrm{g}^{-1}\,\mathrm{s}^{-1}$.

Since the reaction occurs in the liquid phase within the catalyst pellets, one would expect the limiting reagent under diffusion controlled conditions to be the gaseous component which has to diffuse from the gaseous phase through the liquid phase to the active sites. In the case of propylene hydration or etherification the mass transfer limited reagent would thus be expected to be the propylene. Since it has been shown that the diffusivity of propylene is only about 20% greater in IPA than in water (Appendix I), diffusion effects should become apparent at similar rates of propylene consumption. Experimental etherification data, however, exhibit no mass transfer limitations over the temperature range examined, even at propylene consumption rates an order of magnitude greater than in IPA synthesis.

At 120°C and 50bar the liquid phase propylene mole fraction is $1.2 \cdot 10^{-3}$ in water as opposed to 0.49 in IPA. During hydration, even low conversions will thus significantly affect the liquid phase propylene concentration and additional propylene has to diffuse into the liquid phase to compensate for propylene consumed by reaction. At fast reaction rates this leads to mass transfer limitations. In etherification, low conversion levels will not significantly affect the propylene concentration, minimal propylene thus has to diffuse into the liquid phase and reaction rates are apparently not affected by diffusion. Consequently, even though diffusion may be slower than the reaction rate, there is sufficient propylene

in the liquid phase to compensate for consumption and thus no diffusion limitations are observed.

3.3.3.2 Effect of reaction pressure

The effect of pressure on the initial rate of propylene hydration and etherification was investigated between 1 and 70 bar at a temperature of 120°C. At atmospheric pressure all the reactants were in the vapour phase whilst for any pressure above 2 bar, for hydration, or 4 bar, for etherification, the reactor behaved as a trickle bed with all reaction occurring in the liquid phase within the catalyst particles. As for the temperature study, reactants were fed in the stoichiometric ratio for DIPE synthesis (2:1 propylene:water or 1:1 propylene:IPA) and conversion was limited to 10%, so as to operate differentially. The variation of reaction rate with system pressure is shown in Figures 3.28 and 3.29.

As in Section 3.3.3.1, negligible side reactions were observed. During hydration traces of DIPE were detected, during etherification traces of water were formed from IPA dehydration. The rate of hydration was always below $2.0 \cdot 10^{-6}\,\mathrm{mol}_{IPA}\,\mathrm{g}^{-1}\,\mathrm{s}^{-1}$ so rate data were free of mass transfer limitations. The rate of formation of IPA from propylene and water appeared to increase linearly while the rate of formation of DIPE from IPA and propylene appeared to increase non-linearly, becoming more dependent on pressure as this was increased. For both sets of reactions, the vapour phase rate at atmospheric pressure was greater than that in the liquid phase. The difference between the vapour phase rate and the liquid phase rate being considerably more pronounced for etherification than for hydration.

The hydration and etherification of isobutylene or isoamylene can be performed at low temperatures ($\approx 60\,^{\circ}\mathrm{C}$) due to the high activity of the tertiary carbocation intermediate. At these temperatures isobutylene and isoamylene are well below their critical temperatures of $145\,^{\circ}\mathrm{C}$ and $\approx 194\,^{\circ}\mathrm{C}$ and any increase in pressure above their vapour pressure will

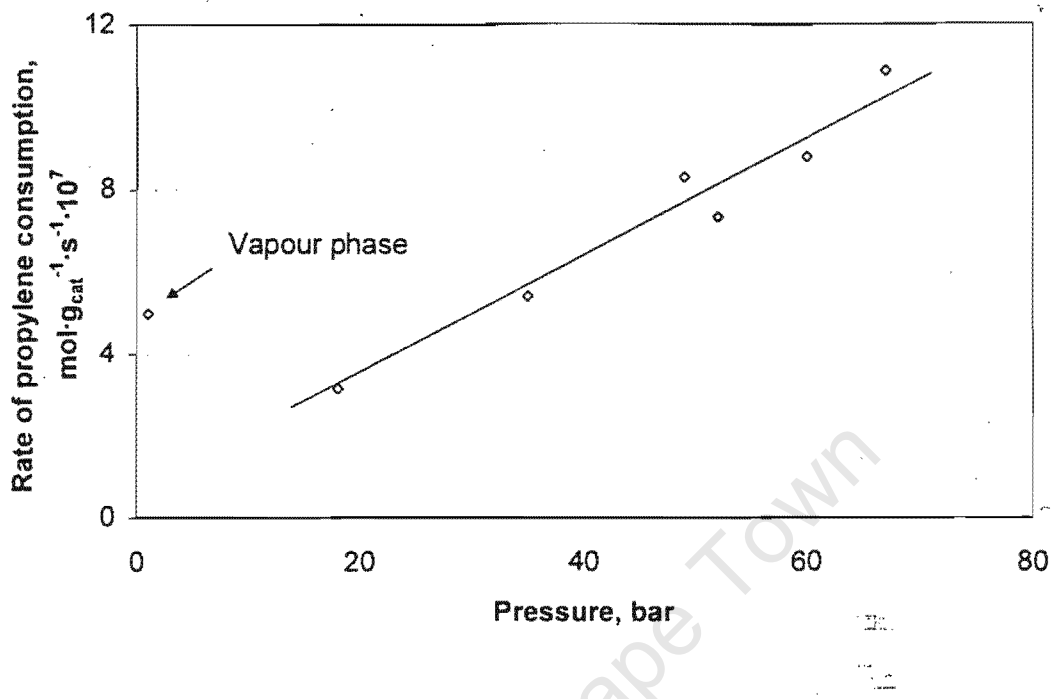

Figure 3.28: Effect of pressure on the rate of propylene hydration. Temperature = 120°C, propylene:water ratio = 2:1.

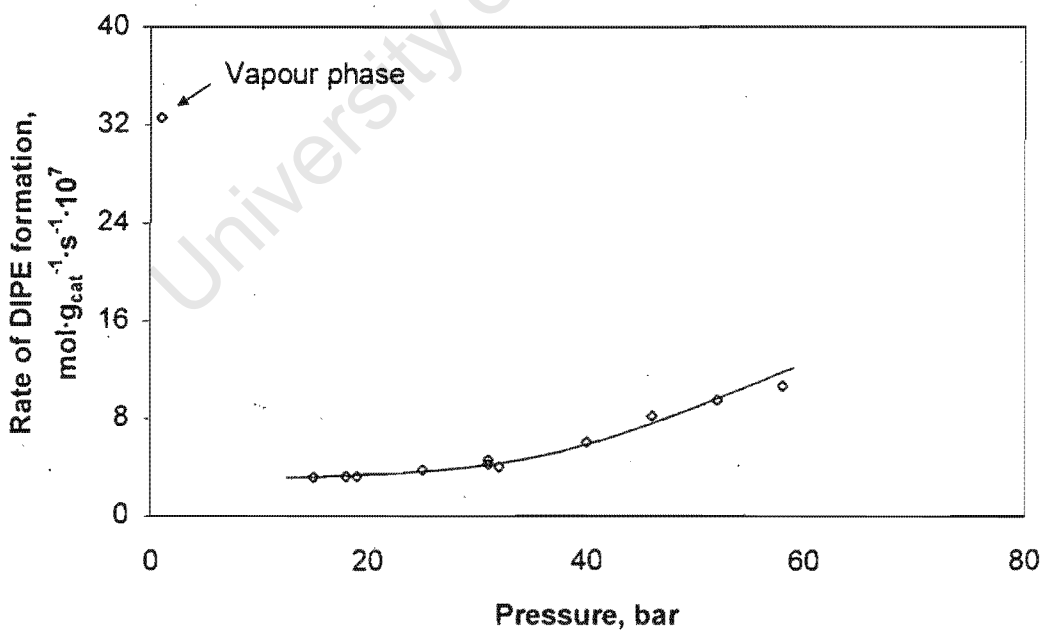

Figure 3.29: Effect of pressure on the rate of DIPE formation. Temperature = 120°C, propylene:IPA ratio = 1:1.

have a negligible effect on their activity. Once the system is liquid phase, pressure thus has no further effect on the reaction rate. This was confirmed by the work of Oost and Hoffman [35] who observed no effect on pressure on the rate of TAME formation between 16 and 21 bar.

Propylene hydration and etherification on the other hand are performed at elevated temperatures ($> 100\,^{\circ}C$) to compensate for the lower reactivity of the propyl carbocation. Propylene is thus super-critical ($T_c = 92\,^{\circ}C$) and any increase in pressure will increase its activity and, consequently, the reaction rate. This has been found in literature for IPA synthesis. Petrus et al. [47] and Hiestand [155] observed that the rate of hydration approximately doubles from 30 to 100 bar. The activities of the reactants for hydration and etherification along with the liquid phase mole fraction of propylene in this study were calculated using the WS-PRSV model and are shown in Figures 3.30 and 3.31 respectively.

Over the pressure range of 10 to 90bar, the activity of water remains constant (Fig. 3.30). That of IPA in the propylene/IPA system decreases slightly (from 3.1. to 2.7) between 10 and 30bar, but remains constant for greater pressures as the liquid phase propylene concentration does not change any longer (Fig. 3.31). The increase in hydration and etherification rate with pressure can thus be attributed solely to the increasing propylene activity rather than to changes in the water or IPA activities. Indeed, the reported doubling in hydration rate [47, 155] between 30 and 100bar corresponds excellently with the two-fold increase in propylene activity (from 22.9 to 46.8). In the present study, the almost linear increase in propylene activity as calculated by the WS-PRSV model is reflected in the linear increase of the experimental propylene hydration rate data. Between 18 and 67 bar, the propylene activity in the system rises from 14.2 to 39.8 whilst the etherification rate increases from $3.4 \cdot 10^{-7}\,mol\,g^{-1}\,s^{-1}$ to $1.1 \cdot 10^{-6}\,mol\,g^{-1}\,s^{-1}$ - a 2.8 fold increase in activity and 3.2 fold increase in reaction rate. This shows that the rate of hydration is first order with respect to propylene activity. The order of dependency of reaction rate on the activity of water could not be determined as this was always in large

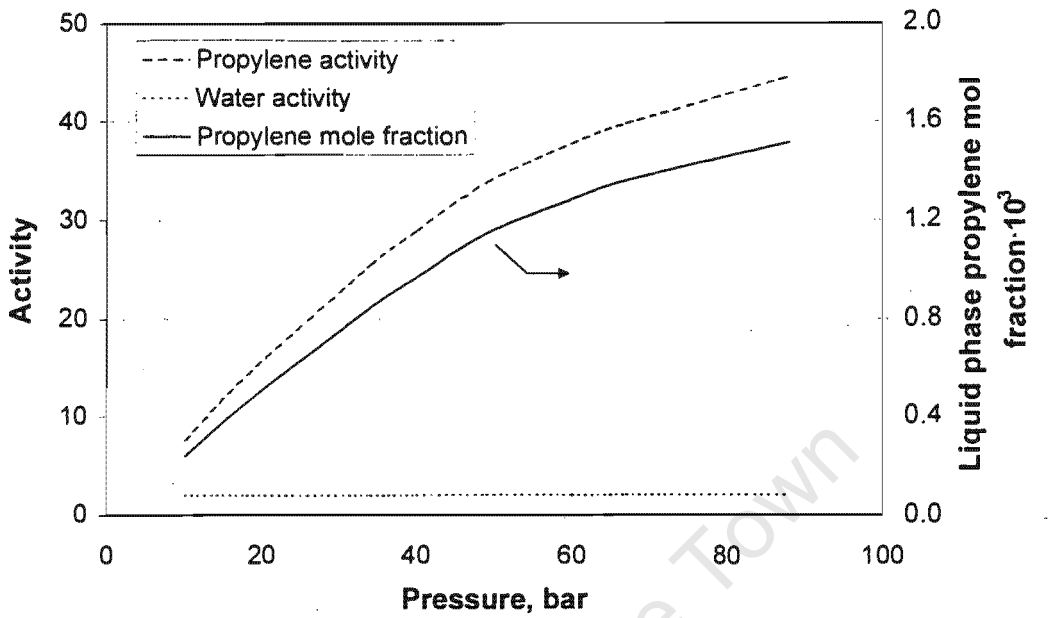

Figure 3.30: Change in the liquid phase propylene mole fraction and the thermodynamic activity of propylene and water with pressure.

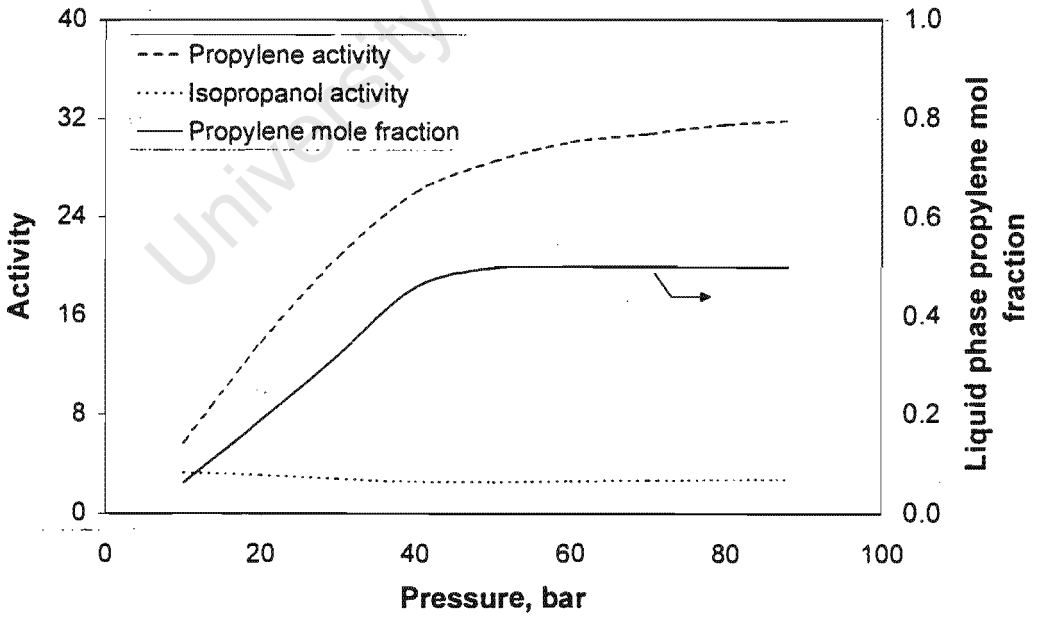

Figure 3.31: Change in the liquid phase propylene mole fraction and the thermodynamic activity of propylene and IPA with pressure.

excess and thus nearly constant.

For DIPE synthesis from propylene and IPA, though, the relationship between activity and etherification rate is rather different. Up to a pressure of approximately 30bar both the propylene activity and the etherification rate increase almost linearly, though not at a 1:1 ratio as for hydration. Above 30bar, however, the situation changes. The propylene activity increases less rapidly with increasing pressure, yet the rate of etherification seems to increase ever faster with pressure, considerably faster than the rise in activity. This phenomenon may be explained by means of a kinetic analysis as demonstrated below.

Since the conversions were low in these experiments, one could assume that reverse reactions did not occur to any great extent. For both hydration and to some extent for etherification, the liquid phase consisted mostly of the polar species and consequently the pseudo-homogeneous reaction model may be assumed to represent the kinetic data (Section 3.1.5). Assuming mass-action kinetics, the rates of hydration and etherification (the sum of the rate of bimolecular dehydration, r_{bimol}, and the rate of IPA alkylation, r_{alkyl}) can now be written as

$$r_{IPA} = k_{r1} \cdot a_{propylene}^{\alpha} \cdot a_{water}^{\beta} \tag{3.11}$$

$$r_{DIPE} = r_{alkyl} + r_{bimol} = k_{r2} \cdot a_{propylene}^{\gamma} \cdot a_{IPA}^{\delta} + k_{r3} \cdot (a_{IPA} \cdot a_{IPA})^{\varepsilon} \tag{3.12}$$

The activities of water, a_{water}, and IPA, a_{IPA}, do not change much with pressure, thus these rate equations may be reduced to

$$r_{IPA} = k'_{r1} \cdot a_{propylene}^{\alpha} \tag{3.13}$$

$$r_{DIPE} = k'_{r2} \cdot a_{propylene}^{\gamma} + c_1 \tag{3.14}$$

Taking the natural logarithm of these rate equations leads to

$$\ln r_{IPA} = c_2 + \alpha \ln (a_{propylene}) \tag{3.15}$$

$$\ln r_{DIPE} = c_3 + \ln\left(a^{\gamma}_{propylene} + \frac{c_1}{k'_{r2}}\right) \quad (3.16)$$

The order of the hydration and etherification reactions with respect to propylene can be obtained from the slope of the plot of the natural logarithm of the reaction rate against the natural logarithm of the propylene activity, Figures 3.32 and 3.33 respectively.

The slope of the plot for hydration rate, i.e. α, was found to be 1.1 ± 0.03. This slope is close enough to unity, to indicate that the reaction is first order with respect to propylene activity, as mentioned previously. For etherification, it is not as clear cut. There are two distinct linear sections to the plot - these were fit separately. The first section, between 15 and 30 bar, has an average slope of 0.45 ± 0.03 whilst the second section, at pressures above 30 bar, has an average slope of 2.62 ± 0.04.

If DIPE were to be formed only from the bimolecular dehydration of IPA then its rate of formation would be independent of propylene activity and the slope of the etherification rate vs. propylene activity plot would be 0. On the other hand, Ancillotti et al. [105] found the rate of methanol alkylation with isobutylene to be first order with respect to isobutylene concentration. Thus, if DIPE were to be formed exclusively from the alkylation of IPA, then the slope with respect to the natural logarithm of propylene activity should be 1. Since the slope of the initial section equals 0.45 one can conclude that at least between 15 and 30 bar at 120 °C, DIPE is formed from *both* bimolecular dehydration and from IPA alkylation.

For pressure greater than approximately 30 bar, the average slope of the experimental data changes from 0.45 to 2.6. In etherification at low reaction pressure the reaction medium was predominantly polar and the matrix was fully swelled. A kinetic equation based on the pseudo-homogeneous mechanism could thus be used to represent the data (see Section 3.1.5). At higher pressures, i.e. above 30 bar, the propylene concentration is greater (see Figure 3.31) and one can expect that the catalytic mechanism shifts from the less active pseudo-homogeneous to a more active concerted mechanism (compare Fig.

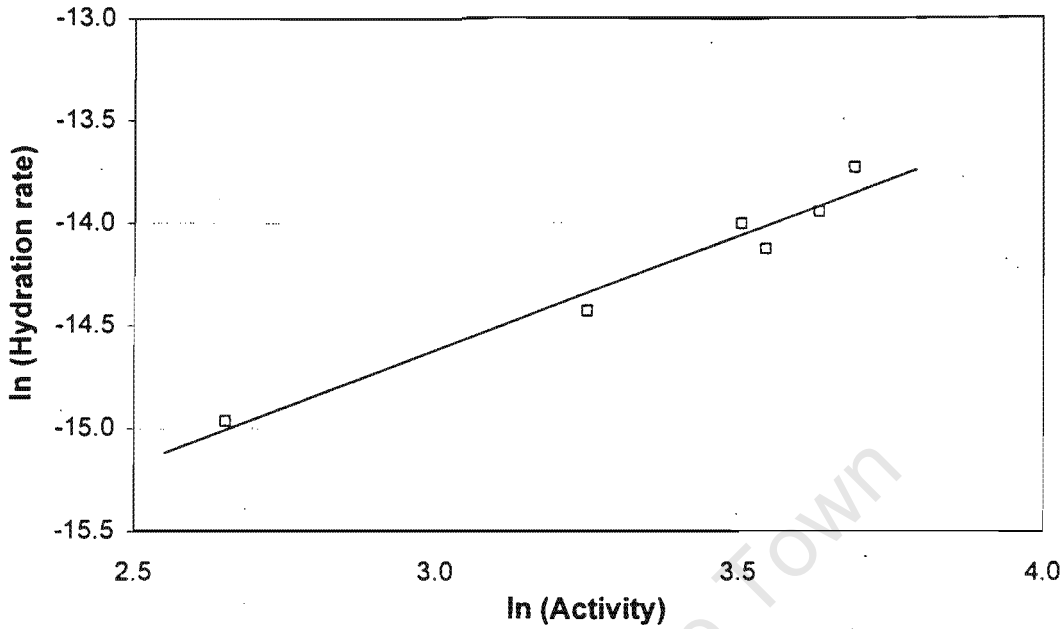

Figure 3.32: Plot of the natural logarithm of the rate of propylene hydration against the natural logarithm of propylene activity.

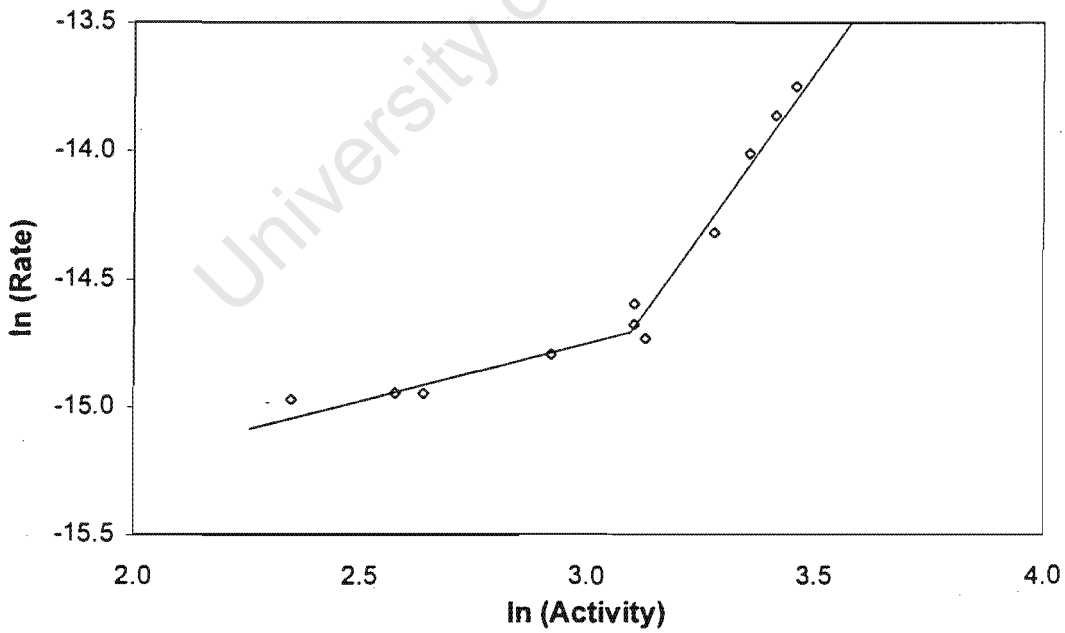

Figure 3.33: Plot of the natural logarithm of the rate of DIPE formation against the natural logarithm of propylene activity.

3.18 and Section 3.1.5). The increased dependency of reaction rate on propylene activity for pressures above 30 bar thus results from a combination of the increasing propylene activity *and* a changing reaction mechanism. Strictly speaking, in this mechanistic regime the pseudo-homogeneous model no longer applies and the increased slope of the plot only gives an indication of the greater order of dependency of reaction rate on propylene activity.

Consequently, using the pseudo-homogeneous reaction model for etherification, only the slope at low activities can be used to determine the reaction order with respect to propylene activity and the extent to which each of the DIPE formation reactions occur. Since the propylene concentration in water is extremely small, this mechanistic transition cannot take place during hydration and the entire data range can be used.

The linear pseudo-homogeneous kinetic model given by Eq. 3.14 was fit to the experimental data between 15 and 30 bar assuming a constant IPA activity. This time, the bimolecular dehydration parameter, c_1, was fit too. The rate of bimolecular dehydration, given by the constant c_1, was determined as $2.6 \cdot 10^{-7} \pm 1.3 \cdot 10^{-8}\,\mathrm{mol\,g^{-1}\,s^{-1}}$. The value of the modified rate constant, k'_{r2}, was found to be $1.0 \cdot 10^{-8}\,\mathrm{mol\,g^{-1}\,s^{-1}}$. The rate of bimolecular dehydration will remain constant as long as the temperature and the IPA activity do not change. At any point, the rate of IPA alkylation is simply the difference between the nett rate of DIPE formation and the bimolecular dehydration rate. The ratio of the rate of bimolecular dehydration to the rate of IPA alkylation and the fit of the rate equation to the initial rate data for low pressure is shown in Figure 3.34.

At low pressure, the activity of propylene is low and the dominant DIPE formation reaction is bimolecular dehydration. As the pressure increases, the activity of propylene increases and the IPA alkylation reaction begins to accelerate until, at approximately 30 bar, it overtakes the rate of bimolecular dehydration. Unfortunately, for pressures much higher than 30 bar, the contribution of each reaction to DIPE formation is masked by the abrupt change in the relationship between rate and activity as discussed above -

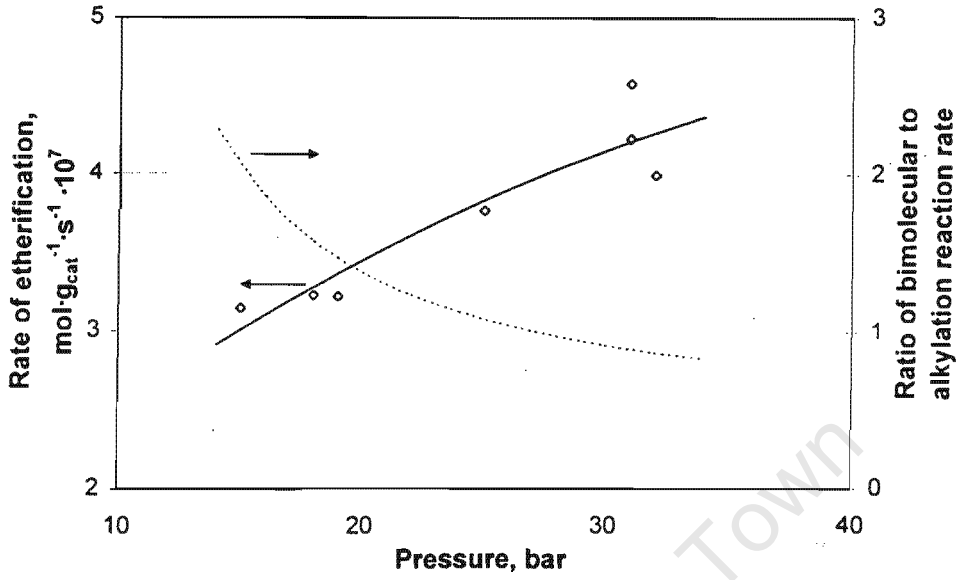

Figure 3.34: Ratio of the rate of bimolecular dehydration to the rate of IPA alkylation and the fit of the rate equation to the initial rate data at low pressures.

extrapolation of the low pressure data is difficult as the hypothesised change in mechanism may affect the ratio of reaction.

However, feeding *only* IPA at a pressure of 50 bar and a temperature of 120°C, an initial rate of DIPE formation of $7.2 \cdot 10^{-7}$ mol g^{-1} s^{-1} was observed. During differential operation the only DIPE formation reaction which can occur in this system is the bimolecular dehydration of IPA. The IPA activity at these conditions is 4.0. Under the conditions of etherification for the pressure series, the average activity of IPA was approximately 2.7 (See Figure 3.31). If one assumes that the rate of bimolecular dehydration is proportional to the square of IPA activity (see Eq. 3.12) then extrapolation of the rate of DIPE formation from pure IPA to the experimental conditions used for the pressure study gives a revised value of the bimolecular dehydration rate at 50bar and 120 °C of $3.3 \cdot 10^{-7}$ mol g^{-1} s^{-1}. While this value does not agree exactly with the constant rate of bimolecular dehydration obtained above ($2.6 \cdot 10^{-7}$ mol g^{-1} s^{-1}), it is close enough that it

can be assumed that the extrapolated ratio line can be used to give an indication of the extent to which each DIPE formation reaction occurs at higher pressure.

At 120°C and atmospheric pressure the system is entirely vapour phase for both hydration and etherification. The activities of the species in the system are thus approximately equal to their mole fraction. For hydration this means the activity of water is 0.333 while that of propylene is 0.666. For etherification both the propylene and the IPA activity are equal to 0.5. If the same catalytic mechanism applied under vapour phase conditions. the rate of hydration and etherification should be significantly smaller than at higher pressure. However, the rate of reaction was found to be larger than that at high pressure. Were the same pseudo-homogeneous kinetic model to apply, the values of the rate constants would have to be respectively 200 and 1200 times greater than those for hydration and etherification at high pressure. However, in this case the ratio of apolar to polar species in the reaction medium was greater (2:1 and 1:1 for propylene hydration and IPA etherification respectively) and the total concentration of species was obviously lower than during the liquid phase high pressure experiments. Under these conditions, it is probable that the reactions would have been occurring via the most catalytically more active mechanisms. the Type III mechanisms (see Section 3.1.5).

3.3.3.3 Propylene to water ratio

In industry propylene hydration is performed at high water to propylene mole ratios (between 15:1 and 10:1) principally to limit the formation of by-products such as DIPE and propylene oligomers [49, 22]. At these high ratios the propylene hydration reaction is thermodynamically favoured over propylene oligomerisation or propylene etherification. However, since the aim of this study is to synthesise DIPE, it is necessary to operate at low water to propylene ratios so as to thermodynamically favour propylene etherification.

The effect of olefin to water ratio during hydration has been studied previously only

over a very narrow range of ratios by Gupta and Douglas [125] during isobutylene hydration and Petrus et al. [47] during propylene hydration. The rate of hydration was not affected by the ratio and no enhancement of side-reactions was observed. The issue of olefin to alcohol ratio during etherification has been the subject of extensive study due to the large variations in reaction rate, refer to Section 3.1.5. These studies have, however, all focussed on the etherification of subcritical isobutylene or isoamylene and the extent to which they apply to supercritical propylene etherification is unknown.

In the present study, the influence of the overall propylene to water ratio on hydration and etherification was investigated between propylene to water mole ratios of 1:5 and 10:1 and propylene to IPA mole ratios of 1:5 and 6:1. Once again, operating conditions of 120 °C and 50bar were chosen. The effect of the propylene to water feed ratio on hydration rate is shown in Figure 3.35 and the effect of the propylene to IPA ratio on etherification rate is shown in Figure 3.36.

The ratio of propylene to water had no effect on the rate of hydration between ratios of 1:5 and 10:1. At these ratios the only products were IPA (selectivity > 98%) and DIPE (selectivity < 2%). For ratios of propylene to water greater than 10:1 the formation of dimers of propylene was observed with a corresponding increase in the rate of propylene consumption. During etherification it was observed that as the ratio of propylene to IPA increased from 1:5 to 1:1 the rate of DIPE formation increased. For higher ratios there was no further change in the etherification rate. No oligomers were detected over the range of ratios studied.

At 120 °C and 50 bar the activities of propylene and water remain constant at 33.8 and 2.0, respectively, between propylene to water ratios of 1:20 and 20:1. Furthermore, the liquid phase propylene mole fraction also remains constant at $1.14 \cdot 10^{-3}$. Thus, neither the reaction mechanism (dependent on the liquid phase propylene concentration) nor the reaction rate (dependent on the reactant activities) should vary over this range of molar ratios. However, this only applies if one assumes vapour-liquid phase equilibrium and

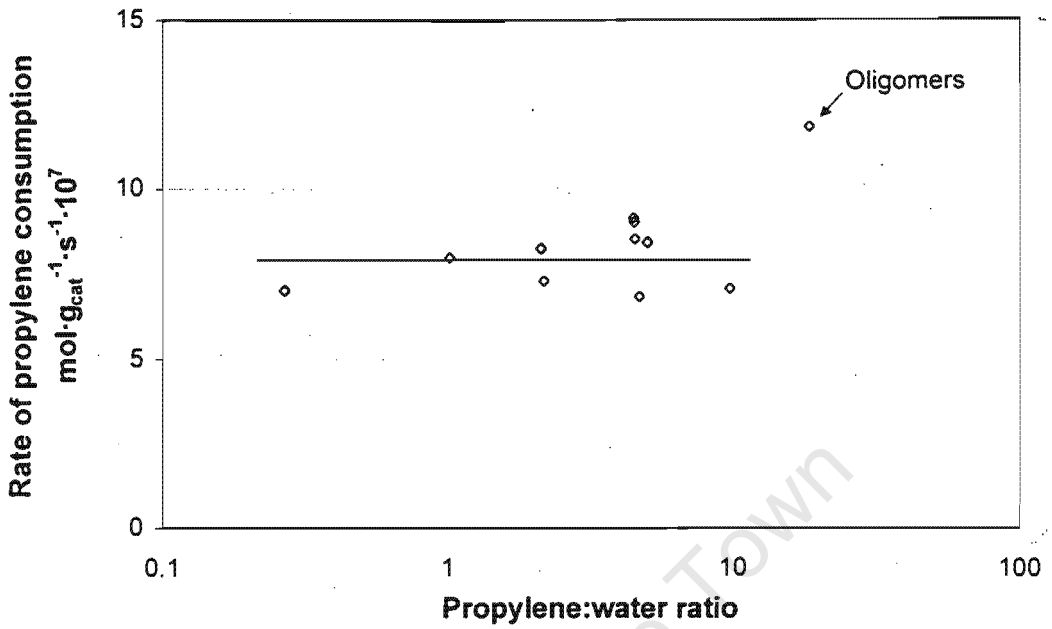

Figure 3.35: Effect of the propylene to water feed ratio on the hydration rate. Temperature = 120 °C and Pressure = 50 bar.

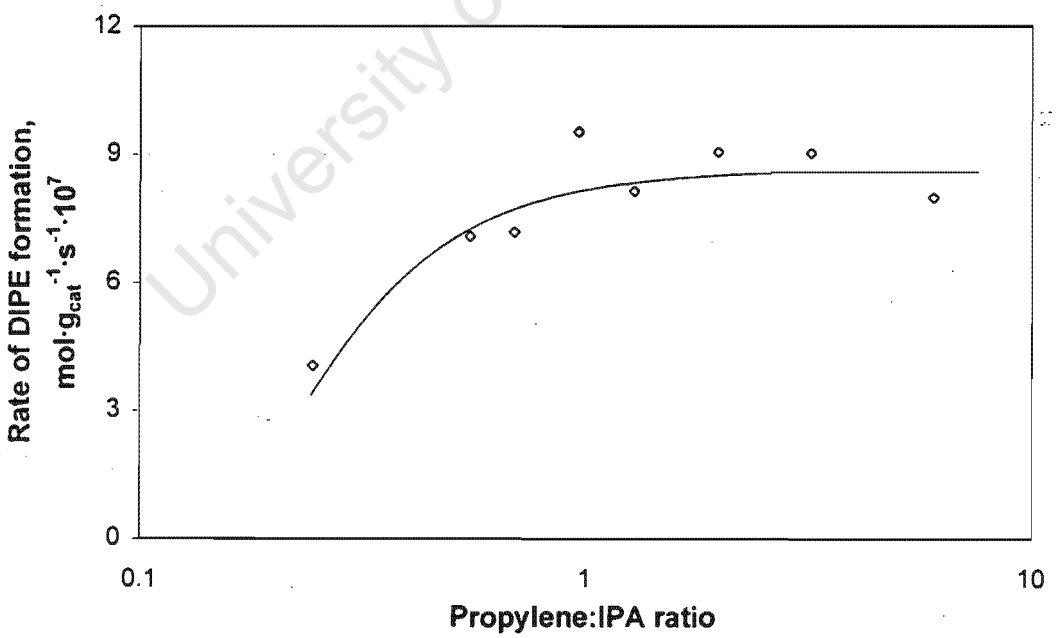

Figure 3.36: Effect of the propylene to IPA feed ratio on the etherification rate. Temperature = 120 °C and Pressure = 50 bar.

complete wetting at every point down the reactor.

In trickle-bed systems it has been observed that high ratios of gas to liquid flow can lead to channeling and decreased wetting efficiency [145, 140]. Under these conditions interphase mixing would be poor and phase-equilibrium might not be reached. The activity of the more volatile species in the gas phase would be increased relative to the activity of the less volatile species in the gas phase and contact between the unsaturated gas phase and "unwetted" catalyst may result in the enhancement of undesirable side reactions.

This is exactly what was in fact observed. At propylene to water ratios below 10:1. the vapour and liquid phases in the trickle-bed reactor were in equilibrium and the catalyst was practically fully wetted (see Appendix I). The rate of hydration was, consequently, unaffected by changing propylene to water ratios. As the ratio of propylene to water was increased, however, the ratio of gas-phase to liquid-phase increased, the wetting efficiency decreased and mixing became poorer until the system was no longer in vapour-liquid equilibrium. At this point, at a propylene to water ratio of approximately 10:1, the activity of water in the gas phase was lower than the activity under saturated conditions and propylene adsorption on unwetted catalyst portions was thus enhanced. The greater rate of propylene consumption at high propylene to water ratios thus results from additional propylene consumption in oligomerisation reactions which are no longer suppressed to the same extent by competitive adsorption.

Since propylene is completely miscible in IPA, the propylene activity, the IPA activity and the liquid phase propylene concentration vary with changing propylene to IPA ratios. These changes affect both the reaction rate and the reaction mechanism. The WS-PRSV model was used to determine the reactant activities and the liquid phase mole fraction with changing propylene to IPA ratio (see Figure 3.37).

At low propylene to IPA ratios the resin is fully solvated and catalysis occurs via a pseudo-homogeneous mechanism. As the propylene to IPA ratio is increased, the

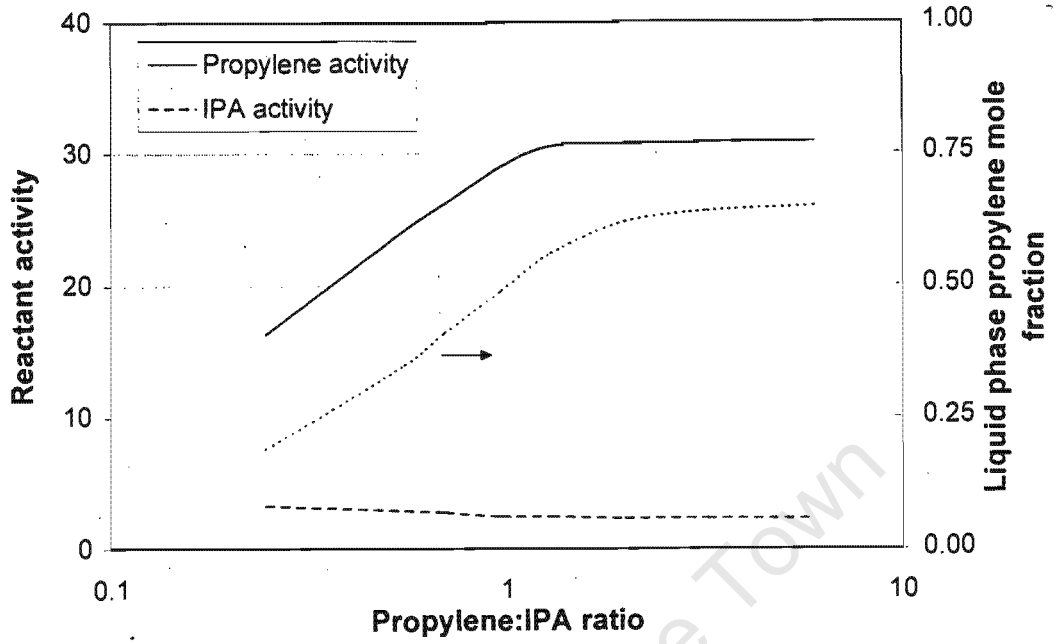

Figure 3.37: Reactant activities and liquid phase propylene mole fraction as a function of changing propylene to IPA ratio. Temperature = 120 °C and Pressure = 50 bar.

concentration of apolar species in the liquid phase increases and the mechanism gradually changes to a more active concerted one (ref. Section 3.1.5). This transition in mechanism together with the changes in propylene and IPA activity account for the increase in the rate of etherification observed at low propylene to IPA ratios. This change in catalytic action is analogous to that believed to occur for changing pressure during etherification (Section 3.3.3.2). At propylene to IPA ratios greater than 1:1, the reactant activities and the liquid phase propylene concentration remain constant. Consequently, no further shift in mechanism takes place and the reaction rate remains constant.

The same general trends in reaction rate with changing olefin to alcohol ratio are observed in supercritical propylene etherification as are observed in subcritical isobutylene or isoamylene etherification. In comparison, the effects of changing olefin to alcohol ratio are considerably less pronounced for propylene etherification, though, since the range of

possible ratios is restricted by the vapour-liquid nature of the system. In isobutylene or isoamylene etherification the ratio can be changed at will since the species are subcritical and completely miscible. However, in propylene etherification, the range of possible ratios is dependent on the system temperature and pressure. Exactly as for hydration, one would also expect propylene oligomerisation to occur at some point during the etherification study. In MTBE synthesis, the formation of diisobutylene has been found to increase with increasing isobutylene to methanol ratio [32]. Over the range of propylene to IPA ratios studied, however, oligomers were never detected, though they may have been present in amounts below the detection limits of the analysis techniques.

3.3.3.4 Effect of contact time

The effect of contact time on single stage DIPE synthesis, firstly, from propylene and water in a 2:1 molar ratio and, secondly, from pure IPA was studied under low pressure, vapour phase conditions and high pressure, trickle-bed conditions. All experiments were carried out at a temperature of 120 °C. In each case contact time was increased until chemical equilibrium was attained. In the case of the two atmospheric pressure series and the pure IPA series at a pressure of 50 bar, the contact time was varied simply by varying the feed flowrate (see Figures 3.38, 3.39 and 3.40).

Limitations in the ability to pump propylene necessitated a different experimental method to study the effect of contact time on the reaction between propylene and water at 120°C and 50 bar. This experimental series started from a feed of propylene and water in a 2:1 molar ratio, stoichiometric for DIPE formation. The effective contact time was then increased in small steps by feeding the reactor product composition from the previous run as the reactor feed in the following experimental run. Every experiment in this series was performed twice, or more often, to ensure accurate results. The variation in mole fraction of water, propylene, IPA and DIPE with contact time is shown in Figure 3.41.

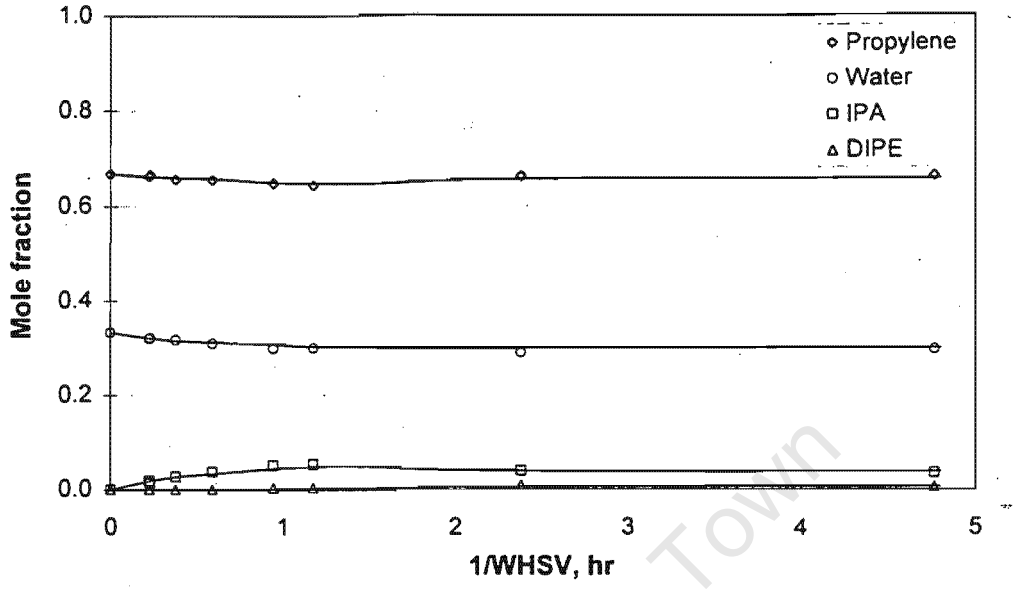

Figure 3.38: Effect of contact time on DIPE synthesis from propylene and water at atmospheric pressure. Temperature = 120 °C, Pressure = 1 atm, initial propylene:water ratio = 2 : 1.

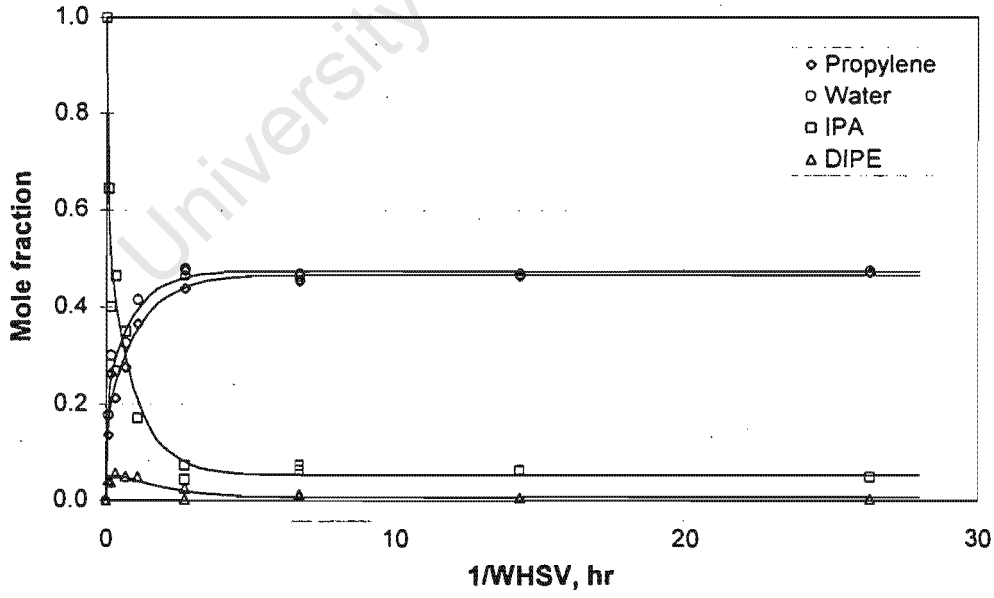

Figure 3.39: Effect of contact time on DIPE synthesis from IPA at atmospheric pressure. Temperature = 120 °C, Pressure = 1 atm.

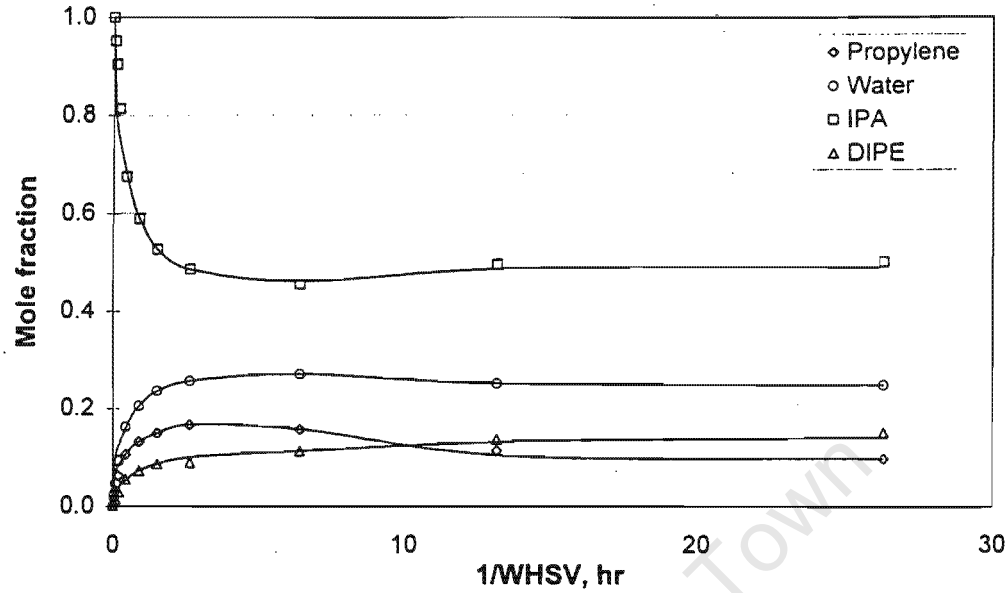

Figure 3.40: Effect of contact time on DIPE synthesis from IPA at high pressure. Temperature = 120 °C, Pressure = 50 bar.

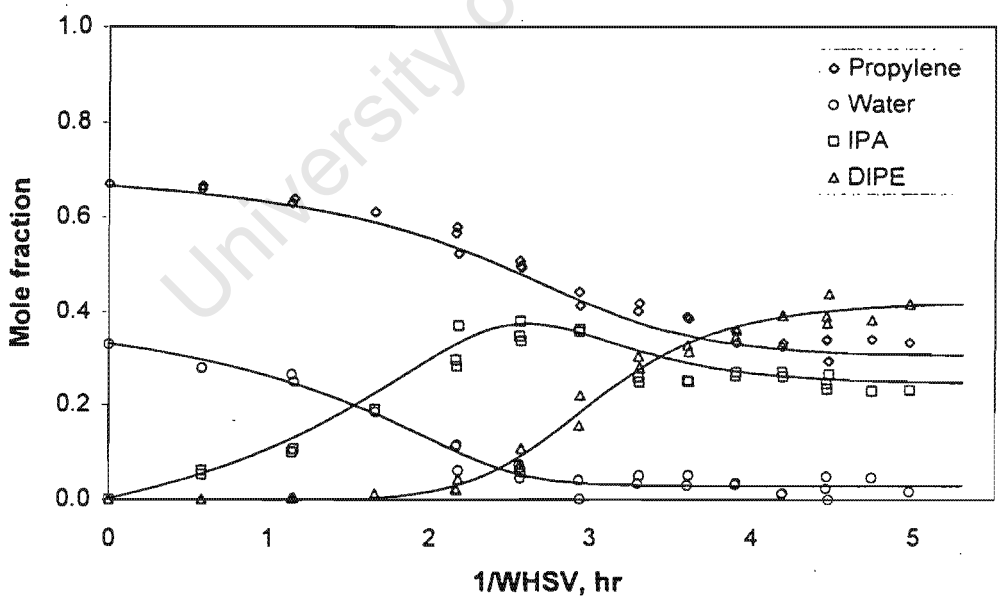

Figure 3.41: Effect of contact time on DIPE synthesis from propylene and water at high pressure. Temperature = 120 °C, Pressure = 50 bar, initial propylene:water ratio = 2 : 1.

Knözinger [159] studied the reaction scheme of vapour-phase ethanol dehydration over $\gamma - Al_2O_3$. The main products of ethanol decomposition were ethylene, water and diethyl ether. The dehydration of ethanol to form ethylene and water and the bimolecular dehydration of ethanol to form diethyl ether and water were the primary parallel reaction steps. In a secondary reaction diethyl ether, one of the primary products, decomposed to give ethanol and ethylene.

The identical reaction network apparently occurs during DIPE synthesis over the sulphonic ion exchange resin, Amberlyst 15. It has been shown (Section 3.3.3.2) that DIPE is formed from two parallel reactions: the bimolecular dehydration of IPA and the alkylation of IPA with propylene. IPA, obviously, is formed from the hydration of propylene. No detectable amounts of by-products, i.e. dimers or trimers of propylene, were produced at any stage during DIPE synthesis. This reaction network can be thought of as cyclic, any two reactions in series having the same nett effect on the system as the remaining reaction on its own (see Figure 3.42)

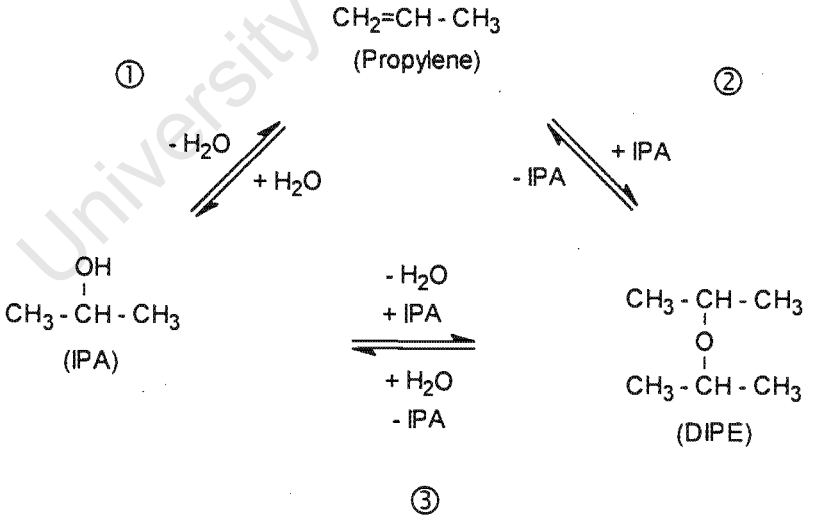

Figure 3.42: Cyclic reaction network of DIPE formation

The observed trends in mole fractions in all the contact time experiments are typical of the above series-parallel network. Feeding propylene and water (Figures 3.38 and 3.41),

the first product which became apparent at both low and high pressure was IPA. The concentration of IPA increased to a maximum, overshot the equilibrium mole fraction and then decreased again as it was consumed (by alkylation and/or dehydration) to produce DIPE in a series reaction step. This makes IPA the primary, intermediate product and DIPE the secondary, final product.

At atmospheric pressure and at 50 bar, feeding only the intermediate product IPA (Figures 3.39 and 3.40), the non-zero initial rates of formation of propylene, water and DIPE indicated that these were all primary reaction products. Propylene and some water resulted from the dehydration of IPA whilst DIPE, as a primary product from an IPA feed, could only be formed from the bimolecular dehydration of IPA. The latter reaction produces the excess water. Since water was produced in both dehydration reactions, its mole fraction increased faster than that of propylene.

Feeding IPA at atmospheric pressure, the concentration of DIPE increased rapidly at low contact times, exceeding equilibrium. Under these conditions chemical equilibrium lay far towards propylene and water though, and DIPE was subsequently consumed, most likely by dealkylation, to give propylene and IPA. Feeding IPA at high pressure, it was the mole fraction of propylene which overshot its chemical equilibrium value. At greater contact times, this excess propylene was again consumed, most probably in the forward IPA alkylation reaction to give DIPE.

An interesting phenomenon for the high pressure series starting from a feed of propylene and water is the point of inflection at a 1/WHSV of approximately 1.2 h, which indicates that the rate of IPA formation increased up to this point. This is counter-intuitive. In an ideal system, the rate of formation is greatest initially when the concentration of reactants is greatest, then decreases as reactants are consumed. In this case though, the rate of IPA formation increases even though the bulk concentrations of the reactants, water and propylene, are decreasing.

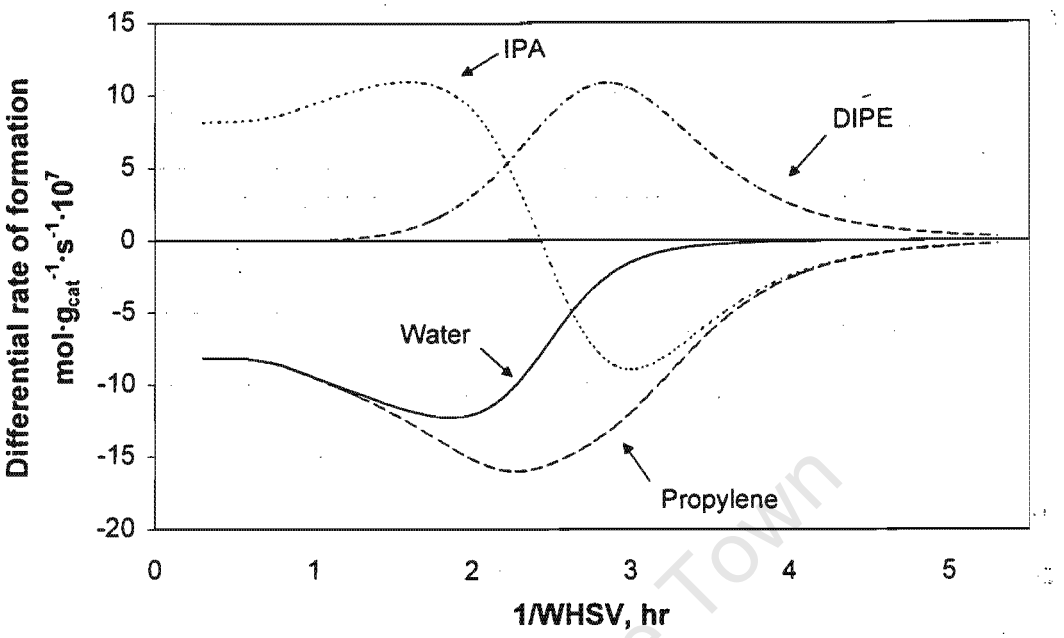

Figure 3.43: Differential rate of species formation with contact time. Temperature = 120°C, Pressure = 50 bar, initial propylene:water ratio = 2:1.

Figure 3.43 presents an alternate view of this situation. Arbitrary smooth curves were fitted to the experimental data. Differentiation of these curves allowed the calculation of the instantaneous rate of formation of every species within the system. These instantaneous rates were then plotted against contact time.

IPA was the primary product and as such its initial rate of formation was non-zero and equal to the rates of consumption of propylene and water. As contact time increased, though, the rate of IPA formation began to increase until it reached a maximum of $11.5 \cdot 10^{-7}\,\mathrm{mol\,g_{cat}^{-1}\,s^{-1}}$ at a 1/WHSV of 1.6h. In fact, the rate of IPA formation was even higher than this, since, by that stage, some IPA was being consumed to form DIPE in a secondary reaction. As the concentration of IPA was still quite low, DIPE was most likely almost exclusively produced by IPA alkylation. The overall rate of hydration was thus equal to the sum of the nett rate of IPA formation and the DIPE formation rate, i.e. $13.5 \cdot 10^{-7}\,\mathrm{mol\,g_{cat}^{-1}\,s^{-1}}$. This represented an almost 70% increase in hydration rate

as compared to the initial hydration rate. Possible causes of the increase in rate are discussed below. After a 1/WHSV of 1.6h, the rate of IPA formation declined as the rate of DIPE formation accelerated due to an increased concentration of IPA. Eventually, the rate of IPA consumption to form DIPE exceeded the rate of hydration and its nett rate of formation became negative.

The rates of consumption of water and propylene, identical when only hydration was taking place, began to diverge as soon as DIPE was formed. Regardless of whether DIPE is formed from alkylation or bimolecular dehydration, the rate of propylene consumption will always be greater than that of water, as two molecules of propylene to one of water are required for every DIPE molecule. The rate of water consumption began to decrease soon after the point of greatest IPA formation rate.

The greatest rate of propylene consumption ($16.2 \cdot 10^{-7}\,\mathrm{mol\,g_{cat}^{-1}\,s^{-1}}$) was attained at a 1/WHSV of 2.3h, more than double the initial rate. This resulted from the formation of IPA (at a nett rate of $4.0 \cdot 10^{-7}\,\mathrm{mol\,g_{cat}^{-1}\,s^{-1}}$) and the formation of DIPE (at a nett rate of $6.1 \cdot 10^{-7}\,\mathrm{mol\,g_{cat}^{-1}\,s^{-1}}$). The extent to which DIPE was formed from bimolecular dehydration of IPA or IPA alkylation can not be determined from these data. Since DIPE was a secondary product, its rate of formation was initially zero. As the intermediate IPA was formed, the rate of DIPE began to accelerate. It reached a maximum rate of formation at a 1/WHSV of 2.8 h. After which it declined and asymptoted to zero rate as the system neared chemical equilibrium.

The initial increase in hydration and propylene consumption rate cannot be due to any physical effects, stemming from greater propylene diffusivity through a mainly IPA-water liquid phase than through an almost pure water liquid phase. It has been shown in Section 3.3.2.2 that the propylene:water system is free of any mass transport limitations up to a temperature of 130 °C. Even if the system were initially mass transfer limited, the 20% increase in propylene diffusivity through IPA rather than water (see the Wilke-Change correlation in Appendix I) would not be sufficient to account for the 70% increase

in the hydration rate. This improvement in the rate must thus either be due to a chemical or to a catalytic effect.

The increase in propylene consumption was not due to increasing species activities either. It has been shown previously (Section 3.3.3.2), that the rate of hydration is linearly dependent on the propylene activity, a_P. Similarly, under water limited conditions, the rate of hydration should also exhibit a first-order dependence on the activity of water, a_W. The initial rate of hydration should thus be proportional to the product of the activities of propylene and water. It can be shown, however, that the activities (calculated by the WS-PRSV model) of both propylene and water actually decrease with contact time (Figure 3.44). Clearly, the product of the activities must then also decrease. In fact, at the point of maximum IPA formation ($1/\mathrm{WHSV} = 1.6\,\mathrm{h}$), the magnitude of the product of activities had declined by 15%, even though the hydration rate had increased by 70%. At the point of greatest propylene consumption ($1/\mathrm{WHSV} = 2.3\,\mathrm{h}$), the product of the activities had decreased to 57% of its original value, but the rate had doubled. Changing activities can thus also not be responsible for the increase in reaction rate.

The changes in species liquid phase mole fraction (calculated from the WS-PRSV model) with contact time are shown in Figure 3.45. At the start of the experimental series, the solubility of propylene in water was extremely small - the liquid phase propylene mole fraction at saturation being only $1.1 \cdot 10^{-3}$. Propylene and IPA on the other hand are completely miscible, as are water and IPA. Consequently, as IPA was produced from the hydration reaction, propylene became more miscible in the IPA-water liquid phase until, at the maximum hydration rate, the liquid phase propylene mole fraction was 0.18, a 150-fold increase in concentration. As ever more IPA and, later, DIPE were produced, the propylene concentration rose ever higher and achieved a maximum liquid phase mole fraction of 0.50, which coincided almost exactly with the maximum propylene consumption rate.

It has been observed previously [160], that increasing the olefin content of the liq-

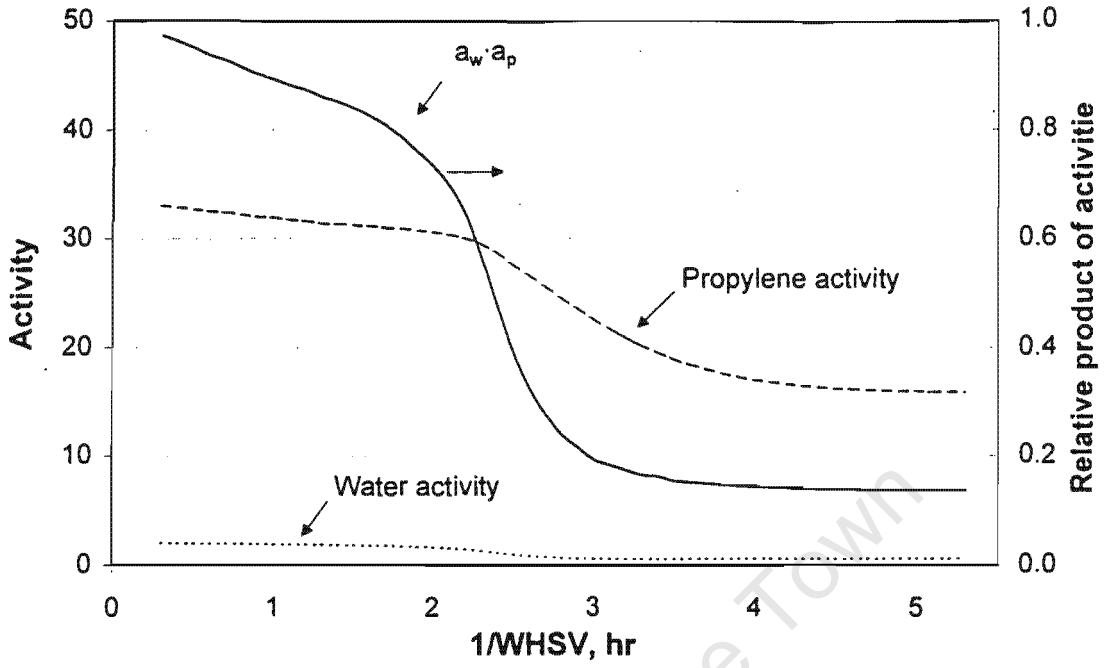

Figure 3.44: Effect of contact time on propylene and water activity and on the relative product of their activities. Temperature = 120°C, Pressure = 50 bar, Initial propylene:water = 2:1.

uid phase by means of an inert cosolvent, or by recycling some of the product alcohol, the rate of hydration reactions over ion exchange resins could be significantly enhanced. This scenario mirrors the situation in the contact time experiment. The production of IPA increased the solubility of propylene in the liquid phase, thus apparently enhancing the rate. However, this does not contradict the fact that activity rather than species concentration is the driving force for chemical reaction.

It has been shown for the hydration of cyclohexene [160] that this increase in the hydration rate is *not* due to the higher liquid phase alkene concentration directly enhancing the rate, but rather due to an increase in the catalytic activity of the active sites due to the changed polarity of the reaction medium resulting from the increased propylene concentration. Whether this enhanced activity manifests itself as a change in reaction mechanism and/or as a change in some other property of the resin is not known. How-

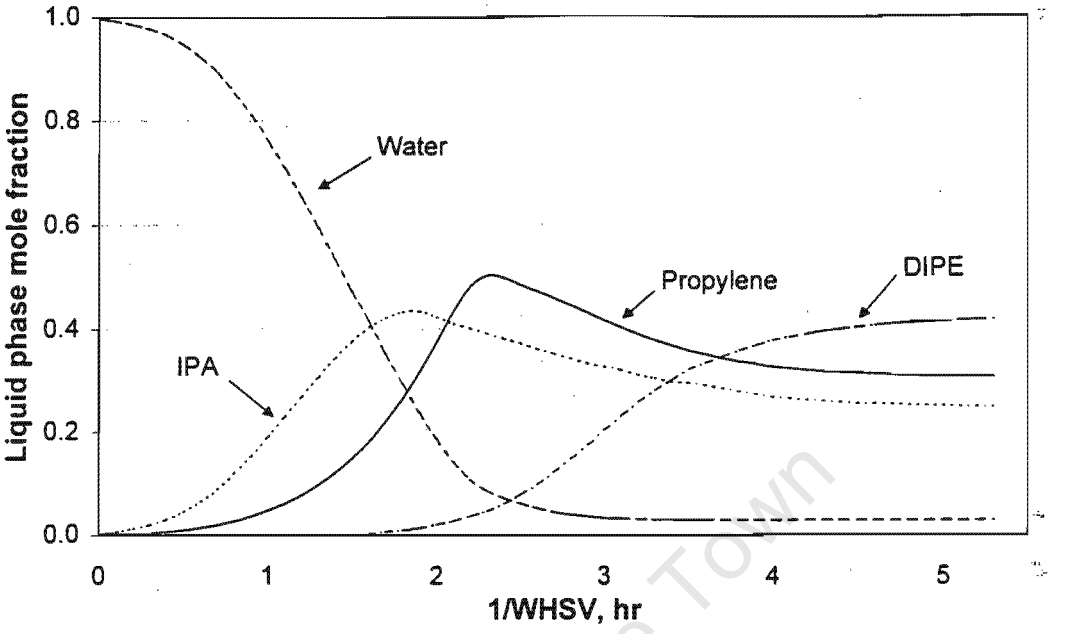

Figure 3.45: Effect of contact time on liquid phase mole fraction. Temperature = 120°C, Pressure = 50 bar, Initial propylene:water = 2:1.

ever, the situation corresponds remarkably well with certain literature findings [99, 132] and the findings of the study of the effects of system pressure (see Section 3.3.3.2).

Both Tejero et al. [132] and Kalló and Mihályi [99] observed changes in the catalytic mechanism deriving from changes in the polar to apolar species ratio. The rate of MTBE synthesis was found to increase substantially over Amberlyst 15 at methanol to isobutylene ratios smaller than 1.4:1. Similarly, the rate of isobutylene hydration to form tert-butyl alcohol began to increase once the ratio of polar/apolar species dropped below 5:1. The maximum change in rate occurred at a ratio of approximately 3:1 (see Section 3.1.5). Also, in the present study of the effects of system pressure, it was found that the rate of etherification increased dramatically at a liquid phase mole fraction of propylene in IPA above 0.3, i.e. a polar to apolar ratio of approximately 3:1. In this study, changes in the reaction rate at lower ratios would have been hard to detect due to a shift in the predominant etherification reaction from bimolecular dehydration to alkylation. In the

current situation, the rate begins to increase gradually once the liquid phase propylene mole fraction exceeds 0.1. The rate of greatest increase in propylene consumption rate at a 1/WHSV of 1.8 h, however, corresponds to a propylene to polar species ratio of 1:3, practically identical to that of the pressure series (ratio = 1:2) and the findings of Kalló and Mihályi [99] for isobutylene hydration (ratio = 1:3).

The increase in the rate of propylene consumption thus stems not from physical changes to the system, nor from an increase in reactant activity, but rather from a decrease in the polarity of the reaction medium affecting the reaction mechanism. As the apolar propylene dissolves in the liquid phase, the concentrations of the polar species (water and IPA) decreases. The mechanism changes from a slow ionic mechanism operating through a solvated proton at high polar species concentrations to a faster concerted mechanism at lower polar species concentrations, in keeping with the theory of Section 3.1.2.4 and Section 3.1.5.

No such increase in rate is observed in the other contact time series. When feeding propylene and water at atmospheric pressure, the reaction phase propylene concentration is already high, so the concerted mechanism dominates from the outset. During the high pressure decomposition of IPA the propylene concentration never rises high enough (maximum mole fraction 0.17) to cause a noticeable increase in rate, whilst the experimental data is not good enough to make any pronouncements for the low pressure IPA decomposition, due to the very high initial IPA dehydration rate.

For every series, experiments were continued until no further change in product composition of the system was observed with increasing contact time. This final composition was taken to be the chemical equilibrium composition. The chemical equilibrium data as well as the discussion of the chemical equilibrium results follows in Section 3.3.7.

3.3.4 The effect of acid site density

An interesting aspect of ion exchange resin catalysis which has thus far not been touched upon in the present study is the effect of acid site density on the reaction rate. The acid site density of Amberlyst 15 was varied by ion-exchange with NaOH (Appendix F details the procedure). Modified catalyst samples with capacities of 0, $0.24 \cdot 10^{-3}$eq g^{-1}, $0.98 \cdot 10^{-3}$eq g^{-1}, $2.24 \cdot 10^{-3}$eq g^{-1} and $3.52 \cdot 10^{-3}$eq g^{-1} were prepared and their catalytic performance compared to the unmodified parent catalyst (capacity of $4.79 \cdot 10^{-3}$eq g^{-1}). Both the hydration of propylene (2 : 1 ratio of propylene to water) and the etherification of IPA (1 : 1 ratio of propylene to IPA) were performed at a temperature of 120 °C and a pressure of 50 bar. Conversion of the reactants was limited to 10% to ensure differential operation. The change in the initial rate of propylene hydration with acid site density is shown in Figure 3.46. The change in initial etherification rate (the sum of the rate of IPA alkylation and the rate of bimolecular dehydration of IPA) with acid site density is shown in Figure 3.47.

No side reactions were observed during the propylene hydration and the IPA etherification experiments. The completely exchanged catalyst samples exhibited no catalytic activity whatsoever, indicating that the active sites are indeed the HSO_3^- species. The rate of propylene hydration increased linearly with acid site density. The rate of IPA etherification, i.e. the rate of DIPE formation, however, displayed a 2^{nd} to 3^{rd} order dependence on acid site density.

There are three schools of thought regarding the cause of the non-linear dependency of reaction rate on acid site concentration. These are:

1. **A heterogeneous distribution in the strength of acid sites.** Uematsu [161] supposed that the non-linear effect of acid site concentration on reaction rate was attributable to a nonhomogeneous distribution of acidic HSO_3^- active sites. Neu-

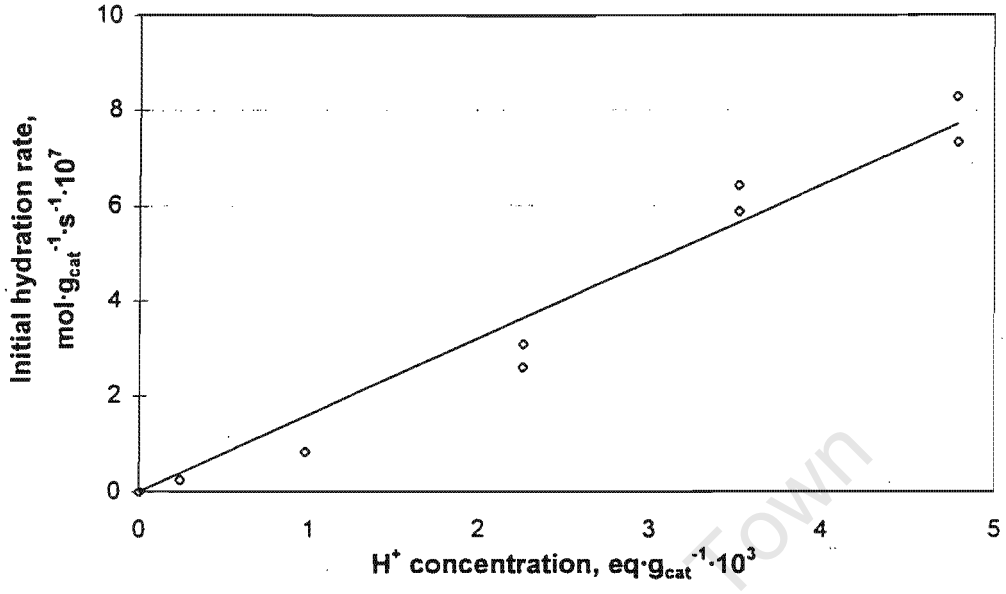

Figure 3.46: The effect of acid site density on the initial rate of propylene hydration. Temperature = 120 °C, pressure = 50 bar and propylene:water ratio = 2 : 1.

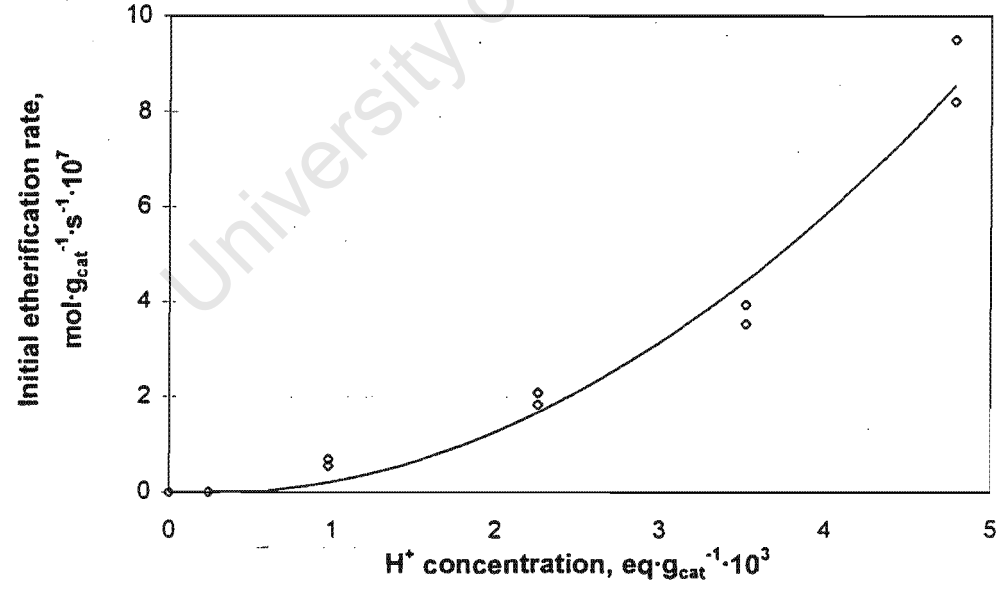

Figure 3.47: The effect of acid site density on the etherification rate (the sum of the initial rate of IPA alkylation and bimolecular dehydration of IPA). Temperature = 120 °C, pressure = 50 bar and propylene:IPA ratio = 1 : 1.

tralization of these sites would proceed from the strongest sites to the weakest ones. Partial neutralization would thus lead to a preferential deactivation of the strongest sites, leading to a non-linear decrease in the reaction rate.

2. **A non-linear increase in the effective acidity of the catalyst.** The rate of homogeneously catalysed reactions has been shown to be proportional to the hydrogen ion concentration at low concentrations of hydrogen ions (up to $2\,\mathrm{mol}\,l^{-1}$). At greater concentrations, however, the reaction rate increases substantially faster than the H^+ concentration increases. The rate, however, remains linearly correlated to the Hammett acidity function (an expression for the effective acidity of the catalyst) over the entire concentration range [162, 163]. The H^+ concentration in ion exchange resins ($[H^+]$ in Amberlyst 15 $\approx 4.0\,\mathrm{mol}\,l^{-1}$) is considerably greater than the threshold value of approximately $2\,\mathrm{mol}\,l^{-1}$ and, consequently, Ancillotti et al. [105] proposed that the non-linear rate dependence in acidic resins is due to a similar non-linear increase in the effective acidity of the active sites of the catalyst.

3. **A disruption of the concerted catalytic mechanism.** It has been shown (Section 3.1.2.4 and Section 3.1.5) that the catalytic action of ion-exchange resins depends on the concentration of the polar species within the resin matrix. At high polar species concentrations the resin behaves similar to a homogeneous catalyst. At low polar species concentrations, multiple centres may take part in a concerted mechanism; the number of active sites involved in the reaction depending on the species involved. Gates and co-workers [121, 122, 123] thus hypothesised that the non-linear dependence of rate was a result of the neutralization step breaking the concerted array by the physical insertion of a Na^+ ion. This step disrupts the concerted counter-ion array, strongly reducing the carbocation stability and, therefore, the catalytic activity.

A fourth possibility which has thus far not been considered is the possibility of a non-uniform ion exchange profile. It is known that ion exchange processes over gelular ion

exchange resins are mass transfer limited, the ion exchange reaction being considerably faster than the diffusion of the ions into the catalyst matrix [164]. During a partial ion exchange, or during a partial catalyst deactivation, the exchange sites on the periphery of the catalyst particle are thus preferentially poisoned in comparison to the interior sites. If, in addition, the catalytic reaction were to be mass transfer limited, then reactants would have to diffuse considerably further to contact unexchanged active sites. This would have a pronounced effect on the reaction rate. The magnitude of this effect would depend on both the extent of ion-exchange and on the relative rates of diffusion versus reaction. However, catalysts are generally macroreticular in nature. During a partial ion exchange, the mean diffusion path through a microgel particle is orders of magnitude smaller than that through a gelular catalyst bead and the ion exchange profile through a macroreticular particle is consequently more uniform. In a macroreticular catalyst, if it can in addition be shown that the kinetics are reaction rate controlled (such as in the present study), it is unlikely that this will have a major impact on the global reaction rate. In a gelular catalyst, this effect would have to be considered.

If the reaction rates were to increase non-linearly due to a heterogeneous distribution of acid sites, this effect should apply equally to all reactions. However, different reactions have distinctly different orders of dependence on the acid site density, ranging from 1 for propylene hydration to 7 for benzene alkylation [123]. This explanation thus seems unlikely.

Similarly, if the rate were simply dependent on the effective acid site strength then the increase in rate for any two reactions should be reasonably similar, as the increase in the effective acid strength would be reasonably similar. Variations in the effective acid strength may be caused by stabilization of the carbocation species or changes in the H^+ ion activity [160, 148] (due to changes in the composition of the reactant medium), but this effect would not explain the differing dependence on acid site density ranging between orders of 1 and of 7. Furthermore, in homogeneous catalysis at low concentrations, it

was observed that reaction rates were linearly dependent on hydrogen ion concentration. At low concentrations of H-form active sites, reactions catalysed by ion-exchange resins should similarly be linearly dependent on the site density. With the possible exception of the data from the dehydration of TBA [122], neither the data from literature nor that from the present study exhibit any such trend.

It appears that Gates' explanation for the changes in reaction rate remains the most likely. Table 3.7 gives the order of dependence of reaction rate on acid site density for alkylation, dehydration and hydration reactions from literature and from the present study. In addition, the dielectric constant (a measure of the charge a substance can withstand at a given field strength) of the dominant compound in the reactant medium is shown. It is evident that the order of dependence of reaction rate on active site density increases with decreasing dielectric constant and with decreasing concentration of polar reactant.

Table 3.7: The order of the reaction rate dependence on the hydrogen ion concentration and the dielectric constant of the predominant reactant in the reaction medium.

Reaction (phase*)	Product	Order on $[H^+]$	Dielectric constant# of reactant at 20°C
Propylene hydration (l)[1]	IPA	1	78.5
Methanol dehydration (v)[2]	dimethyl ether, H_2O	2	32.6
Methanol alkylation (l)[3]	MTBE	2-3	32.6
Ethanol dehydration (v)[3]	diethyl ether, H_2O	2	24.3
IPA dehydration (v)[4]	DIPE, H_2O	2-3	18.3
IPA etherification (l)[1]	DIPE, H_2O	2-3	18.3
TBA dehydration (l)[5]	isobutylene, H_2O	4	10.9
Benzene propylation (l)[6]	isopropyl benzene	7	2.28

* 'l' = liquid phase, 'v'= vapour phase, # CRC Handbook [165]

[1] Present study, [2] Gates and Johanson [121], [3] Panneman and Beenackers [148]

[4] Sivanand et al. [166], [5] Gates et al. [122], [6] Wesley and Gates [123]

For propylene hydration, the reaction medium consists almost exclusively of liquid water, with a little dissolved propylene (propylene mole fraction $1.2 \cdot 10^{-3}$). The active sites are fully solvated (i.e. polyhydrated) and the homogeneous mechanism dominates. Changes in the active site density would consequently cause a linear response, i.e. an order on $[H^+]$ of one. In methanol and ethanol dehydration the reactant phase is still highly polar. However, in this instance the reaction takes place in the vapour phase at atmospheric pressure and the concentration of the reactant is thus insufficient to fully "solvate" the active sites. The reaction thus takes place via a concerted reaction scheme, probably involving two active sites. Similarly, in IPA etherification, though the reaction medium is liquid, it contains equimolar amounts of propylene and IPA. There is thus insufficient IPA to fully solvate the active sites and a highly active concerted mechanism (involving 2 or 3 sites) dominates.

On the other hand, the dehydration of tert-butyl alcohol (TBA) takes place in the liquid phase yet displays a fourth order dependence on acid site density. It is a highly polar molecule and thus, in the liquid phase, would be expected to fully solvate the active sites. However, TBA has quite a low dielectric constant. It is thus less able to hold and/or transfer a charge and thus multiple active sites are required to stabilise the protonated TBA cation. As benzene is apolar, it is unable to solvate the active sites and all reactions take place via concerted mechanisms. Like TBA it has a low dielectric constant and, for the same reason as TBA, multiple active sites are required to stabilise the benzene cation. This is in agreement with IR work which has shown that apolar organic species (e.g. benzene, diethyl ether and propylene) hydrogen bond into "nests" of active sites [123] on acidic ion exchange resin catalysts. These "nests" may involve up to seven active species - in perfect agreement with the order of reaction rate with acid site density for benzene alkylation.

The order of the reaction rate on the acid site density thus depends on a combination of the reactant polarity, the concentration of the polar compound within the resin matrix and

on the dielectric constant of the dominant species within the resin matrix. The polarity and the concentration of the reacting species determines whether or not the reaction can take place via a homogeneous mechanism (if it is present at a high concentration). The dielectric constant determines the number of active sites required to stabilise the charged reaction intermediate in a concerted mechanism. Even if the reaction intermediate did not result from the dominant species in the resin matrix, the dielectric constant would give an indication of the extent to which it might stabilise the actual intermediate species. In methanol alkylation, for example, the isobutyl carbocation is stabilised by the surrounding methanol molecules and only two active sites are required to catalyse the reaction. In contrast, propylene is less able to stabilise the phenyl carbocation and consequently seven sites are needed to catalyse benzene propylation. If the concentration of active sites is decreased by ion exchange, the concerted mechanisms are disrupted. The protonated reaction intermediates can no longer be stabilised to the same extent and the catalytic activity decreases dramatically. As the activity of these less active mechanisms is most likely considerably lower than that of the preferred multi-site concerted mechanism, the order of reaction rate dependence on acid site density gives an indication of the number of sites involved in the mechanism. The mechanism of propylene hydration thus involves one active site, that for IPA etherification involves two or three sites.

3.3.5 Decomposition of DIPE

The decomposition of pure DIPE and of DIPE with traces of water and/or IPA was studied at 120 °C and 50 bar over "dry" and over "wet" Amberlyst 15. The "dry" catalyst had been dried at 120 °C for 18 hours under vacuum and then washed with anhydrous methanol followed by washing with anhydrous DIPE. "Wet" catalyst had been pretreated in the standard manner (Appendix F). The effect of small amounts of polar compounds on DIPE decomposition was studied by co-feeding 2 mol % or 5 mol % water or IPA or by co-feeding 2 mol % of water and 2 mol % of IPA. The rate of DIPE decomposition from an arbitrary

feed composition (20 mol % propylene, 2 mol % water, 12 mol % IPA and 66 mol % DIPE), but still with an overall propylene to water ratio of 2 : 1, was also studied.

Figures 3.48 and 3.49 respectively show the product distribution and instantaneous rates of the decomposition of pure DIPE with inverse space velocity over "dry" catalyst. Figure 3.50 gives the initial rate of DIPE decomposition for "dry" and "wet" catalyst and for varying amounts of co-fed water and/or IPA.

Over Amberlyst 15 DIPE decomposed by dealkylation to form propylene and IPA. At low contact times carbon selectivity was 50% to propylene and 50% to IPA. At greater contact times water and additional propylene were formed from the subsequent dehydration of IPA. At a space velocity of 29 h^{-1} for example, carbon selectivity was 55% to propylene and 45% to IPA, some of the IPA having decomposed to water and propylene in a secondary reaction step. It was found that co-feeding small amounts of water or IPA did not appear to change the DIPE decomposition pathway. No dimers or trimers resulting from the subsequent oligomerisation of propylene were detected in the contact time experiments.

The rate of DIPE decomposition changes markedly with 1/WHSV. At low contact times the rate of DIPE decomposition is $6.6 \cdot 10^{-8}$ mol g_{cat}^{-1} s^{-1}. As contact time increases, though, the rate of decomposition decreases exponentially up to a 1/WHSV of 5 h. After this time, the rate of DIPE decomposition drops off sharply to approximately $1.2 \cdot 10^{-8}$ mol g_{cat}^{-1} s^{-1} at a 1/WHSV of 29 h.

The initial rate of DIPE decomposition was slowest ($6.6 \cdot 10^{-8}$ mol g_{cat}^{-1} s^{-1}) over the so-called "dry" catalyst. Reaction over the so-called "wet" catalyst proceeded significantly quicker, at a rate of $3.0 \cdot 10^{-7}$ mol g_{cat}^{-1} s^{-1}. Co-feeding small amounts of polar compounds (either water or IPA or a mixture of both) also increased the decomposition rate in comparison to pure DIPE over the "dry" catalyst. Co-feeding 2 mol % water, raised the reaction rate to $3.4 \cdot 10^{-7}$ mol g_{cat}^{-1} s^{-1}. Increasing the amount of water being co-

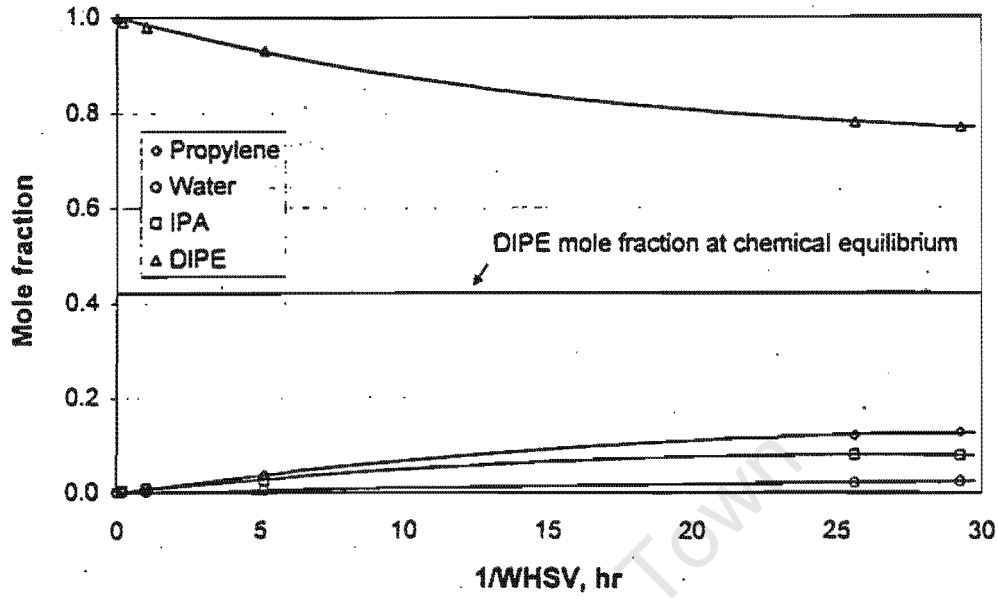

Figure 3.48: Product distribution as a function of inverse space velocity for pure DIPE decomposition over "dry" Amberlyst 15. Temperature = 120 °C and pressure = 50 bar.

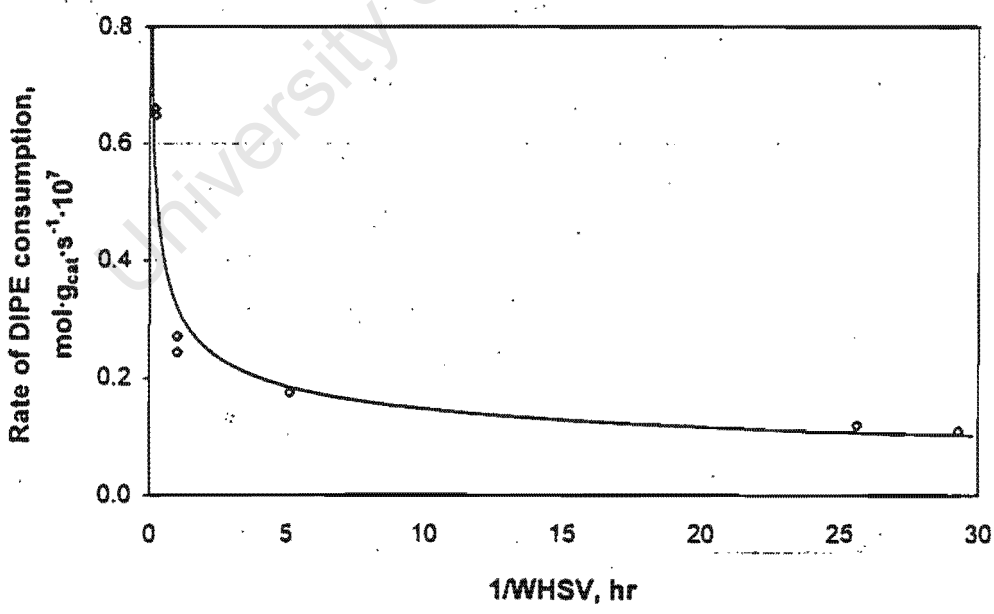

Figure 3.49: Instantaneous rate of pure DIPE decomposition over "dry" Amberlyst 15 as a function of inverse space velocity. Temperature = 120 °C and pressure = 50 bar.

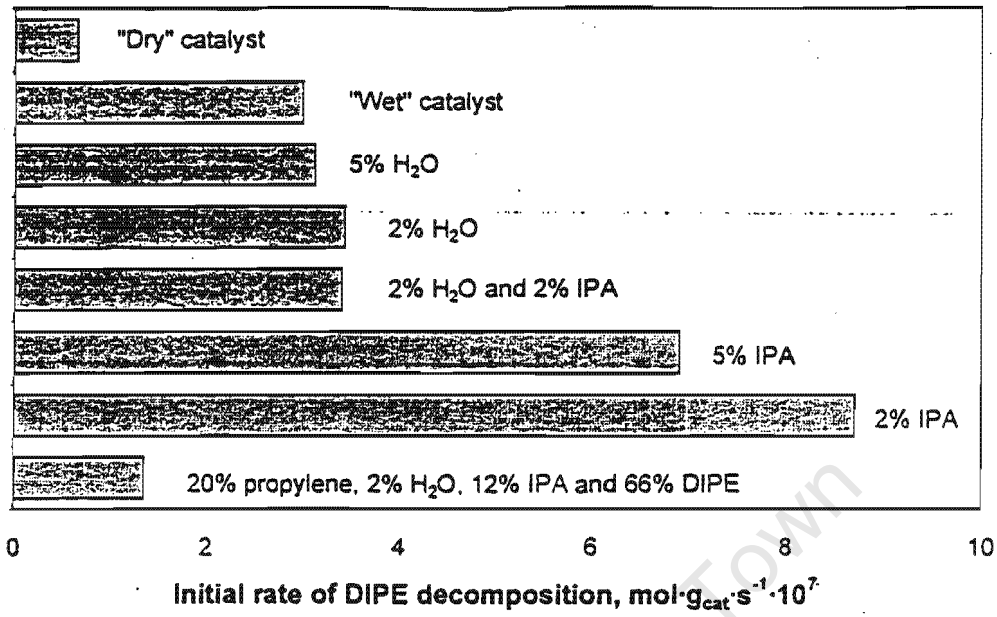

Figure 3.50: Initial rate of DIPE decomposition over "dry" and "wet" Amberlyst 15 and with varying amounts of polar co-feed. Temperature = 120 °C and pressure = 50 bar.

fed to 5 mol % slightly decreased the rate to $3.1 \cdot 10^{-7}$ mol $g_{cat}^{-1} s^{-1}$. DIPE decomposition proceeded quickest when co-feeding small amounts of IPA. At a level of 2 mol % of IPA in DIPE, the rate of decomposition was found to be $8.7 \cdot 10^{-7}$ mol $g_{cat}^{-1} s^{-1}$. Similarly as for co-feeding water, raising the amount of IPA being co-fed to 5 mol % slightly decreased this rate to $6.9 \cdot 10^{-7}$ mol $g_{cat}^{-1} s^{-1}$. Feeding an arbitrary mixture of water, propylene, IPA and DIPE gave a rate of DIPE decomposition of $1.4 \cdot 10^{-7}$ mol $g_{cat}^{-1} s^{-1}$; faster than pure DIPE over the "dry" catalyst, yet significantly slower than any of the other DIPE decomposition rates.

Table 3.8 gives the initial rates of ether formation, of ether decomposition and the ratio of the two rates from the present study and from literature. The ratio of the rate of DIPE formation to the rate of DIPE decomposition is significantly greater than the ratio for MTBE or TAME. Most likely, the comparatively low rate of DIPE decomposition is due to a steric effect. The mechanism of DIPE decomposition almost certainly proceeds

via a protonation of the electrophilic bridging oxygen followed by the elimination of the alkyl group. In MTBE or TAME decomposition this yields methanol and isobutylene or methanol and isoamylene; in DIPE this process yields IPA and propylene. Whereas in MTBE and TAME a methyl group is attached to the oxygen which allows ready access for electrophilic attack, two bulky propyl groups are attached to the oxygen in DIPE. These groups shield the oxygen and inhibit the decomposition reaction (steric hindrance). Based on the forgoing argument, the ratio of the rates of formation and decomposition for ETBE should lie between the ratio for MTBE and TAME and the ratio for DIPE. However, the decomposition of ethers over ion exchange resins has been little studied and no ETBE decomposition study has been performed to date.

Table 3.8: Comparison of the rate of ether formation and decomposition for MTBE, TAME and DIPE starting from 'dry' catalyst.

		Initial rate, $\mathrm{mol\,g_{cat}^{-1}\,s^{-1}}$		Ratio of formation
Ether	T, °C	Formation*	Decomposition#	to decomposition
DIPE[1]	120	$1.3 \cdot 10^{-6}$	$6.6 \cdot 10^{-8}$	19.7
MTBE[2]	90	$1.4 \cdot 10^{-3}$	$7.1 \cdot 10^{-4}$	2.0
TAME[3]/TAEE[4]	80	$2.6 \cdot 10^{-5}$	$2.1 \cdot 10^{-5}$	1.2

1 Present study. Catalyst Amberlyst 15.

2 Rehfinger and Hoffmann [32]. Catalyst Amberlyst 15, rate of formation scaled to 90°C

3 Rihko and Krause [34]. Catalyst Amberlyst 16, rate of formation scaled to 80°C

4 Linnekoski et al. [147]. Catalyst Amberlyst 16

* Rate of ether formation from an equimolar mixture of alcohol and olefin

\# Rate of ether decomposition of pure ether over "dry" catalyst

The rate of DIPE decomposition decreased rapidly with contact time. At a 1/WHSV of 0.2 h the reaction rate was $6.6 \cdot 10^{-8}\,\mathrm{mol\,g_{cat}^{-1}\,s^{-1}}$, at 1 h it was $2.5 \cdot 10^{-8}\,\mathrm{mol\,g_{cat}^{-1}\,s^{-1}}$ and by 29 h it had decreased to $1.2 \cdot 10^{-8}\,\mathrm{mol\,g_{cat}^{-1}\,s^{-1}}$. This decrease was not a result of approaching chemical equilibrium as even at very low DIPE conversions the reaction rate had already decreased substantially, and throughout the entire contact time study the conversion of DIPE was far from equilibrium (see Figures 3.48 and 3.49). Most probably, this rapid

decrease was caused by competitive adsorption. Due to their low polarity, propylene and diethyl ether do not interact strongly with the acidic ion exchange resin matrix, exhibiting only weak adsorption in multiply-hydrogen bonded complexes [123] - DIPE can be expected to show similar behaviour. When DIPE decomposes, it forms propylene and IPA. Since IPA is a strongly polar molecule, it will preferentially adsorb on the active sites, blocking access for DIPE. This will inhibit the rate of DIPE decomposition. Since multiple active sites are involved in the reactions of apolar molecules on ion exchange resin catalysts (e.g. Wesley and Gates [123] report seven sites taking part in benzene propylation), even small amounts of polar molecules are sufficient to cause significant disruptions in the concerted reaction mechanisms, resulting in the almost exponential decrease in the rate of DIPE decomposition (comparable to the findings of Section 3.3.4).

Even though water and IPA inhibit the rate of DIPE decomposition due to competitive adsorption, when these compounds are co-fed, even in small amounts, they can once again cause an increase in the reaction rate. Co-feeding 2 mol % water, the reaction rate of DIPE decomposition is $3.4 \cdot 10^{-7}\,\mathrm{mol\,g_{cat}^{-1}\,s^{-1}}$; a co-feed of 2 mol % of IPA causes an increase in the decomposition rate to $8.7 \cdot 10^{-7}\,\mathrm{mol\,g_{cat}^{-1}\,s^{-1}}$. This increase in rate is caused by a greater number of active sites becoming accessible for reaction. Apolar molecules are incapable of swelling the resin matrix (Section 3.1.2.2) and consequently only active sites on the periphery of the resin particle are available for reaction. However, ion exchange resin catalysts preferentially adsorb polar molecules and co-feeding even small amounts will result in a significant swelling of the matrix. This swelling allows DIPE access to a far greater number of active sites, so even though the majority of active sites may be blocked by water and IPA, sufficient new sites are accessible to cause the increase in the DIPE decomposition rate.

This is practically identical to decomposing DIPE over the "wet" resin which had been preswelled with methanol and then with "water". The matrix was already fully swelled and a maximum number of active sites were accessible for reaction. As above, even

though a number of the sites would have been "deactivated" for DIPE decomposition by the adsorption of water, sufficient new sites were now accessible to result in the increased decomposition rate.

Additional evidence for competitive adsorption affecting the rate of DIPE decomposition can be obtained from the initial rates of decomposition resulting from different levels of polar co-feed and from different species of polar co-feed. Increasing the level of water or IPA co-feed from 2 mol % to 5 mol % decreased the rate of DIPE decomposition as additional polar species adsorbed on the active sites. These would have "blocked" additional sites for DIPE decomposition and caused the observed decrease in the reaction rate. As IPA is less polar than water, co-feeding IPA in preference to water resulted in fewer sites being blocked for DIPE decomposition. Increased amounts of DIPE could adsorb on the active sites which caused the observed increase in the rate of DIPE decomposition.

Co-feeding mixtures of polar species (e.g. water and IPA) or feeding an arbitrary mixture beyond the chemical equilibrium composition (20 mol % propylene, 2 mol % water, 12 mol % IPA and 66 mol % DIPE) results in increases in the rate of DIPE decomposition. When feeding 2 mol % water and 2 mol % IPA, the rate of DIPE decomposition increased from $6.6 \cdot 10^{-8}\,\mathrm{mol\,g_{cat}^{-1}\,s^{-1}}$ to $3.4 \cdot 10^{-7}\,\mathrm{mol\,g_{cat}^{-1}\,s^{-1}}$. Once again, this increase is caused by the polar species swelling the resin matrix and making more active sites available for reaction. Similarly, the rate of DIPE decomposition resulting from the arbitrary mixture is greater than the rate of DIPE decomposition over the "dry" catalyst the resin matrix is swollen. The rate is not as great as that for the other experiments due to the proximity to chemical equilibrium.

3.3.6 Single component adsorption of propylene and water

To gauge the extent to which polar and apolar species adsorb onto acidic ion exchange resin catalysts, single component adsorption studies were performed over Amberlyst 15

with propylene and water. For a comparative study, the adsorption experiments had to be carried out under conditions where propylene would not oligomerise over the catalyst and water would not swell the resin matrix. Consequently, the adsorption studies could not be carried out under the conditions of DIPE synthesis and this study was thus purely qualitative in nature. The adsorption experiments were performed at an absolute pressure of 1.4 bar at temperatures of 30 °C, 45 °C, 60 °C and 75 °C. Partial pressures of propylene and water were varied between 1.4 kPa and 14 kPa (the balance being helium) at each temperature. At these low partial pressures, it was found that the resin did not swell noticeably, so the water and the propylene data could be compared. Appendix K gives further details on the adsorption experiments and explains how the various adsorption parameters were calculated. Langmuir isotherms were fitted to the adsorption data to obtain a qualitative measure of the saturation loading and the heats of adsorption. Figures 3.51 and 3.52 show the adsorption data with the best-fit Langmuir isotherms for water and propylene respectively. Table 3.9 gives the obtained Henry's constants of adsorption, the saturation capacities and the heats of adsorption (see Appendix K for the calculational procedures).

Table 3.9: Henry's constants, saturation capacities and heats of adsorption of water and propylene on Amberlyst 15

	Propylene		Water	
Temperature, °C	H	C_m, mol g_{cat}^{-1}	H	C_m, mol g_{cat}^{-1}
30	1200	$8.4 \cdot 10^{-4}$	-	–
45	1300	$8.1 \cdot 10^{-4}$	19000	$6.4 \cdot 10^{-2}$
60	1400	$7.0 \cdot 10^{-4}$	12000	$5.0 \cdot 10^{-2}$
75	–	–	4700	$5.4 \cdot 10^{-2}$
ΔH_{ads}	5.4 ± 11.5 kJ mol^{-1}		-42.6 ± 4.3 kJ mol^{-1}	

Considerably more water than propylene adsorbs onto Amberlyst 15 as water is a polar molecule. At a temperature of 45 °C, for example, the saturation loading of propylene is $8.1 \cdot 10^{-3}$ mol g_{cat}^{-1} whilst that of water is $6.4 \cdot 10^{-2}$ mol g_{cat}^{-1}, almost 80 times greater. This

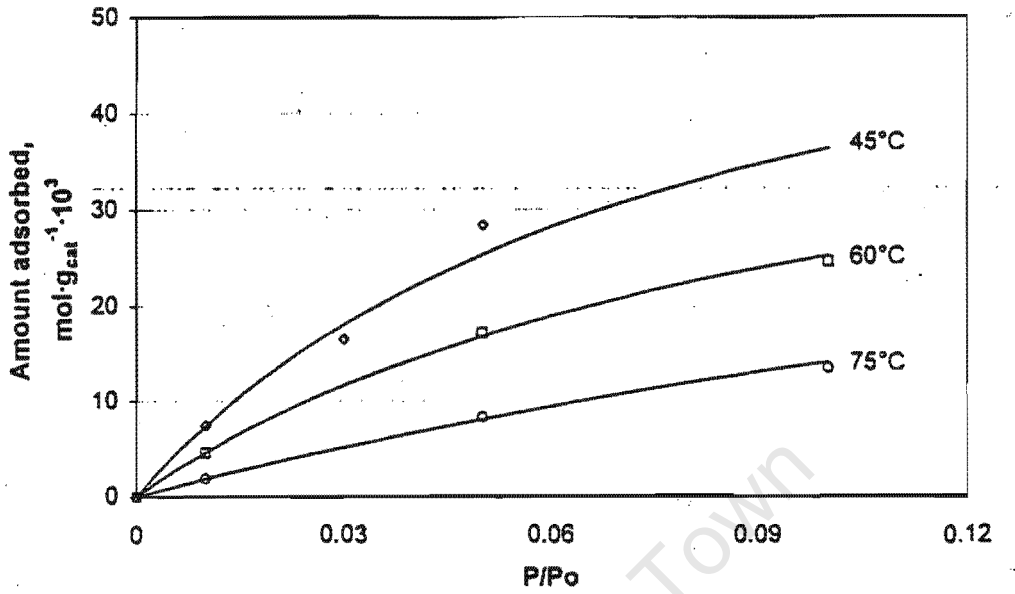

Figure 3.51: Experimental adsorption data and the best-fit Langmuir isotherms for single component water adsorption over Amberlyst 15. Absolute pressure, $P_o = 1.4$ bar.

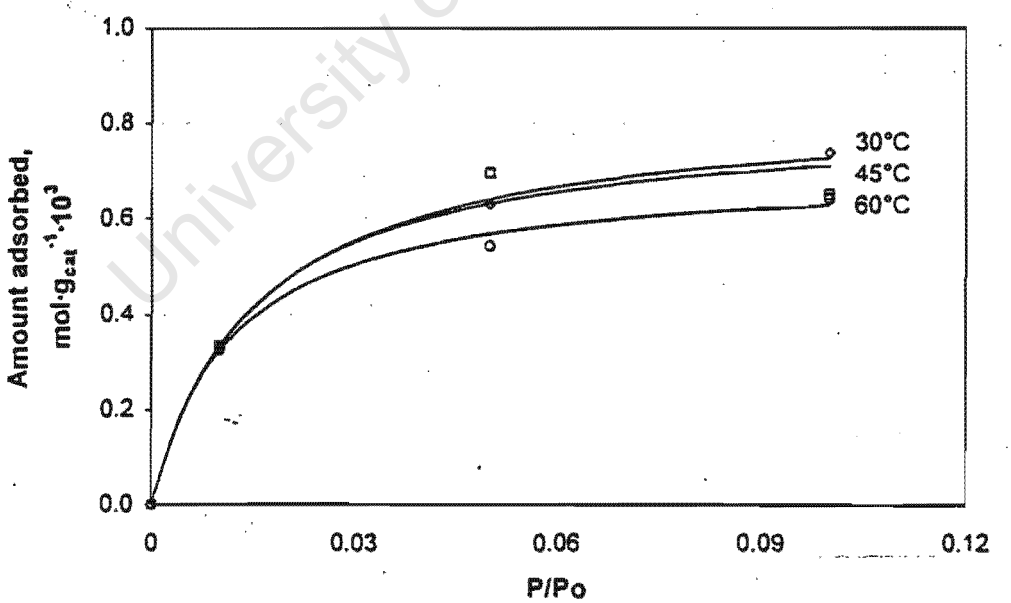

Figure 3.52: Experimental adsorption data and the best-fit Langmuir isotherms for single component propylene adsorption over Amberlyst 15. Absolute pressure, $P_o = 1.4$ bar.

agrees with literature findings. Rehfinger and Hoffmann [32] report methanol adsorbing onto Amberlyst 15 in 3.5 times greater amounts than isobutylene. Since methanol is a less polar molecule than water, it should adsorb to a lesser extent and consequently the ratio between the saturation loading of methanol and an olefin should be smaller than that between water and an olefin.

The Henry constant for water is approximately an order of magnitude greater than that of propylene at the same temperature. As the magnitude of the Henry's constant gives an indication of the strength of adsorption, not only does Amberlyst 15 adsorb more water than propylene, but it also adsorbs this water approximately an order of magnitude more strongly than it does the propylene. Further evidence for this comes from the heat of adsorption. The heat of adsorption of water, $-42.6 \pm 4.3\,\mathrm{kJ\,mol^{-1}}$, is indicative of a strong exothermic interaction between water and the resin matrix. The water is chemisorbed, likely through strong hydrogen bonds in concerted arrays of active sites. Propylene, on the other hand, displays a very weak interaction with the resin matrix. The heat of propylene adsorption on the catalyst is $5.4 \pm 11.5\,\mathrm{kJ\,mol^{-1}}$. It is unlikely that this is in fact an endothermic adsorption in light of the poor quality of the experimental data. However, it does indicate that the heat of adsorption is very small and most likely only physical adsorption occurs. Any chemical interaction that does take place under these conditions would most likely only occur through weak hydrogen bonds with a number of active sites, probably the origin of the "nesting" behaviour witnessed in the IR studies of Wesley and Gates [123].

While the quantitative results of the single component adsorption measurements at low pressure and low temperature in the vapour phase almost certainly do not hold in multicomponent systems at high pressure and high temperature in the liquid phase, the qualitative findings should still apply. Basically, the strength and the amount of adsorption of the species occurring in the DIPE system on acidic ion exchange resins should

follow the order of polarity of the molecules, i.e.

$$water > IPA > DIPE > propylene$$

Consequently, if water or IPA are present in a system to any significant extent, they will largely prevent propylene and DIPE from adsorbing on the catalyst. Any reactions which require a propylene or DIPE molecule to be adsorbed on the active sites will thus be strongly inhibited. For this reason the rate of DIPE decomposition decreased significantly once a little IPA and water had been produced (see Section 3.3.5) and propylene oligomerisation was not witnessed so long as the catalyst had been properly wetted.

3.3.7 Chemical reaction equilibrium

Chemical reaction equilibrium in the DIPE system was measured at three temperatures (100 °C, 120 °C and 140 °C) at a constant pressure of 50 bar and a propylene to water ratio of 2:1; at four pressures (1 atm, 30 bar, 50 bar and 70 bar) at a constant temperature of 120 °C and a propylene to water ratio of 2:1; and at two propylene to water mole ratios (2 : 1 and 1 : 1) at a temperature of 120 °C and pressures of 1 atm and 50 bar. The experimental method was identical in every case. Starting from an initial feed composition (either pure IPA (i.e. an overall propylene to water ratio of 1:1), a 2:1 molar mixture of propylene and water or an arbitrary mixture containing all four species with an overall propylene to water ratio of 2:1), contact time was increased until no further change in product composition was observed. This point was presumed to be chemical equilibrium.

To determine the accuracy with which the chemical equilibrium product distribution was determined, an additional chemical equilibrium experimental series was performed at conditions identical to that from a previous series (120 °C, 50bar and 2:1 propylene to water ratio). This time, however, instead of reacting "forwards" from propylene and

water, the starting composition was purposely chosen to be beyond the previously determined chemical equilibrium distribution, such that reaction had to proceed in the"reverse" direction.

Raw data from the experiments together with the chemical equilibrium constant determined from the experimental product distribution and the WS-PRSV model are shown in Table 3.10 while the experimental results from the reverse series are shown in Figure 3.53. Unfortunately, the chemical equilibrium product distributions obtained in this study could not be compared with values obtained from literature as the overall ratios of propylene to water were not equal.

The chemical equilibrium distributions determined from the "forward" and the "reverse" experimental series were practically identical. The greatest variation in mole fraction occurred for IPA (an absolute deviation of 0.02), suggesting that either the forward or reverse series had possibly not yet attained chemical equilibrium. The remainder of the species mole fractions agreed to within 0.01. Assuming the same confidence in having reached chemical equilibrium and with the exception of the DIPE mole fraction for the atmospheric runs, the chemical equilibrium product mole fractions of the remainder of the series consequently can be assumed to be accurate within absolute bounds of ± 0.02. The very small amounts of DIPE formed at atmospheric pressure were at the detection limits of the analytical apparatus such that the DIPE mole fraction could not be determined to a high accuracy (relative standard deviations in DIPE mole fraction of 60% were obtained).

The experimental equilibrium conversion of propylene and carbon product selectivity resulting from the hydration and etherification of propylene and water were strongly affected by the reaction temperature, pressure and the overall propylene to water ratio. As temperature was increased from 100°C to 140°C, the equilibrium propylene conversion decreased from 87% to 74%. At the same time DIPE selectivity decreased from 87% to 77% while IPA selectivity increased from 13% to 23%. Similarly, increasing the system pressure from 1 atm to 30 bar increased the chemical equilibrium conversion of propylene

Table 3.10: Experimental chemical equilibrium product distribution, propylene conversion, carbon selectivity and chemical equilibrium constants. Activities used to calculate the chemical equilibrium constants were calculated from the WS-PRSV model using the experimental equilibrium product distributions.

Propylene:water	2:1							1:1	
Temperature, °C	100	120[1]	120[2]	140	120	120	120	120	120
Pressure, bar	50	50	50	50	1.01	30	70	1.01	50
Experimental product distribution									
Propylene	0.21	0.31	0.30	0.34	0.66	0.33	0.30	0.47	0.10
Water	0.03	0.05	0.04	0.05	0.30	0.04	0.04	0.48	0.25
IPA	0.18	0.22	0.24	0.23	0.035	0.20	0.21	0.049	0.50
DIPE	0.58	0.42	0.42	0.38	0.007	0.43	0.45	0.005	0.15
Propylene conversion and carbon selectivity, mol%									
Conversion	87	77	78	74	6.9	76	79	11	76
IPA selectivity	13	21	22	23	71	19	19	83	63
DIPE selectivity	87	79	78	77	29	81	81	17	38
Experimental chemical equilibrium constant*									
$K_{a,1}$	0.241	0.096	0.137	0.075	0.177	0.090	0.123	0.219	0.122
$K_{a,2}$	0.315	0.081	0.079	0.051	0.306	0.077	0.092	0.220	0.071
$K_{a,3}$	1.307	0.851	0.577	0.678	1.727	0.847	0.746	1.006	0.579

[1] "Forward" series

[2] "Reverse" series

* '1' refers to propylene hydration, '2' to IPA alkylation and '3' to bimolecular IPA dehydration

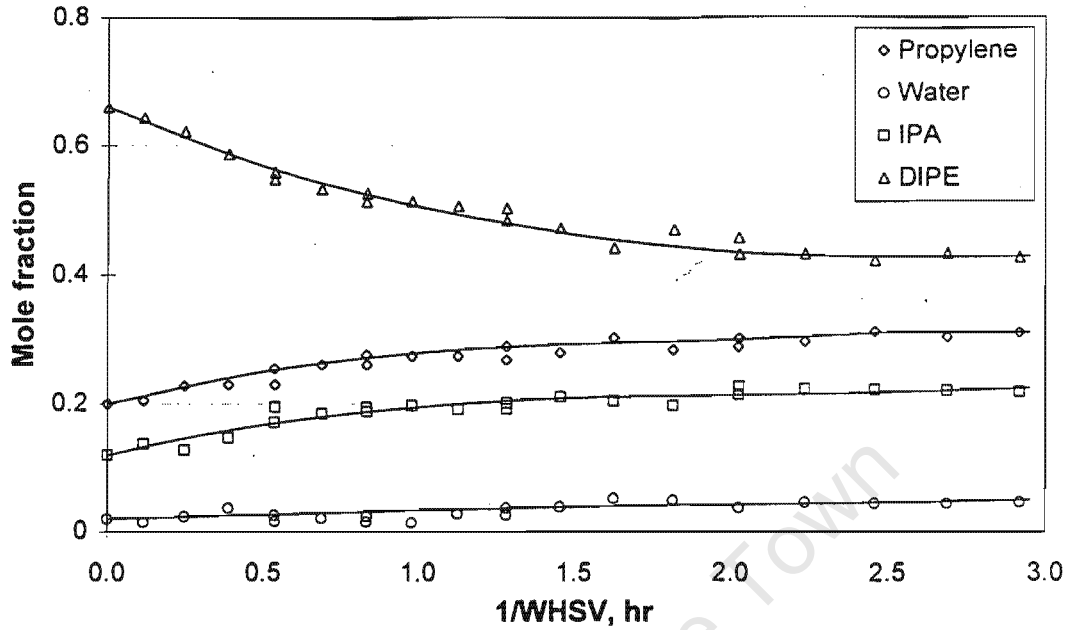

Figure 3.53: Approach to chemical reaction equilibrium starting from beyond chemical equilibrium relative to propylene and water as feed materials. Temperature = 120 °C, pressure = 50 bar and propylene:water ratio = 2 : 1.

from 7% to 76% and the DIPE selectivity from 29% to 81%. Any increase in pressure beyond 30 bar had little effect on the propylene conversion or DIPE selectivity. Decreasing the propylene to water mole ratio at 50 bar from 2 : 1 to 1 : 1 had very little effect on the propylene conversion, yet the selectivity to DIPE decreased from 79% to 38%. At atmospheric pressure, the same change in the propylene to water ratio resulted in a slight increase in propylene conversion from 7% to 11%, while DIPE selectivity decreased yet again from 29% to 17%.

All these changes in the equilibrium distribution can simply be explained by LeChateliers principle. Both the hydration and the two etherification reactions are exothermic reactions. Consequently, as temperature increases the equilibrium conversion of propylene decreases. As conversion decreases, the selectivity to DIPE (which is the final product) must decrease and the selectivity to IPA, the intermediate product, must increase.

The synthesis of IPA and DIPE involves a contraction in the number of moles in the system relative to the starting materials propylene and water. Hence, at low pressure the reactants propylene and water are thermodynamically favoured whilst at high pressure the reaction products IPA and DIPE are favoured. At a pressure of 30 bar the system is practically entirely liquid phase. Any further increase in pressure has very little effect on the system and thus has little effect on the equilibrium product distribution.

High ratios of propylene to water favour products with a higher propylene "content" relative to water, i.e. high propylene to water ratios favour DIPE formation whilst low ratios favour IPA. Thus, as the ratio of propylene to water is decreased from 2 : 1 to 1 : 1, the selectivity to DIPE decreases, i.e. that to IPA increases.

The experimental chemical equilibrium product distribution and the WS-PRSV model were used to obtain species activities at chemical equilibrium, thus enabling calculation of the experimental chemical equilibrium constants for the hydration and etherification reactions. The comparisons of the experimental chemical equilibrium constants obtained by this method with those from literature and the theoretical predictions are shown in Figures 3.54, 3.55 and 3.56 for the hydration of propylene, the alkylation of IPA and the bimolecular dehydration of IPA, respectively.

For every reaction, the majority of the experimental values of the chemical equilibrium constant lie above those of the theoretically determined chemical equilibrium constants. Even the chemical equilibrium constants of the two atmospheric pressure series display the same discrepancy. At atmospheric pressure and 120 °C the species can be considered to behave as ideal gases and the chemical equilibrium constant can thus be calculated directly from the mole fractions, without the need to resort to recalculation of the experimental data by the WS-PRSV model. Since these points (see Table 3.10) also lie above the theoretical values, the differences between the experimental and the theoretical values of the chemical equilibrium constants therefore cannot be attributed to the model used to calculated species activity, and the difference thus either results from the theoretical

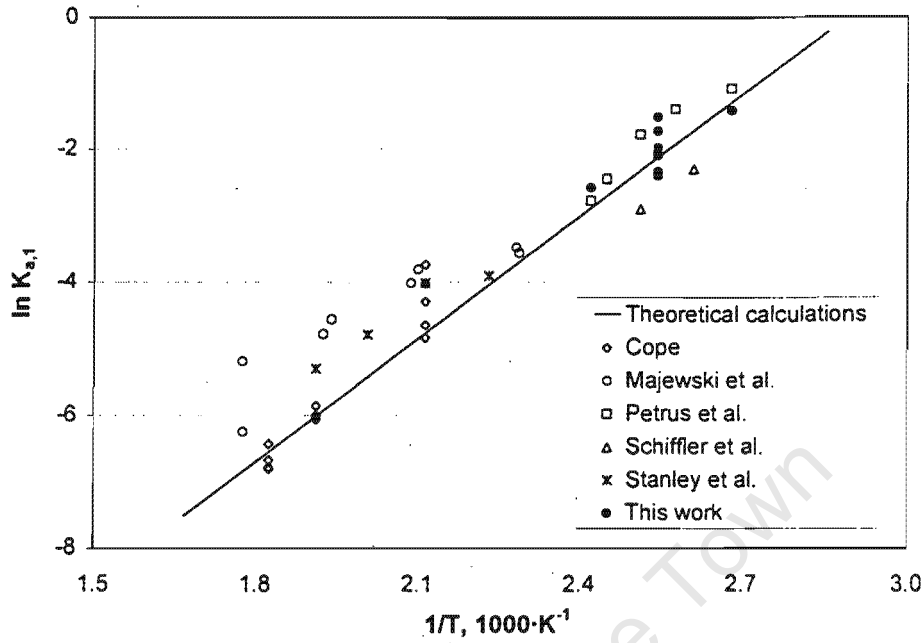

Figure 3.54: Comparison of the theoretical chemical equilibrium constant for propylene hydration with experimental data from literature and from this work.

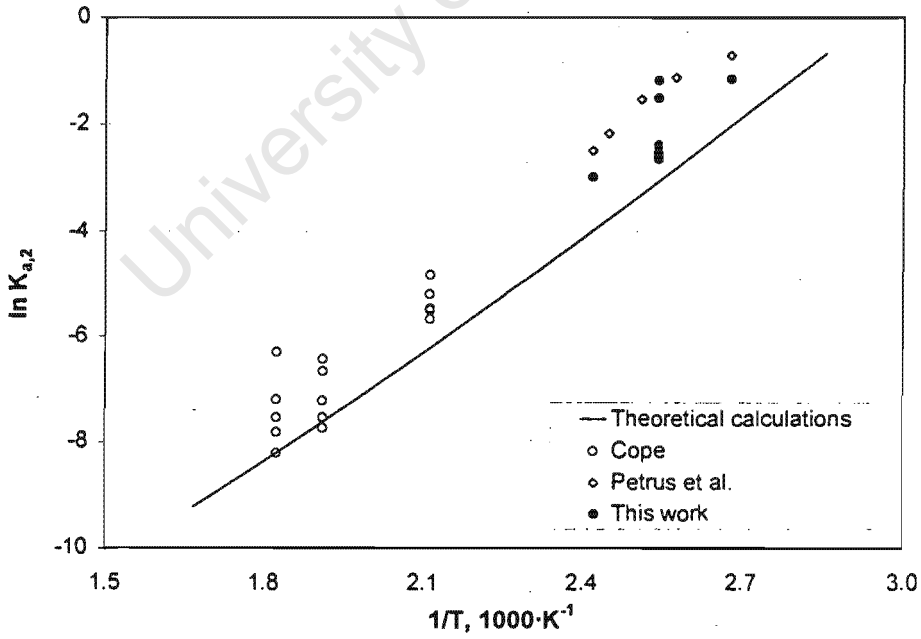

Figure 3.55: Comparison of the theoretical chemical equilibrium constant for IPA alkylation with experimental data from literature and from this work.

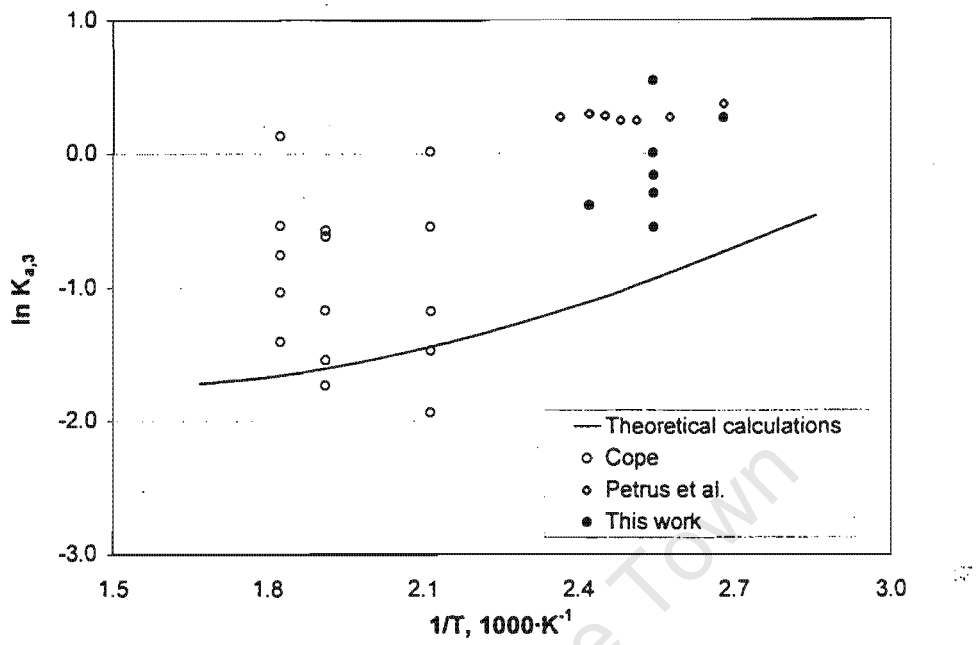

Figure 3.56: Comparison of the theoretical chemical equilibrium constant for the bimolecular dehydration of IPA with experimental data from literature and from this work.

calculations or from the experimental data. As the experimental data of so many authors gave such consistently higher values of the chemical equilibrium constant, it is reasonable to assume that the discrepancy can be ascribed to the theoretical calculations; more precisely, it can be ascribed to errors in the values of the pure component properties cited in literature.

Revised values of the chemical equilibrium constants were obtained from linear regression of the experimental $ln\ K_{a,i}$ vs $1/T$ data (both from literature and from this study). The best-fit lines to the experimental chemical equilibrium constants along with the theoretical predictions from literature are shown in Figures 3.57, 3.58 and 3.59. The best-fit linearisations of the chemical equilibrium constant for propylene hydration, IPA alkylation and the bimolecular dehydration of IPA, between temperatures of 100 °C and

290 °C, are given by

$$\ln K_{a,1} = \frac{5742}{T} - 16.58 \tag{3.17}$$

$$\ln K_{a,2} = \frac{7800}{T} - 21.81 \tag{3.18}$$

$$\ln K_{a,3} = \frac{2058}{T} - 5.23 \tag{3.19}$$

with 95% confidence limits of ±3.7%, ±2.2% and ±11.2% respectively.

Using these correlations, one can extrapolate to the value of the chemical equilibrium constant at 298 K and in so doing obtain a revised estimate of the standard Gibbs free energy of reaction. The revised values of the standard Gibbs free energies of reaction at 298 K obtained from the best-fit lines are shown in Table 3.11 along with the standard Gibbs free energies of reaction calculated from Stull et al. [65], Daubert and Danner [62] and Coulson et al. [63].

Table 3.11: Standard Gibbs free energies of reaction at 298 K for the reactions in the DIPE system. Literature values and the revised values from this work.

	Gibbs free energy of reaction, kJ·mol^{-1}		
Source	$\Delta G^o_{rxn,1}$	$\Delta G^o_{rxn,2}$	$\Delta G^o_{rxn,3}$
Daubert and Danner[1]	−6.94	−7.99	−1.05
Coulson et al.[2] and Stull et al. [3]	−7.49	−11.2	−3.73
Revised value	−6.62 ± 3.7%	−10.8 ± 2.2%	−4.18 ± 11.2%

[1] Daubert and Danner [62]

[2] Coulson et al. [63]

[3] Stull et al. [65]

The best-fit lines give significantly better predictions of the chemical equilibrium constant than those obtained from theoretical calculations using pure component data from literature [62]. The best-fit lines are not only offset from the theoretical predictions at

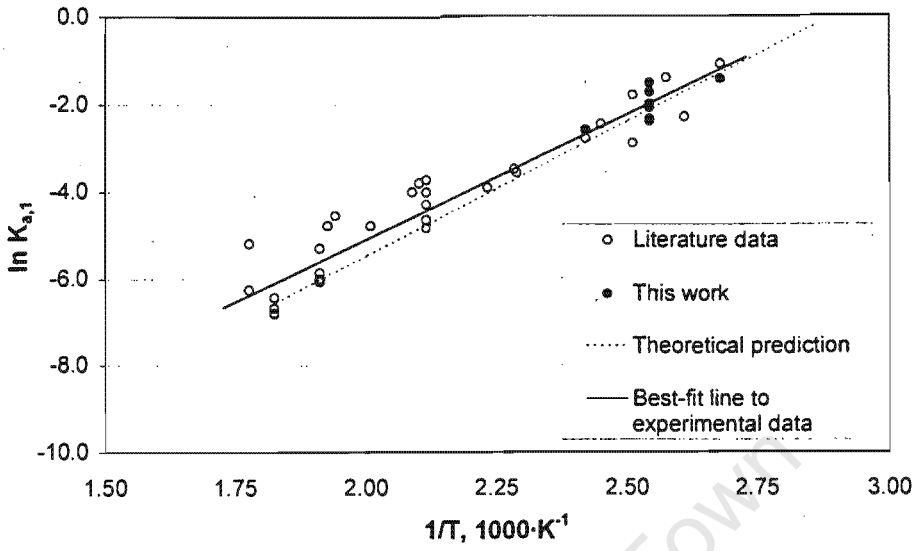

Figure 3.57: Comparison of the theoretical predictions of the chemical equilibrium constant for propylene hydration to experimental data from literature and from the present work. Both the theoretical predictions and the best-fit line giving the revised standard Gibbs free energy of reaction are shown.

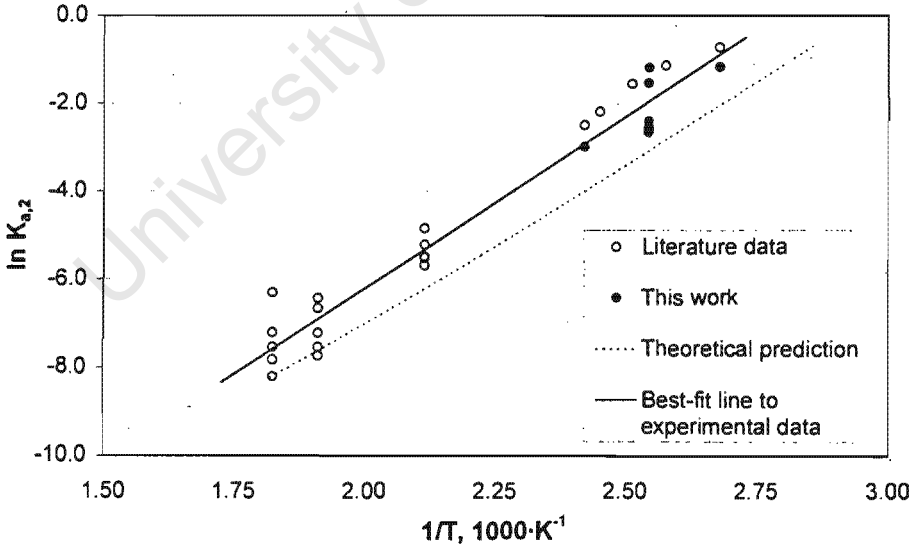

Figure 3.58: Comparison of the theoretical predictions of the chemical equilibrium constant for IPA alkylation to experimental data from literature and from the present work. Both the theoretical predictions and the best-fit line giving the revised standard Gibbs free energy of reaction are shown.

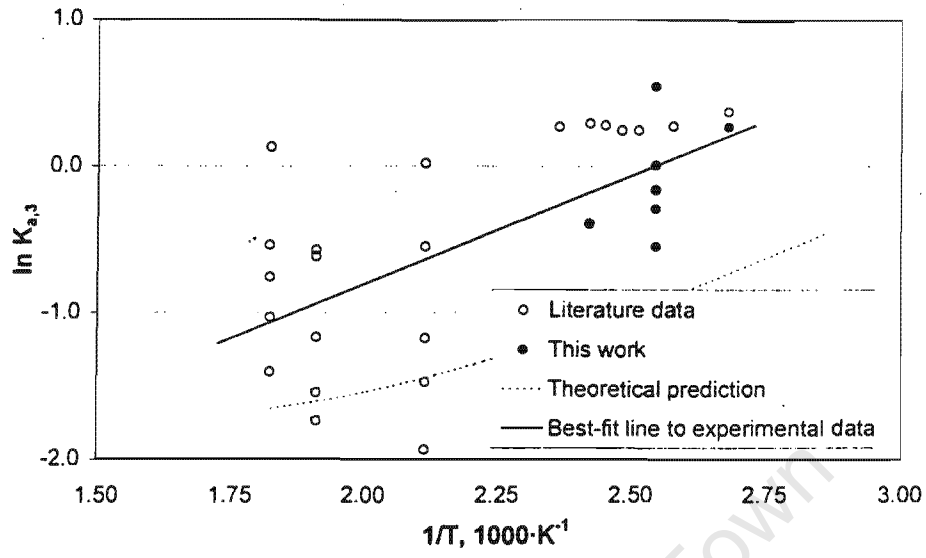

Figure 3.59: Comparison of the theoretical predictions of the chemical equilibrium constant for the bimolecular dehydration of IPA to experimental data from literature and from the present work. Both the theoretical predictions and the best-fit line giving the revised standard Gibbs free energy of reaction are shown.

298 K, they also display considerably different slopes. Should the best-fit line and the theoretical line be parallel but differ by a constant value, an incorrect value of the standard Gibbs energy of reaction at 298 K was used. A difference in slope between the best-fit line and the theoretical line indicates, in addition, that the heat capacity data may be inaccurate.

For propylene hydration, the value of the standard Gibbs free energy of reaction at 298 K was close to that calculated from literature data. This was consistent with the behaviour of the best-fit line and the theoretical line which intersected at a temperature of 300 K. The slope of the best-fit line to experimental chemical equilibrium data and that of theoretical line, though, are significantly different, which indicated that whilst the standard pure component Gibbs free energies of formation given in literature were correct, the heat capacity data, used to calculate the value of the chemical equilibrium constant

at temperatures other than 298 K, may have been inaccurate. For IPA alkylation, the theoretical line and the best-fit line were not only offset at 298 K, but also showed a different slope. This indicated that both the standard Gibbs free energy of reaction as well as the heat capacity data used for the compounds may have been in error. For the bimolecular dehydration of IPA, the best-fit line and the theoretical line were parallel for temperatures below 150 °C, the offset between the two lines being constant. In this case, only the value of the standard Gibbs free energy of reaction from literature [62] was inaccurate.

Since the only theoretical chemical equilibrium constants for which the Gibbs free energy of reaction was imprecise were those involving DIPE, most likely the standard Gibbs free energy of formation of DIPE as given by Daubert and Danner [62] was the source of the error in the theoretical chemical equilibrium constant. Assuming that the standard Gibbs free energy of formation of the other compounds involved in the reactions was correct, a revised estimate of the standard Gibbs free energy of formation of DIPE at 298 K gave -122.04 kJmol^{-1}. This value is larger than that given by Daubert and Danner [62] (-119.24 kJmol^{-1} $\pm$ 5%) though still within the cited error margin and compares excellently with the value given by Stull et al. [65] and Coulson et al. [63] of -121.96 kJmol^{-1}. The only reactions for which the experimental chemical equilibrium constant differed from the theoretical values were those involving propylene, i.e. propylene hydration and IPA alkylation. Most likely the heat capacity data for propylene was incorrect, but insufficient experimental data was available to estimate more accurate values.

The revised values of the chemical equilibrium constants with temperature are shown in Figure 3.60.

In addition to revising the standard Gibbs free energy of reaction, one can now also re-estimate the standard enthalpy and entropy of reaction for all three reactions. The standard enthalpy of reaction can be estimated from the rate of change of the natural logarithm of the chemical equilibrium constant with respect to temperature using the

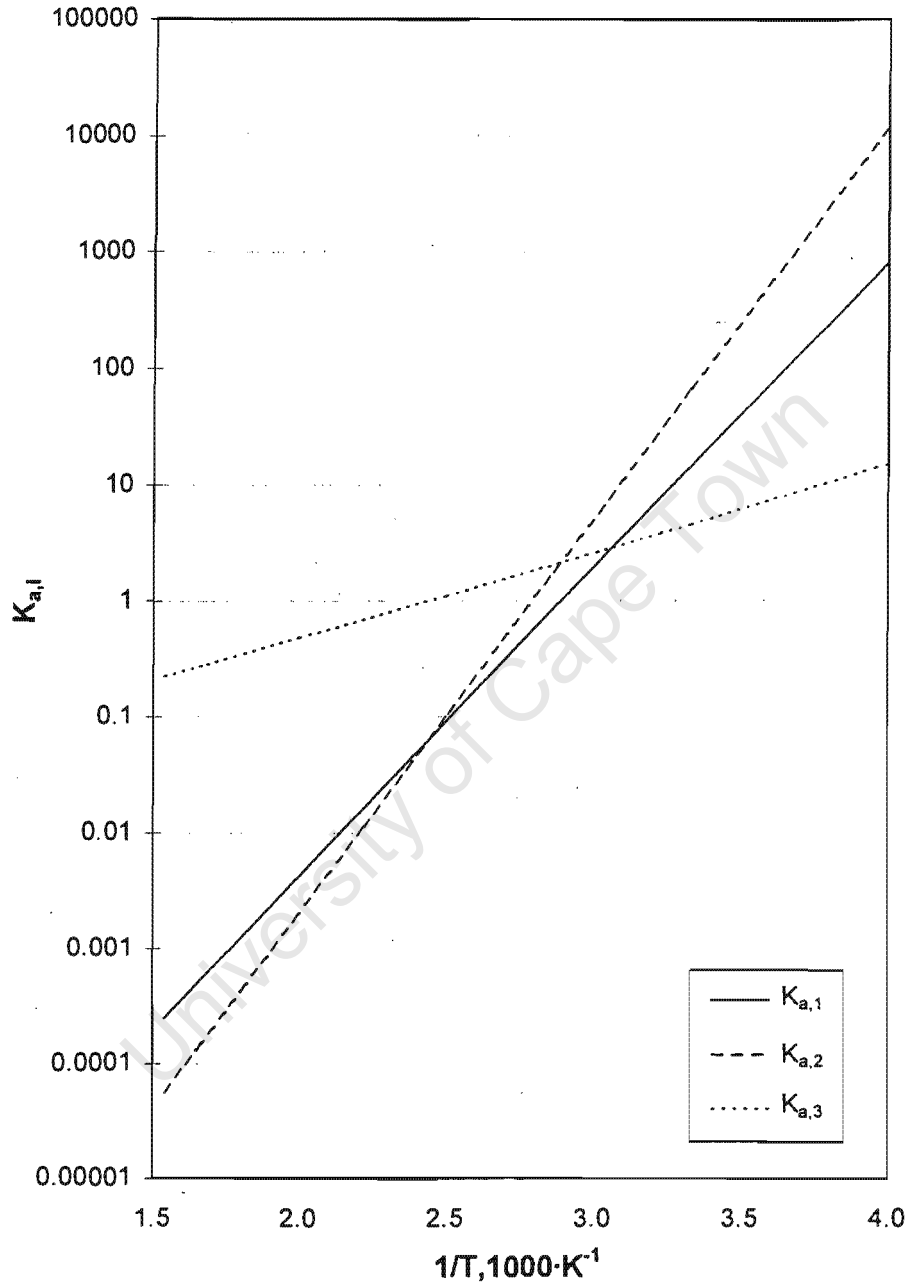

Figure 3.60: Revised values of the chemical equilibrium constant; variation with temperature. $K_{a,1}$ = chemical equilibrium constant for hydration, $K_{a,2}$ = chemical equilibrium constant for IPA alkylation, $K_{a,3}$ = chemical equilibrium constant for bimolecular dehydration.

van't Hoff equation (see Section 2.2.4),

$$\left(\frac{\partial \ln K_a(T)}{\partial T}\right)_P = \frac{\Delta \overline{H}^{\circ}_{rxn}(T)}{RT^2} \tag{3.20}$$

and since

$$G = H - TS \tag{3.21}$$

the standard entropy of reaction is given by

$$\Delta \overline{S}^{\circ}_{rxn} = \frac{\Delta \overline{H}^{\circ}_{rxn} - \Delta \overline{G}^{\circ}_{rxn}}{T} \tag{3.22}$$

The standard Gibbs free energy, standard enthalpy and standard entropy of reaction for propylene hydration, IPA alkylation and bimolecular dehydration of IPA are given in Table 3.12 in comparison to those of the other octane enhancing ethers.

The standard entropy of reaction for bimolecular dehydration of IPA is the lowest of all the reactions shown as there is no net reduction in the number of molecules and, consequently, the reduction in the number of degrees of freedom is smaller than for any other reaction. This reaction also has the smallest standard enthalpy of reaction. The hydration of propylene and the alkylation of IPA display the greatest standard entropies of reaction.

The experimental chemical equilibrium constants show considerable scatter about the theoretical value (see Figures 3.57 to 3.59). It was shown in Section 2.3.3 that the squared fractional error in the chemical equilibrium constant given an exact system composition, temperature and pressure could be calculated from

$$\left(\frac{\Delta K_a}{K_a}\right)^2 = \nu_1^2\left(\frac{\Delta a_1}{a_1}\right)^2 + \nu_2^2\left(\frac{\Delta a_2}{a_2}\right)^2 + \nu_3^2\left(\frac{\Delta a_3}{a_3}\right)^2 + \nu_4^2\left(\frac{\Delta a_4}{a_4}\right)^2 \tag{3.23}$$

In the case of the error in the experimentally determined chemical equilibrium constant, however, the mole fraction, pressure and temperature are no longer exact, thus a

Table 3.12: Standard Gibbs free energy, enthalpy and entropy of reaction for propylene, isobutylene and isoamylene hydration and etherification

	Properties of reaction at 298 K		
Compound	ΔG^o_{rxn}, kJmol^{-1}	ΔH^o_{rxn}, kJmol^{-1}	ΔS^o_{rxn}, Jmol^{-1}K^{-1}
Propylene[1]			
Hydration	-6.62	-47.7	-137
Alkylation with IPA	-10.8	-64.8	-181
Bimolecular IPA dehydration	-4.18	-17.1	-43.4
Isobutylene			
Hydration[2]	3.23	-24.5	-93.0
Alkylation with methanol[3]	-13.9	-38.5	-82.5
Alkylation with ethanol[4]	-11.7	-34.8	-77.3
Isoamylene[5]			
Hydration	-13.1	-41.2	-94.3
Alkylation with methanol	-9.91	-34.3	-81.8

1 This work, revised values

2 Coulson et al. [63]

3 Using correlation of Zhang and Datta [128]

4 Cunill et al. [167]

5 Linnekoski et al. [157]

more detailed error analysis is required. The fractional error in the chemical equilibrium constant as a function of the error in mole fraction, temperature and pressure can be shown (Appendix J) to equal

$$\begin{aligned}\left(\frac{\Delta K_a}{K_a}\right)^2 &= \sum_i \nu_i^2 \left(\frac{\Delta x_i}{x_i}\right)^2 \left(1+\left(\frac{\partial \ln \phi_i}{\partial \ln x_i}\right)^2\right) \\ &+ \sum_i \nu_i^2 \left(\frac{\Delta P}{P}\right)^2 \left(1+\left(\frac{\partial \ln \phi_i}{\partial \ln P}\right)^2\right) \\ &+ \sum_i \nu_i^2 \left(\frac{\Delta T}{T}\right)^2 \left(\frac{\partial \ln \phi_i}{\partial \ln T}\right)^2\end{aligned} \tag{3.24}$$

where the partial derivatives of the fugacity coefficient with respect to mole fraction,

system pressure and temperature can be obtained numerically. The error in temperature measurement was ±1 °C for all experiments. The error in pressure measurement was ±0.5 bar for the high pressure and ±0.5 kPa for the low pressure experiments. It has been shown that the error in the estimation of the mole fraction is approximately ±0.02 absolute for all compounds except for DIPE at low pressure, where the error was ±60% based on the scatter in the analytical measurements. The error in the calculation of the theoretical chemical equilibrium constant, within 95% confidence limits, has already been shown to equal 3.7% for $K_{a,1}$ and 11.2% for $K_{a,3}$ (see Table 3.11). The values of the theoretical and experimental chemical equilibrium constants with associated error margins are shown in Figure 3.61. For clarity only $K_{a,1}$ and $K_{a,3}$ are displayed.

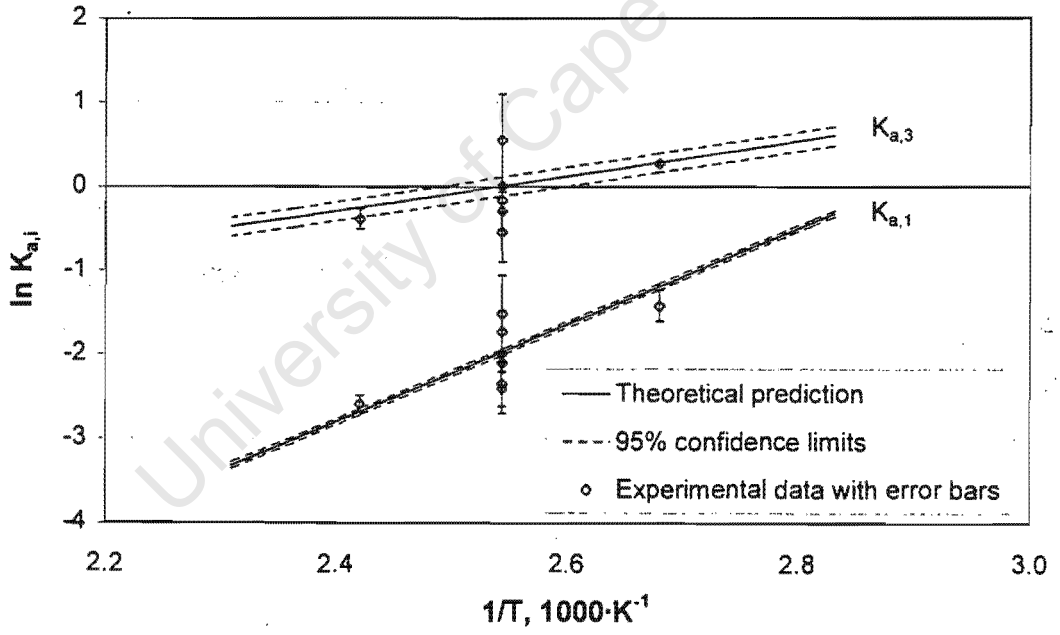

Figure 3.61: The values and error margins in the theoretically and experimentally determined chemical equilibrium constants.

For every experimental point except the "reverse" run at 120 °C and 50 bar, the experimental value of the chemical equilibrium constant either lies within the 95% confidence limits of the theoretical value or at least the error margins overlap. For these data points,

the experimentally determined chemical equilibrium constant thus lies within the expected error margins of the theory and the experimental method.

By far the greatest source of error in the experimental determination of the chemical equilibrium constant lay in the accuracy of determination of the chemical equilibrium distribution. This is well illustrated by the experimental chemical equilibrium at 140 °C and 50 bar, for example. The only difference between the experimental product distribution and the product distribution predicted by the WS-PRSV model (using accurate values of the chemical equilibrium constants) at chemical equilibrium occurred for the propylene mole fraction which was under-predicted by 2.9% and for DIPE mole fraction which was over-predicted by 2.6%. The predictions of the IPA and water mole fractions were identical to the experimental values. Nevertheless, these relatively small errors between the predicted and experimental product distributions led to errors in the chemical equilibrium constants of propylene hydration and bimolecular dehydration of 10% and 13% respectively. Larger errors in mole fractions, especially in the water mole fraction, led to considerably larger errors in the values of the chemical equilibrium constants.

Figures 3.62 and 3.63 show the effect of temperature and pressure on the product distribution at chemical reaction equilibrium in comparison to the predicted product distribution using the revised values of the chemical equilibrium constant and the WS-PRSV model. Qualitatively the correspondence between the experimental data and the model predictions is good, but the model appears to overpredict the DIPE mole fraction while underpredicting the propylene and IPA mole fractions.

As stated above, the error in the experimental determination of the chemical equilibrium mole fraction was shown to be ± 0.02 with the exception of the DIPE mole fraction at atmospheric pressure, where the error was estimated to be $\pm 60\%$. The prediction of the chemical equilibrium product distribution of any system depends not only on the temperature, pressure and system composition, but also on the accuracy in the calculation of the chemical equilibrium constant(s) and the species activity. In this case, the

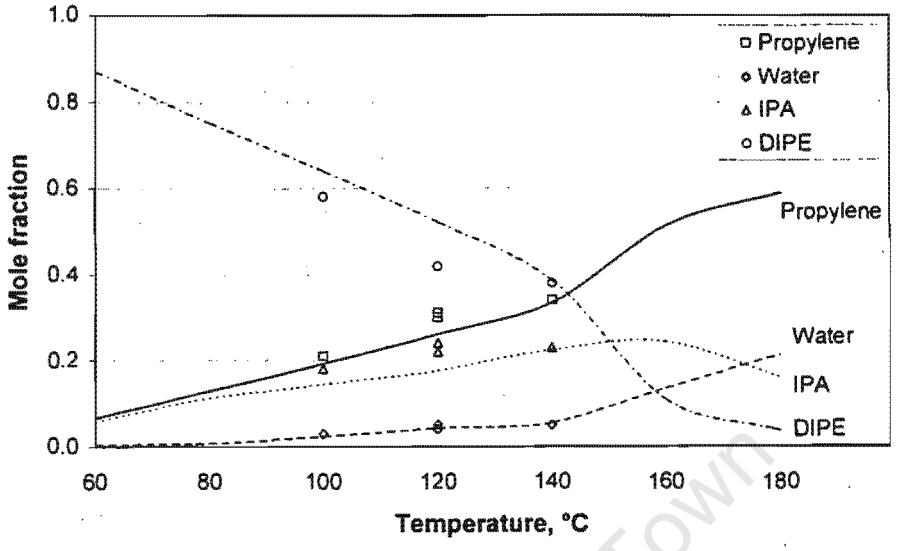

Figure 3.62: Chemical equilibrium product distribution variation with temperature. Pressure = 120 °C and propylene to water ratio of = 2 : 1. The lines show the WS-PRSV model predictions, the points show the experimental data.

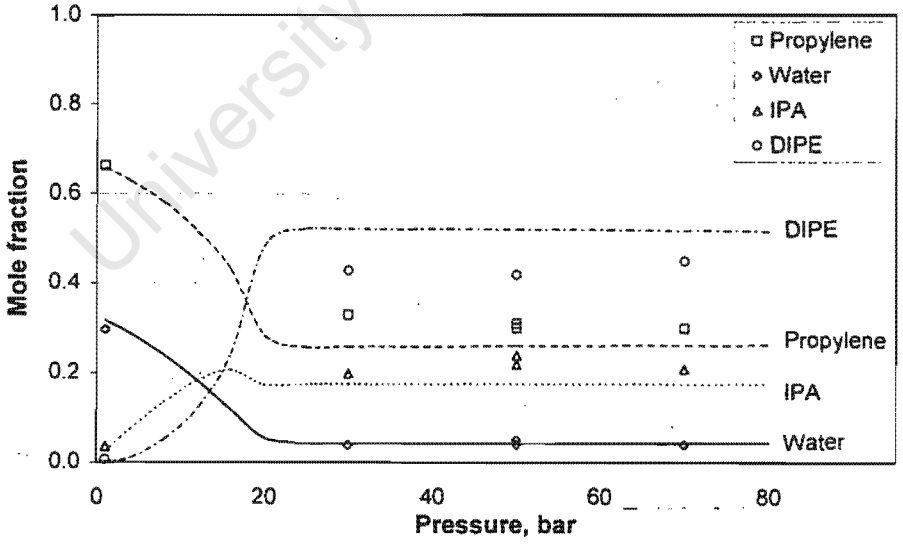

Figure 3.63: Chemical equilibrium product distribution variation with pressure. Temperature = 120 °C and propylene to water ratio of = 2 : 1. The lines show the WS-PRSV model predictions, the points show the experimental data.

temperature, pressure and system composition are given, so the error in prediction depends solely on the error in the calculation of the chemical equilibrium constants and the species activity. In terms of propagation of error theory, the fractional squared error in the chemical equilibrium mole fraction of a species i is

$$\left(\frac{\Delta z_i}{z_i}\right)^2 = \left(\frac{\Delta K_{a,1}}{K_{a,1}}\right)^2 \left(\frac{\partial \ln z_i}{\partial \ln K_{a,1}}\right)^2 + \left(\frac{\Delta K_{a,3}}{K_{a,3}}\right)^2 \left(\frac{\partial \ln z_i}{\partial \ln K_{a,2}}\right)^2 + \sum_j \left[\left(\frac{\Delta a_j}{a_j}\right)^2 \left(\frac{\partial \ln z_i}{\partial \ln a_j}\right)^2\right] \tag{3.25}$$

where only two chemical equilibrium constants need be considered as the third is a function of the other two, $K_{a,2} = K_{a,3} \cdot K_{a,1}$. The error in calculating the values of $K_{a,1}$ and $K_{a,3}$, from the best-fit linearisations, within 95% confidence limits have been shown to be 3.7% and 11.2% respectively. In Section 2.3.3 it was shown that the error in determining the activity of an individual species given an exact temperature, pressure and system composition was less than 6%. Finding an analytical solution for the partial derivatives of the species chemical equilibrium mole fraction with respect to $\ln K_{a,1}$, $\ln K_{a,3}$ and $\ln a_j$ is not possible, so these quantities were determined numerically.

Figures 3.64 and 3.65 show the chemical equilibrium IPA mole fractions and error margins of the experimental data and the WS-PRSV model predictions. As IPA displayed the greatest fractional deviation between the predicted and the experimental chemical equilibrium mole fractions, similar figures for the other three components would not have been instructive and thus are not shown.

Exactly as was the case for the comparison of the experimental and theoretical chemical equilibrium constant, for every run other than the "reverse" series at 120 °C and 50 bar the experimental IPA mole fraction either lay within the 95% confidence limits of the WS-PRSV model predictions or the error bars at least overlapped. The "reverse" series had probably not yet entirely attained chemical equilibrium as both the mole fraction and the chemical equilibrium constant lay outside the combined error margins.

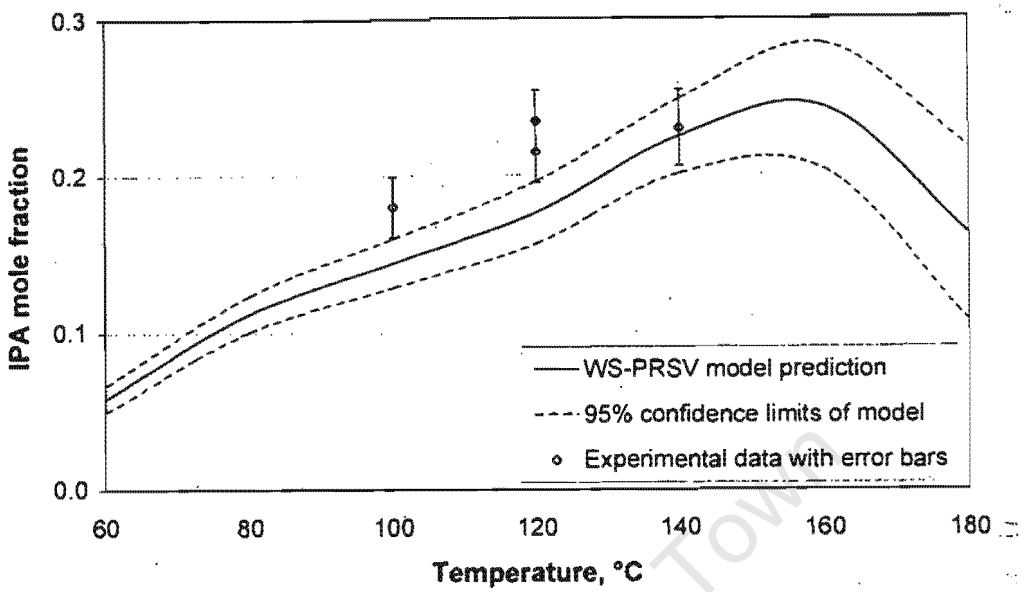

Figure 3.64: Variation with temperature of the experimental and WS-PRSV model predictions of the IPA mole fraction at chemical reaction equilibrium. Pressure = 50 bar and propylene to water ratio = 2 : 1.

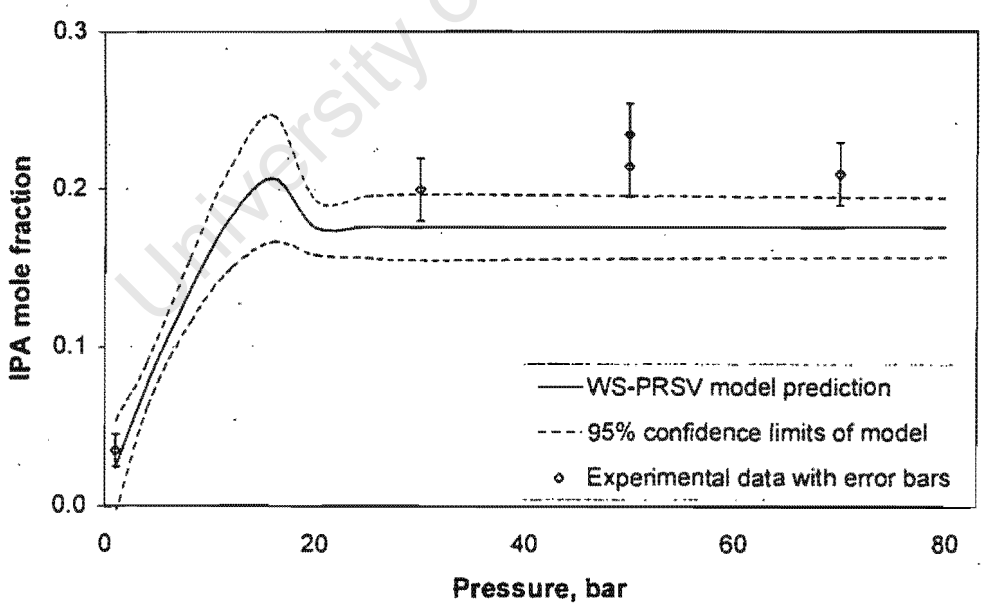

Figure 3.65: Variation with pressure of the experimental and WS-PRSV model predictions of the IPA mole fraction at chemical reaction equilibrium. Temperature = 120 °C and propylene to water ratio = 2 : 1.

3.3.8 Catalysts

As all catalytic results in the present study thus far had been obtained from reaction over Amberlyst 15 sulphonic acid ion exchange resin, it was decided to at least qualitatively examine the performance of other catalysts for DIPE synthesis. One of the difficulties in choosing a catalyst for the DIPE system is that it must be catalytically highly active at low temperatures. This is necessary for two reasons:

- At a pressure of 50 bar, an overall propylene to water mole ratio of 2 : 1 and a temperature of 100 °C the maximum thermodynamic yield of DIPE (on a carbon basis) is 79%. This rapidly decreases to 71% at 120 °C, to 50% at 150 °C and to 3% at 200 °C. For a high yield it is thus necessary to operate at relatively low temperatures.
- The propyl carbocation (the intermediate in the hydration and etherification reactions) is relatively unstable as opposed to the isoamyl or isobutyl carbocation. In comparison to MTBE, ETBE or TAME synthesis the rate of the reactions in the DIPE system consequently proceed considerably slower (see Section 3.3.3.1) and a highly active catalyst is thus required to compensate.

Consequently, two additional sulphonic acid ion exchange resin catalysts, Amberlyst 35 and Amberlyst 36, a zeolite, H-Y, and an organofunctional polysiloxane, D-ASP, were chosen for the study (Table 3.4 in Section 3.2.1 gives the catalyst properties). The catalysts were evaluated under "process" conditions, i.e. it was decided not to compare the initial rates, but rather to choose a realistic feed composition such as would enter a commercial DIPE reactor. The composition of the system just before the point of maximum propylene consumption rate in the contact time series performed at 120 °C, 50 bar and an overall propylene to water mole ratio of 2 : 1 was chosen as the starting point (see Section 3.3.3.4). At this point, at a 1/WHSV of 2h, the mole fractions of water,

propylene, IPA and DIPE were 0.16, 0.57, 0.25 and 0.02 respectively. The differential rates of propylene consumption during the reaction on a mass basis, on an equivalent basis and based on catalyst bed volume are shown in Table 3.13.

Table 3.13: The rate of propylene consumption in DIPE synthesis over various acidic catalysts on a mass basis, on an equivalent basis and on a catalyst bed volume basis (wet catalyst)

	Propylene consumption rate		
Catalyst	$mol \cdot g_{cat}^{-1} \cdot s^{-1}$	$mol \cdot eq^{-1} \cdot s^{-1}$	$mol \cdot cm^3 \cdot s^{-1}$
Amberlyst 15	$1.3 \cdot 10^{-6}$	$2.7 \cdot 10^{-4}$	$3.1 \cdot 10^{-7}$
Amberlyst 35	$1.1 \cdot 10^{-6}$	$2.1 \cdot 10^{-4}$	$2.2 \cdot 10^{-7}$
Amberlyst 36	$1.2 \cdot 10^{-6}$	$2.1 \cdot 10^{-4}$	$2.5 \cdot 10^{-7}$
H-Y	$5.5 \cdot 10^{-8}$	$5.5 \cdot 10^{-5}$	$1.6 \cdot 10^{-8}$
D-ASP	$1.2 \cdot 10^{-6}$	$8.8 \cdot 10^{-4}$	$1.7 \cdot 10^{-7}$

None of the catalysts exhibited any deactivation over the duration of the experiments (approximately 8 h on-line in each case), nor were any compounds other than the above-mentioned four detected in the effluent stream for any catalyst.

It was to be expected that H-Y would exhibit the least catalytic activity for the hydration and etherification reactions, as it is well known to be highly hygroscopic. Any water (or any other highly polar compound for that matter) present in the reaction medium would adsorb strongly on the active sites and inhibit both the hydration and the etherification reactions.

On a mass basis Amberlyst 15, Amberlyst 35, Amberlyst 36 and D-ASP displayed approximately the same reaction rate. On an equivalent basis, however, the rate of propylene consumption over D-ASP was approximately 4 times greater than over the Amberlyst ion exchange resin catalysts. Interestingly, the active sites in both sets of catalyst are sulphonic acid sites. Presumably, the difference in activity stems from the different interactions between the sulphonic acid groups and the polystyrene backbone on the one hand and the sulphonic acid groups and the polysiloxane backbone on the other.

On a catalyst bed volume basis Amberlyst 15 exhibited the greatest rate of etherification followed by Amberlyst 35 and Amberlyst 36. From a reactor design point of view, in light of similar deactivation and selectivities, it would appear that Amberlyst 15 is the catalyst of choice for DIPE synthesis.

Chapter 4

The mechanism and kinetics of DIPE synthesis

4.1 The mechanism of DIPE formation

The reaction mechanisms thought to occur in olefin hydration and ether formation reactions over acidic ion exchange resin catalysts have evolved from simple pseudo-homogeneous type mechanisms to complex mechanisms involving multiply adsorbed species reacting on varying numbers of acid sites in distinct catalytic regimes (see Section 3.1.5). Which catalytic regime is dominant and the number of acid sites taking part in the reaction is determined by the ratio (R) of apolar to polar species within the resin matrix and by the overall concentration of polar and apolar species. The phase of the reaction has no effect other than to determine the concentration, i.e. the mechanisms in the vapour and liquid phase are identical. Figure 4.1 gives a representation of the transition between the three regimes of catalytic action (names Type I, Type II and Type III for convenience).

I: At low apolar to polar species mole ratios ($R < R_1$) and at concentrations high enough that the catalyst is fully saturated, the dominant mechanism is Type I (see Figure 4.5 for a pictorial representation of the Type I mechanisms). This mechanism is similar in nature to the mechanisms encountered in true homogeneous

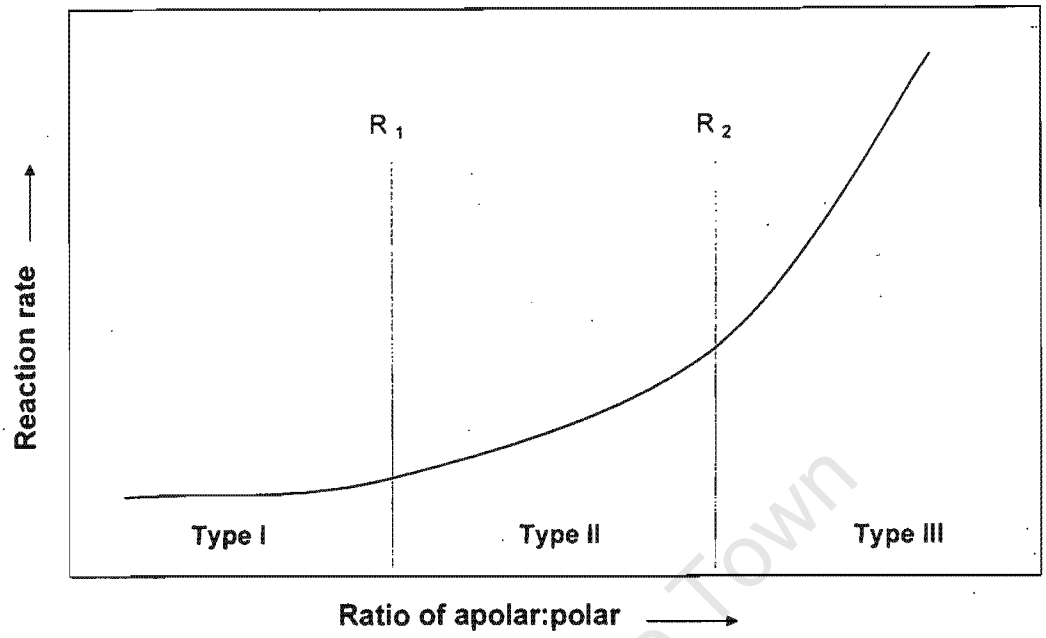

Figure 4.1: The type of catalytic mechanism and the change in the catalytic activity as a function of the ratio of apolar to polar species at saturated conditions. Type I - pseudohomogeneous mechanism, Type II - adsorbed polar species and solution phase apolar species mechanism, Type III - adsorbed polar species and adsorbed apolar species mechanism.

catalysis. Polyadsorbed complexes of polar species form on individual active sites, where the number of polar molecules adsorbed on the active sites is determined by the concentration and the polarity of the species. Apolar molecules are not adsorbed and remain in the solution phase. The active sites are surrounded by a "solvation" sphere. The hydrogen ions are delocalised with transference of the protons to form the reaction intermediates occurring via the polyadsorbed species. The order with respect to acid site density is one. Any side reactions involving only apolar species are suppressed by competitive adsorption. This is the least active mechanism.

II: At intermediate ratios of apolar to polar species ($R_1 < R < R_2$) reaction still occurs between adsorbed phase polar species and solution phase apolar species. However,

the higher concentrations of the apolar species disrupt the molecular ordering of the polar species such that polyadsorbed complexes no longer occur (see Figure 4.6 for a pictorial representation of Type II mechanisms). Polar molecules now hydrogen-bond into single or multiple active site complexes, so-called "nests" of active sites. The number of active sites involved in these concerted complexes is determined by the polarity and the concentration of the polar species. The order of dependence of reaction rate on active site density depends on the number of active sites involved in the mechanism. Reactions involving only apolar species are still inhibited by competitive adsorption. The adsorbed reaction intermediate is stabilised by increased hydrogen bonding to additional active sites and the mechanism is thus more catalytically active than the Type I mechanism.

III: At high ratios of apolar to polar species ($R > R_2$) or at very low overall concentrations, apolar species also adsorb onto the active sites. Reactions now take place between adsorbed phase polar and adsorbed phase apolar species with both types of species adsorbed on multiple active sites. As for the Type II mechanism, the number of active sites involved in the concerted Type III mechanism depends on the polarity and the concentration of the adsorbed species. The order with respect to active site density, once again, depends on the number of active sites involved in the mechanism. Side reactions between apolar species are now possible. As even more active sites take part in this mechanism, allowing an even greater stabilisation of the reaction intermediate compared to Type II, this mechanism is the most catalytically active.

Besides the overall concentration and the ratio of apolar to polar species in the reaction medium, the type of catalytic mechanism is also determined by catalyst factors such as the acid site density, the extent of cross-linking and the extent of ion exchange or deactivation. These factors influence the mechanism by determining the average distance between active sites. Even though macroreticular catalytic resins are heterogeneous structures, if the

active site density is very low, then the distance between individual sites may be too large for the concerted Type II and Type III mechanisms to take place. Conversely, if the active site density is high, active sites will be closer together and Type II and Type III mechanisms can occur. The extent of cross-linking has a more subtle effect. In resins with a high degree of cross-linking, the matrix is not able to swell as extensively as it would in resins with a low degree of cross-linking. Decreased swelling translates to a higher active site density which leads to the more active Type II and Type III mechanisms However, decreased swelling may also result in reduced accessibility to the internal sites and possible mass transfer limitations which may inhibit the desired reactions.

Ion exchange and/or deactivation of active sites has a dramatic effect on catalyst activity. Figure 4.2 gives a pictorial representation of a heterogeneous ion exchange resin with randomly distributed active sites at varying extents of ion exchange. Clearly, the unmodified catalyst not only has the greatest number of active sites, but also has the greatest number of nests with two, three or four sites etc. As active sites are deactivated by ion exchange with inactive ions, the total number of active sites declines linearly with the extent of ion exchange. The number of multi-site nests, however, decreases with the extent of ion exchange with an order equal to the number of active sites situated within the nests. This accounts for the non-linear dependence of reaction rate with respect to acid site density. The rate of a reaction taking place via a three-site mechanism, for example, would decrease with extent of increased ion exchange to the third order. The effect of ion exchange on the total number of active sites and on the number of multi-site active site nests is shown in Figure 4.3.

This study has shown (see Section 3.3.3.2 and Section 3.3.3.4) that the reactions which occur in the DIPE system are the hydration of propylene, the alkylation of IPA and the bimolecular dehydration of IPA. No other reactions occur. The reaction network is shown in Figure 4.4.

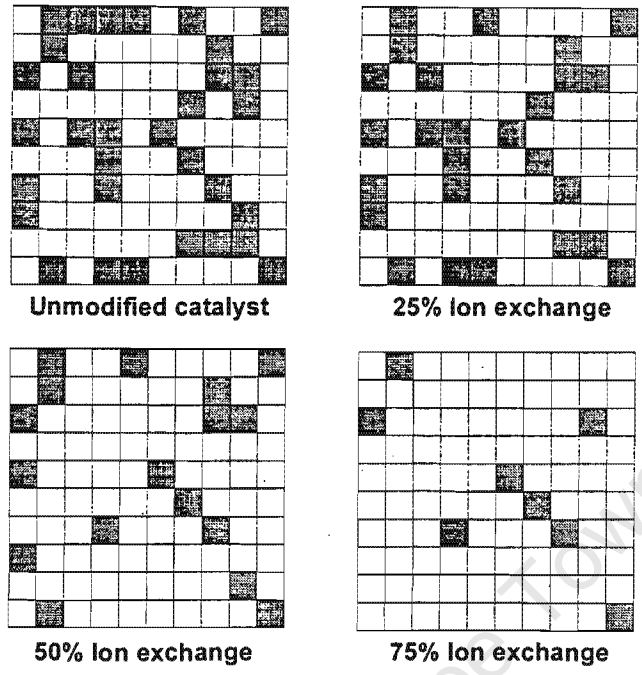

Figure 4.2: Pictorial representation of a heterogeneous ion exchange resin with randomly distributed active sites at varying extents of ion exchange. Dark squares represent active sites, light squares represent catalyst matrix or inactive sites.

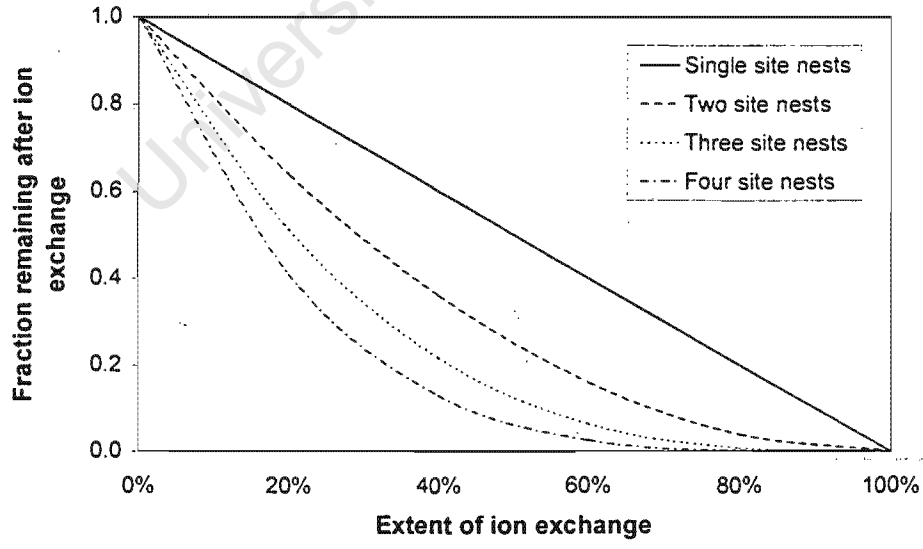

Figure 4.3: The effect of ion exchange on the total number of active sites and on the number of multi-site active site nests.

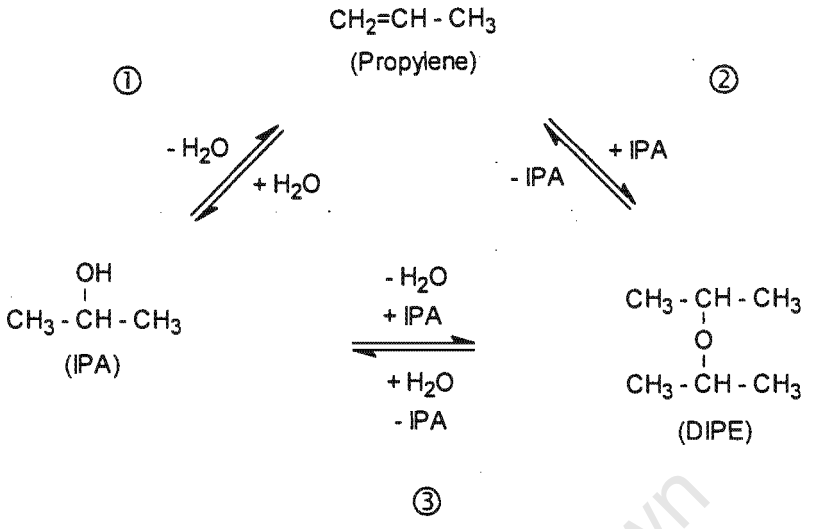

Figure 4.4: Cyclic reaction network of DIPE formation.

When feeding only propylene and water, the initial rate of propylene hydration was observed to be first order with respect to acid site density (Section 3.3.4) and first order with respect to the concentration of propylene in the liquid phase (Section 3.3.3.2), so long as the concentration of propylene remained very small. No by-products, i.e. dimers or trimers of propylene were produced at any stage, oligomerisation likely having been suppressed by the competitive adsorption of water. At greater concentrations of propylene in the liquid phase, e.g. after sufficient IPA had been produced to extensively solubilise propylene, it was observed that the rate of propylene hydration increased markedly (Section 3.3.3.4). These findings are consistent with the transition from a Type I mechanism at low propylene to water ratios to a Type II mechanism at higher propylene to water ratios. At low ratios of propylene to water, water is polyadsorbed on single active sites. The protons from the active sites are solvated within these polyadsorbed complexes and can react with solution phase propylene to form the propyl carbocation intermediate. This then reacts further with water to form IPA.

As IPA is produced, propylene becomes ever more soluble and disrupts the Type I mechanism, causing the Type II mechanism to dominate. This appears to occur at an

apolar (propylene) to polar (water and IPA) mole ratio of approximately 1:2 (Section 3.3.3.4). This is consistent with the findings for isobutylene hydration, where the shift in mechanism appears at a ratio of approximately 1:3 [99]. In the Type II mechanism, water is adsorbed to multiple active sites. Propylene from solution then reacts with the adsorbed water to form IPA. In both types of mechanisms the presence of only small amounts of water is sufficient to displace propylene from the active sites and thus prevent oligomerisation, in agreement with the findings in Section 3.3.6 that the adsorption constant for water was considerably greater than that for propylene. Figures 4.5 and 4.6 show the Type I and the Type II mechanisms over catalytic ion exchange resins.

Both etherification reactions behave identically to the hydration reactions. At low ratios of propylene to IPA (i.e. at low apolar to polar species ratio), the etherification reactions are slow. As one increases the ratio of propylene to IPA, the rate of etherification accelerates dramatically, but then levels off again (Sections 3.3.3.2 and 3.3.3.3). As for the hydration reaction, no by-products, i.e. dimers or trimers of propylene were produced at any stage, indicating a competitive adsorption effect which prevents propylene from adsorbing on the active sites, thus preventing the oligomerisation reaction. As before, this is consistent with the transition from a Type I mechanism (at low propylene to IPA ratios) to a Type II mechanism. The order of reaction on acid site density in the more active regime was found to be two or three, indicating that either two or three sites are involved in the mechanism (Section 3.3.4). Similarly as for hydration, the switch between a predominantly Type I and a predominantly Type II mechanism occurs at an apolar (propylene and DIPE) to polar (water and IPA) mole ratio of approximately 1:1. For MTBE synthesis this shift appears at a ratio of approximately 1:1.4 [132]. In the Type I mechanism, IPA is polyadsorbed to the active sites and reacts either with solution phase propylene or IPA to form DIPE. In the Type II mechanism, each IPA molecule is adsorbed to multiple sites (likely two or three) and then reacts with solution phase propylene or IPA to form DIPE. Figures 4.5 and 4.6 show the Type I and the Type II mechanisms over catalytic ion exchange resins.

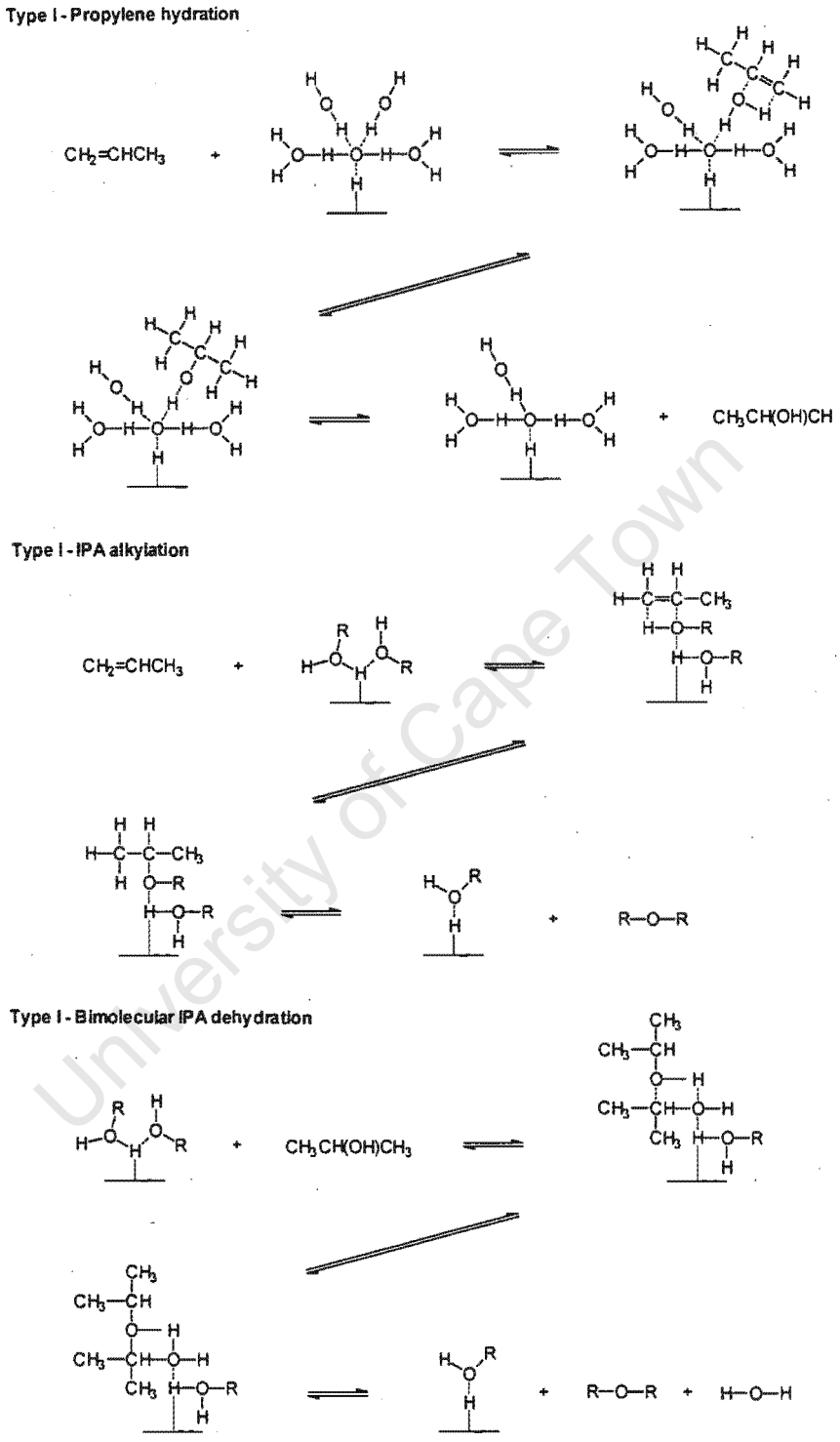

Figure 4.5: Type I mechanisms for propylene hydration, IPA alkylation and bimolecular dehydration of IPA over ion exchange resins.

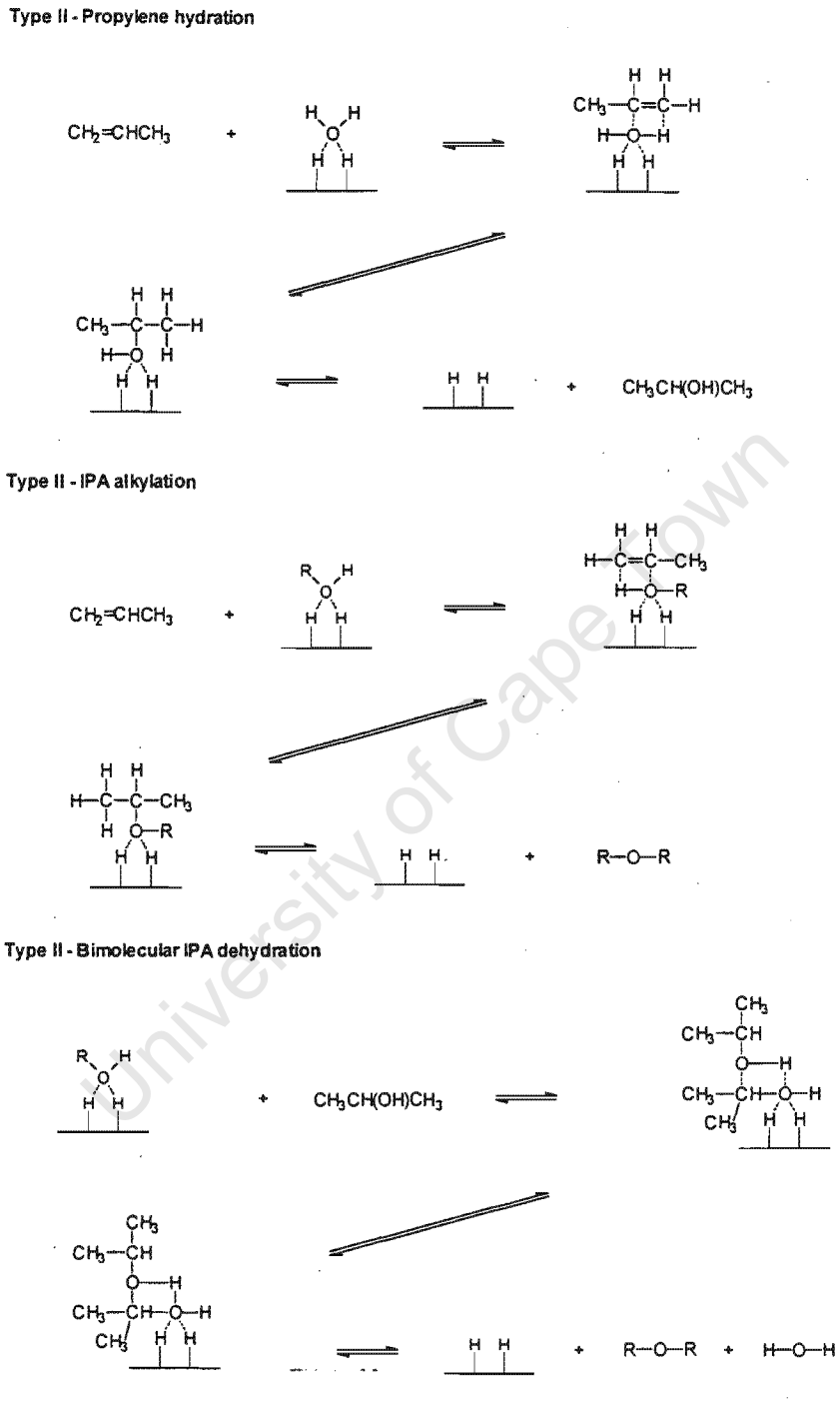

Figure 4.6: Type II mechanisms for propylene hydration, IPA alkylation and bimolecular dehydration of IPA over ion exchange resins. Polar molecules are shown adsorbed to two active sites for illustrative purposes.

In summary, the mechanisms of both hydration and etherification (whether IPA alkylation or bimolecular IPA dehydration) in the DIPE system initially take place via a Type I mechanism between polyadsorbed polar species (water or IPA) and solution phase apolar species (propylene). As the ratio of apolar to polar species within the reaction medium increases, the mechanism switches from Type I to Type II, where multiply hydrogen bonded polar species react with solution phase apolar species. The shift in mechanism occurs at a ratio between 1:2 and 1:1. The proposed subsequent shift into a Type III mechanism was never observed in the present study, as the overall ratio of apolar to polar species in the DIPE system never rose high enough. In MTBE synthesis, for example, this shift occurs at a ratio of approximately 4:1 [132], considerably higher than any ratio used in this work.

4.2 Kinetic modelling of DIPE formation

The reactor in which the catalytic experiments were performed was understood to be an integral plug flow reactor. In such a system the molar flow rate, F, of a component, i, with respect to contact catalyst mass, m_{cat}, can be obtained from the plug flow performance equation. This involves substitution of the appropriate rate expressions into the integrated form of the reactor mass balance equation, i.e.

$$F_i = \int_0^{m_{cat}} \left(\sum_j \sigma_{i,j} \cdot r_i \right) dm_{cat} \tag{4.1}$$

where the total mass of catalyst within the reactor is given by m_{cat}, r_j is the instantaneous rate of reaction j and $\sigma_{i,j}$ is the matrix of stoichiometric coefficients of component i in reaction j.

If the instantaneous rate of the propylene hydration reaction is denoted as r_1, IPA alkylation as r_2 and bimolecular IPA dehydration as r_3 and considering that water is consumed in reaction 1 and produced in reaction 3; propylene is consumed in reactions

1 and 2; IPA is produced in reaction 1 and consumed in reactions 2 and 3 and DIPE is produced in both reactions 2 and 3, the molar flow rates of the four species in the DIPE system as a function of the contact mass of catalyst, in differential form, can be written as

$$\frac{dF_W}{dm_{cat}} = -r_1 + r_3 \tag{4.2}$$

$$\frac{dF_P}{dm_{cat}} = -r_1 - r_2 \tag{4.3}$$

$$\frac{dF_A}{dm_{cat}} = r_1 - r_2 - 2r_3 \tag{4.4}$$

$$\frac{dF_E}{dm_{cat}} = r_2 + r_3 \tag{4.5}$$

where water is indicated by W, propylene by P, IPA by A and DIPE by E and the instantaneous rates of reaction (r_1, r_2 and r_3) are functions of temperature, pressure, the composition of the reaction medium and of the catalyst mechanism. To solve for the flowrates of the various species in the DIPE system as a function of catalyst mass, rate expressions in terms of these parameters have to be developed and the resulting system of four first order differential equations integrated by Eq. 4.1.

To account for non-ideal species behaviour, rate expressions were developed in terms of component activities rather than concentrations. As thermodynamic phase equilibrium was assumed between all phases within the reactor, the fugacity (and therefore the activity) of each species could be assumed to be the same in every phase. It was thus possible to describe the kinetics of the reaction by bulk phase activities and it was not necessary to consider different vapour, liquid and catalyst phase concentrations in the kinetic modelling. The species activities were calculated using the WS-PRSV model as described in Chapter 2. The three kinetic models which will be examined for their applicability to the DIPE system are: the pseudo-homogeneous kinetic model, the Eley-Rideal kinetic model and an additional model which accounts empirically for mechanistic changes.

The following assumptions were common to all three models:

- The only reactions occurring in the system were the hydration of propylene, the alkylation of IPA and the bimolecular dehydration of IPA.
- All of the above three reactions were reversible.
- The rate limiting step was the chemical reaction, whether it took place on the surface or in the solution phase. Neither the rate of adsorption nor the rate of mass transfer (whether internal or external) affected the overall reaction rate.
- The vapour phase, the liquid phase and non-adsorbed species within the catalyst particle were at thermodynamic phase equilibrium at every point along the reactor.
- The WS-PRSV model developed in Chapter 2 describes the phase behaviour of the species in the DIPE system.
- No catalyst deactivation took place during the catalytic experiments.
- The catalyst bed was isothermal throughout all experiments.

4.2.1 The pseudo-homogeneous kinetic model

The simplest form of rate expression is the pseudo-homogeneous model which assumes reactions taking place between solution-phase species and does not account for adsorption on the catalyst surface. In terms of the DIPE system, either water or IPA is considered to solvate the protons of the active sites. The solvated protons combine with solution phase species to form the carbocation intermediates (by combining either with propylene or with IPA) which then react with other solution phase species to form IPA or DIPE (see Section 3.1.5, Figure 3.16 for the homogeneous reaction mechanism). Both propylene hydration [47] and the MTBE reaction [148] have been modelled successfully using this approach,

providing the polar species (be it water or methanol) is in large excess within the system. This model can be thought to be loosely representative of Type I mechanisms.

The system of rate equations, containing three adjustable parameters (the three rate constants: k_1, k_2 and k_3), for propylene hydration, IPA alkylation and bimolecular IPA dehydration can, respectively, be written as (see Appendix L for the derivation)

$$r_1 = k_1 \left(a_W \cdot a_P - \frac{1}{K_{a,1}} a_A \right) \tag{4.6}$$

$$r_2 = k_2 \left(a_P \cdot a_A - \frac{1}{K_{a,2}} a_E \right) \tag{4.7}$$

$$r_3 = k_3 \left(a_A^2 - \frac{1}{K_{a,3}} a_E \cdot a_W \right) \tag{4.8}$$

4.2.2 The Eley-Rideal kinetic model

The Eley-Rideal model takes account of the chemical reaction and the adsorption behaviour of the species in the DIPE system in a mechanistically relevant fashion. In addition to the assumptions mentioned above, it assumes multi-site Langmuir-type adsorption of the polar species and negligible adsorption of apolar species. It has been used successfully to describe MTBE synthesis when alcohol is in large excess [156]. This model can account for the characteristics of both Type I and Type II mechanisms.

The Eley-Rideal model for propylene hydration, IPA alkylation and bimolecular dehydration of IPA is given by Eq.'s 4.9 to 4.11. The derivation of the rate expressions is given in Appendix L.

$$r_1 = \frac{k_1 H_W \left(a_W \cdot a_P - \frac{1}{K_{a,1}} a_A \right)}{\left(1 + H_W a_W + H_A a_A + H_E a_E \right)^n} \tag{4.9}$$

$$r_2 = \frac{k_2 H_A \left(a_A \cdot a_P - \frac{1}{K_{a,2}} a_E \right)}{\left(1 + H_W a_W + H_A a_A + H_E a_E \right)^m} \tag{4.10}$$

$$r_3 = \frac{k_3 H_A^2 \left(a_A^2 - \frac{1}{K_{a,3}} a_E a_W\right)}{\left(1 + H_W a_W + H_A a_A + H_E a_E\right)^{2m}} \tag{4.11}$$

If one fixes the number of active sites (i.e. n and m) involved in the reactions, then this model contains 6 parameters: the three reaction rate constants (k_1, k_2 and k_3) and the three adsorption constants (H_W, H_A and H_E). If the number of active sites involved in the reactions is not fixed, then the number of parameters increases to eight.

4.2.3 The "changing-mechanism" model

One of the shortcomings of the above two models is that they assume a fixed reaction mechanism, i.e. they assume a constant number of active sites take part in the reaction(s) regardless of the composition of the reaction medium. However, as discussed in Section 4.1, the catalyst mechanism changes and the catalytic activity increases as the overall ratio of apolar (propylene and DIPE) to polar (water and IPA) species increases. To account for this change in mechanism an additional model, based on the pseudo-homogeneous model, was developed where the value of the rate constant depends on the ratio of the polar to apolar species in the reaction medium. The additional empirical term, $\exp\left(k_m \cdot (x_P + x_E)\right)$, simulates the increase in catalytic activity due to the mechanism changing from Type I to Type II. As the concentration of propylene and DIPE in the liquid phase increases, the rate constants increase continuously, i.e. the magnitude of the rate constant increases as the ratio of apolar polar species in the liquid phase increases.

In terms of the pseudo-homogeneous model, this additional term may almost be viewed as an autocatalytic step. As the reaction products (IPA or DIPE) are produced, the ratio of apolar species increases. In the case of propylene hydration, the production of IPA solubilises additional propylene which raises the liquid phase propylene concentration and thus the catalyst phase propylene concentration. This increases the reaction rate. In the case of the etherification reactions, the production of DIPE (being an apolar species)

also increases the reaction rate.

In this case the rate equations, in terms of four adjustable parameters, for propylene hydration, IPA alkylation and bimolecular IPA dehydration are (see Appendix L for the derivation)

$$r_1 = k_1 \cdot \exp\left(k_m \cdot (x_P + x_E)\right) \left(a_W \cdot a_P - \frac{1}{K_{a,1}} a_A\right) \tag{4.12}$$

$$r_2 = k_2 \cdot \exp\left(k_m \cdot (x_P + x_E)\right) \left(a_P \cdot a_A - \frac{1}{K_{a,2}} a_E\right) \tag{4.13}$$

$$r_3 = k_3 \cdot \exp\left(k_m \cdot (x_P + x_E)\right) \left(a_A^2 - \frac{1}{K_{a,3}} a_E \cdot a_W\right) \tag{4.14}$$

4.2.4 Evaluation of the kinetic models

Four different kinetic models were evaluated. These were the pseudo-homogeneous model, the Eley-Rideal model with a fixed number of acid sites involved in each mechanism, the Eley-Rideal model with an adjustable number of acid sites involved in each mechanism and the "changing-mechanism" model. The number of parameters which could be adjusted in each model was 3, 6, 8 and 4 respectively. The kinetic models were fit to the two experimental contact time series performed at 120 °C and 50 bar with overall propylene to water ratios of 2:1 and 1:1 (see Figures 3.40 and 3.41 for the two sets of experimental data). These two sets of experimental data had different initial feeds, and thus different reaction conditions.

The system of four differential equations, i.e. Eq.'s 4.2 to 4.5, was solved using the ODEPACK algorithm [168] for solving systems of linear ordinary differential equations. The simplex optimisation method of Nelder and Mead [74] was used to determine the best-fit set of kinetic parameters. The objective function was the sum of squared relative

residuals ($SSRR$) based on species molar flows, i.e.

$$SSRR = \sum_{all\ data\ points} \left(\frac{\exp_i - calc_i}{\exp_i} \right)^2 \tag{4.15}$$

The best-fit set of parameters for each of the four models and the sum of relative square residuals of the best-fit set of parameters are shown in Table 4.1. The model fits to both sets of experimental data are shown graphically in Figures 4.7 and 4.8 for the pseudo-homogeneous model, in Figures 4.9 and 4.10 for the Eley-Rideal model with a fixed number of active centres involved in the mechanisms, in Figures 4.11 and 4.12 for the Eley-Rideal model with a variable number of active centres involved in the reaction and in Figures 4.13 and 4.14 for the changing-mechanism model.

The eight parameter Eley-Rideal model contains two parameters which determine the number of active sites water, n, and IPA, m, are adsorbed to. Fitting the eight parameter model to the experimental data gave values for n and m of 1.1 and 2.2 respectively. This was in agreement with the order of dependence on acid site density observed in Section 3.3.4, though n and m are empirical parameters and any agreement is most likely just coincidental. Since the number of acid sites a molecule adsorbs to in Langmuir-type adsorption must be integer, this model was then re-fit with the values of n and m fixed as one and two respectively, i.e. water adsorbs to a single active site and IPA to two active sites. This reduced the number of adjustable parameters in the model to six.

When fitting the "changing-mechanism" model to the experimental data, the magnitude of the rate constant for the IPA alkylation reaction tended to zero. No deterioration in the quality of the model fit occurred if only the rate constants for propylene hydration and bimolecular dehydration of IPA in addition to the empirical mechanistic parameter were fit, i.e. k_1, k_2 and k_m. The number of parameters in this model could thus be reduced from four to three.

In view of the fact that it had the most parameters, it is not surprising that the

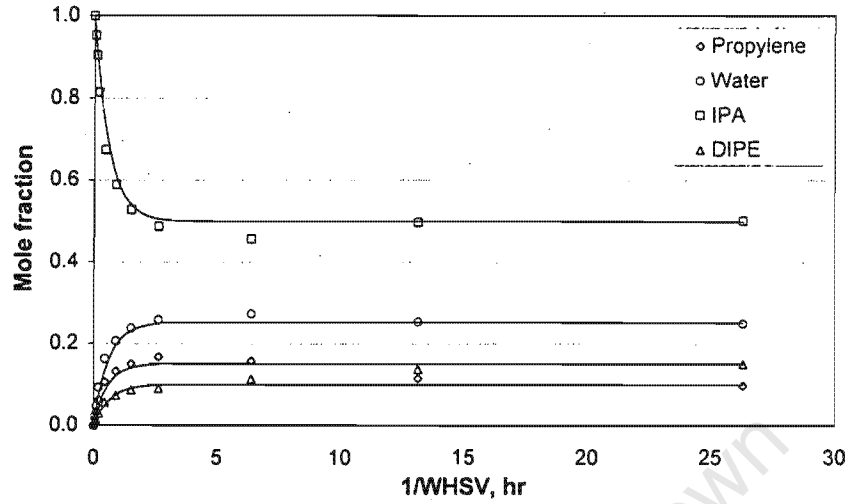

Figure 4.7: Pseudo-homogeneous model fit to the experimental contact time series performed at 120 °C and 50 bar with an overall propylene to water ratio of 1:1, starting from a pure IPA feed. The solid lines are the model predictions, the points are the experimental data.

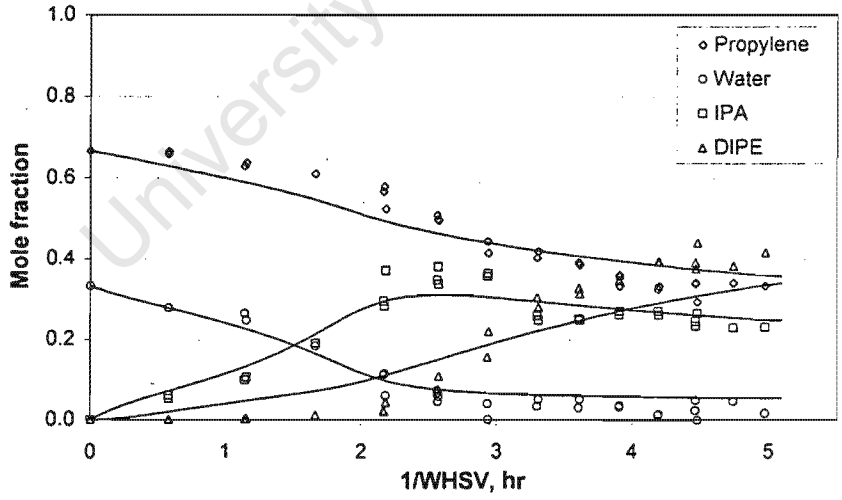

Figure 4.8: Pseudo-homogeneous model fit to the experimental contact time series performed at 120 °C and 50 bar with an overall propylene to water ratio of 2:1, starting from a feed of propylene and water. The solid lines are the model predictions, the points are the experimental data.

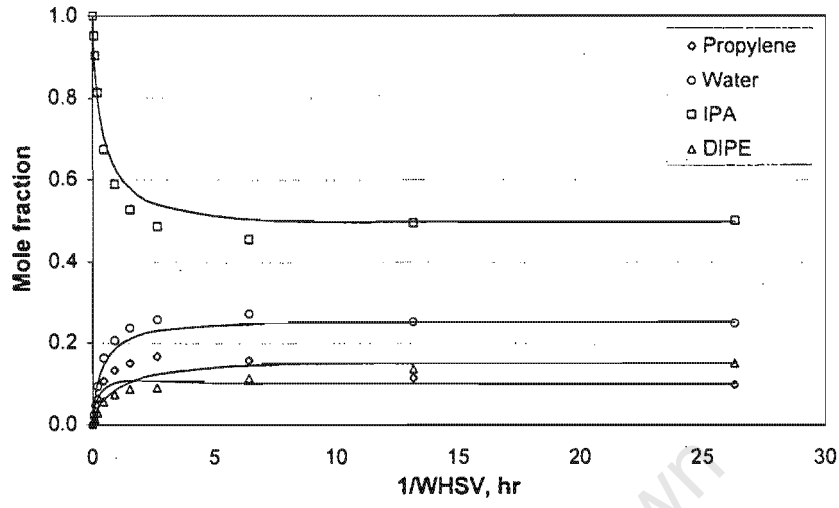

Figure 4.9: Eley-Rideal model with a fixed number of active sites involved in the reaction mechanism fit to the experimental contact time series performed at 120 °C and 50 bar with an overall propylene to water ratio of 1:1, starting from a pure IPA feed. The solid lines are the model predictions, the points are the experimental data.

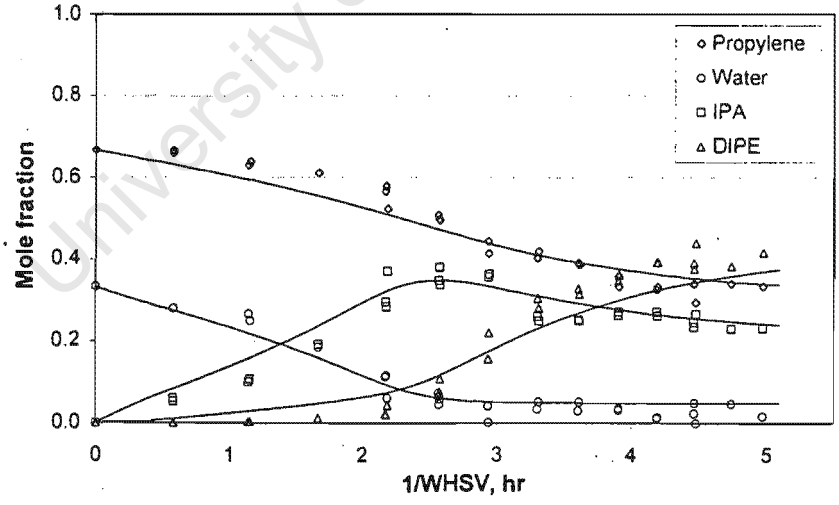

Figure 4.10: Eley-Rideal model with a fixed number of active sites involved in the reaction mechanism fit to the experimental contact time series performed at 120 °C and 50 bar with an overall propylene to water ratio of 2:1, starting from a feed of propylene and water. The solid lines are the model predictions, the points are the experimental data.

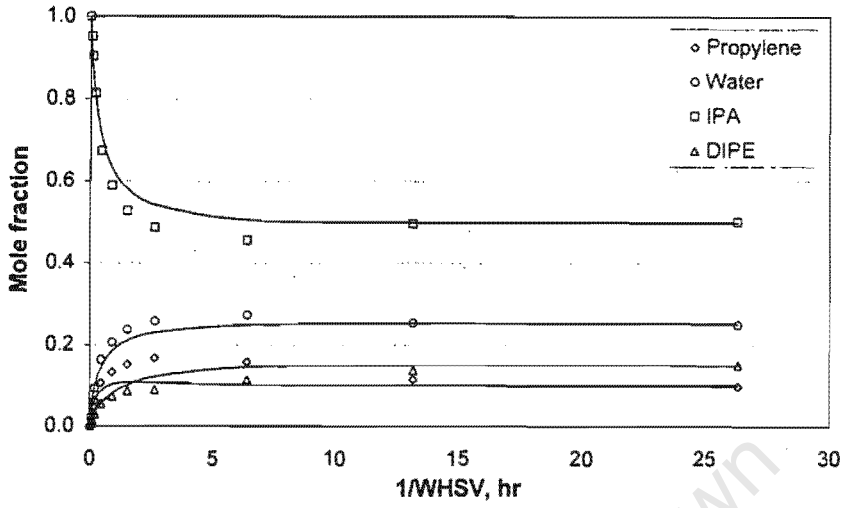

Figure 4.11: Eley-Rideal model with a variable number of active sites involved in the reaction mechanism fit to the experimental contact time series performed at 120 °C and 50 bar with an overall propylene to water ratio of 1:1, starting from a pure IPA feed. The solid lines are the model predictions, the points are the experimental data.

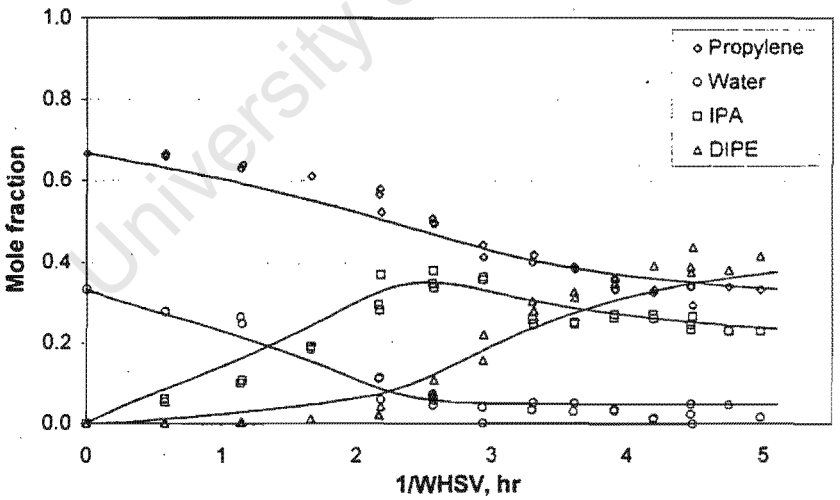

Figure 4.12: Eley-Rideal model with a variable number of active sites involved in the reaction mechanism fit to the experimental contact time series performed at 120 °C and 50 bar with an overall propylene to water ratio of 2:1, starting from a feed of propylene and water. The solid lines are the model predictions, the points are the experimental data.

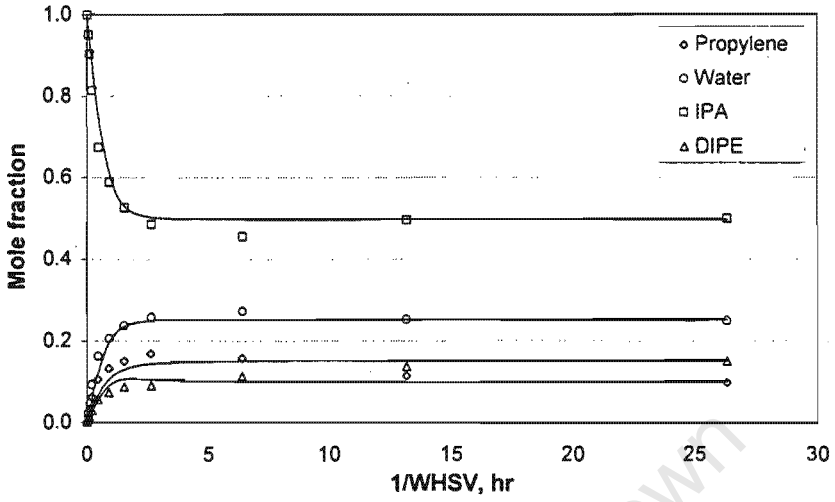

Figure 4.13: "Changing-mechanism" model fit to the experimental contact time series performed at 120 °C and 50 bar with an overall propylene to water ratio of 1:1, starting from a pure IPA feed. The solid lines are the model predictions, the points are the experimental data.

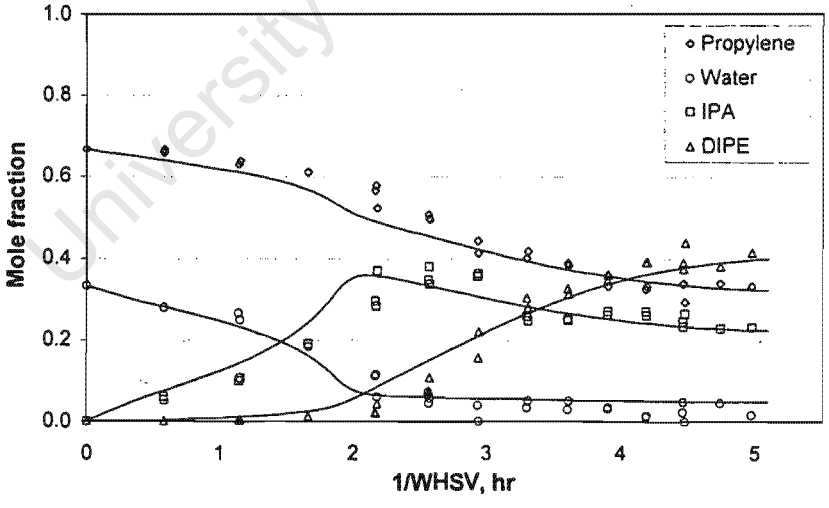

Figure 4.14: "Changing-mechanism" model fit to the experimental contact time series performed at 120 °C and 50 bar with an overall propylene to water ratio of 2:1, starting from a feed of propylene and water. The solid lines are the model predictions, the points are the experimental data.

Table 4.1: Best-fit values of the parameters used in the four kinetic models. P-H - pseudo-homogeneous model, E-R (6) - 6 constant Eley-Rideal model, E-R (8) - 8 constant Eley-Rideal model and M - empirical changing mechanism model

	Kinetic models			
Parameters	**P-H**	**E-R (6)**	**E-R (8)**	**M**
Rate constants, $\mathrm{mol\,g_{cat}^{-1}\,s^{-1}}$				
k_1	$2.1 \cdot 10^{-8}$	$4.3 \cdot 10^{-8}$	$7.1 \cdot 10^{-8}$	$1.8 \cdot 10^{-8}$
k_2	$8.8 \cdot 10^{-9}$	$1.8 \cdot 10^{-5}$	$2.5 \cdot 10^{-5}$	≈ 0
k_3	$8.1 \cdot 10^{-8}$	$2.0 \cdot 10^{-4}$	$3.5 \cdot 10^{-4}$	$5.1 \cdot 10^{-8}$
Henry constants				
H_W	–	46	47	–
H_A	–	2.4	3.9	–
H_E	–	0.020	0.016	–
Number of active sites				
n	–	1	1.1	–
m	–	2	2.2	–
Empirical mechanistic parameter				
k_m	–	–	–	3.0
Sum of squared relative residuals				
$SSRR$	138	89	55	61

kinetic model which gave the best fit to the experimental data on the basis of the sum of squared relative residuals was the Eley-Rideal model with eight parameters ($SSRR = 55$). Interestingly, the next best was the three parameter "changing-mechanism" model ($SSRR = 61$) followed by the six parameter Eley-Rideal model ($SSRR = 89$) and the pseudo-homogeneous model ($SSRR = 138$).

The Henry adsorption equilibrium constants determined from the Eley-Rideal kinetic models have no quantitative connection with the actual Henry constants of adsorption. The best-fit Henry constants are merely an indication of the strength of adsorption of the various species. Nevertheless, the order of the Henry constants is exactly in the order one

would expect. Water, the most polar molecule has the greatest constant of adsorption in both the six parameter and the eight parameter Eley-Rideal models. IPA, being less polar than water, has a Henry constant an order of magnitude smaller than that for water but still more than two orders of magnitude larger than the Henry constant for apolar DIPE. As presumed previously (Section 3.3.5) this indicates that water and IPA are strongly adsorbed on the active sites whilst DIPE is weakly adsorbed.

One of the shortcomings of the Eley-Rideal model as well as the pseudo-homogeneous model is that they assume a constant reaction mechanism for the entirety of the experimental data. As was shown in Section 4.1, however, the mechanism changes as the ratio of apolar to polar species within the reaction medium changes. The dominant reaction mechanisms in the experimental series starting from a pure IPA feed are most likely Type I mechanisms, as the ratio of apolar to polar species was always below 1 : 4. In the experimental series starting from a feed of propylene and water, the reaction mechanisms were initially Type I as the liquid phase consisted almost entirely of water. From a 1/WHSV of 1.8 h onwards, however, the dominant mechanisms became Type II mechanisms as the ratio of apolar to polar species exceeded 1 : 3 (see Section 3.3.3.4). The number of sites involved in the reaction as well as the rate of reaction will be affected by this change in mechanism. Consequently, neither the pseudo-homogeneous model nor the Eley-Rideal model was able to qualitatively represent the entire set of experimental data as accurately as the empirical "changing-mechanism" model.

None of the models was able to accurately reproduce the experimental data of the IPA decomposition series performed at 120 °C and 50 bar. Every model predicted a greater initial DIPE formation rate and a lower initial propylene formation rate than was obtained from experiment. Consequently, the peak in the propylene mole fraction was not reproduced by any model. In contrast to expectations, the two Eley-Rideal models, while still failing to reproduce the propylene data accurately, came the closest to describing the initial region of the this set of experimental data accurately. This indicated that species

adsorption behaviour may have been influencing the reaction rate to some degree even though a Type I mechanism was prevailing.

The only model that appeared to be able to qualitatively reproduce the set of experimental data starting from a propylene and water feed was the "changing-mechanism" model. Every other model considerably over-predicted the initial rate of DIPE formation (whether from IPA alkylation or bimolecular IPA dehydration). Even so, the "changing-mechanism" model still predicted an initial rate of IPA formation greater than the experimentally observed rate.

The initial rates of propylene hydration and etherification as a function of system pressure and feed ratio as predicted by "changing-mechanism" model compared to experiment are shown in Figures 4.15 to 4.18.

As mentioned above, the rate of IPA formation was over-predicted by the "changing-mechanism" model. However, it predicts the identical, near-straight line behaviour as was observed experimentally (Section 3.3.3.2). For etherification the reaction rate was once again over-predicted. However, qualitatively it reproduces the shape of the experimental data. At low pressures (below 30 bar) where the propylene concentration in IPA is low, the reaction takes place via a slow Type I mechanism. Any increase in reaction rate is due only to an increase in the activity of propylene with pressure. As pressure increases, the propylene concentration in IPA increases and the mechanism changes from a Type I to the more catalytically active Type II (between 30 bar and 45 bar). Above 45 bar the model predicts a flattening-off of the reaction rate, as the mechanism has already changed and any further increase in reaction rate, once again, is due solely to the increasing activity of propylene. The behaviour of the last portion was not observed experimentally, but this may be due to the fact that experiments were not carried out at sufficiently high pressures to observe the effect.

The "changing-mechanism" model predicts the same trends in reaction rate with

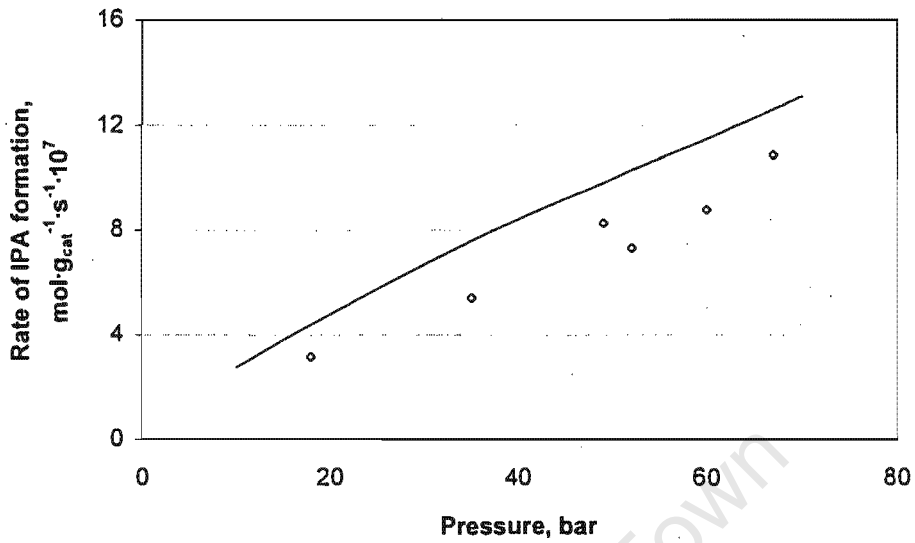

Figure 4.15: Predictions of the initial rates of propylene hydration using the three parameter "changing-mechanism" model with changing pressure. Temperature = 120 °C, propylene to water feed ratio = 2:1 and MHSV = 0.05 mol· g_{cat}^{-1} ·hr^{-1}.

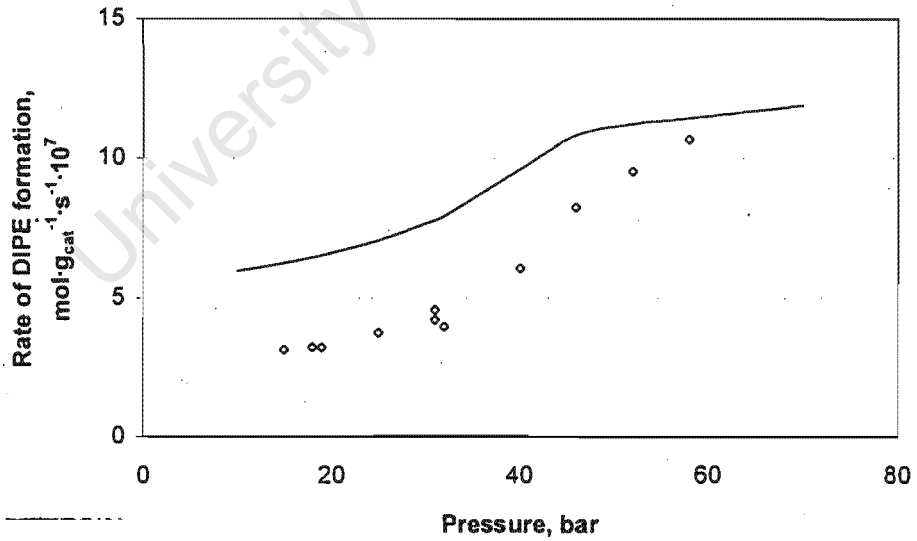

Figure 4.16: Predictions of the initial rates of etherification using the three parameter "changing-mechanism" model with changing pressure. Temperature = 120 °C, IPA to propylene feed ratio of 1:1 and MHSV = 0.05 mol· g_{cat}^{-1} ·hr^{-1}.

changing apolar to polar species feed ratio as were found experimentally (Section 3.3.3.3). As the ratio of propylene to water increased, no change in the propylene hydration rate was predicted as the activities of propylene and water remained constant. Obviously, oligomer formation (as observed experimentally at high ratios) was not predicted by the model as this reaction was not considered in the kinetic formulation. As the ratio of propylene to IPA increased, it was observed experimentally that the reaction rate initially increased and then flattened off, once the concentration of propylene in IPA had reached the saturation level at the system conditions (see Section 3.3.3.3). The identical behaviour was predicted by the model.

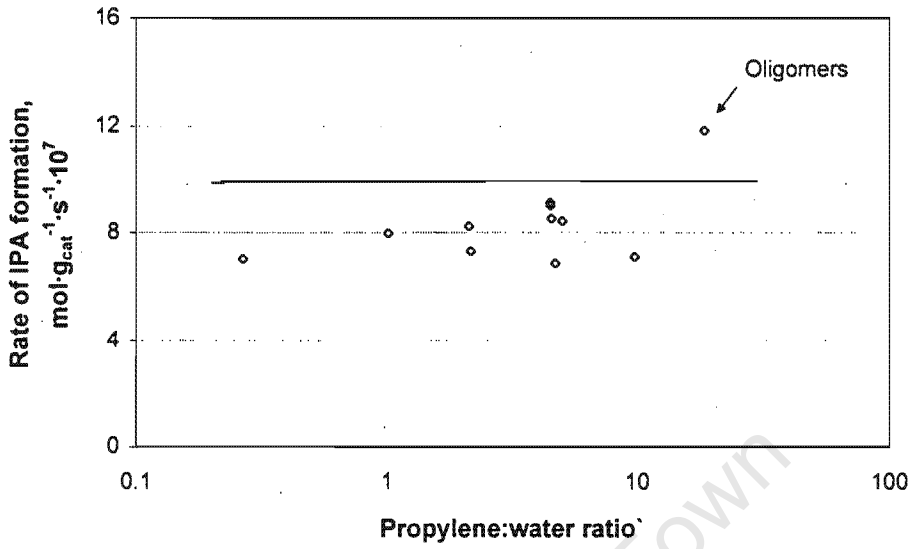

Figure 4.17: Predictions of the initial rates of propylene hydration using the three parameter "changing-mechanism" model with changing propylene to water molar ratio. Temperature = 120 °C, pressure = 50 bar and MHSV = 0.05 mol· g_{cat}^{-1} ·hr^{-1}.

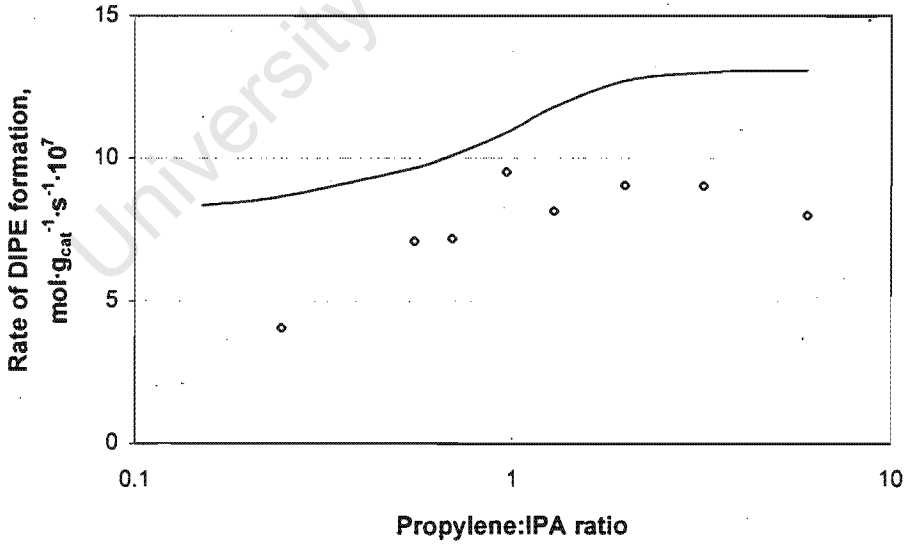

Figure 4.18: Predictions of the initial rates of etherification using the three parameter "changing-mechanism" model with changing propylene to IPA molar ratio. Temperature = 120 °C, pressure = 50 bar and MHSV = 0.05 mol· g_{cat}^{-1} ·hr^{-1}.

Chapter 5

Conclusions

DIPE can be produced in a single step from a feed of propylene and water over Amberlyst 15 sulphonic acid ion exchange resin catalyst. It was produced in a trickle bed reactor at pressures between 1 bar and 60 bar, at temperatures between 70 °C and 160 °C and at overall propylene to water ratios between 1 : 5 and 10 : 1. Reaction proceeded in the liquid phase in the catalyst particles. The only reactions that occurred in the system were the hydration of propylene to form IPA, the alkylation of IPA with propylene to form DIPE and the bimolecular dehydration of IPA to form DIPE and water. No side reactions such as propylene oligomerisation occurred. Starting from a feed of propylene and water the primary reaction product was IPA. IPA was subsequently consumed in two secondary reactions which produced DIPE. DIPE was produced either by the alkylation of IPA with propylene or by the bimolecular dehydration of IPA.

The reactions to produce IPA and DIPE over Amberlyst 15 catalytic ion exchange resin proceed via two different mechanistic routes. The ratio of apolar to polar species and the overall species concentration in the reaction medium determine which reaction mechanism dominates. At low ratios of apolar to polar species, a so-called Type I mechanism is dominant. According to this mechanism, a number of polar molecules cluster around a single active site (a sulphonic acid functional group). The proton from the sulphonic acid

site is solvated within this cluster of polar molecules and reaction proceeds similarly to homogeneous catalysis. For propylene hydration, this means that the proton combines with solution-phase propylene to form a secondary carbocation. This carbocation then reacts with one of the water molecules within the cluster to form IPA. In IPA alkylation, the proton, solvated by a cluster of IPA molecules (and presumably water, if also present), likewise reacts with solution phase propylene to form the carbocation intermediate. This then reacts further, with one of the adsorbed IPA molecules, to form DIPE. In the case of the bimolecular dehydration of IPA, the proton attaches to an IPA molecule. The isopropyl carbocation then reacts with another IPA molecule (whether from solution or similarly adsorbed) to form DIPE and water.

The threshold ratio, above which so-called Type II mechanisms prevail, lies at apolar to polar species ratios of approximately 1:2. In the Type II mechanism the clusters of polar molecules around single active sites from Type I mechanisms are disrupted by the increased concentration of apolar molecules (be they propylene or DIPE). Single polar molecules hydrogen-bond with multiple active sites and reaction proceeds between these adsorbed species and other solution phase molecules. Adsorbed water reacts with solution phase propylene to form IPA; adsorbed IPA reacts with solution phase propylene to form DIPE and adsorbed IPA reacts with solution phase IPA to form DIPE and water. As polar species hydrogen bond with multiple active sites in Type II mechanisms, the intermediate species are stabilised relative to the intermediates that occur in Type I mechanisms which results in higher concentrations of these species. This causes increased reaction rates of propylene hydration, IPA alkylation and bimolecular IPA dehydration. For greatest catalytic activity in the DIPE system, one should thus attempt to operate in a Type II mechanistic regime.

The polar species adsorb onto the active sites far more strongly than the apolar species. Regardless of the type of mechanism, so long as there are sufficient polar species to saturate the active sites, practically all apolar species will be displaced from the active

sites. Any reactions which take place between apolar species only, are thus severely inhibited by competitive adsorption. Consequently, only reactions involving adsorbed polar species take place and side reactions such as propylene oligomerisation do not occur to any significant extent.

The DIPE system contains highly polar water and IPA components together with apolar DIPE and apolar propylene under supercritical conditions. The Peng-Robinson-Stryjek-Vera [41, 42] equation of state in conjunction with the Wong-Sandler [40, 43] mixing rule accurately correlates the thermodynamic behaviour of this highly nonideal mixture. The binary interaction parameters used in the mixing rule were regressed from binary vapour-liquid equilibrium data found in literature. Where no binary mixture data was found, "pseudo-experimental" vapour-liquid equilibrium data were generated using the UNIFAC predictive activity coefficient model together with the Peng-Robinson-Stryjek-Vera equation of state. The accuracy of this model was corroborated by a comparison of the predicted chemical equilibrium compositions under non-ideal conditions with experimental chemical equilibrium compositions at the same conditions. This model (the WS-PRSV model) allows the calculation of the chemical equilibrium composition, the enthalpies of reaction and the calculation of species activity in the DIPE system under both ideal and highly non-ideal conditions.

In contrast to the production of the other octane enhancing ethers, e.g. MTBE and TAME, low temperature ($\pm 60\,^{\circ}C$) synthesis of DIPE is not practical as reactions proceed via secondary carbocation rather than tertiary carbocation intermediates. Since tertiary carbocations are more stable than secondary carbocations, the reactions to produce MTBE and TAME take place approximately three orders of magnitude more rapidly than the reaction rates in DIPE synthesis. Exactly as for the other octane enhancing ethers, DIPE synthesis is thermodynamically limited and the proper tailoring of process parameters to obtain the greatest rate of DIPE synthesis, yet still obtain a high yield is of crucial importance, especially if DIPE is to compete economically.

The most obvious method to overcome this kinetic constraint is to operate at temperatures greater than those in MTBE or TAME synthesis. Unfortunately, whilst high temperature operation may favour DIPE production from a kinetic viewpoint, chemical equilibrium favours DIPE formation at low temperature. Furthermore, the maximum operating temperature is limited by the ion exchange resin catalyst which begins to deactivate by thermal decomposition at temperatures greater than 120 °C. The extent to which kinetics can be enhanced by operating at higher temperatures is thus limited.

Alternatively, DIPE can be synthesised at elevated pressure. This is beneficial as chemical equilibrium favours DIPE at high pressure and increased pressure increases the formation rates of both IPA and DIPE. Unlike the synthesis of the other octane enhancing ethers which takes place below the critical temperature of the primary olefin, DIPE synthesis takes place above the critical temperature of propylene. Any increase in operating pressure will increase the activity of propylene and will thus increase reaction rates. Furthermore, as the system consists of a mostly polar liquid phase in phase equilibrium with a vapour phase composed mainly of supercritical propylene, an increase in pressure will also increase the concentration of propylene in the liquid phase. This increases the concentration of apolar species in the liquid phase and may lead to the transition from the less active Type I mechanism to the more active Type II mechanism.

Changing the overall propylene to water feed ratio has no effect on the reaction rates of IPA or DIPE nor on the catalyst selectivity. Only at ratios of propylene to water or propylene to IPA above 10:1 does oligomer formation become noticeable as the system is no longer at phase equilibrium due to poor feed distribution. However, the greatest yield of DIPE relative to the total number of moles in the system can be obtained at the stoichiometric ratio for DIPE formation, i.e. at a propylene to water ratio of 2:1. At low ratios of propylene to water, the formation of IPA is favoured above the formation of DIPE due to chemical equilibrium constraints. At high ratios of propylene to water, DIPE may be the thermodynamically favoured product, but relative to the total number

of moles fed to the system the yield is very low. For the most efficient use of reactor volume, DIPE synthesis should thus be carried out at an overall propylene to water mole ratio of 2 : 1.

The catalyst used for the majority of the experimental work in this study was Amberlyst 15. It showed no loss of activity over a period of three months on-line at a temperature of 120 °C. The same lifetime behaviour can be expected for Amberlyst 35 and Amberlyst 36 as they are almost identical in structure, differing only in acid site density and in the extent of cross-linking. The deactivation behaviour of zeolite H-Y and Deloxan ASP is not known. It is thus difficult to compare catalysts on the basis of lifetime or selectivity. Amberlyst 15, though, displayed the greatest activity per unit volume of catalyst bed under "process" conditions. Any process design utilising this resin would thus result in the most economical reactor design. Amberlyst 35 and Amberlyst 36 are reported to be more thermally stable [134, 135] than Amberlyst 15. The lifetime of these catalysts may thus extend beyond that of Amberlyst 15 and, consequently, even though the initial reactor costs may be greater due to their lower activity, the catalyst replacement costs may be lower. No side reactions were observed on any of the tested catalysts.

The three parameter "changing-mechanism" model can be used to describe the kinetics of the system. It is an empirical model based on the pseudo-homogeneous kinetic model, which incorporates an empirical term that changes the magnitude of the kinetic rate constant of each reaction to account for changes in the reaction mechanism from a Type I to a Type II, as the ratio of apolar to polar species changes. Even though it consistently overpredicts the initial reaction rates of all reactions by between 10% and 20%, this model was shown to qualitatively reproduce the behaviour of the DIPE system in response to changes in the operating pressure or the overall apolar to polar species mole ratio.

DIPE is a symmetric dialkyl ether. It can thus be produced simply from the primary olefin and water. This gives one increased flexibility in the choice of process technology in

comparison to the synthesis of the other octane enhancing ethers. It can be synthesised in a single step from a feed of propylene and water, in a two stage process where IPA is produced in the first reactor and DIPE in the second reactor, or, as in MTBE synthesis, it may be produced by catalytic distillation. For catalytic distillation to be implemented for DIPE synthesis, the reaction would have to fulfil certain criteria [17]:

- Distillation must be a practical method of separating the reagents and products.
- The reaction cannot be overly exothermic.
- A viable catalyst with a long lifetime must be available for the reaction.
- The reaction(s) must take place at a temperature equivalent to the boiling point of the liquid at the operating pressure of the distillation column.

DIPE synthesis directly from propylene and water fulfils the first three criteria, but fails to meet the last. For any practical DIPE process, operating pressures would have to be considerably greater than the boiling point of the liquid in the catalytic distillation column to overcome the kinetic limitations. For DIPE to be synthesised directly from propylene and water in a catalytic distillation column at lower pressure, a significantly more active catalyst than Amberlyst 15 would need to be found. If IPA were first produced in a fixed bed reactor, however, reaction pressures in the catalytic distillation column could be decreased significantly as the rate of the primary propylene hydration reaction is no longer of importance. In this case, catalytic distillation may prove to be a viable reactor technology. Ultimately, though, the choice of reactor technology, whether one-stage, two-stage or hydration followed by catalytic distillation will be answered by process economics.

Appendix A

Pure component properties

Pure component properties were obtained from Daubert and Danner [62], Stryjek and Vera [42], Coulson et al. [63], Reid et al. [44], Stull et al. [65], Sandler [45] and Perry and Green [64].

A.1 Pure component properties that were used in this study - from Daubert and Danner, Stryjek and Vera and Coulson et al.

Table A.1: Pure component structure, molar mass, liquid density and PRSV equation of state factor

Compound	Structural formula	M $[\frac{g}{mol}]$	$\rho^{o,\#}$ $[\frac{kg}{m^3}]$	κ_1^*
Water	HOH	18.0152	998	−0.06635
Propylene	CH_2CHCH_3	42.0804	612	0.04400
IPA	$CH_3CHOHCH_3$	60.0956	786	0.23264
DIPE	$CH_3CH(CH_3)OCH(CH_3)CH_3$	102.1760	724	0.03751

$^{\#}$ water, IPA and DIPE measured at 20°C, propylene at -50°C

* from Stryjek and Vera [42]

Table A.2: Pure component critical properties

Compound	T_c $[K]$		P_c $[bar]$		V_c $\frac{m^3}{kmol}$	
Water	647.13	±0.2%	220.550	±0.2%	0.056	±0.2%
Propylene	364.76	±1%	46.126	±1%	0.181	±5%
IPA	508.31	±1%	47.643	±3%	0.220	±5%
DIPE	500.05	±1%	28.776	±3%	0.386	±5%

Table A.3: Pure component accentric factor, normal boiling point, standard Gibbs free energy and standard enthalpy of formation

Compound	ω	T_{bp} $[K]$	$\Delta G_f^{\circ,IG}$ $[\frac{kJ}{mol}]$		$\Delta H_f^{\circ,IG}$ $[\frac{kJ}{mol}]$	
Water	0.3449	373.15	−228.59	±0.2%	−241.81	±0.2%
Propylene	0.1424	225.43	62.14	±3%	19.71	±5%
IPA	0.6689	355.41	−173.39	±0.2%	−272.42	±1%
DIPE	0.3383	341.45	−119.24	±5%	−318.99	±3%

Table A.4: Pure component ideal gas heat capacity parameters

Compound	Ideal gas heat capacity parameters*				
	Cp_A	Cp_B	Cp_C	Cp_D	Cp_E
Water	$3.3363 \cdot 10^4$	$2.679 \cdot 10^4$	$2.6105 \cdot 10^3$	$8.896 \cdot 10^3$	$1.169 \cdot 10^3$
Propylene	$4.13 \cdot 10^4$	$1.525 \cdot 10^5$	$1.352 \cdot 10^3$	$7.44 \cdot 10^4$	$5.78 \cdot 10^2$
IPA	$4.746 \cdot 10^4$	$1.935 \cdot 10^5$	$1.124 \cdot 10^3$	$9.38 \cdot 10^4$	$4.6 \cdot 10^2$
DIPE	$1.151 \cdot 10^5$	$2.144 \cdot 10^5$	$-7.066 \cdot 10^2$	$1.86 \cdot 10^5$	$-2.031 \cdot 10^3$

$$^*Cp[\tfrac{J}{kmol \cdot K}] = Cp_A + Cp_B \left[\frac{\frac{Cp_C}{T}}{\sinh \frac{Cp_C}{T}}\right]^2 + Cp_D \left[\frac{\frac{Cp_E}{T}}{\cosh \frac{Cp_E}{T}}\right]^2, \; T \; in \; K$$

A.2 Vapour pressure correlation parameters

Table A.5: Antoine vapour pressure correlation parameters from Coulson et al.

Compound	Parameters*			Limits [°C]	
	A	B	C	T_{min}	T_{max}
Water	18.3036	3816.44	−46.13	11	168
Propylene	15.7027	1807.53	−26.15	−113	−33
IPA	18.6929	3640.20	−53.54	0	111
DIPE	16.3417	2895.73	−43.15	−24	91

*$P_{vap}[mmHg] = \exp\left(A - \frac{B}{T+C}\right)$

Table A.6: Wagner vapour pressure correlation parameters from Reid et al.

Compound	Parameters*				Limits [°C]	
	A	B	C	D	T_{min}	T_{max}
Water	−7.76451	1.45828	−2.77580	−1.23303	2	T_c
Propylene	−6.64231	1.21857	−1.81005	−2.48212	−133	T_c
IPA	−8.16927	−0.094321	−8.10040	7.85000	−23	T_c
DIPE	−7.62613	1.29308	−2.90101	−6.14467	24	T_c

*$P_{vap} = P_c \exp\left(\frac{a\tau + b\tau^{1.5} + c\tau^3 + d\tau^6}{T_r}\right), \tau = 1 - T_r$

A.3 Pure component properties from Sandler and Perry and Green

Table A.7: Standard Gibbs free energies and enthalpies of formation and heat capacity parameters

Compound	$\Delta G_f^{\circ,IG}$	$\Delta H_f^{\circ,IG}$	Heat capacity parameters*			
	$[\frac{kJ}{mol}]$	$[\frac{kJ}{mol}]$	Cp_A	Cp_B	Cp_C	Cp_D
Water	-228.75	-241.99	32.238	$1.923 \cdot 10^{-3}$	$1.055 \cdot 10^{-5}$	$-3.595 \cdot 10^{-9}$
Propylene	62.65	20.43	3.153	$2.383 \cdot 10^{-1}$	$1.218 \cdot 10^{-4}$	$2.462 \cdot 10^{-8}$
IPA	-159.94	-261.30	3.323	$3.560 \cdot 10^{-1}$	$-2.100 \cdot 10^{-4}$	$4.840 \cdot 10^{-8}$

*$Cp[\frac{J}{mol \cdot K}] = Cp_A + Cp_B \cdot T + Cp_C \cdot T^2 + Cp_D \cdot T^3$, T in K

A.4 Pure Component Properties from Coulson et al.

Table A.8: Critical constants, standard Gibbs energies and enthalpies of formation

Compound	T_c	P_c	V_c	$\Delta G_f^{\circ,IG}$	$\Delta H_f^{\circ,IG}$
	$[K]$	$[bar]$	$[\frac{m^3}{kmol}]$	$[\frac{kJ}{mol}]$	$[\frac{kJ}{mol}]$
Water	647.3	220.5	0.056	-228.77	-242.00
Propylene	365.0	46.2	0.181	62.76	20.43
IPA	508.3	47.6	0.220	-173.50	-272.60
DIPE	500.0	28.8	0.386	-121.96	-319.03

Table A.9: Pure component ideal gas heat capacity parameters

Compound	**Ideal gas heat capacity parameters***			
	Cp_A	Cp_B	Cp_C	Cp_D
Water	32.243	$1.923 \cdot 10^{-3}$	$1.055 \cdot 10^{-5}$	$-3.596 \cdot 10^{-9}$
Propylene	3.710	$2.345 \cdot 10^{-1}$	$-1.160 \cdot 10^{-4}$	$2.204 \cdot 10^{-8}$
Isopropanol	32.427	$1.886 \cdot 10^{-1}$	$6.405 \cdot 10^{-5}$	$-9.261 \cdot 10^{-8}$
Diisopropyl Ether	7.503	$5.849 \cdot 10^{-1}$	$-3.026 \cdot 10^{-4}$	$5.844 \cdot 10^{-8}$

*$Cp[\frac{J}{mol \cdot K}] = Cp_A + Cp_B \cdot T + Cp_C \cdot T^2 + Cp_D \cdot T^3,\ T\ in\ K$

A.5 Pure component properties from Stull et al.

Table A.10: Pure component Gibbs free energies of formation at different temperatures

Compound	**Standard Gibbs free energy of formation,** $\frac{kcal}{mol}$					
Temperature, K	298	300	400	500	600	700
Water	−54.64	−54.62	−53.52	−52.36	−51.16	−49.91
Propylene	14.99	15.05	18.62	22.45	26.46	30.60
IPA	−41.49	−41.34	−33.17	−24.66	−15.94	−7.07
DIPE	−29.13	−28.84	−12.65	−4.10	21.23	38.61

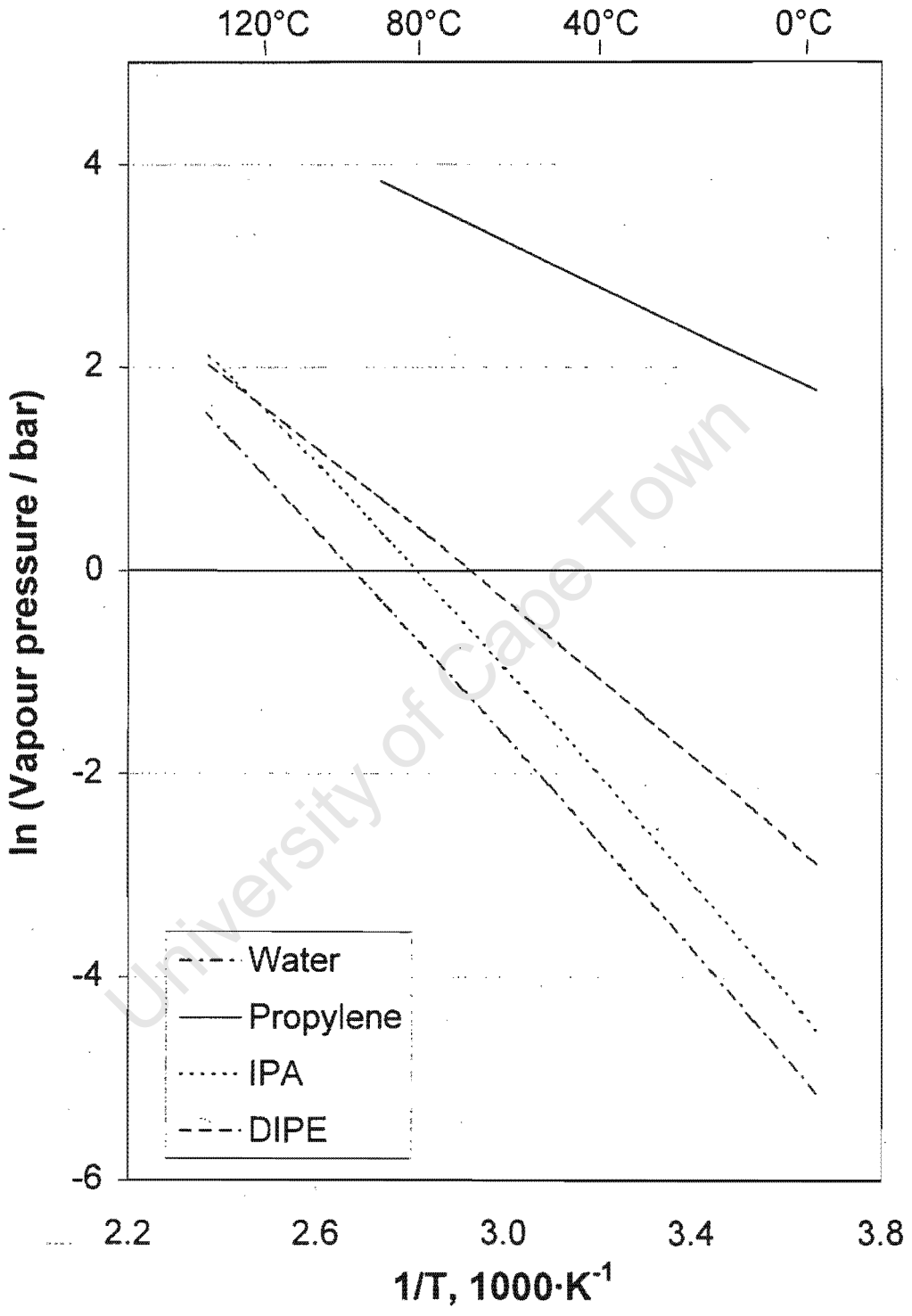

Figure A.1: Pure component vapour pressures calculated using the PRSV equation of state.

Appendix B

General solution for the fugacity coefficient

B.1 Derivation of general solution

To obtain the general solution of $\ln \phi_i$, regardless of mixing rule, for Peng-Robinson type equations of state, one must solve

$$\ln \phi_i = \frac{1}{RT} \int_{\bar{V}=\infty}^{\bar{V}=\frac{ZRT}{P}} \left[\frac{RT}{\bar{V}} - N \cdot \left(\frac{\partial P}{\partial N_i} \right)_{T,\bar{V},N_{j \neq i}} \right] d\bar{V} - \ln Z \tag{B.1}$$

where

$$P = f(T, \bar{V}, a, b) = \frac{RT}{\bar{V} - b} - \frac{a}{\bar{V}^2 + 2b\bar{V} - b^2} \tag{B.2}$$

and $T, N_i, Z, a = f(T, N_i)$ and $b = f(N_i)$ are constant.

Now, differentiating P with respect to N_i gives

$$\left(\frac{\partial P}{\partial N_i}\right)_{T,\bar{V},N_{j\neq i}} = -\frac{RT}{\left(\bar{V}-b\right)^2}\cdot\left[\left(\frac{\partial \bar{V}}{\partial N_i}\right)_{T,\bar{V},N_{j\neq i}} - \left(\frac{\partial b}{\partial N_i}\right)_{T,\bar{V},N_{j\neq i}}\right] - \frac{\left(\frac{\partial a}{\partial N_i}\right)_{T,\bar{V},N_{j\neq i}}}{\bar{V}^2+2b\bar{V}-b^2} + \frac{a}{\left(\bar{V}^2+2b\bar{V}-b^2\right)^2}\left[2\bar{V}\left(\frac{\partial \bar{V}}{\partial N_i}\right)_{T,\bar{V},N_{j\neq i}} + 2\bar{V}\left(\frac{\partial b}{\partial N_i}\right)_{T,\bar{V},N_{j\neq i}} + 2b\left(\frac{\partial \bar{V}}{\partial N_i}\right)_{T,\bar{V},N_{j\neq i}} - 2b\left(\frac{\partial b}{\partial N_i}\right)_{T,\bar{V},N_{j\neq i}}\right] \tag{B.3}$$

Let

$$da = \frac{\partial a}{\partial N_i}_{T,\bar{V},N_{j\neq i}} \tag{B.4}$$

and

$$db = \frac{\partial b}{\partial N_i}_{T,\bar{V},N_{j\neq i}} \tag{B.5}$$

Also

$$\bar{V} = \frac{V}{N_{tot}} = \frac{V}{\sum N_i} \tag{B.6}$$

thus

$$\left(\frac{\partial \bar{V}}{\partial N_i}\right)_{T,\bar{V},N_{j\neq i}} = -\frac{V}{\left(\sum N_i\right)^2} = -V \tag{B.7}$$

when flows are normalised, i.e. $\sum N_i = N_{tot} = 1$. Also, da and db are constant since T and N_i are constant.Then, considering only the integral part of Equation B.1 and expanding,

$$\int_{\bar{V}=\infty}^{\bar{V}=\frac{ZRT}{P}}\left[\frac{RT}{\bar{V}} - N\cdot\left(\frac{\partial P}{\partial N_i}\right)_{T,\bar{V},N_{j\neq i}}\right]d\bar{V} = \int_{\bar{V}=\frac{ZRT}{P}}^{\bar{V}=\infty}\left[\left(\frac{\partial P}{\partial N_i}\right)_{T,\bar{V},N_{j\neq i}} - \frac{RT}{\bar{V}}\right]d\bar{V} =$$

$$\ldots = \int_{\bar{V}=\frac{ZRT}{P}}^{\bar{V}=\infty} -\frac{RT(-\bar{V}-db)}{(\bar{V}-b)^2} - \frac{da}{\bar{V}^2+2b\bar{V}-b^2} + \frac{2a\bar{V}db - 2a\bar{V}^2 - 2ab\bar{V} - 2abdb}{\left(\bar{V}^2+2b\bar{V}-b^2\right)^2} - \frac{RT}{\bar{V}}d\bar{V} \tag{B.8}$$

where the denominator in all terms is always greater than 0 between $\frac{ZRT}{P}$ and ∞ since $\bar{V} > b > 0$ thus $\bar{V}^2 - b^2 > 0$ and also $2b\bar{V} > 0$. Now, we have 4 distinct integrals in $d\bar{V}$ to solve:

1. $\int \frac{RT(\bar{V})+\partial b)}{(\bar{V}-b)^2} d\bar{V}$
2. $\int \frac{\partial a}{(\bar{V}^2+2b\bar{V}-b^2)} d\bar{V}$
3. $\int -\frac{2a\left[\bar{V}(b-\partial b)+b\partial b\right]^2}{\left(\bar{V}^2+2b\bar{V}-b^2\right)^2} d\bar{V}$
4. $\int \frac{RT}{\bar{V}} d\bar{V}$

These were solved with the aid of integration tables [169], to give for each of the four above integrals

1. $\int \frac{RT(\bar{V})+\partial b)}{(\bar{V}-b)^2} d\bar{V} = RT \ln(\overline{V} - b) - \frac{RT(\overline{V}+\partial b)}{\overline{V}-b}$
2. $\int \frac{\partial a}{(\bar{V}^2+2b\bar{V}-b^2)} d\bar{V} = -\frac{\partial a}{2\sqrt{2}b} \ln\left[\frac{\overline{V}+\left(1+\sqrt{2}\right)b}{\overline{V}+\left(1-\sqrt{2}\right)b}\right]$
3. $\int -\frac{2a\left[\bar{V}(b-\partial b)+b\partial b\right]^2}{\left(\bar{V}^2+2b\bar{V}-b^2\right)^2} d\bar{V} = \frac{\sqrt{2}a}{4}\left(\frac{\partial b-b}{b^2}\right) \ln\left[\frac{\overline{V}+\left(1+\sqrt{2}\right)b}{\overline{V}+\left(1-\sqrt{2}\right)b}\right] + \frac{b+\partial b}{b}\left(\frac{\overline{V}RT}{\overline{V}-b} - P\overline{V}\right)$
4. $\int \frac{RT}{\bar{V}} d\bar{V} = RT \ln \overline{V}$

This gives for $\ln \phi_i$

$$\ln \phi_i = \frac{1}{RT}\left[(1) - (2) + (3) - (4)\right]_{\overline{V}=\frac{ZRT}{P}}^{\overline{V}=\infty} - \ln Z \tag{B.9}$$

Which, when simplified, gives

$$\ln \phi_i = \frac{b+\partial b}{b}(Z-1) - \ln\left(Z - \frac{bP}{RT}\right) - \frac{a}{2\sqrt{2}bRT} \ln\left[\frac{\overline{V}+\left(1+\sqrt{2}\right)b}{\overline{V}+\left(1-\sqrt{2}\right)b}\right]\left[\frac{\partial a}{a} - \frac{\partial b - b}{b}\right] \tag{B.10}$$

B.2 Verification of general solution

B.2.1 Pure components

For pure components $\partial a = \partial b = 0$, thus

$$\ln \phi_i = (Z-1) - \ln\left(Z - \frac{bP}{RT}\right) - \frac{a}{2\sqrt{2}bRT} \ln\left[\frac{\overline{V} + \left(1+\sqrt{2}\right)b}{\overline{V} + \left(1-\sqrt{2}\right)b}\right] \tag{B.11}$$

which is the standard form for $\ln \phi_i$ for pure components using the Peng-Robinson equation of state

B.2.2 Simple quadratic mixing rule

Using the simple quadratic mixing rule given by Sandler [45]

$$a = \sum_i \sum_j x_i x_j a_{ij} \qquad and \qquad b = \sum_i b_i x_i \tag{B.12}$$

which when differentiated gives

$$\partial a = \left(\frac{\partial a}{\partial N_i}\right)_{T,\overline{V},N_{j\neq i}} = 2\sum_i x_j a_{ij} - 2a \tag{B.13}$$

$$\partial b = \left(\frac{\partial b}{\partial N_i}\right)_{T,\overline{V},N_{j\neq i}} = b_i - b \tag{B.14}$$

This, substituted into Eq B.11 gives

$$\ln \phi_i = \frac{b_i}{b}(Z-1) - \ln\left(Z - \frac{bP}{RT}\right) - \frac{a}{2\sqrt{2}bRT} \ln\left[\frac{\overline{V} + \left(1+\sqrt{2}\right)b}{\overline{V} + \left(1-\sqrt{2}\right)b}\right] \left(\frac{2\sum_j x_j a_{ij}}{a} - \frac{b_i}{b}\right) \tag{B.15}$$

Once again, this is the same form as given in Sandler [45].

Appendix C

Vapour-liquid equilibrium mixing parameters

C.1 UNIFAC predictive activity coefficient model parameters

Table C.1: UNIFAC functional group interaction parameters a_{mn} [K]

	a_{mn}[K]					
	H_2O	$-CH_3$	-CH	$-CH=CH_2$	-OH	-CHO-
H_2O	0.00	300.00	300.00	496.10	-229.10	540.50
$-CH_3$	1318.00	0.00	0.00	86.02	986.50	251.50
-CH	1318.00	0.00	0.00	86.02	986.50	251.50
$-CH=CH_2$	270.60	-35.36	-35.36	0.00	524.10	214.50
-OH	-150.00	156.40	156.40	457.00	0.00	28.06
-CHO-	-314.70	83.36	83.36	26.51	237.70	0.00

Table C.2: Stoichiometric number of functional groups in each component

Component	Number of Functional Groups, $v_k^{(i)}$					
	H_2O	-CH_3	-CH	-CH=CH_2	-OH	-CHO-
Water	1	-	-	-	-	-
Propylene	-	1	-	1	-	-
Isopropanol	-	2	1	-	1	-
Diisopropyl Ether	-	4	1	-	-	1

Table C.3: UNIFAC functional groups specifications

Functional Group	$\mathbf{R}_i$	$\mathbf{Q}_i$
H_2O	0.9200	1.4000
-CH_3	0.9011	0.8480
-CH	0.4469	0.2280
-CH=CH_2	1.3454	1.1760
-OH	1.0000	1.2000
-CHO-	0.6908	0.4680

C.2 Wyczesany binary mixing rule parameters

Table C.4: Mixing Parameters for the Wyczesany-Stryjek-Vera mixing rule

Binary Mixture	**Binary Interaction Parameters** [39]			
	$k_{ij}^{(1)}$	$k_{ij}^{(2)}$	$k_{ji}^{(1)}$	$k_{ji}^{(2)}$
Water - Propylene	0.4192	-190.5	-0.4337	243.4
Water - Isopropanol	-0.07513	-36.72	0.2291	-128.7
Propylene - Isopropanol	0.1552	-37.52	0.1630	-39.60

C.3 Regressed Wong-Sandler binary mixing rule parameters

Table C.5: Regressed mixing rule parameters for the Wong-Sandler mixing rule

Binary Mixture	Binary Interaction Parameters			
	τ_{ij}	τ_{ji}	α	k_{ij}
Water - Propylene	4.6318	6.1483	0.3941	0.5823
Water - Isopropanol	1.4629	1.3404	0.6024	0.0462
Water - Diisopropyl Ether	3.6547	4.6947	0.7848	0.8488
Propylene - Isopropanol	0.7197	0.2798	0.1559	0.1404
Propylene - Diisopropyl Ether	-0.1329	-0.2996	0.0041	0.1428
Isopropanol - Diisopropyl Ether	-0.1537	2.0058	1.3750	0.4069

Appendix D

The general solution for chemical equilibrium

The general solution for the chemical reaction equilibrium constant Ka_2 at temperature T_2 given the chemical reaction equilibrium constant Ka_1 at temperature T_1 is given by the equation

$$\ln \frac{K_a(T_2)}{K_a(T_1)} = \int_{T_1}^{T_2} \frac{\Delta H^\circ_{rxn}(T)}{RT^2} dT \tag{D.1}$$

where the enthalpy of reaction, $\Delta H^\circ_{rxn}(T)$, can be shown to equal

$$\Delta H^\circ_{rxn}(T) = \Delta H^\circ_{rxn}(T = 25°C) + \sum_i \nu_i \int_{T=25°C}^{T} Cp_i^\bullet(T')dT' \tag{D.2}$$

Pure component heat capacities are related to temperature in a variety of empirical forms. Depending on the form of the correlation, the solution to the integral in the above equation varies.

If Cp is given by the form of Coulson et al. [63] or Sandler [45],

$$Cp = A + BT + CT^2 + DT^3 \tag{D.3}$$

then,

$$\Delta H^{\circ}_{rxn}(T) = \Delta H^{\circ}_{rxn}(T_1) + \sum_i \nu_i \int_{T_1}^{T} \left\{ A + BT + CT^2 + DT^3 \right\} dT' \tag{D.4}$$

which can be solved to give

$$\begin{aligned} \ln \frac{K_{a,2}(T_2)}{K_{a,1}(T_1)} &= \frac{\Delta A}{R} \ln \frac{T_2}{T_1} + \frac{\Delta B}{2R}(T_2 - T_1) + \frac{\Delta C}{6R}(T_2^2 - T_1^2) + \frac{\Delta D}{12R}(T_2^3 - T_1^3) \\ &+ \frac{T_1 - T_2}{RT_1T_2} \left\{ -\Delta H^{\circ}_{rxn}(T_1) + \Delta AT) + \frac{\Delta B}{2} T_1^2 + \frac{\Delta C}{3} T_1^3 + \frac{\Delta D}{4} T_1^4 \right\} \end{aligned} \tag{D.5}$$

If the temperature dependency of the heat capacity is given by the empirical form of Daubert and Danner [62],

$$Cp = A + B \left[\frac{C}{T \sinh\left(\frac{C}{T}\right)} \right]^2 + D \left[\frac{E}{T \cosh\left(\frac{E}{T}\right)} \right]^2 \tag{D.6}$$

then

$$\Delta H^{\circ}_{rxn}(T) = \Delta H^{\circ}_{rxn}(T_1) + \sum_i \nu_i \int_{T_1}^{T} \left\{ A + B \left[\frac{C}{T \sinh\left(\frac{C}{T}\right)} \right]^2 + D \left[\frac{E}{T \cosh\left(\frac{E}{T}\right)} \right]^2 \right\} dT' \tag{D.7}$$

and one can then solve for the chemical equilibrium at T_2 such that

$$\begin{aligned} \ln \frac{K_{a,2}(T_2)}{K_{a,1}(T_1)} &= \left\{ \frac{T_2 - T_1}{RT_1T_2} \left[\Delta H^{\circ}_{rxn}(T_1) + \sum_i \nu_i \left(DE \tanh \frac{E}{T_1} - BC \coth \frac{C}{T_1} - AT_1 \right) \right] \right\} \\ &+ \frac{\sum_i \nu_i}{R} \left\{ A \ln \frac{T_2}{T_1} - B \ln \left[\frac{\sinh \frac{C}{T_2}}{\sinh \frac{C}{T_1}} \right] + D \ln \left[\frac{\cosh \frac{E}{T_2}}{\cosh \frac{E}{T_1}} \right] \right\} \end{aligned} \tag{D.8}$$

Appendix E

DIPE system composition at equilibrium

Table E.1: Predicted DIPE yield at chemical and phase equilibrium as a function of temperature and pressure

	Temperature, °C										
Press., bar	0	20	40	60	80	100	120	140	160	180	200
1	0.99	0.97	0.94	0.53	0.19	0.04	0.01	0.00	0.00	0.00	0.00
20	0.98	0.97	0.94	0.91	0.86	0.79	0.71	0.19	0.07	0.02	0.01
40	0.98	0.97	0.94	0.91	0.86	0.79	0.71	0.57	0.14	0.06	0.02
60	0.98	0.96	0.94	0.91	0.86	0.79	0.71	0.57	0.33	0.10	0.04
80	0.98	0.96	0.94	0.90	0.85	0.78	0.71	0.58	0.38	0.15	0.05
100	0.98	0.96	0.93	0.90	0.85	0.78	0.70	0.58	0.40	0.21	0.07
120	0.98	0.96	0.93	0.90	0.85	0.78	0.70	0.58	0.41	0.24	0.09
140	0.98	0.96	0.93	0.90	0.84	0.78	0.70	0.58	0.42	0.26	0.11
160	0.98	0.95	0.93	0.89	0.84	0.77	0.70	0.59	0.43	0.27	0.13
180	0.98	0.95	0.92	0.89	0.84	0.77	0.70	0.59	0.44	0.29	0.14
200	0.97	0.95	0.92	0.89	0.83	0.77	0.70	0.59	0.45	0.30	0.16

Table E.2: Predicted liquid phase mole fraction in the DIPE system at chemical and phase equilibrium as a function of temperature and pressure

	Temperature, °C										
Press., bar	0	20	40	60	80	100	120	140	160	180	200
1	1.00	1.00	0.98	0.00	0.00	0.00	0.00	0.00	0.00	0.00	0.00
20	1.00	1.00	1.00	1.00	1.00	1.00	1.00	0.07	0.00	0.00	0.00
40	1.00	1.00	1.00	1.00	1.00	1.00	1.00	1.00	0.08	0.00	0.00
60	1.00	1.00	1.00	1.00	1.00	1.00	1.00	0.98	0.78	0.07	0.00
80	1.00	1.00	1.00	1.00	1.00	0.99	0.99	0.96	0.72	0.14	0.02
100	1.00	1.00	1.00	1.00	1.00	0.99	0.98	0.95	0.74	0.23	0.03
120	1.00	1.00	1.00	1.00	1.00	0.98	0.97	0.94	0.76	0.35	0.01
140	1.00	1.00	1.00	1.00	1.00	0.97	0.96	0.92	0.77	0.43	0.05
160	1.00	1.00	1.00	1.00	1.00	0.96	0.95	0.91	0.78	0.49	0.10
180	1.00	1.00	1.00	1.00	1.00	0.94	0.94	0.90	0.79	0.54	0.16
200	1.00	1.00	1.00	1.00	1.00	0.92	0.92	0.89	0.79	0.58	0.22

Table E.3: Predicted DIPE mole fraction at chemical and phase equilibrium as a function of the propylene to water mole ratio and temperature

	Overall propylene:water mole ratio										
Temp., °C	1:100	1:40	1:16	1:6	1:2	1:1	2:1	6:1	16:1	40:1	100:1
0	0.00	0.00	0.01	0.02	0.06	0.27	0.66	0.19	0.07	0.03	0.01
20	0.00	0.00	0.01	0.02	0.06	0.29	0.66	0.19	0.07	0.03	0.01
40	0.00	0.00	0.01	0.02	0.06	0.29	0.66	0.19	0.07	0.03	0.01
60	0.00	0.00	0.01	0.02	0.06	0.28	0.65	0.19	0.07	0.03	0.01
80	0.00	0.00	0.01	0.02	0.06	0.27	0.63	0.19	0.07	0.03	0.01
100	0.00	0.00	0.00	0.02	0.05	0.25	0.58	0.19	0.07	0.03	0.01
120	0.00	0.00	0.00	0.01	0.04	0.21	0.50	0.17	0.06	0.02	0.01
140	0.00	0.00	0.00	0.01	0.03	0.16	0.38	0.12	0.04	0.02	0.01
160	0.00	0.00	0.00	0.01	0.03	0.09	0.09	0.06	0.03	0.01	0.00
180	0.00	0.00	0.00	0.01	0.01	0.02	0.03	0.02	0.01	0.00	0.00
200	0.00	0.00	0.00	0.00	0.00	0.01	0.01	0.01	0.00	0.00	0.00

Appendix F

Catalyst modification and characterisation

F.1 Pretreatment of ion-exchange resins

1. Rinsing with benzene. A maximum of 200ml of catalyst was placed in a 1000 ml beaker. Three bed volumes of benzene were added to the ion-exchange resin and agitated by a magnetic stirrer for 10 minutes. Excess benzene was poured off.

2. Rinsing with methanol. Three bed volumes of methanol were added whilst stirring the catalyst. Excess liquid was again poured off and the catalyst transferred into a 1000 mm long, 25 mm diameter glass column. Three bed volumes of methanol were then used to wash the catalyst free of benzene.

3. Rinsing with deionised water. Three bed volumes of deionised water were passed over the resin bed, which removed all methanol from the catalyst.

4. Exchange with 1 mol/l sulphuric acid (H_2SO_4). A 400% excess of acid was used relative to the capacity of the catalyst. The exchange was done over 10 minutes, although the conversion is supposedly complete within 60 seconds [112]. The volume

of acid was calculated from

$$V_{H_2SO_4}[ml] = 5 \cdot \frac{capacity\ of\ catalyst\left[\frac{meq}{g}\right] \cdot dry\ mass\ of\ catalyst\,[g]}{concentration\ of\ H_2SO_4\left[\frac{mmol}{ml}\right]} \qquad \text{(F.1)}$$

5. Washing with deionised water. Deionised water was passed over the catalyst bed until the effluent from the column was neutral to universal indicator paper. A futher 3 bed volumes of deionised water were then passed over the catalyst.

6. Drying of catalyst. The catalyst was removed from the column and and placed in an oven at 120°C for 24 hours to dry. After cooling, it was stored over silica gel in an air tight container for future use.

F.2 Modification of acid site density

1. An amount of pretreated catalyst was weighed out ($\pm 50g$), transferred to the glass column (Section F.1), preswelled with methanol and then washed with deionised water.

2. The wet catalyst was transferred to a beaker containing 50ml of deionised water.

3. NaOH was added to the beaker to ion-exchange the catalyst. The volume of 1 mol/l NaOH required to attain the desired catalyst capacity was calculated from

$$V_{NaOH}[ml] = \frac{catalyst\ mass[g] \cdot \left(parent\ capacity - desired\ capacity\left[\frac{meq}{g}\right]\right)}{1\frac{mmol}{ml}} \qquad \text{(F.2)}$$

4. The beaker was covered and left standing for four hours to equilibrate. During this period the beaker was stirred.

5. The catalyst was transferred back to the glass column.

6. Deionised water was passed over the catalyst bed until the effluent from the column was neutral to universal indicator paper. A futher 3 bed volumes of deionised water were then passed over the catalyst.

7. The catalyst was removed from the column and placed in an oven at 120°C for 24 hours to dry. After cooling, it was stored over silica gel in an air tight container.

8. A portion of the sample was used to determine the new catalyst capacity.

F.3 Measurement of acid site density

1. About 0.5g of dry catalyst were weighed out into a conical flask containing 25ml of deionised water

2. 10ml of 1 mol/l NaOH were added to the flask. The flask was stoppered and gently stirred for four hours.

3. The liquid was filtered off and 25ml of the filtrate transferred to a beaker.

4. The contents of the beaker were then back-titrated with 0.1 mol/l HCl using thymolphthalein as an indicator.

5. The catalyst capacity could then be calculated from

$$catalyst\ capacity\left[\frac{meq}{g}\right] = \frac{35ml \cdot \left[\frac{1\frac{mmol}{ml}\cdot 10ml}{35ml} - \frac{0.1\frac{mmol}{ml}\cdot V_{HCl}[ml]}{25ml}\right]}{mass\ of\ catalyst[g]} \qquad \text{(F.3)}$$

6. Steps 1-5 were repeated 4 times per sample. The capacity of the catalyst was taken as the mean these four measurements. The average error of measurement was $\pm 0.06\frac{meq}{g}$.

Appendix G

Calculational procedures

G.1 Adsorption experiments

G.1.1 Calculation procedures

The amount of sorbate adsorbed onto the resin catalyst was calculated from the adsorption breakthrough curve, see Figure G.1 for an example. Once the curve had been obtained for the entire run, the average TCD GC bypass response was determined by averaging over all the initial analyses, i.e.

$$average\ response = \frac{\sum_n (blank\ response)_n}{n} \tag{G.1}$$

All the responses were then normalised to the bypass response. The "missing-area" caused by adsorption was calculated from the normalised response data using the trapezoidal integration rule. The total volume adsorbed could then be calculated from

$$V_{adsorbed}[ml] = Area \cdot Sorbate\ flow[\frac{ml}{\text{min}}] \tag{G.2}$$

and the amount of sorbate adsorbed per catalyst mass from

$$Capacity = \frac{\frac{P \cdot V_{adsorbed}}{R \cdot T}}{Mass_{cat}} \tag{G.3}$$

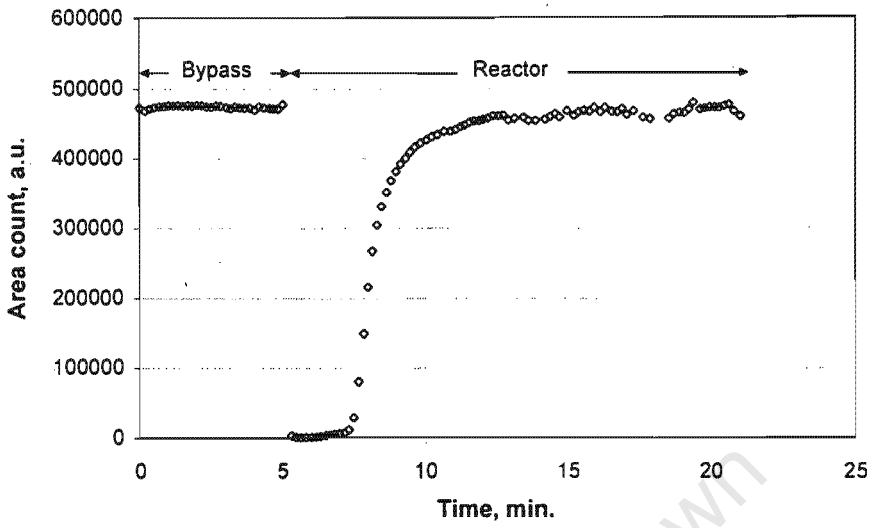

Figure G.1: Typical example of an adsorption breakthrough curve.

G.1.2 Sample run

An example of an adsorption run done with propylene is shown in Figure G.1 and the results in Table G.1.

Table G.1: Example of an adsorption run

Run conditions	
Temperature, $°C$	60
Pressure, kPa	40
He flow, ml/min	30
C_3H_6 flow, ml/min	30
Calculations	
Average initial response	473946.2
Area under normalised curve, min	3.44
Volume adsorbed, ml	103.3
Capacity, mol/g_{cat}	0.00170

G.2 Reaction experiments

G.2.1 Calculation procedures

The feed flowrates were determined from the mass of reactants fed to the reactor during the course of the experiment. The product flowrates of the organic compounds were calculated from the known methane internal standard flowrate, the response factors and the analysed area ratios obtained from FID GC analysis

$$F_i = F_{IStd} \cdot \frac{Area_i \cdot RF_i \cdot \mathcal{M}_{Istd}}{Area_{IStd} \cdot RF_{IStd} \cdot \mathcal{M}_i} \tag{G.4}$$

The product water flowrate was determined by subtracting the product oxygen contained in IPA and DIPE from the total oxygen feed flowrates

$$F_{H_2O,out} = F_{H_2O,in} + F_{IPA,in} + F_{DIPE,in} - F_{IPA,out} - F_{DIPE,out} \tag{G.5}$$

The carbon balance around the reactor was calculated by comparing the flow of carbon in the product stream to the flow of carbon in the feed stream

$$carbon\ balance = \frac{carbon\ out}{carbon\ in} = \frac{(F_{propylene} + F_{IPA} + 2 \cdot F_{DIPE})_{product}}{(F_{propylene} + F_{IPA} + 2 \cdot F_{DIPE})_{feed}} \tag{G.6}$$

and the conversion of a reactant was calculated from

$$conversion = \frac{F_{in} - F_{out}}{F_{in}} \tag{G.7}$$

whilst the selectivity, e.g. of propylene to DIPE, was defined by

$$selectivity_{propylene \rightarrow DIPE} = \frac{2 \cdot (F_{DIPE,in} - F_{DIPE,out})}{F_{propylene,in} - F_{propylene,out}} \tag{G.8}$$

The so-called weight hourly space velocity (WHSV) and mole hourly space velocity (MHSV) were respectively defined by

$$WHSV = \frac{feed\ mass\ flowrate}{mass\ of\ catalyst} \tag{G.9}$$

$$MHSV = \frac{feed\ molar\ flowrate}{mass\ of\ catalyst} \tag{G.10}$$

G.2.2 Sample run sheet

An example of a typical reaction run done with propylene and water is shown in Figure G.2 with the results in Table G.2.

Table G.2: Example of a reaction experiment

Run: Sample Run **Date:** 99 December 1999

Run conditions

System conditions		Equipment setpoints		Liquid feed mass fractions	
P, bar	50	HP HPLC	0.070	H_2O, g	1.00
T, °C	120	LEWA	8.0	IPA, g	0.00
Catalyst, g	24.30	MFC 1	80%	DIPE, g	0.00

Propylene feed

	Start of run	End of run
Time	8h53	17h41
Propylene mass, kg	5.597	5.213

Mass of liquid fed

Reaction time	0	15	30	45	60	75	90	105	120
Liquid mass, g	0.0	1.0	2.1	3.1	4.1	5.2	6.2	7.2	8.3
Feed rate, g/min	-	0.067	0.070	0.069	0.068	0.069	0.069	0.069	0.069

On-line GC analyses, area%

GC Trace	1	2	3	4	5	6	7	8	9
Methane	5.107	4.783	4.781	4.766	5.088	5.000	4.963	5.067	4.892
Propylene	89.883	89.788	90.093	89.849	89.398	89.527	89.352	89.197	90.158
IPA	4.786	5.244	4.919	5.163	5.279	5.230	5.437	5.498	4.757
DIPE	0.225	0.184	0.206	0.222	0.235	0.242	0.248	0.238	0.193

Calculations

Carbon Balance	97.1	104.2	104.1	104.6	97.7	99.5	100.3	98.2	101.6
Conversion, mol%									
Propylene	6.8	7.3	6.9	7.3	7.5	7.4	7.7	7.8	6.7
Water	30.0	32.6	30.7	32.2	33.0	32.7	34.0	34.4	29.7
IPA	0.0	0.0	0.0	0.0	0.0	0.0	0.0	0.0	0.0
DIPE	0.0	0.0	0.0	0.0	0.0	0.0	0.0	0.0	0.0
Selectivity, C%									
IPA	96.6	97.5	97.0	96.9	96.8	96.7	96.7	96.9	97.1
DIPE	3.4	2.5	3.0	3.1	3.2	3.3	3.3	3.1	2.9

Averaged calculated results

Average GC r.s.d., area%		Calculations		Other	
Methane	2.64	Propylene conversion, mol%	7.3	C-balance	100.7
Propylene	0.36	Water conversion, mol%	32.4	WHSV	1.97
IPA	4.91	IPA selectivity, C%	96.9	MHSV	0.0522
DIPE	9.58	DIPE selectivity, C%	3.1	P:W molar ratio	4.50

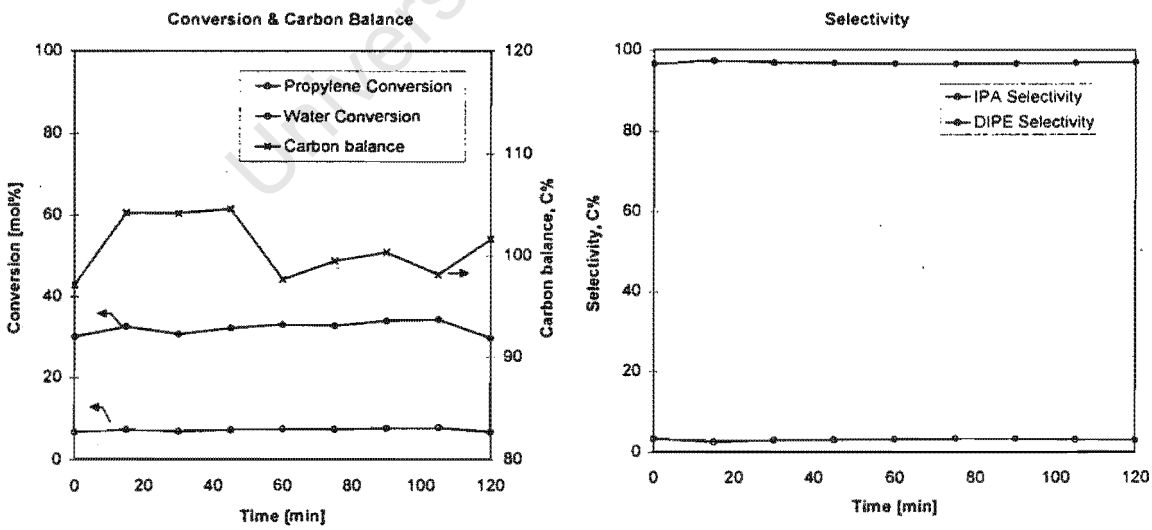

Figure G.2: Steady state conversion, carbon balance and selectivity for the sample experimental run

Appendix H

Gas chromatographic analysis

H.1 Gas chromatograph settings

Table H.1: Gas chromatograph settings

Gas chromatograph	Varian 3700	Varian 1400	HP 5890A
Column	HP PONA	SP 1000	HP PONA
Length and I.D.	50 m x 0.2 mm	1.8 m x 3 mm	50 m x 0.2 mm
Stationary phase	Crosslinked methyl silicone gum	0.1% Carbopack C	Crosslinked methyl silicone gum
Film thickness	0.2 μm	Packed column	0.2 μm
Carrier gas	Hydrogen	Helium	Helium
Column head pressure	200 kPa	130 kPa	100 kPa
Injector	Split-injector	Splitless injector	Split-injector
Injector temperature	240^{o}C	150^{o}C	250^{o}C
Split	1:200	-	1:300
Detector	FID	TCD	MS
Detector temperature	250^{o}C	150^{o}C	280^{o}C
Temperature programme	Isothermal	Isothermal	Isothermal
Oven temperature	40^{o}C	110^{o}C	80^{o}C

H.2 Response factors

H.2.1 Response factor determination for flame ionization detector

A number of binary mixtures of isopropanol (IPA) or diisopropyl ether (DIPE) with n-hexane were prepared. The mass ratios of the components in these mixtures varied significantly to ensure that the obtained response factor was linear with concentration over a large range. Five GC analyses were performed on each of the prepared mixtures by manual injection of $1\mu l$ of the mixture. The relative response factor was then calculated from linear regression of the area ratios obtained from the flame ionisation detector (FID) and the mass ratio of the components in the mixture. It was assumed that the response factors of n-hexane, propylene and methane were 1.00. The FID response to IPA and DIPE was thus determined relative to its response to hydrocarbons. Linear regression gave a response factor for IPA of $0.560 \pm 0.37\%$ and for DIPE of $0.848 \pm 0.36\%$. Table H.2 gives the raw data, where the ratio is always the ratio of hydrocarbon to oxygenate. The calibration plots for IPA and DIPE are shown in Figure H.1.

Table H.2: Absolute flame ionization detector response factor determination for IPA and DIPE

	IPA					DIPE				
Sample #	**1**	**2**	**3**	**4**	**5**	**6**	**7**	**8**	**9**	**10**
Actual mass ratio	5.059	0.863	0.476	1.649	0.107	6.284	0.158	10.854	2.354	1.782
GC ratio										
1	8.818	1.544	0.816	2.834	0.184	7.235	0.178	12.468	2.864	2.151
2	9.276	1.468	0.825	2.923	0.175	7.198	0.185	12.135	2.784	2.099
3	9.076	1.484	0.826	2.805	0.179	7.312	0.186	12.215	2.658	1.995
4	8.894	1.493	0.829	2.881	0.191	7.229	0.172	12.384	2.737	2.033
5	8.926	1.459	0.800	2.892	0.184	7.395	0.189	12.698	2.811	2.006

H.2.2 Response factor determination for thermal conductivity detector

The response factors of the thermal conductivity detector (TCD) for water and DIPE were obtained in the same manner as for the FID, except that instead of n-hexane being used as the internal standard, IPA was used. IPA was convenient since it is a mutual solvent for both water and DIPE. As only the liquid fraction was to be analysed by TCD, it was not necessary to determine the response factors for the gaseous species methane and propylene. The response of IPA was assumed to be 1.00 and those for DIPE and water were calculated relative to it. Linear regression gave a relative response factor for water of $1.255 \pm 0.73\%$ and for DIPE of $0.888 \pm 0.28\%$. Table H.3 gives the raw data where, once again, the ratio is given as the ratio of the standard to the compound in question. The calibration plots for water and DIPE are shown in Figure H.2.

Table H.3: Relative TCD response factor determination for water and diisopropyl ether

	Water					DIPE				
Sample #	**1**	**2**	**3**	**4**	**5**	**6**	**7**	**8**	**9**	**10**
Actual mass ratio	0.153	0.251	0.505	1.621	4.241	0.273	1.035	0.324	1.936	6.943
GC ratio										
1	0.092	0.164	0.422	1.180	3.473	0.292	1.121	0.357	2.200	7.883
2	0.092	0.163	0.418	1.211	3.365	0.291	1.125	0.358	2.231	7.667
3	0.093	0.162	0.445	1.183	3.499	0.293	1.116	0.355	2.228	7.887
4	0.093	0.163	0.445	1.199	3.357	0.294	1.122	0.352	2.215	7.841
5	0.094	0.160	0.421	1.215	3.357	0.290	1.123	0.356	2.217	7.940

H.3 Sample gas chromatograph traces

Typical traces obtained from the various GC's used in this work are shown in Figures H.3, H.4 and H.5.

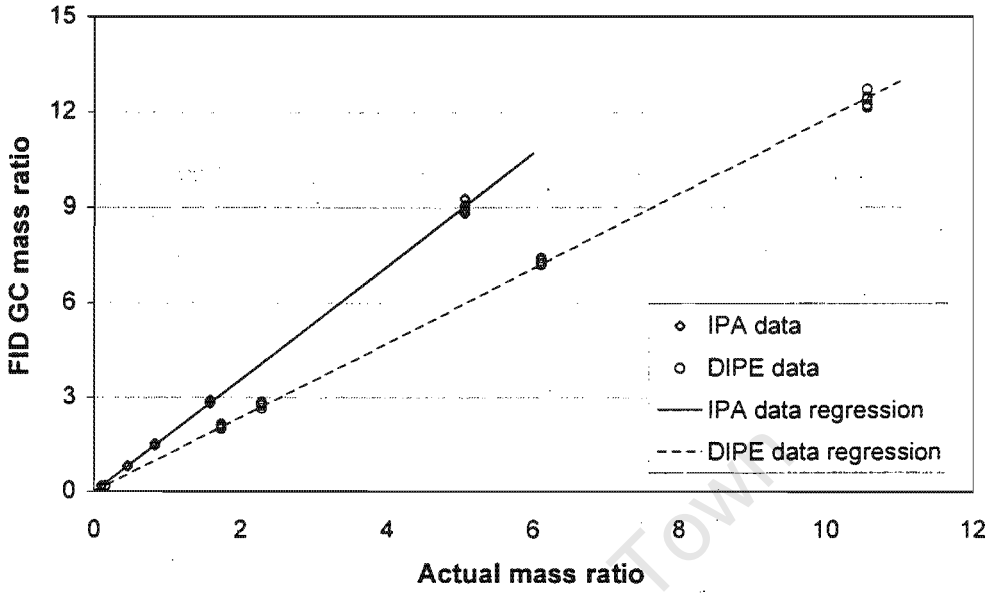

Figure H.1: Calibration plot for FID GC response factor determination for IPA and DIPE.

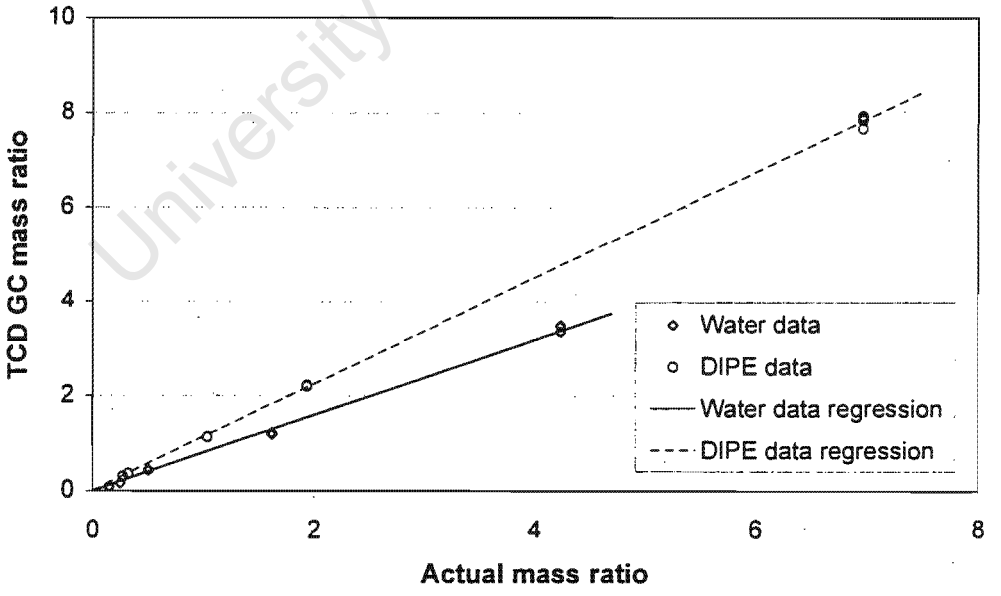

Figure H.2: Calibration plot for TCD GC response factor determination for water and DIPE.

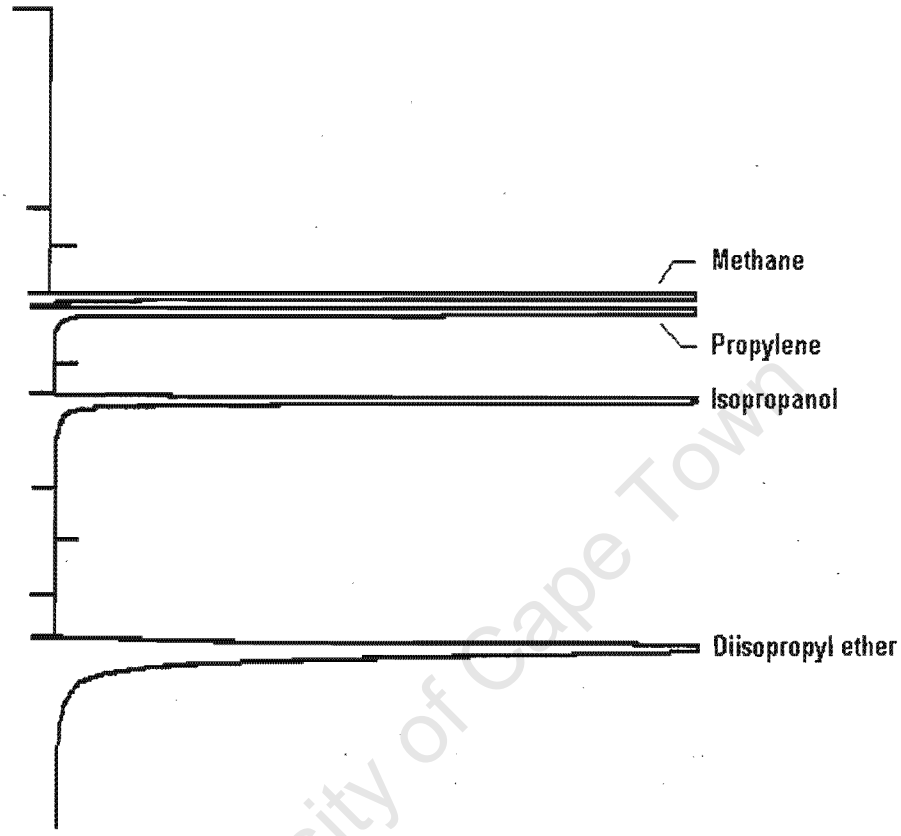

Figure H.3: Representative flame ionisation detector GC trace

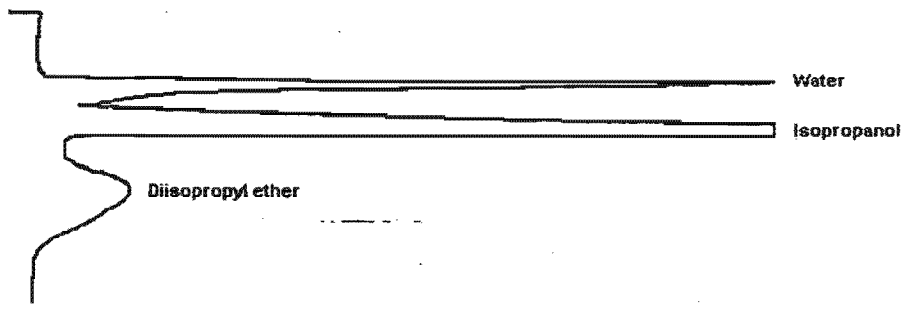

Figure H.4: Representative thermal conductivity detector GC trace

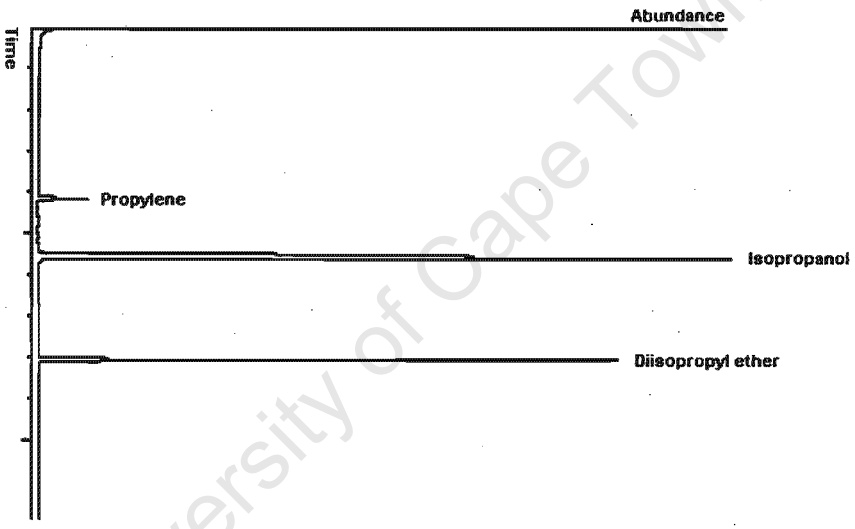

Figure H.5: Representative mass spectrometer GC trace

Appendix I

Internal and external transport effects

I.1 Wetting efficiency

The wetting efficiency, f_e, of catalyst particles in a trickle bed may be estimated by the empirical wetting efficiency correlation developed by Mills and Dudukovic [146] which is a function of the Reynolds, Weber and Froude numbers,

$$f_e = \tanh\left[0.664\,\mathrm{Re}_L^{0.333}\,Fr_L^{0.195}We_L^{-0.171}\left(\frac{a_p d_p^2}{\epsilon^2}\right)^{-0.0615}\right] \tag{I.1}$$

where the liquid phase particle Reynolds number (Re_L), the Weber number (We_L) and the Froude number (Fr_L) respectively are given by

$$\mathrm{Re}_L = \frac{u_L \rho_L d_p}{\mu_L} \tag{I.2}$$

$$We_L = \frac{G^2}{\sigma_L \rho_L a_p} \tag{I.3}$$

$$Fr_L = \frac{a_p G^2}{\rho_L^2 g} \tag{I.4}$$

Poorest catalyst wetting will occur at the beginning of the reaction when the system consists purely of water and propylene - under these conditions the liquid phase can be assumed to be only water. The theoretical wetting efficiency of catalyst in the trickle bed reactor used in this project was calculated for conditions of 120°C, 50bar and commercial catalyst particles. The wetting efficiency is shown in Figure I.1 as a function of the water to propylene ratio. The physical properties of propylene and water were taken from Daubert and Danner [62].

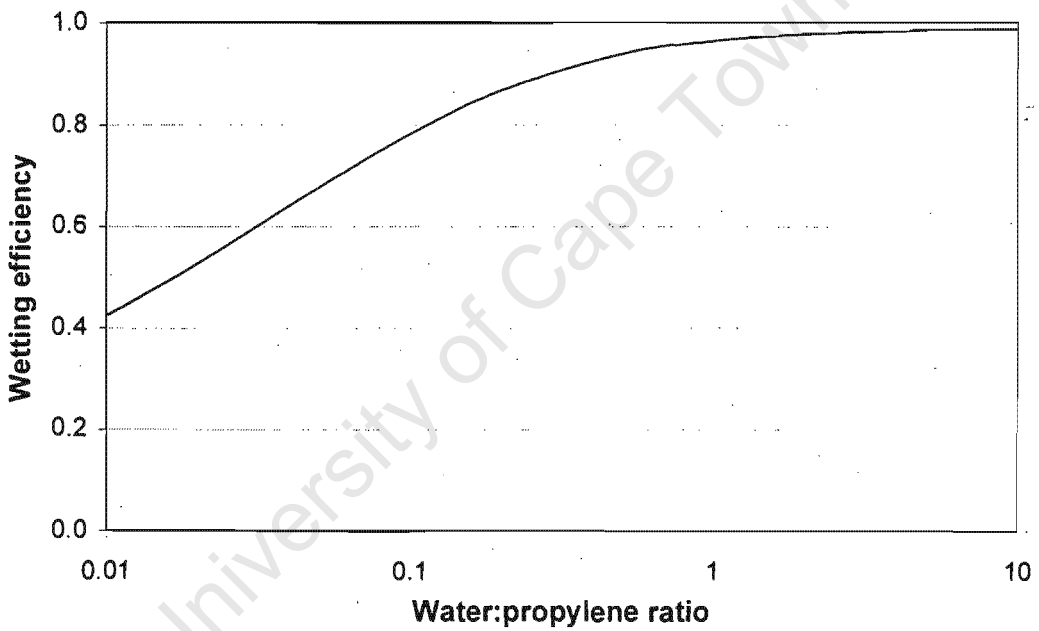

Figure I.1: Wetting efficiency of catalyst particles in the trickle-bed reactor at 120 °C and 50 bar.

For water:propylene ratios greater than 0.2, the wetting efficiency is greater than 0.9, i.e. more than 90% of the catalyst surface is covered by liquid. Since the ion exchange resin beads are highly hygroscopic, it can be assumed that this is a conservative estimate of the wetting and consequently, above ratios of 0.2, the beads are almost completely wetted.

I.2 Wilke-Chang Correlation

The Wilke-Chang correlation can be used to estimate liquid diffusivities. It gives satisfactory predictions (±10%) for the diffusivity of organic compounds in water and for organic compounds in other organic compounds [63]. It cannot, however, be used to determine the diffusivities of water through organic solvents. The liquid diffusivity, D_L, can be estimated from

$$D_L = \frac{1.173 \cdot 10^{-13} (\phi M)^{0.5} T}{\mu V_m^{0.6}} \tag{I.5}$$

Where ϕ is an association factor for the solvent (2.6 for water and 1.3 for isopropanol), M is the molecular weight of the solvent, μ is the viscosity of the solvent and V_m is the molar volume of the solute at its boiling point. The ratio of the diffusivity of propylene through IPA and through water can thus be calculated from

$$\frac{D_{L_{IPA}}}{D_{L_{H_2O}}} = \left(\frac{(\phi M)^{0.5}}{\mu}\right)_{IPA} \cdot \left(\frac{\mu}{(\phi M)^{0.5}}\right)_{H_2O} \tag{I.6}$$

At 120°C this is equal to 1.2, i.e. propylene diffuses approximately 20% faster through IPA than through water. The viscosities of the pure components at 120°C were obtained from Daubert and Danner [62].

I.3 Satterfield criterion

Satterfield et al. [151] studied mass transfer limitations in industrial trickle-bed reactors. It was determined that mass transfer from the gas phase to the liquid outer surface of the catalyst pellets will not be significant so long as

$$\frac{5 \cdot d_p \cdot \epsilon \cdot r_{obs}}{3 \cdot C_{eqm} \cdot D_e \cdot a} < 1 \tag{I.7}$$

The bulk diffusion coefficient, D_e, of the gas (in this case propylene) through the liquid (either water or isopropanol) was obtained for the relevant system from Perry and Green [64]. The equilibrium concentration of the gas phase in the liquid phase at the system conditions was calculated from the WS-PRSV model described in Section [?].

At 120 °C and 50 bar a value of 0.993 was obtained for the hydration reaction at a propylene to water ratio of 5:1. A value of 0.152 was obtained for the etherification reaction at a propylene to IPA ratio of 1:1. Whilst the etherification reaction would thus not appear to be diffusion limited, the hydration reaction, on the other hand, may very well be occurring at the borderline of a mass transfer constrained regime.

I.4 Weisz-Prater criterion

The Weisz-Prater criterion [149] for negligible intraparticle diffusion limitations assuming first-order reversible kinetics in a spherical particle is given by

$$\Phi = \frac{\rho_{cat} \cdot r_{obs} \cdot (\frac{d_p}{6})^2}{D_e(C_{bulk} - C_{eqm})} \ll 1 \tag{I.8}$$

Assuming a temperature of 120 °C and a pressure of 50 bar values of the Weisz-Prater modulus, Φ, of $2.84 \cdot 10^{-3}$ and $9.24 \cdot 10^{-4}$ were calculated for the hydration and etherification reactions respectively. These values are sufficiently smaller than unity that one can assume negligible intraparticle diffusion limitations. Indeed, Levenspiel [152] cites a value of 0.15 as being small enough to discount internal diffusion effects. As before, component properties were obtained from Daubert and Danner [62]. The effective diffusivity of the propylene through the relevant liquid phase was estimated from Perry and Green [64].

I.5 Hougen correlation

The temperature difference between the catalyst particle surface and the bulk fluid temperature in a packed bed can be estimated by the Hougen correlation [153]. This method correlates the temperature difference with three dimensionless groups, the overall Reynolds number, Re, the Prandtl number, Pr, and the heat transmission number, Q, which in this case, for spherical particles, are given by

$$\mathrm{Re} = \frac{G}{a_p \mu} \tag{I.9}$$

$$\mathrm{Pr} = \frac{C_p \mu}{k} \tag{I.10}$$

$$Q = \frac{r_{obs} \Delta H_{rxn}}{a_m C_p G_m} \tag{I.11}$$

The temperature difference, ΔT, can then be estimated with the aid of Figure I.2.

At 120 °C and 50 bar, the Hougen correlation indicates that the external temperature gradients are smaller than 0.1 °C for both the hydration and etherification reactions (species parameters obtained form Daubert and Danner [62]). One can thus assume that no external temperature gradients exist during reaction.

I.6 Anderson criterion

Anderson [154] derived a criterion for significant temperature gradients inside a catalyst pellet from the two Damköhler dimensionless groups which assess the relative importance of gradients of concentration or temperature in a reacting system without convection. It assumes spherical pellets and an Arrhenius dependence of rate on temperature and holds even if diffusional limitations apply. The Anderson criterion is

$$\frac{\Delta H_{rxn} \cdot r_{obs} \cdot d_p^2 \cdot E_a}{3 \cdot R \cdot \lambda_p \cdot T_s^2} < 1 \tag{I.12}$$

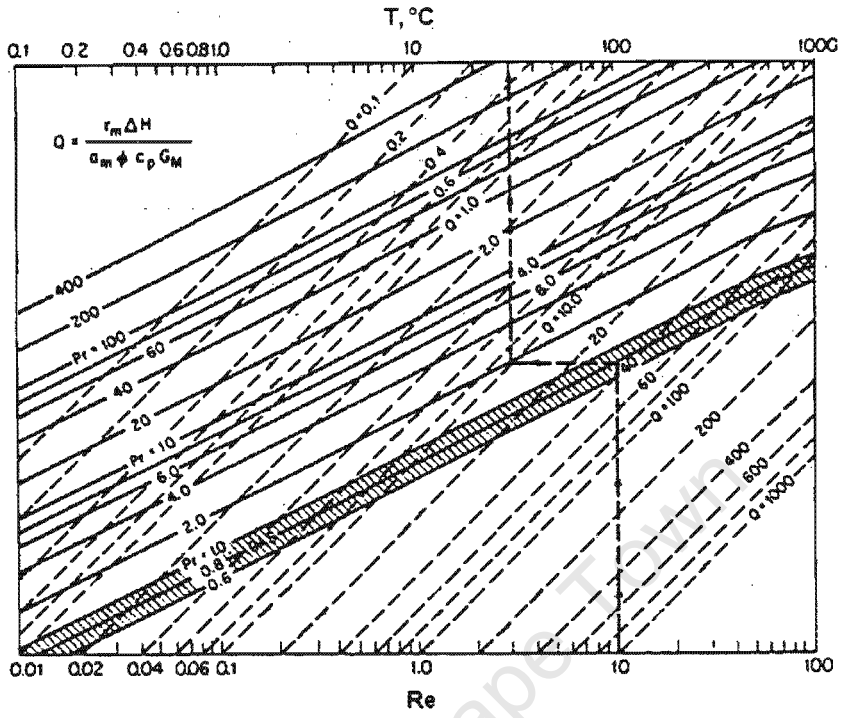

Figure I.2: Hougen correlation for external temperature gradients

Where the thermal conductivity of the entire catalyst pellet, λ_p, including the intra-particle fluid, can be estimated by a correlation from Smith [96],

$$\lambda_p = \lambda_{cat} \left(\frac{\lambda_f}{\lambda_{cat}} \right)^{1-\epsilon} \tag{I.13}$$

As it has been shown by the Hougen criterion that the temperature at the catalyst surface is practically identical to that of the bulk fluid, the external surface of the catalyst particle can be assumed to be at the same temperature as the bulk fluid, i.e. 120 °C. Assuming completely wetted particles containing only water, values of the Anderson criterion of $1.21 \cdot 10^{-3}$ were calculated for the hydration reaction. At a ratio of propylene to IPA of 1:1, a value of $1.18 \cdot 10^{-3}$ was calculated for the etherification reaction. Species properties were obtained from Daubert and Danner [62]. These values are sufficiently smaller than unity, that one can assume that no temperature gradients existed within the catalyst beads during reaction.

Appendix J

Propagation of error in chemical equilibrium

As stated previously in Section 2.3.3, the fractional error in a dependent variable, say Ω, which is a function of independent variables $\alpha_1 ... \alpha_m$ is given by [96]

$$\left(\frac{\Delta\Omega}{\Omega}\right)^2 = \sum_{i=1}^{m}\left[\left(\frac{\partial(\ln\Omega)}{\partial(\ln\alpha_i)}\right)^2\left(\frac{\Delta\alpha_i}{\alpha_i}\right)^2\right] \tag{J.1}$$

If, now, the chemical equilibrium constant is defined as

$$K_a = \prod_i (a_i)^{\nu_i} = \frac{a_1^{\nu_1} a_2^{\nu_2} \ldots}{a_3^{\nu_3} a_4^{\nu_4} \ldots} \tag{J.2}$$

then it was also shown that the fractional error in determining K_a is

$$\left(\frac{\Delta K_a}{K_a}\right)^2 = \nu_1^2\left(\frac{\Delta a_1}{a_1}\right)^2 + \nu_2^2\left(\frac{\Delta a_2}{a_2}\right)^2 + \nu_3^2\left(\frac{\Delta a_3}{a_3}\right)^2 + \nu_4^2\left(\frac{\Delta a_4}{a_4}\right)^2 \tag{J.3}$$

Now, the activity of a species is defined as the ratio between the partial molar fugacity and the standard pure component fugacity, i.e.

$$a_i = \frac{f_i^*}{f_i^o} \tag{J.4}$$

Applying Eqn. J.1 the fractional error in the activity is thus

$$\left(\frac{\Delta a_i}{a_i}\right)^2 = \left(\frac{\Delta f_i^*}{f_i^*}\right)^2\left(\frac{\partial \ln a_i}{\partial \ln f_i^*}\right)^2 + \left(\frac{\Delta f_i^o}{f_i^o}\right)^2\left(\frac{\partial \ln a_i}{\partial \ln f_i^o}\right)^2 = \left(\frac{\Delta f_i^*}{f_i^*}\right)^2 + \left(\frac{\Delta f_i^o}{f_i^o}\right)^2 \tag{J.5}$$

but the error in determining the standard activity of the gas phase pure component at 1 atm and the system temperature is negligible, thus the fractional error in activity depends only on the fractional error in the partial molar fugacity,

$$\left(\frac{\Delta a_i}{a_i}\right)^2 = \left(\frac{\Delta f_i^*}{f_i^*}\right)^2 \tag{J.6}$$

The partial molar fugacity is given by the product of the system pressure, the fugacity coefficient and the mole fraction of the species in the phase under consideration

$$f_i^* = x_i \cdot P \cdot \phi_i \tag{J.7}$$

Once again applying Eqn. J.1, the fractional error in the activity now becomes

$$\begin{aligned}\left(\frac{\Delta a_i}{a_i}\right)^2 &= \left(\frac{\Delta x_i}{x_i}\right)^2\left(\frac{\partial \ln a_i}{\partial \ln x_i}\right)^2 + \left(\frac{\Delta P}{P}\right)^2\left(\frac{\partial \ln a_i}{\partial \ln P}\right)^2 + \left(\frac{\Delta \phi_i}{\phi_i}\right)^2\left(\frac{\partial \ln a_i}{\partial \ln \phi_i}\right)^2 \\ &= \left(\frac{\Delta x_i}{x_i}\right)^2 + \left(\frac{\Delta P_i}{P_i}\right)^2 + \left(\frac{\Delta \phi_i}{\phi_i}\right)^2\end{aligned} \tag{J.8}$$

However, the fugacity coefficient is not an indendent variable, but is itself a function of the mole fraction, the system pressure and the system temperature. The fractional error in the fugacity coefficient is thus given by

$$\left(\frac{\Delta \phi_i}{\phi_i}\right)^2 = \left(\frac{\Delta x_i}{x_i}\right)^2\left(\frac{\partial \ln \phi_i}{\partial \ln x_i}\right)^2 + \left(\frac{\Delta P}{P}\right)^2\left(\frac{\partial \ln \phi_i}{\partial \ln P}\right)^2 + \left(\frac{\Delta T}{T}\right)^2\left(\frac{\partial \ln \phi_i}{\partial \ln T}\right)^2 \tag{J.9}$$

The partial derivatives of the fugacity coefficient with respect to pressure, temperature and mole fraction can be obtained by differentiation of the equation of state and the relevant mixing rule. Due to the complexity of mixing rules and equations of state, determining the partial derivative analytically can, however, prove to be extremely tedious and is not particularly instructive, thus it is generally easier to obtain the partial derivatives by numerical means.

The fractional error in determing the value of the chemical equilibrium constant from experimental data, using an equation of state to calculate the species activities, can thus

be estimated from

$$\left(\frac{\Delta K_a}{K_a}\right)^2 = \sum_i \nu_i^2 \left(\frac{\Delta x_i}{x_i}\right)^2 \left(1 + \left(\frac{\partial \ln \phi_i}{\partial \ln x_i}\right)^2\right) + \sum_i \nu_i^2 \left(\frac{\Delta P}{P}\right)^2 \left(1 + \left(\frac{\partial \ln \phi_i}{\partial \ln P}\right)^2\right) + \sum_i \nu_i^2 \left(\frac{\Delta T}{T}\right)^2 \left(\frac{\partial \ln \phi_i}{\partial \ln T}\right)^2 \quad \text{(J.10)}$$

Appendix K

Single component adsorption studies

K.1 Basic adsorption theory

In a microscopic sense, even the smoothest of surfaces are irregular. These irregular features, be they valleys or peaks, are regions of unsaturated surface forces and thus attract other atoms or molecules from the surrounding gas or liquid phase (so-called adsorption). Certain materials may even exhibit regions of concentrated surface forces, which in catalysts are often termed active-sites. Two types of adsorption may occur:

- Physical adsorption is a non-specific process, thought to be similar in nature to condensation. Typically, the heat evolved during the exothermic adsorption process is of the same magnitude as the heat of condensation, 2 to 20 kJ/mol.
- Chemical adsorption on the other hand is a specific process and involves forces considerably stronger than in physical adsorption. The name derives from the fact that the exothermic heat of chemical adsorption is of the same magnitude as the heat of chemical reaction, 20 to 400 kJ/mol.

In order to develop rate equations for catalytic reactions quantitative expressions for the adsorptive processes are often required. A number of adsorption models have been

proposed, but the most widely used remains the approach of Langmuir [96]. The Langmuir isotherm can be written in the form

$$C_c = \frac{HC_b}{1 + \frac{H}{C_m}C_b} \tag{K.1}$$

where one assumes:

- An energetically uniform surface. In the case of a catalyst with active centres this assumption implies that all centres have the same activity for adsorption and that the remainder of the surface has none.
- No interaction between adsorbed molecules on the surface.
- All adsorption occurs by the same mechanism and each adsorbed complex has the same structure.
- Adsorption extends up to one complete monolayer.

The value of the Henry's constant of adsorption, H, is a measure of the strength of adsorption of the sorbing species. The saturation loading, C_m, specifies the maximum amount of the relevant species which can adsorb at the temperature of interest.

K.2 Residence time distribution

When measuring adsorption data, it is important to ensure that all the adsorption which is observed is due to adsorption on the material under investigation and not due to adsorption on the experimental apparatus. A pulse input of adsorbent into the adsorption apparatus without catalyst should give a pulse response if no extraneous adsorption is occurring. Also, two different adsorbents should give the same residence time. If some adsorption were occurring on the apparatus itself, then the pulse input should show peak

broadening and, due to the different chemical properties of water and propylene, the residence times should differ. Figures K.1 and K.2 give the normalised response curves for water and propylene for a pulse input with no catalyst present.

The average residence time, $\bar{t}$, of the adsorbent in the apparatus without catalyst may be calculated from

$$\bar{t} = \frac{\int_0^\infty C \cdot t \, dt}{\int_0^\infty C \, dt} \tag{K.2}$$

this allows one to calculate the variance of the response from

$$\sigma_{out}^2 = \frac{\int_0^\infty C \cdot (t - \bar{t})^2 \, dt}{\int_0^\infty C \, dt} \tag{K.3}$$

and thus the vessel dispersion number, N_D, for a closed system resulting from a pulse input may be calculated from the experimental data by

$$N_D = \frac{\sigma_{out}^2}{2 \cdot \bar{t}^2} \tag{K.4}$$

The average residence times of water and propylene within the adsorption apparatus were calculated to be 53.3 s and 53.7 s respectively whilst vessel dispersion numbers of $1.3 \cdot 10^{-2}$ and $7.1 \cdot 10^{-3}$ were obtained - such low dispersion numbers are indicative of plug flow. It is clear from the response that neither of the compounds were adsorbed in the adsorption apparatus if no catalyst was loaded. When catalyst was loaded, all observed adsorption was thus only due to adsorption on the catalyst.

K.3 Langmuir isotherm evaluation of adsorption data

The simplest method of fitting Langmuir isotherms to adsorption data is by linearising the isotherm and then fitting the Henry's constant and the saturation loading parameters

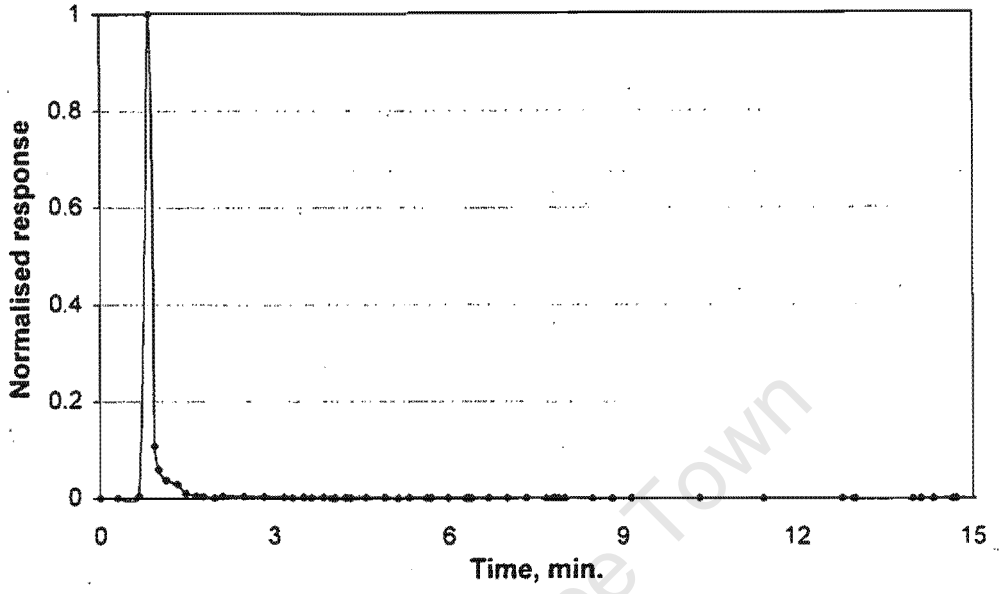

Figure K.1: Normalised response curve for water in the adsorption apparatus with no catalyst present.

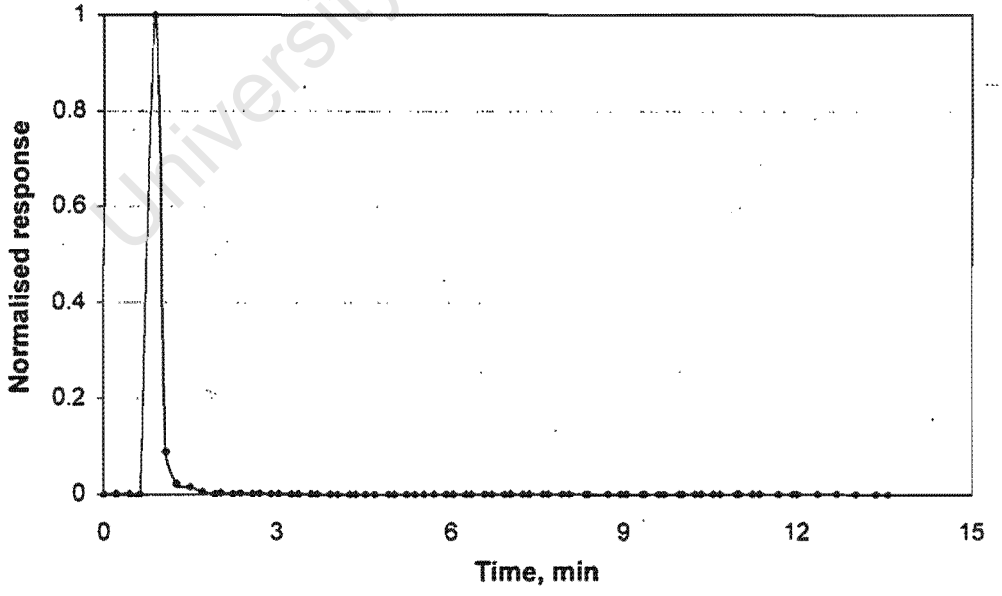

Figure K.2: Normalised response curve for propylene in the adsorption apparatus with no catalyst present.

by linear regression of the experimental data. The Langmuir isotherm, Eq. K.1, may be rewritten as

$$\frac{1}{C_c} = \frac{1}{HC_b} + \frac{1}{C_m} \tag{K.5}$$

where the slope of the regressed line gives the Henry's constant and the intercept gives the saturation loading. This method was used to fit the single component adsorption data. The linearisations of the water and the propylene data along with the best-fit Langmuir isotherms are shown in Figures K.3 and K.4 respectively. Table K.1 gives the obtained values for the Henry's constant and the saturation capacity.

Table K.1: Henry's constants and saturation capacities from the adsorption of water and propylene on Amberlyst 15

	Propylene		Water	
Temperature, °C	H	C_m, mol g_{cat}^{-1}	H	C_m, mol g_{cat}^{-1}
30	1200	$8.4 \cdot 10^{-4}$		–
45	1300	$8.1 \cdot 10^{-4}$	19000	$6.4 \cdot 10^{-2}$
60	1400	$7.0 \cdot 10^{-4}$	12000	$5.0 \cdot 10^{-2}$
75	–	–	4700	$5.4 \cdot 10^{-2}$

At low coverages the change in the logarithm of the Henry's constant has been found to be proportional to the quotient of the heat of adsorption and the temperature such that

$$\ln H = \ln H_o - \frac{\Delta H_{ads}}{RT} \tag{K.6}$$

Linearisation of the Henry's constant obtained from experimental data at different temperatures should thus give an indication of the heat of adsorption of water and propylene on Amberlyst 15. Figure K.5 shows the linearisation of the Henry's constants for water and propylene with the best-fit lines obtained from regression. Heats of adsorption for water and for propylene of -42.6 kJ mol^{-1} and 5.4 kJ mol^{-1} respectively were obtained.

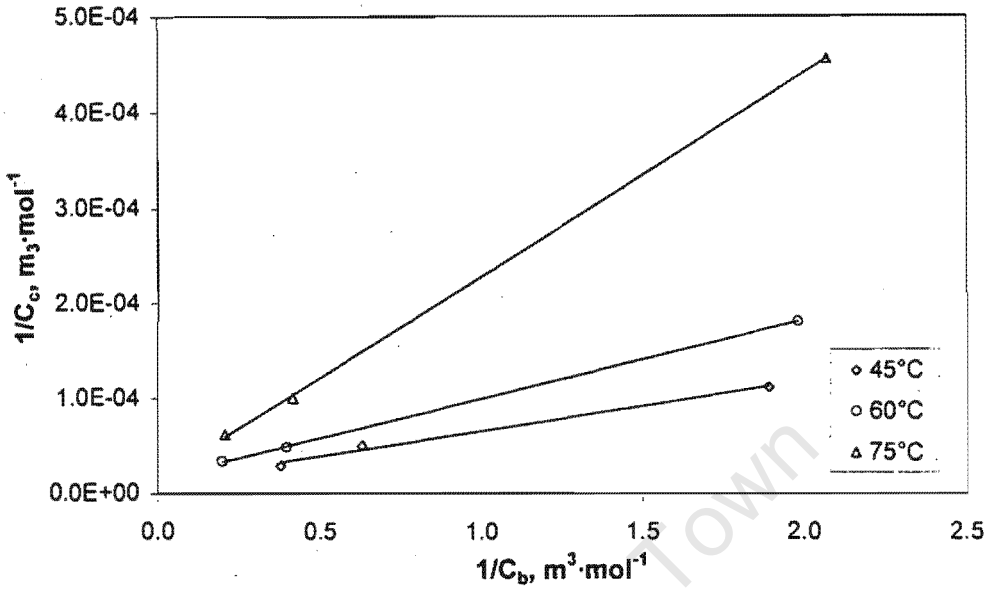

Figure K.3: Linear regression of experimental single component water adsorption data on Amberlyst 15 and the best-fit Langmuir isotherms.

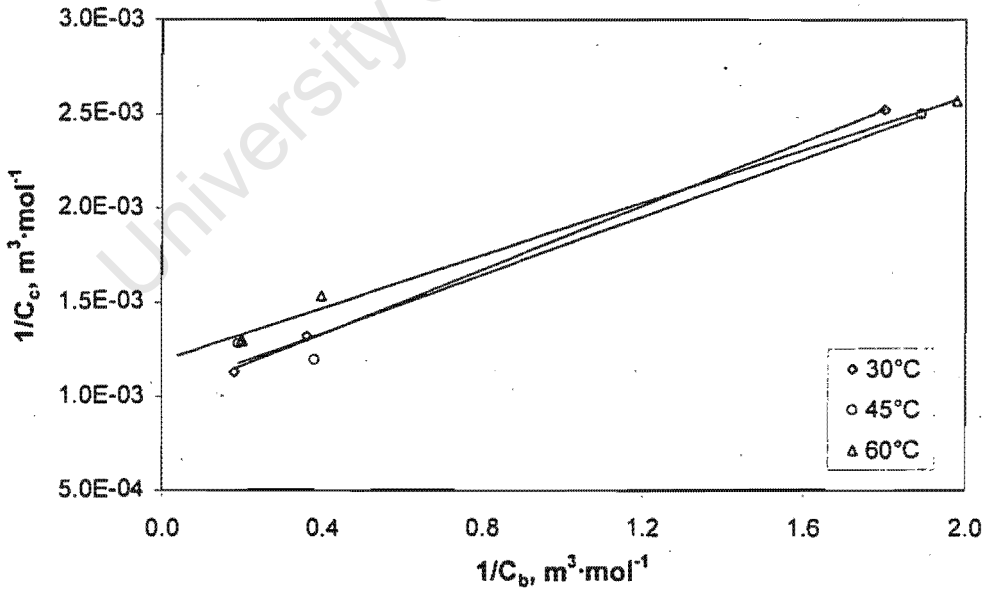

Figure K.4: Linear regression of experimental single component propylene adsorption data on Amberlyst 15 and the best-fit Langmuir isotherms.

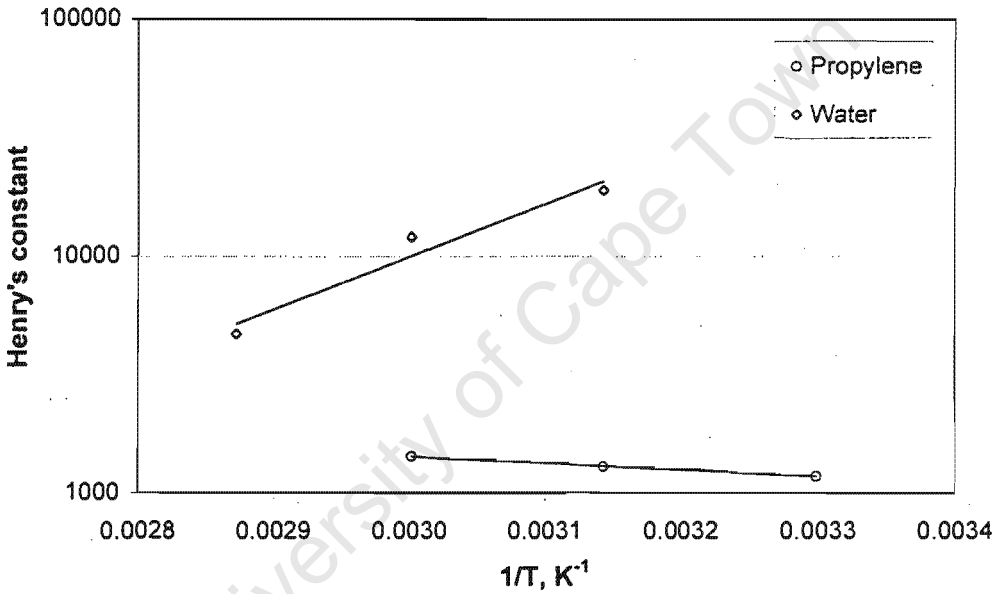

Figure K.5: Linearisation of the Henry's constants for water and propylene to obtain the heat of adsorption on Amberlyst 15.

Appendix L

Kinetic model derivations

L.1 Reactions in the DIPE system

The propylene hydration, IPA alkylation and bimolecular IPA dehydration reactions can be written as represented in Figure L.1

For a Type I mechanism, n, m and k are less than one as species are polyadsorbed to a single site. For a Type II mechanism, n, m and k would be equal to or greater than one. In every case it was assumed that the chemical reaction, be it on the surface or in the bulk phase, was the rate limiting step. In the following model developments, water was denoted by W, propylene by P, IPA by A and DIPE by E.

L.2 The pseudo-homogeneous kinetic model

The pseudo-homogeneous model assumes simple reversible mass action kinetics, such that the rate equations for propylene hydration (reaction 1), IPA alkylation (reaction 2) and bimolecular IPA dehydration (reaction 3) become

$$r_1 = k_1 \left(a_W \cdot a_P - \frac{1}{K_{a,1}} a_A \right) \tag{L.1}$$

1. Propylene hydration

$H_2O + n\otimes \rightleftharpoons H_2O\otimes_n$

$H_2O\otimes_n + C_3H_6 \rightleftharpoons IPA\otimes_m + (n-m)\otimes$

$IPA\otimes_m \rightleftharpoons IPA + m\otimes$

2. IPA alkylation

$IPA + m\otimes \rightleftharpoons IPA\otimes_m$

$IPA\otimes_m + C_3H_6 \rightleftharpoons DIPE\otimes_k + (m-k)\otimes$

$DIPE\otimes_k \rightleftharpoons DIPE + k\otimes$

3. Bimolecular IPA dehydration

$2IPA + 2m\otimes \rightleftharpoons 2IPA\otimes_m$

$2IPA\otimes_m \rightleftharpoons DIPE\otimes_k + H_2O\otimes_n + (m-k)\otimes$

$DIPE\otimes_k \rightleftharpoons DIPE + k\otimes$

$H_2O\otimes_n \rightleftharpoons H_2O + n\otimes$

Figure L.1: Elementary reaction steps of propylene hydration, IPA alkylation and bimolecular dehydration of IPA over ion exchange resins for Type I and Type II mechanisms. Where $\otimes$ represents an active site, n the number of sites water is adsorbed to, m the number of sites IPA is adsorbed to and k the number of sites DIPE is adsorbed to ($n > m > k$).

$$r_2 = k_2 \left(a_P \cdot a_A - \frac{1}{K_{a,2}} a_E \right) \tag{L.2}$$

$$r_3 = k_3 \left(a_A^2 - \frac{1}{K_{a,3}} a_E \cdot a_W \right) \tag{L.3}$$

The only parameters used in this model are the three rate constants: k_1, k_2 and k_3.

L.3 The Eley-Rideal kinetic model

For each reaction, the mechanism involves three basic steps:

1. The adsorption of the polar species from the solution phase onto the active site(s)

2. The surface reaction between the adsorbed polar species and solution phase propylene or IPA

3. The desorption of the surface reaction products from the active site(s) to the solution phase

If one assumes multi-site Langmuir-type adsorption isotherms in terms of the bulk phase species activities and adsorbed phase concentrations and assumes that chemical reaction occurs only on the surface, then the rate equations for each of these three basic mechanistic steps may, for propylene hydration, be written as

$$r_{W,ads} = k_{W,ads}\left(a_W \cdot C_{VS}^n - \frac{1}{H_W} \cdot C_{W,ads}\right) \tag{L.4}$$

$$r_1 = k_1'\left(C_{W,ads} \cdot a_P - \frac{1}{K_{1,S}} C_{A,ads} \cdot C_{VS}^{(n-m)}\right) \tag{L.5}$$

$$r_{A,ads} = k_{A,ads}\left(a_A \cdot C_{VS}^m - \frac{1}{H_A} \cdot C_{A,ads}\right) \tag{L.6}$$

If one assumes further that the surface reaction is rate controlling, then the two adsorption reactions are always at equilibrium, such that

$$C_{W,ads} = H_W \cdot a_W \cdot C_{VS}^n \tag{L.7}$$

and

$$C_{A,ads} = H_A \cdot a_A \cdot C_{VS}^m \tag{L.8}$$

Substituting these equations into the rate equation for the surface reaction one obtains

$$r_1 = k_1' \cdot C_{VS}^n\left(H_W \cdot a_W \cdot a_P - \frac{1}{K_{1,S}} H_A \cdot a_A\right) \tag{L.9}$$

The overall concentration of active sites, however, is equal to the sum of the concentration of vacant sites, the concentration of sites where water has adsorbed, the concentration of sites where IPA has adsorbed and the concentration of sites where DIPE has adsorbed:

$$C_{S,tot} = C_{VS} + C_{W,ads} + C_{A,ads} + C_{E,ads} = C_{VS}\left(1 + H_W a_W + H_A a_A + H_E a_E\right) \quad \text{(L.10)}$$

thus

$$C_{VS} = \frac{C_{S,tot}}{\left(1 + H_W a_W + H_A a_A + H_E a_E\right)} \quad \text{(L.11)}$$

Also, the chemical equilibrium constant for the surface reaction between adsorbed water and solution phase propylene to give adsorbed IPA is

$$K_{1,S} = \frac{C_{A,ads} \cdot C_{VS}^{(n-m)}}{C_{W,ads} \cdot a_P} = \frac{H_A \cdot a_A \cdot C_{VS}^{m} \cdot C_{VS}^{(n-m)}}{H_W \cdot C_{VS}^{n} \cdot a_W \cdot a_P} = \frac{H_A}{H_W} K_{a,1} \quad \text{(L.12)}$$

Substituting these formulations for the concentration of vacant sites and for the adsorbed phase chemical equilibrium constant into the rate equations, the final form of the rate equation in terms of the bulk phase species activities, a_i, the Henry constants of adsorption, H_i, the activity-based chemical equilibrium constant, $K_{a,1}$, and the hydration rate constant, k_1, is

$$r_1 = \frac{k_1 H_W \left(a_W \cdot a_P - \frac{1}{K_{a,1}} a_A\right)}{\left(1 + H_W a_W + H_A a_A + H_E a_E\right)^n} \quad \text{(L.13)}$$

where the rate costant, k_1, incorporates the total concentration of active sites, $C_{S,tot}$. Similar model developments lead to the following equations for IPA alkylation and the bimolecular dehydration of IPA, respectively

$$r_2 = \frac{k_2 H_A \left(a_A \cdot a_P - \frac{1}{K_{a,2}} a_E\right)}{\left(1 + H_W a_W + H_A a_A + H_E a_E\right)^m} \quad \text{(L.14)}$$

$$r_3 = \frac{k_3 H_A^2 \left(a_A^2 - \frac{1}{K_{a,3}} a_E a_W\right)}{\left(1 + H_W a_W + H_A a_A + H_E a_E\right)^{2m}} \quad \text{(L.15)}$$

If one fixes the number of active sites involved in the reactions, i.e. fixes n and m, then this model contains 6 parameters: the three reaction rate constants (k_1, k_2 and k_3) and the three adsorption constants (H_W, H_A and H_E). If the number of active sites involved in the reactions is not fixed, then the number of parameters increases to eight.

L.4 The "changing-mechanism" model

This model is essentially a variation on the pseudo-homogeneous model with the addition of an exponential term which accounts for changes in the reaction mechanism as the ratio of apolar to polar species in the reaction medium changes. As the ratio of apolar to polar species increases, i.e. as the sum of the propylene and DIPE mole fractions increases, the magnitude of the rate constant is scaled to simulate the increased catalytic activity of the Type II mechanism in comparison to the Type I mechanism. The rate equations for propylene hydration (reaction 1), IPA alkylation (reaction 2) and bimolecular IPA dehydration (reaction 3) are given by

$$r_1 = k_1 \cdot \exp\left(k_m \cdot (x_P + x_E)\right)\left(a_W \cdot a_P - \frac{1}{K_{a,1}} a_A\right) \tag{L.16}$$

$$r_2 = k_2 \cdot \exp\left(k_m \cdot (x_P + x_E)\right)\left(a_P \cdot a_A - \frac{1}{K_{a,2}} a_E\right) \tag{L.17}$$

$$r_3 = k_3 \cdot \exp\left(k_m \cdot (x_P + x_E)\right)\left(a_A^2 - \frac{1}{K_{a,3}} a_E \cdot a_W\right) \tag{L.18}$$

This model contains 4 kinetic parameters: the three reaction rate constants (k_1, k_2 and k_3) and k_m which, at least empirically, simulates changes in the reaction mechanism.

Bibliography

[1] A. Douaud. Tomorrow's engines and fuels. *Hydrocarbon Processing*, pages 55–61, February 1995.

[2] I. Kroschwitz, editor. *Kirk-Othmer Encyclopedia of Chemical Technology*, volume 9 - 20. John Wiley and Sons, New York, 4th edition, 1993-1998.

[3] E. Pescarollo, R. Trotta, and P.R. Sarathy. Etherify light gasolines. *Hydrocarbon Processing*, pages 53–60, February 1993.

[4] P. Crow. US refiners face more challenges in wake of RFG introduction. *Oil and Gas Journal*, pages 23–26, Apr. 22 1996.

[5] J. Ignatius, H. Järvelin, and P. Lindqvist. Use TAME and heavier ethers to improve gasoline properties. *Hydrocarbon Processing*, pages 51–53, February 1995.

[6] A. Jezak. C_5 alkylate: A superior blending component. *Hydrocarbon Processing*, pages 47–50, February 1994.

[7] J. Haggin. Alternative fuels to petroleum gain increased attention. *Chemical and Engineering News*, pages 25–27, August 14 1989.

[8] T.L. Marker, W.H. Keesom, R. Schmidt, S. Davis, and R. Marinangeli. Low-cost DIPE production. *Conference on Clean Air Act and Reformulated Gasoline*, 1994.

[9] T.L. Marker, H.U. Hammerschaimb, R. Marinangeli, W.H. Keesom, and U.G. Bozzano. Production of IPA and DIPE from propylene using ion-exchange resin catalysts. *AIChE Annual Meeting*, 1993.

[10] New process produces alternative oxygenate from propylene. *Oil and Gas Journal*, pages 39–41, May 25 1992.

[11] H.U. Hammerschaimb, U.G. Bozzano, W.H. Keesom, and T.L. Marker. Produce IPA and DIPE from propylene. *Fuel Reformulation*, pages 36–42, September 1993.

[12] H.L. Brockwell, P.R. Sarathy, and R. Trotta. Synthesize ethers. *Hydrocarbon Processing*, pages 133–141, September 1991.

[13] G. Ertl, H. Knözinger, and J. Weitkamp, editors. *Handbook of Heterogeneous Catalysis*, volume 1 - 5. VCH Verlagsgesellschaft, Weinheim, 1997.

[14] W.R. Hartley, A.J. Englande, and D.J. Harrington. Health risk assessment of groundwater contaminated with methyl tertiary butyl ether (MTBE). *Department of Environmental and Health Sciences, Tulane University*, 1997.

[15] Petrochemical processes '95. *Hydrocarbon Processing*, pages 110–114, March 1995.

[16] Refining 1996. *Hydrocarbon Processing*, pages 110–116, November 1996.

[17] G.G. Podrebarac, F.T.T. Ng, and G.L. Rempel. More uses for catalytic distillation. *CHEMTECH*, pages 37–45, May 1997.

[18] New etherification process commercialized in Finland. *Oil and Gas Journal*, pages 44–45, Jan. 6 1997.

[19] A. Wood. Mobil cuts the alcohol out of oxygenate production. *Chemical Week*, April 15 1992.

[20] World ethylene capacity increased marginally in 1995. *Oil and Gas Journal*, pages 49–54, May 13 1996.

[21] W. Weirauch. Chem System petrochemical outlook. *Hydrocarbon Processing*, pages 23–27, April 1995.

[22] W. Neier and J. Woellner. Isopropyl alcohol by direct hydration. *CHEMTECH*, February:95–99, 1973.

[23] W. Neier, W. Webers, M. Dettmer, and G. Osterburg. Process for the production of alcohols. *US Patent No. 4579984*, April 1 1986.

[24] R. Ramachandran and L.H. Dao. Process for the production of ethanol and isopropanol. *US Patent No. 5488185*, January 30 1996.

[25] W. Neier. Ionentauscher-katalysatoren bei der herstellung organischer zwischenprodukte. *Chemische Industrie*, 33(10):632–636, 1981.

[26] T.L. Marker, G.A. Funk, P.T. Barger, and H.U. Hammerschaimb. Two-stage process for producing diisopropyl ether using catalytic distillation. *US Patent No. 5504258*, April 2 1996.

[27] T.L. Marker, R.J. Schmidt, R.E. Marinangeli, and T.A. Brandvold. Process for producing diisopropyl ether with removal of acid material. *US Patent No. 5504257*, April 2 1996.

[28] J.E. Child, B.C. Choi, and F.P. Ragonese. Dual stage process for the production of ethers. *US Patent No. 4935552*, June 19 1990.

[29] M.N. Harandi, W.O. Haag, H. Owen, and W.K. Bell. Ether production. *US Patent No. 5144086*, September 1 1992.

[30] R.J. Taylor, P.E. Dai, and J.F. Knifton. Gradient catalyst system for the integrated production of isopropyl alcohol and diisopropyl ethers. *US Patent No. 5550300*, August 27 1996.

[31] R.J. Taylor, P.E. Dai, and J.F. Knifton. Integrated process for the production of isopropyl alcohol and diisopropyl ethers. *US Patent No. 5583266*, December 10 1996.

[32] A. Rehfinger and U. Hoffmann. Kinetics of methyl tertiary butyl ether liquid phase synthesis catalyzed by ion exchange resin - I. Intrinsic rate expression in liquid phase activities. *Chemical Engineering Science*, 45(6):1605–1617, 1990.

[33] L. Sola, M.A. Pericas, F. Cunill, and M. Iborra. Reaction calorimetry study of the liquid-phase synthesis of tert-butyl methyl ether. *Industrial and Engineering Chemistry Research*, 33(11):2578–2583, 1994.

[34] L.K. Rihko and A.O.I. Krause. Kinetics of heterogeneously catalyzed tert-amyl methyl ether reactions in the liquid phase. *Industrial and Engineering Chemistry Research*, 34(4):1172–1180, 1995.

[35] C. Oost and U. Hoffman. The synthesis of tertiary amyl methyl ether (TAME): Microkinetics of the reactions. *Chemical Engineering Science*, 51(3):329–340, 1996.

[36] C.S. Cope. Equilibria in the hydration of propylene and of butylenes. *Journal of Chemical and Engineering Data*, 11(3):379–383, 1966.

[37] J.J. Carroll and A.E. Mather. A model for the solubility of light hydrocarbons in water and aqueous solutions of alkanolamines. *Chemical Engineering Science*, 52(4):542–552, 1997.

[38] I.G. Economou and C. Tsonopolous. Associating models and mixing rules in equations of state for water/hydrocarbon mixtures. *Chemical Engineering Science*, 52(4):511–525, 1997.

[39] A. Wyczesany. Nonstoichiometric algorithm of calculation of simultaneous chemical and phase equilibria. 2. High-pressure hydration of propene to 2-propanol. *Industrial and Engineering Chemistry Research*, 33(8):1971–1978, 1994.

[40] D.S.H. Wong and S.I. Sandler. A theoretically correct mixing rule for cubic equations of state. *AIChE Journal*, 38(5):671–680, 1992.

[41] R. Stryjek and J.H. Vera. PRSV - An improved Peng-Robinson equation of state with new mixing rules for strongly nonideal mixtures. *The Canadian Journal of Chemical Engineering*, 64:334–340, 1986.

[42] R. Stryjek and J.H. Vera. PRSV: An improved Peng-Robinson equation of state for pure compounds and mixtures. *The Canadian Journal of Chemical Engineering*, 64:323–333, 1986.

[43] H. Orbey and S.I. Sandler. Reformulation of Wong-Sandler mixing for cubic equations of state. *AIChE Journal*, 41(3):683–690, 1995.

[44] J.M. Prausnitz R.C. Reid and B.E. Poling. *The Properties of Gases and Liquids.* McGraw-Hill Book Company, New York, 1987.

[45] S.I. Sandler. *Chemical and Engineering Thermodynamics.* John Wiley and Sons, New York, 1989.

[46] F.M. Majewski and L.F. Marek. Hydration of propylene under pressure. *Industrial and Engineering Chemistry*, 30(2):203–210, 1938.

[47] L. Petrus, R.W. De Roo, E.J. Stamhuis, and G.E.H. Joosten. Kinetics and equilibria of the hydration of propene over a strong acid ion exchange resin as catalyst. *Chemical Engineering Science*, 39(3):433–446, 1984.

[48] J.R. Kaiser, H. Beuther, L.D. Moore, and R.C. Odioso. Direct hydration of propylene over ion-exchange resins. *Industrial and Engineering Chemistry Product Research and Development*, 1(4):296–302, 1962.

[49] W. Neier and J. Woellner. Use cation catalyst for IPA. *Hydrocarbon Processing*, November:113–116, 1972.

[50] Y. Izumi. Hydration / hydrolysis by solid acids. *Catalysis Today*, 33:371–409, 1997.

[51] H.M. Stanley, J.E. Youell, and J.B. Dymock. *Journal of the Society of Chemical Engineers*, 53:205, 1934.

[52] W.H. Schiffler, M.M. Holm, and L.F. Brooke. *Industrial and Engineering Chemistry*, 31:1099, 1939.

[53] C.S. Cope and B.F. Dodge. Equilibria in the hydration of ethylene at elevated pressures and temperatures. *AIChE Journal*, 5(1):10–16, 1959.

[54] C.S. Cope. Equilibria in the hydration of ethylene and propylene. *AIChE Journal*, 10(2):277–281, 1962.

[55] A. Corma. Inorganic solid acids and their use in acid-catalyzed hydrocarbon reactions. *Chemical Reviews*, 95:559–614, 1995.

[56] A. Calderon, J. Tejero, J.F.Izquierdo, M. Iborra, and F. Cunill. Equilibrium constants for the liquid phase synthesis of isopropyl tert-butyl ether from 2-propanol and isobutene. *Industrial and Engineering Chemistry Research*, 36(3):896–902, 1997.

[57] P. Kitchaiya and R. Datta. Ethers from ethanol. 2. Reaction equilibria of simultaneous tert-amyl ethyl ether synthesis and isoamylene isomerization. *Industrial and Engineering Chemistry Research*, 34(4):1092–1101, 1995.

[58] J.F. Izquierdo, F. Cunill, M. Vila, M. Iborra, and J. Tejero. Equilibrium constants for methyl tert-butyl ether and ethyl tert-butyl ether liquid-phase syntheses using C_4 olefinic cut. *Industrial and Engineering Chemistry Research*, 33(11):2830–2835, 1994.

[59] M. Ladisch, P. Westgate, R. Hendrickson, and M. Brewer. Framework for correlating composition dependent equilibrium conversion in methyl tert-butyl ether formation by ion-exchange catalysts. *Industrial and Engineering Chemistry Research*, 34(8):2811–2816, 1995.

[60] K.L. Jensen and R. Datta. Ethers from ethanol. 1. equilibrium thermodynamic analysis of the liquid-phase ethyl tert-butyl ether reaction. *Industrial and Engineering Chemistry Research*, 34(1):392–399, 1995.

[61] C. Fite, M. Iborra, J. Tejero, J.F. Izquierdo, and F. Cunill. Kinetics of the liquid-phase synthesis of ethyl tert-butyl ether (ETBE). *Industrial and Engineering Chemistry Research*, 33(3):581–591, 1994.

[62] T.E. Daubert and R.P. Danner. *Physical and Thermodynamic Properties of Pure Chemicals*, volume 1-4. Hemisphere Publishing Company, Washington, 1992.

[63] J.M. Coulson, J.F. Richardson, and R.K. Sinnot. *Chemical Engineering*, volume 6. Pergamon Press, Oxford, 1991.

[64] R.H. Perry and D. Green. *Perry's Chemical Engineers' Handbook.* McGraw-Hill Book Company, New York, 1984.

[65] D.R. Stull, E.F. Westrum, and G.C. Sinke. *The Chemical Thermodynamics of Organic Compounds.* John Wiley and Sons, New York, 1969.

[66] D.Y. Peng and D.B. Robinson. *Industrial Engineering and Chemistry Fundamentals*, 15:59, 1976.

[67] A. Fredenslund, J. Gmehling, and P. Rasmussen. *Vapor-Liquid Equilibrium Using UNIFAC.* Elsevier, Amsterdam, 1977.

[68] D.S. Abrams and J.M. Prausnitz. Statistical thermodynamics of liquid mixtures: A new expression for the excess Gibbs energy of partly or completely miscible systems. *AIChE Journal*, 21(1):116–128, 1975.

[69] M.J. Huron and J. Vidal. New mixing rules in simple equation of state for representing vapor-liquid equilibria of strongly nonideal mixtures. *Fluid Phase Equilibria*, 3:255, 1979.

[70] R.A. Heidemann. Computation of high pressure phase equilibria. *Fluid Phase Equilibria*, 14:55–78, 1983.

[71] J.M. Smith and H.C. Van Ness. *Introduction to Chemical Engineering Thermodynamics*. McGraw-Hill Book Company, Tokyo, 1983.

[72] G.F.C. Rogers and Y.R. Mayhew. *Thermodynamic and Transport Properties of Fluids*. Basil Blackwell Ltd., Oxford, 1980.

[73] D. Ambrose, J.H. Ellender, C.H.S. Sprake, and R. Townsend. Thermodynamic properties of organic oxygen compounds - XLV - Vapour pressures of some ethers. *Journal of Chemical Thermodynamics*, 9:735–741, 1976.

[74] J.A. Nelder and R. Mead. *The Computer Journal*, 7:308, 1965.

[75] W. Spendley, G.R. Hext, and F.R. Himsworth. *Technometrics*, 4:44, 1962.

[76] C.G. Broyden. *J. Inst. Math. Appl.*, 76:222, 1970.

[77] R. Fletcher. *Comput. J.*, 13:317, 1970.

[78] D. Goldfarb. *Math. Comput.*, 24:23, 1970.

[79] D.F. Shanno. *Mathematical Computations*, 24:647, 1970.

[80] T.F. Edgar and D.M. Himmelblau. *Optimization of Chemical Processes*. McGraw-Hill Publishing Company, New York, 1988.

[81] C.C. Li and J.J. McKetta. Vapor-liquid equilibrium in the propylene-water system. *Journal of Chemical and Engineering Data*, 8(2):271–275, 1963.

[82] C. McAuliffe. Solubility in water of paraffin, cycloparaffin, olefin, acetylene, cycloolefin and aromatic hydrocarbons. *The Journal of Physical Chemistry*, 70(4):1267–1275, 1966.

[83] E.L. Purlee and R.W. Taft. Distribution constants for ethylene and propylene between the gas phase and aqueous perchloric acid. *Journal of the American Chemical Society*, 78:5811–5812, 1956.

[84] F. Barr-David and B.F. Dodge. Vapor-liquid equilibrium at high pressures. The systems ethanol-water and 2-propanol-water. *Journal of Chemical and Engineering Data*, 4(2):107–121, 1959.

[85] V.V. Udovenko and T.F. Mazanko. *Zh. Fiz. Khim.*, 41:1615, 1967.

[86] *International Critical Tables*, volume 3. McGraw-Hill Book Company, New York, 1928.

[87] A.S. Brunjes and M.J.P. Bogart. *Industrial Engineering Chemistry*, 35:255, 1943.

[88] A. Wilson and E.L. Simons. *Industrial Engineering Chemistry*, 44:2214, 1952.

[89] W. Hunsmann and K.H. Simmrock. *Chemical Engineering Technology*, 38:1053, 1966.

[90] M. Yorizane, S. Yoshimura, and Yamamoto T. *Kagaku Kogaku*, 31:451, 1967.

[91] M.S. Zabaloy, G.D.B. Mabe, S.B. Bottini, and E.A. Brignole. *Journal of Chemical Engineering Data*, 38:40, 1993.

[92] L.A.J. Verhoeye. *Journal of Chemical Engineering Data*, 15:222, 1970.

[93] H.C. Miller and H. Bliss. *Industrial Engineering Chemistry*, 32:123, 1940.

[94] B.L. Larsen. A modified UNIFAC group-contribution model for prediction of phase equilibria and heats of mixing. *Industrial and Engineering Chemistry Research*, 26(11):2274–2286, 1987.

[95] S.I. Sandler. 1997. personal communication.

[96] J.M. Smith. *Chemical Engineering Kinetics.* McGraw-Hill Book Company, Singapore, third edition, 1981.

[97] E. Berecz and M. Balla-Achs. *Gas Hydrates.* Akademiai Kiado, Budapest, 1983.

[98] L. Fan, T. Watanabe, and K. Fujimoto. Reaction phase effect on tertiary butyl alcohol synthesis by air oxidation of isobutane. *Applied Catalysis A: General*, 158:L41–L46, 1997.

[99] D. Kalló and R.M. Mihályi. Mechanism of 1-butene hydration over acidic zeolite and ion-exchange resin catalysts. *Applied Catalysis A: General*, 121:45–46, 1995.

[100] E.L. Purlee, R.W. Taft, and C.A. DeFazio. Enthalpies and entropies of activation for the hydration of dissolved isobutene and trimethylethylene from the thermodynamic properties for solution of gaseous olefins in aqueous nitric acid. *Journal of the American Chemical Society*, 77:837–842, 1955.

[101] M.H.W. Sonnemans. Hydration of propene over acidic zeolites. *Applied Catalysis A: General*, 94:215–229, 1993.

[102] K. Tao, W. Li, H. Li, and X. Qi. Effect of modified industrial zeolite beta on one-step catalytic hydration of propylene to isopropanol. *Applied Catalysis A: General*, 139:43–49, 1996.

[103] S. Ahmed, M.Z. El-Faer, M.M. Abdillahi, J. Shirokoff, M.A.B. Siddiqui, and S.A.I. Barri. Production of methyl tert-butyl ether (MTBE) over MFI-type zeolites synthesised by the rapid crystallization method and modified by varying Si/Al ratio and steaming. *Applied Catalysis A: General*, 161:47–58, 1997.

[104] A.M. Al-Jarallah, A.K.K. Lee, and M.A.B. Siddiqui. Kinetics of methyl tertiary butyl ether synthesis catalyzed by sulphuric acid. *The Chemical Engineering Journal*, 39:169–174, 1988.

[105] F. Ancillotti, M.M. Mauri, and E. Pescarollo. Ion exchange resin catalyzed addition of alcohols to olefins. *Journal of Catalysis*, 46:49–57, 1977.

[106] K.H. Chang, G.J. Kim, and W.S. Ahn. Methyl tert-butyl ether synthesis over titanium-silicalite I catalysts. *Industrial and Engineering Chemistry Research*, 31(1):125–130, 1992.

[107] P. Chu and G.H. Kühl. Preparation of methyl tert-butyl ether (MTBE) over zeolite catalysts. *Industrial and Engineering Chemistry Research*, 26(2):365–369, 1987.

[108] A.A. Nikolopoulos, A. Kogelbauer, J.G. Goodwin, and G. Marcelin. Effect of dealumination on the catalytic activity of acid zeolites for the gas phase synthesis of MTBE. *Applied Catalysis A: General*, 119:69–81, 1994.

[109] S. Shikata, S. Nakata, T. Okuhara, and M. Misono. Catalysis by heteropoly compounds. 32. Synthesis of methyl tert-butyl ether catalyzed by heteropolyacids supported on silica. *Journal of Catalysis*, 166:263–271, 1997.

[110] M.H.W. Sonnemans. Hydration and etherification of propene over H-ZSM-5. 1. a kinetic study. *Industrial and Engineering Chemistry Research*, 32(11):2506–2511, 1993.

[111] I G Farbenindustrie. *German Patent No. 882 091*, 1953.

[112] W.K. Schumann. The catalytic conversion of low chain length hydrocarbons to liquid fuels using ion-exchange resin. Master's thesis, University of Cape Town, 1984.

[113] R.L. Albright and I.J. Jakovac. CATALYSIS by functionalized porous organic polymers. Technical Report IE-287, Rohm and Haas, July 1985.

[114] R. Kunin, E. Meitzner, and N. Bortnick. Macroreticular ion exchange resins. *Journal of the American Chemical Society*, 84:305–306, Jan. 1962.

[115] Bayer Polymer-Based Catalysts - Properties and Applications. Technical Report OC/I 20416e, Bayer AG, June 1989.

[116] B.C. Gates and G.M. Schwab. The dehydration of formic acid catalyzed by polystyrene sulfonic acid. *Journal of Catalysis*, 15:430–434, 1969.

[117] G. Zundel, H. Noller, and G.M. Schwab. *Zeitschrift der Elektrochemie*, 66:129, 1962.

[118] G. Zundel. *Hydration and Intermolecular Interaction. Infrared Investigations with Polyelectrolyte Membranes.* Academic Press, New York, 1969.

[119] R. Thornton and B.C. Gates. Catalysis by matrix-bound sulphonic acid groups: Olefin and paraffin formation from butyl alcohols. *Journal of Catalysis*, 34:275–287, 1974.

[120] E. Knözinger and H. Noller. *Zeitschrift der Physikalischen Chemie*, 79:130, 1972.

[121] B.C. Gates and L.N. Johanson. The dehydration of methanol and ethanol catalyzed by polystyrene sulfonate resins. *Journal of Catalysis*, 14:69–76, 1968.

[122] B.C. Gates, J.S. Wisnouskas, and H.W. Heath Jr. The dehydration of t-butyl alcohol catalyzed by sulfonic acid resin. *Journal of Catalysis*, 24:320–327, 1972.

[123] R.B. Wesley and B.C. Gates. Benzene propylation catalyzed by sulphonic acid resin. *Journal of Catalysis*, 34:288–293, 1974.

[124] P.D. Bolton and T. Henshall. *Journal of the Chemical Society*, page 1226, 1962.

[125] V.P. Gupta and W.J.M Douglas. Diffusion and chemical reaction in isobutylene hydration within cation exchange resin. *AIChE Journal*, 13(5):883–889, September 1967.

[126] L. Petrus, E.J. Stamhuis, and G.E.H. Joosten. Thermal deactivation of strong-acid ion-exchange resins in water. *Industrial and Engineering Chemistry Product Research and Development*, 20(2):366–371, 1981.

[127] N. Bothe, F. Döscher, J. Klein, and H. Widdecke. Thermal stability of sulponated styrene-divinylbenzene resins. *POLYMER*, 20:850–854. July 1979.

[128] T. Zhang and R. Datta. Integral analysis of methyl tert-butyl ether synthesis kinetics. *Industrial and Engineering Chemistry*, 34(3):730–740, 1995.

[129] M. Iborra, J.F. Izquierdo, F. Cunill, and J. Tejero. Application of the response surface methodology to the kinetic study of the gas-phase addition of ethanol to isobutene on a sulfonated-divinylbenzene resin. *Industrial and Engineering Chemistry*, 31(8):1840–1848, 1992.

[130] V. J. Nowlan and T. T. Tidwell. Structural effects of acid-catalyzed hydration of alkenes. *Accounts of Chemical Research*, 10:252–258, 1977.

[131] R.T. Morrison and R.N. Boyd. *Organic Chemistry*. Allyn and Bacon, Boston, third edition, 1973.

[132] J. Tejero, F. Cunill, J.F. Izquierdo, M. Iborra, C. Fite, and D. Parra. Scope and limitations of mechanistic inferences from kinetic studies on acidic macroporous resins. The MTBE liquid-phase synthesis case. *Applied Catalysis A: General*, 134:21–36, 1996.

[133] Amberlyst 15WET. Technical Report PDS 0373A, Rohm and Haas, Sep. 1995.

[134] Amberlyst 35WET. Technical Report PDS 0316A, Rohm and Haas, Apr. 1993.

[135] Amberlyst 36WET. Technical Report PDS 0334A, Rohm and Haas, Sep. 1995.

[136] Amberlyst. Technical Report CLP 0396A, Rohm and Haas, Dec. 1993.

[137] Deloxan ASP. Technical report, Degussa.

[138] Catalyst extrudate base LZ-Y82 1/16". Technical Report F-4061B, Linde, Jul. 1979.

[139] K.P. Möller. *The Deactivation of Zeolite-Y and Mordenite During Hexane Cracking and Propylene Oligomerisation.* PhD thesis, University of Cape Town, 1989.

[140] L.B. Møller, C. Halken, J.A. Hansen, and J. Bartholdy. Liquid and gas distribution in trickle-bed reactors. *Industrial and Engineering Chemistry Research*, 35:926–930, 1996.

[141] W.A. Dietz. Response factors for gas chromatographic analyses. *Journal of Gas Chromatography*, pages 68–71, February 1967.

[142] *Eight Peak Index of Mass Spectra.* The Mass Spectrometry Data Centre, The Royal Society of Chemistry, Cambridge, fourth edition, 1991.

[143] H. E. Avery. *Basic Reaction Kinetics and Mechanisms.* The Macmillan Press Ltd., London, 1980.

[144] R. Prins. *Kinetiek.* Technische Hogeschool Eindhoven, Eindhoven, 1984.

[145] M. Herskowitz and J.M. Smith. Trickle-bed reactors: A review. *AIChE Journal*, 29(1):1–18, 1983.

[146] P.L. Mills and M.P. Dudukovic. Analysis of catalyst effectiveness in trickle-bed reactors processing volatile or nonvolatile reactants. *Chemical Engineering Science*, 35:2267, 1980.

[147] J.A. Linnekoski and L.K. Rihko. Kinetics of heterogeneously catalyzed formation of tert-amyl ethyl ether. *Industrial and Engineering Chemistry Research*, 36(2):310–316, 1997.

[148] H.J. Panneman and A.C.M. Beenackers. Synthesis of methyl tert-butyl ether catalyzed by acidic ion-exchange resins. Influence of the proton activity. *Industrial and Engineering Chemistry Research*, 34(12):4318–4325, 1995.

[149] E. Velo, L. Puigjaner, and F. Recasens. Inhibition by product in the liquid-phase hydration of isobutene to tert-butyl alcohol: Kinetics and equilibrium studies. *Industrial and Engineering Chemistry*, 27(12):2224–2231, 1988.

[150] H.A. Massaldi and J.A. Maymo. Error in handling finite conversion reactor data by the differential method. *Journal of Catalysis*, 14:61–68, 1969.

[151] C.N. Satterfield, A.A. Pelossof, and T.K.Sherwood. Mass transfer limitations in a trickle-bed reactor. *AIChE Journal*, 15(2):226–234, 1969.

[152] O. Levenspiel. *The Chemical Reactor Omnibook*. Oregon State University Press, Corvalis, 1979.

[153] OlaF A. Hougen. Engineering aspects of solid catalysis. *Industrial Engineering Chemistry*, 53(7):509–528, 1961.

[154] J.B. Anderson. A criterion for isothermal behaviour of a catalyst pellet. *Chemical Engineering Science*, 18:147–148, 1963.

[155] J.H. Hiestand. PhD thesis, University of Michigan, 1961.

[156] A. Gicquel and B. Torck. Synthesis of methyl tertiary butyl ether catalyzed by ion-exchange resin. Influence of methanol concentration and temperature. *Journal of Catalysis*, 83:9–18, 1983.

[157] J.A. Linnekoski, A.O.I. Krause, and L.K. Struckmann. Etherification and hydration of isoamylenes with ion exchange resin. *Applied Catalysis A: General*, pages 117–126, 1998.

[158] L. Petrus, R.W. De Roo, E.J. Stamhuis, and G.E.H. Joosten. Kinetics and equilibria of the hydration of linear butenes over a strong acid ion-exchange resin as catalyst. *Chemical Engineering Science*, 41(2):217–226, 1986.

[159] H. Knözinger. Dehydration of alcohols on aluminum oxide. *Angewandte Chemie Internationale Edition*, 7(10):791–805, 1968.

[160] H.J. Panneman and A.C.M. Beenackers. Solvent effects on the hydration of cyclohexene catalyzed by a strong acid ion-exchange resin. 2. Effect of sulfolane on the reaction kinetics. *Industrial and Engineering Chemistry Research*, 31(6):1425–1433, 1992.

[161] T. Uematsu. *Bulletin of the Chemical Society of Japan*, 45:3329, 1972.

[162] R.W. Taft. The dependence of the rate of hydration of isobutene on the acidity function, H_o, and the mechanism for olefin hydration in aqueous acids. *Journal of the American Chemical Society*, 74:5372 – 5376, 1952.

[163] F.A. Long and M.A. Paul. Application of the H_o acidity function to kinetics and mechanisms of acid catalysis. *Chemical Reviews*, 57:935–1010, 1957.

[164] R. Albright and E.R. Becker. *Ion Exchange.* Environex, Wayne, Pennsylvania, 1996.

[165] R.C. Weast, editor. *CRC Handbook of Chemistry and Physics.* CRC Press, Boca Raton, Florida, 1988.

[166] S.P. Sivanand, B.V. Kamath, R.S. Singh, and D.K. Chakrabarty. Vapour-phase dehydration of isopropanol on macroporous ion exchange resins. *Journal of Catalysis*, 69:502–505, 1981.

[167] F. Cunill, M. Vila, J.F. Izquierdo, M. Iborra, and J. Tejero. Effect of water presence on methyl tert-butyl ether and ethyl tert-butyl ether liquid phase syntheses. *Industrial and Engineering Chemistry Research*, 32(3):564–569, 1993.

[168] A.C. Hindmarsh. ODEPACK - A Systematized Collection of ODE Solvers. Technical report, Computing and Mathematics Research Division, Lawrence Livermore National Laboratory, 1987.

[169] I.S. Gradshteyn and I.M. Rhyzik. *Table of integrals, series and products.* Academic Press, London, fifth edition, 1994.